SOLUTION PHOTOPHYSICS OF SELECTED METAL COMPLEX IONS

A thesis submitted for the degree of

Doctor of Philosophy

by

WILLIAM JOHN REED

September, 1979

University of Warwick

ACKNOWLEDGEMENTS

I wish to thank Dr. T.J. Kemp for his constant encouragement and interest throughout this work. I am also extremely grateful to Dr. S.R. Allsopp for help with the work on ruthenium(II) and initial investigations of the uranyl, osmium(II) and chromium(III) systems. I thank Dr. A. Cox for many helpful discussions and Professor O. Traverso of the University of Ferrara, Ferrara, Italy, for supplying a number of the complexes.

I am also grateful to the workshops of the Department of Chemistry and Molecular Sciences for invaluable help in both construction of apparatus and maintenance of the laser assembly.

I wish to acknowledge financial support from the S.R.C. in the form of a postgraduate studentship and N.A.T.O. for a grant both to assist with maintenance of the laser assembly and to enable the Warwick-Ferrara collaboration.

Finally, I thank my wife for tolerating the author during the preparation of this manuscript.

CONTENTS

page

page

ABSTRACT

The luminescence lifetimes of a number of selected metal complex ions have been determined in a variety of media over as wide a temperature range as feasible, using laser flash photolysis. The results, together with those of other selected experiments, have been used in conjunction with a re-interpretation of certain others in the literature to either propose or extend simple energy schemes for the individual systems which provide a basis for discussion of the results.

The luminescence kinetics of $[Ru(bipy)_3]^{2+}$ and $[Ru(phen)_3]^{2+}$ can be described completely for 360 > T > 77 K by deactivation of the excited state through two energy-controlled pathways. At T $\geq$ 270 K, the high-energy route (40 to 50 kJ mol^{-1}) dominates,whilst at T < 130 K, the other route becomes important. The latter pathway has an activation energy of a few kJ mol^{-1} in fluid media, but < 1 kJ mol^{-1} in rigid media, indicating the importance of solvation forces. A simple energy level model involving a high-energy photoreactive ^{3}LF state and a lower luminescent level of the low-lying ^{3}CT manifold has been used to explain these results. Two principal routes also provide the deactivation of the excited state for $[Os(phen)_3]^{2+}$ and $[Os(bipy)_3]^{2+}$, namely a higher energy non-radiative pathway ($\sim$ 13 kJ mol^{-1} in 9 mol dm^{-3} LiCl) and a radiative pathway of energy $\sim$ 0.75 kJ mol^{-1}. However, both the discrepancy between the temperature profiles of the luminescence lifetime and relative quantum yield, and the emission wavelength dependence of the luminescence lifetime suggests a more complicated situation prevails than for the ruthenium(II) analogues.

In contrast, the temperature profile of both the luminescence lifetime and relative yield for $[Pt(QO)_2]$ can be attributed to a single low-energy (< 15 kJ mol^{-1}) non-radiative pathway. Further study of this system revealed an intense ESA spectrum (λ_{max} 565, 850 and 930 nm) and a strong dependence of ground state absorption peaks upon solvent (as indicated by a correlation of ν_{max} with the Dimroth parameter, E_T), although the dependence of the luminescence lifetimes is small. A model involving deactivation of the luminescent state through a higher energy level has been proposed.

A number of luminescent chromium(III) complexes of photochemical interest show a similar temperature profile for the luminescence lifetime over the range 77 to 370 K. The energy of this non-radiative pathway is always only a fraction of the $^4T_2$-^2E splitting, and while strongly solvent-dependent is insensitive to solvent deuteration, implying a strongly-coupled mechanism. This pathway is explained in terms of an M-L vibration which may lead to photochemistry and is suggested in preference to the previously proposed possibility of back-ISC. The good correlation of the activation data for individual complexes to a Barclay-Butler plot implies a common mechanism at least for each complex.

The luminescent decay of the uranyl ion has been studied in a number of diverse media, and in those cases where it was possible to work at temperatures as low as 77 K the temperature-dependent kinetics could be rationalised in terms of the equation $k = B + A \exp(-\Delta E^{\ddagger}/RT)$. B, which was similar for all systems studied (within a factor of 3) is considered to reflect a combination of radiative and non-radiative processes of a physical nature. The thermally-activated term which is dominant at 298 K is characterised by high values of $\Delta E^{\ddagger}$ and is thought to refer to a chemical quenching mechanism in all but the aqueous case, for which a physical mechanism is preferred. Both pathways show kinetic isotope effects which can be marked on the B term, but are only slight on the $\Delta E^{\ddagger}$ route. For the case of methanol, selective isotopic substitution suggests a hydrogen abstraction mechanism to give the hydroxyalkyl radical to operate at 298 K while physical deactivation through the O-H bond is preferred at 77 K.

An unusual luminescence which has been reported for a series of Pt(O) complexes is also discussed.

The majority of the work described in this thesis has reached the stage of publication, viz.

(i) Inorganic Photophysics in Solution. Part 1. Temperature activation of decay processes in the luminescence of tris-(2,2'-bipyridine)ruthenium(II) and tris(1,10-phenanthroline)-ruthenium(II) ions, by S.R. Allsopp, A. Cox, T.J. Kemp and W.J. Reed. J.C.S. Faraday I, 1978, 74, 1275.

(ii) Inorganic Photophysics in Solution. Part 2. Temperature activation of decay processes in the luminescence of uranyl $[UO_2]^{2+}$ ion, by S.R. Allsopp, A. Cox, T.J. Kemp, W.J. Reed, V. Carassiti and O. Traverso. J.C.S. Faraday I, 1979, 75, 342.

(iii) Inorganic Photophysics in Solution. Part 3. Temperature activation of decay processes in the luminescence of tris-(2,2'-bipyridine)osmium(II) and tris(1,10-phenanthroline)-osmium(II) ions, by S.R. Allsopp, A. Cox, T.J. Kemp, W.J. Reed, V. Carassiti and O. Traverso. J.C.S. Faraday I, 1979, 75, 353.

(iv) Inorganic Photophysics in Solution. Part 4. Deactivation mechanisms of the ^2E_g state of Cr(III) complexes from life-time studies, by S.R. Allsopp, A. Cox, T.J. Kemp, W.J. Reed, S. Sostero and O. Traverso. J.C.S. Faraday I, 1979, accepted for publication.

(v) Inorganic Photophysics in Solution. Part 5. Bis(8-hydroxy-quinolinato)platinum(II)-absorption, excited state absorption and emission spectra, kinetics and energetics, by C. Bartocci, S. Sostero, O. Traverso, A. Cox, T.J. Kemp and W.J. Reed. J.C.S. Faraday I, 1979, accepted for publication.

(vi) Inorganic Photophysics in Solution. Part 6. Isotope effects in the non-radiative deactivation of photo-excited uranyl $[UO_2]^{2+}$ ion in hydroxylic solvents, by A. Cox, T.J. Kemp, W.J. Reed and O. Traverso. J.C.S. Faraday I, 1979, accepted for publication.

ABBREVIATIONS

acac	acetylacetonate
bipy	2,2'-bipyridine
CA	cellulose acetate
CT	charge-transfer
CTTL	charge-transfer-to-ligand
CTTM	charge-transfer-to-metal
CTTS	charge-transfer-to solvent
cyclam	1,4,8,11-tetraazacyclotetradecane
DMF	dimethylformamide
DMSO	dimethylsulphoxide
E_A	activation energy
E_T	Dimroth parameter
en	ethylenediamine
EPA	ethanol:isopentane:ether (2:5:5)
e.p.r.	electron paramagnetic resonance
ESA	excited state absorption
e.s.r.	electron spin resonance
fmn	fumaronitrile
gly	glycinate
HOMO	highest occupied molecular orbital
i.r.	infra-red
ISC	inter-system crossing
LF	ligand field
LMCT	ligand-to-metal charge-transfer
LUMO	lowest unoccupied molecular orbital
M-L	metal-ligand
MLCT	metal-to-ligand charge-transfer
MO	molecular orbital
MTHF	2-methyltetrahydrofuran
NBD	norbornadiene
Oh	octahedral
phen	1,10-phenanthroline
PMM	polymethylmethacrylate
PQ	paraquat
py	pyridine
QO	8-hydroxyquinoline

Reinecke's salt	trans-$\left[Cr(NH_3)_2(NCS)_4\right]^-$
S	spin quantum number
SOC	spin-orbit coupling
T	temperature
T_g	glassing temperature
tcne	tetracyanoethylene
terpy	2,2',2"-tripyridyl
tfpd	1,1,1-trifluoropentane-2,4-dionato
thexi	thermally equilibrated, excited
tn	trimethylenediamine
u.v.	ultra-violet
X	X-ray
ε	extinction coefficient
τ	lifetime
ϕ	quantum yield
λ	wavelength
$\perp r$	perpendicular to

CHAPTER 1

INTRODUCTION

1-1 Introductory Remarks

An excited state decays by two types of process, broadly termed as radiative and non-radiative. While luminescence studies yield direct information about radiative processes, they can only give indirect evidence concerning non-radiative pathways. To obtain useful information about the nature and extent of the latter, it is necessary to monitor the effects on the luminescence of a system caused by systematic variation of environmental factors such as solvent, ligand field (LF) and temperature. Further information can be obtained by examining the effect of intermolecular processes on the luminescence, usually in the form of quenching experiments, and by examining the photoreactivity of the complexes, which can also be classified as a type of non-radiative process. It is of particular interest to identify the photoreactive state and obtain qualitative and quantitative information about this level, because of its obvious implication in the photochemical mechanism of the system. Therefore, the most complete information can be obtained by examining both the photochemistry and luminescence of a system under the same experimental conditions, and preferably in the same experiment, although it must be stressed that identification of the nature of the photoreactive state does not by any means give a complete picture of the course of photoreaction. The inherent experimental difficulties of performing room-temperature photophysics experiments have now been alleviated to a certain extent by the advent of laser techniques, providing both luminescence lifetime measurements in the nanosecond domain and high-powered coherent excitation sources for photolysis. More recently, the major disadvantage of the laser, that is its fixed wavelength, has been overcome by the introduction of tunable dye lasers, and picosecond lasers now

promise the direct observation of rates of some ultra-fast non-radiative pathways, by recording the rise time of luminescence.[1]

With the notable exception of $[UO_2]^{2+}$, inorganic photophysics and photochemistry have received extensive investigation only within the last two decades, and have advanced in parallel with the refinement of optical and electronic technology and the clarification of LF and molecular orbital (MO) theory. The interest in $[UO_2]^{2+}$ has been stimulated by research into nuclear power and weapons, and a comprehensive survey arising from the Manhattan Project is given by Rabinowitch and Belford in their excellent monograph.[2]

The study of organic systems is well-documented and has been the subject of numerous reviews, books and articles.[3,4] It therefore seems logical to apply the knowledge of this reasonably well-defined subject to its inorganic counterpart, which might be considered simply as a metal-perturbed organic system. The effect of such a perturbation has an analogy in organic photochemistry in the so-called 'heavy atom' effect,[3] which suggests that heavy metal atoms induce large spin-orbit coupling (SOC) leading to mixing of states and thus removing some of their forbidden character and effecting more efficient communication between them. That SOC does play an important role in transition-metal systems has been amply demonstrated by the work of Crosby on some d^6 systems,[5] where it is suggested that SOC is so strong that strict spin and orbital labelling of states is no longer valid. The one-electron SOC constant, ζ_{nl} for a free ion is given by:-[6]

$$\zeta_{nl} = CZ^4/n^3l(l+\tfrac{1}{2})(l+1) \qquad (1\text{-}1)$$

where Z is the atomic number, l is the orbital quantum number, n is the orbital number and C is a constant given by

$$C = e^2h^2/2m^2c^2a_o^3 \qquad (1\text{-}2)$$

where h is Planck's constant/2π, e is the electronic charge, m is

Figure 1

Molecular orbital scheme for an octahedral complex: LF - ligand-field transitions, LMCT - ligand-to-metal charge-transfer, MLCT - metal-to-ligand charge-transfer, LC - ligand-central transitions.

np

ns

(n-1)

plex: ·

o-metal

-transfer,

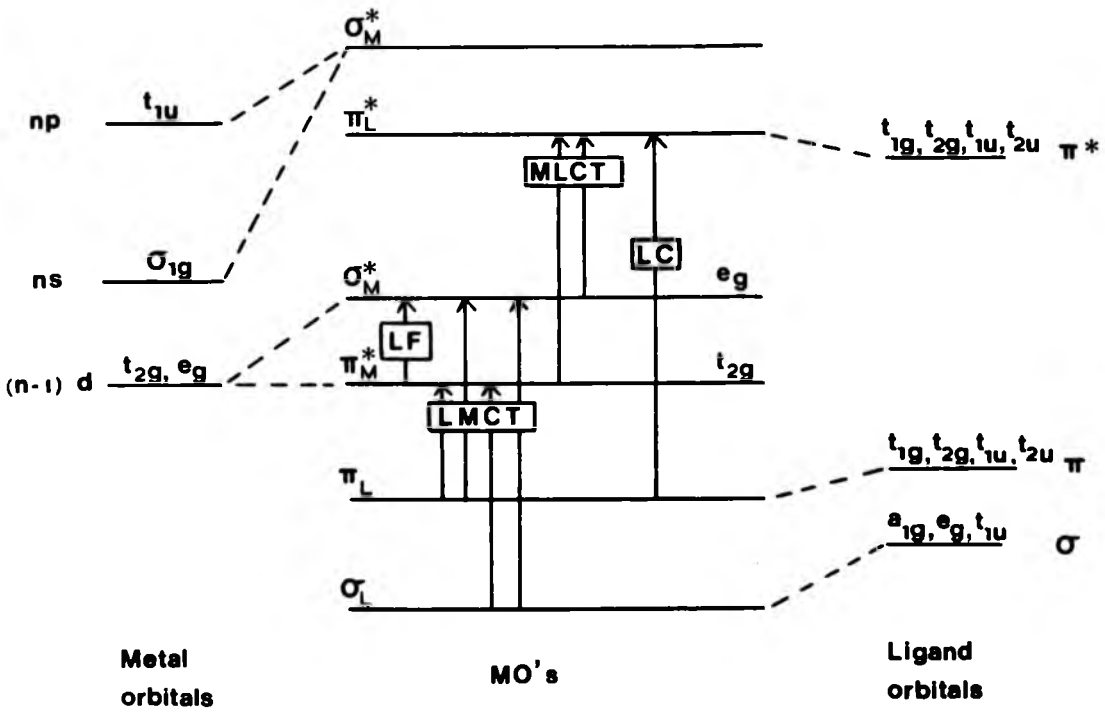

the mass of the electron, a_o is the Bohr radius and c is the velocity of light. This equation shows that SOC increases (through a fourth power dependence) with the mass of the central ion. In the case of chromium(III) complexes (ξ_{3d} = 275 cm^{-1}), SOC is expected to play only a peripheral role, whilst for the platinum(II) and platinum(0) systems we have investigated the effect is predicted to be important ($\xi_{5d} \sim$ 10,000 cm^{-1}).

1-2 Absorption Spectra of Transition-metal Complexes

The absorption of energy by a transition-metal complex may be due to one or more of the electronic transitions depicted in the MO scheme shown opposite (Figure 1). Metal-localised transitions, denoted as LF, involve a transition between the d orbitals of the metal, whereas ligand-localised transitions represent the other extreme, in which a localised transition corresponding to $n-\pi^*$, $\pi-\pi^*$, $\sigma-\sigma^*$ etc. occurs among the ligand orbitals. The latter type of transition is identifiable with that established for the free ligand.

The third type of transition is charge transfer (CT), in which communication between the metal and ligand orbital systems results in an electron being essentially transferred either from a mainly metal-centred MO to an orbital containing mainly ligand character (MLCT), or in the opposite direction (LMCT). One other possible mode is charge transfer to solvent (CTTS) which can result either in a free electron being released into the solvent or in transfer of electronic energy into the vibrational modes of the solvent.

LF (d-d) transitions are invariably treated in terms of LF theory, which considers the effect of the electrostatic field produced by the ligands on the d orbitals of the metal ion, any covalency being accounted for by the two corrective Rac[illegible]

Figure 2

Term diagram (lowest levels) for an octahedral d^3 metal complex (from ref. 36).

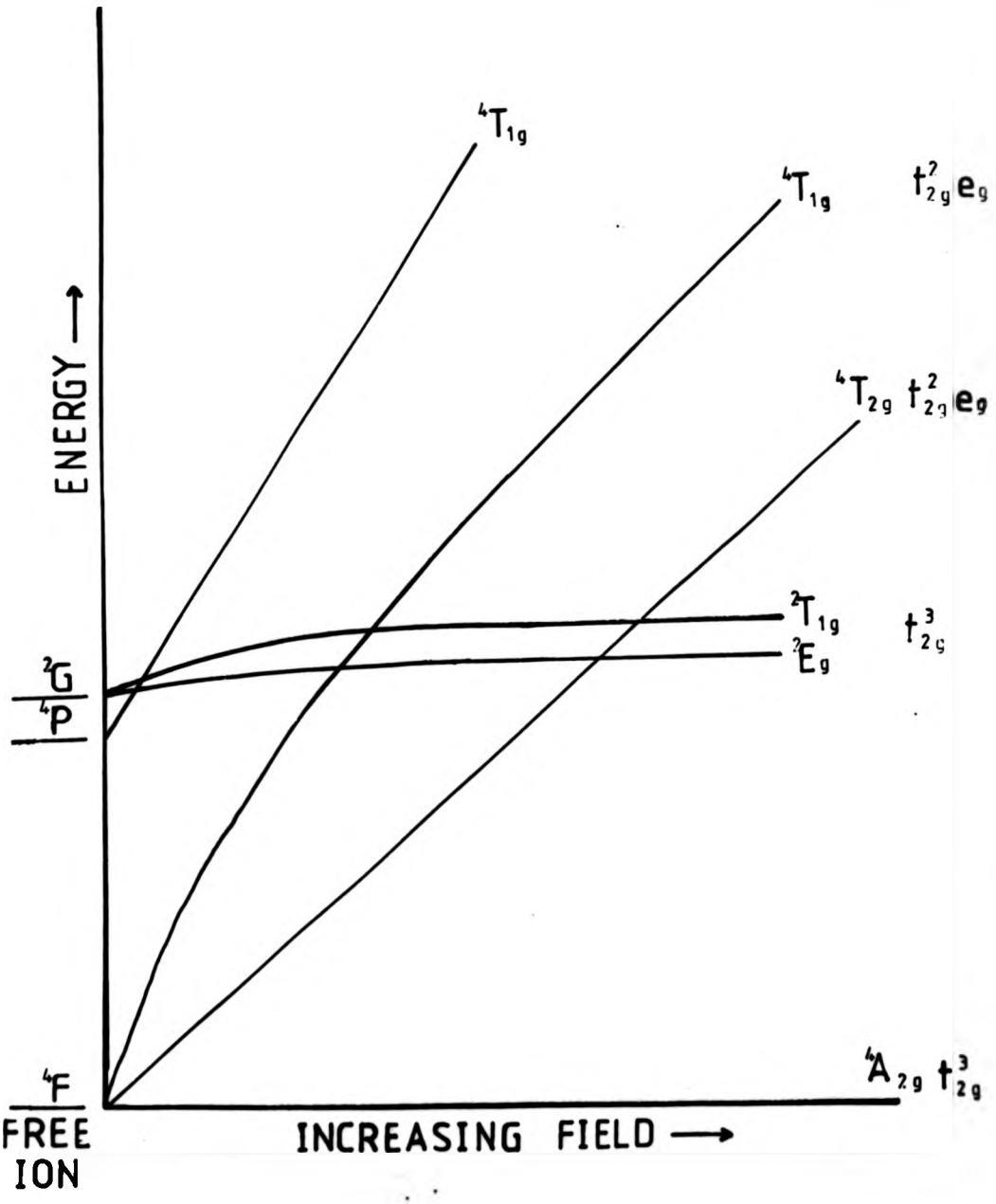
$^4T_{1g}$
$^4T_{1g}$ $t_{2g}^2 e_g$
$^4T_{2g}$ $t_{2g}^2 e_g$
$^2T_{1g}$ t_{2g}^3
^2E_g
^2G
^4P
^4F
$^4A_{2g}$ t_{2g}^3
ENERGY
FREE ION
INCREASING FIELD

parameters, B and C, on the orbital splitting paramater, denoted Δ in octahedral symmetry.

Consideration of the free gaseous metal ion reveals that the d orbitals can combine their orbital and spin-angular momenta as predicted by Russell-Saunders coupling[7] to produce a set of states which are designated bydifferent term symbols and ordered according to Hund's rules.[7] The ligand field splits the d orbitals into two sets, one containing the three orbitals d_{xy}, d_{yz} and d_{xz} (t_2) and the other containing the axial orbitals $d_{x^2-y^2}$ and d_{z^2} (e). The splitting and relative positions of these sets depends upon the overall symmetry of the system and the LF strength. An indication of the latter can be obtained from the spectrochemical series.

For a strong field, terms corresponding to the different orbital configurations ($t_{2g}^{m}e_g^{n}$) are derived from group theory. In reality, the ligand field is often of intermediate strength, and the ordering of the states can be predicted from a term diagram such as those developed by Tanabe and Sugano,[8] which correlate the two extreme cases depicted above. The treatment is illustrated as follows. Chromium(III) is a d^3 system and has the configuration t_{2g}^{3} in Oh symmetry. Promotion of an electron will give rise to a $t_{2g}^{2}e_g$ configuration. The terms for the t_{2g}^{3} configuration are $^4A_{2g}$, ^2E_g, $^2T_{2g}$, $^2T_{1g}$ with the $^4A_{2g}$ term being the ground state by consideration of Hund's rule. The $t_{2g}^{2}e_g$ configuration gives rise to a further set of quartet and doublet terms. The quartet states represent transitions between different orbitals whereas the doublet states refer merely to changes of electron spin within a single orbital. The ordering of these states for the appropriate ligand field strength can now be found by recourse to the d^3 term diagram, as shown opposite (Figure 2).

Transitions between any two of these states are fully allowed only when (i) there is no alteration in the spin quantum number ($\Delta S = 0$), and (ii) a change in symmetry is involved (Laporte-allowed) as satisfaction of these two conditions is required to achieve a non-zero transition moment integral for both the magnetic and electric dipole vectors of the exciting light, respectively. In the case cited above, as for all transition-metal complexes, there are no fully allowed transitions between the ground and first excited states as they are all Laporte-forbidden, and in the doublet case both Laporte- and spin-forbidden. d-d transitions do, however, occur and their mechanism can be understood by considering the selection rules in further detail.

The spin selection rule is only valid in the absence of SOC, an effect which is given by equation (1-1) for a free metal ion and which reaches significance in the case of transition-metals, causing spin-forbidden transitions to occur due to mixing of the same spin-orbit terms in the ground and excited states; although they will not be as intense as spin-allowed transitions, they will get more intense as heavier metal atoms are used. The symmetry rule may also be broken, due to vibronic coupling of the symmetry-forbidden transition with a symmetry-allowed one. These arguments suggest that d-d transitions are relatively weak and indeed their extinction coefficients (ε) are usually ca. 10 to 100 M^{-1} cm^{-1} and can be thought of as "borrowing" intensity from higher energy transitions, mainly through SOC. Charge-transfer transitions are invariably both spin- and symmetry-allowed, and are therefore very intense with ε values ca. 10^3 to 10^4 M^{-1} cm^{-1} or greater. Their position (in the case of LMCT) can be estimated, using the following formula derived by Jörgensen:-[9]

Figure 3

Ground state absorption spectrum of trans-$[Cr(NH_3)_2(NCS)_4]^-$ in methanol at 298 K.

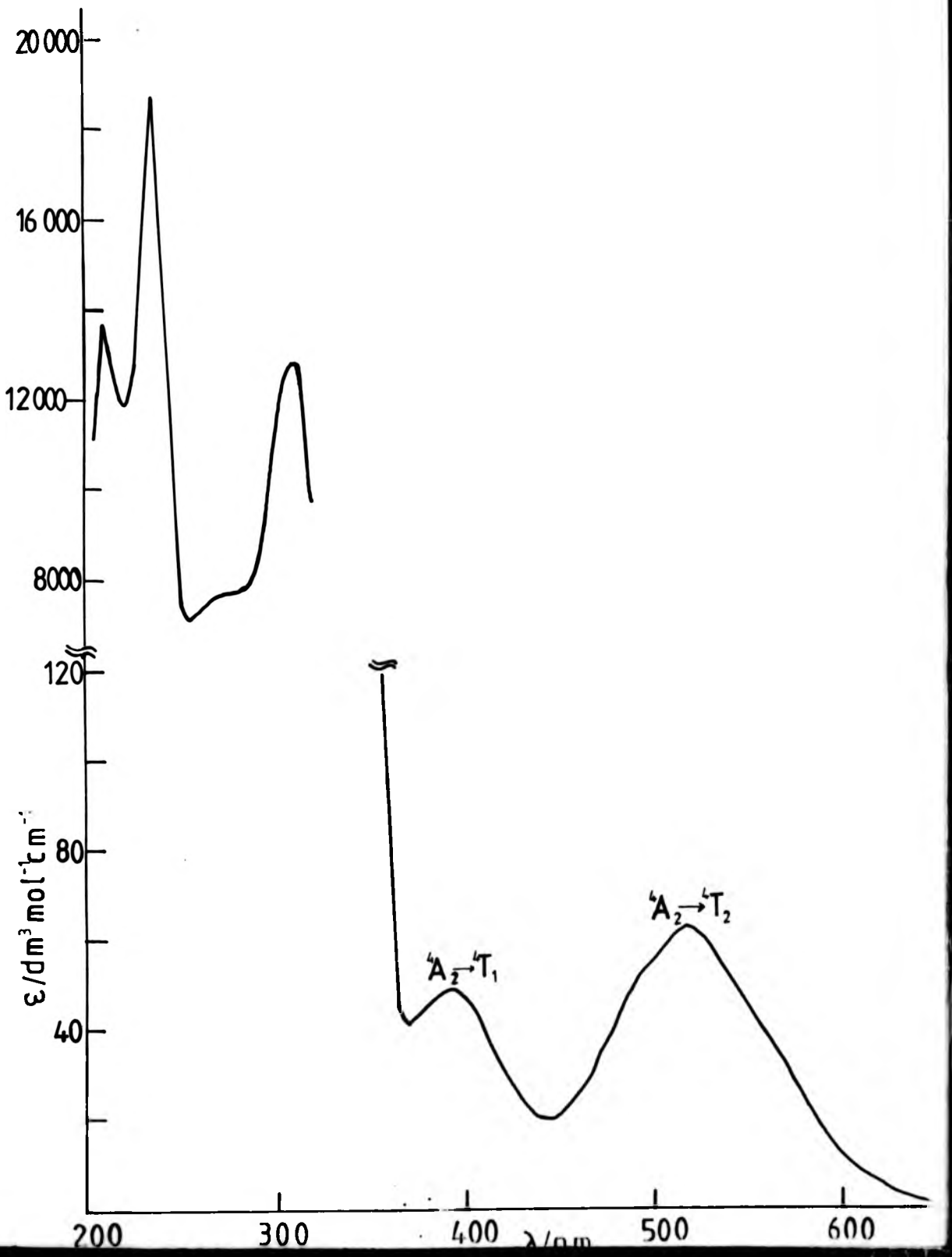
20 000
16 000
12 000
8000
120
80
40
ε/dm³ mol⁻¹ cm⁻¹
⁴A₂ → ⁴T₁
⁴A₂ → ⁴T₂
200
300
400
λ/nm
500
600

$$\bar{\nu}_{max} = 30(\chi_L - \chi_M) + 10Dq + \delta SP + aB \qquad (1\text{-}3)$$

where $\chi_L - \chi_M$ is the difference in electronegativity between metal and ligand, 10Dq is the d orbital energy splitting, δSP is the difference in the spin-pairing energy of the central metal in the ground and excited states, and B is the Racah Parameter. Although this equation does not take into account the nature of the metal-ligand interaction, i.e. the types of donor and acceptor orbitals involved, it is useful in assigning LMCT transitions.

To a first approximation, the energy of the CT bond depicts the ease with which the metal ion is oxidised (MLCT) or reduced (LMCT), and its position will therefore depend upon the nature and oxidation state of the metal, and for readily oxidised or reduced metal cores may well completely envelope the low-intensity d-d bands, as in the case of Ru(II)[10] and Co(III).[11]

Both types of transition are depicted for Reinecke's salt trans-$\left[Cr(NH_3)_2(NCS)_4\right]^-$ in the absorption spectrum shown opposite (Figure 3). The low-intensity, low-energy bands are assigned to the d-d transitions $^4A_2 \rightarrow {}^4T_2$ and $^4A_2 \rightarrow {}^4T_1$, and the intense high-energy bands are attributed to LMCT transitions as their high energy reflects the reluctance of Cr(III) to be reduced and, moreover, there is no resemblance with the absorption bands of the free ligands. The spectrum illustrates that CT and d-d states overlap, which can make the labelling of the excited state initially populated approximate.

The position of the $^4A_2 \rightarrow {}^4T_2$ band gives an indication of the extent of the d orbital splitting, Δ, whereas the intensity of the transition can be used to obtain an estimate of the radiative rate constant, k_r, of the fluorescence, $^4T_2 \rightarrow {}^4A_2$ by using the Strickler-Berg formula:-[12]

$$k_r = 2.88 \times 10^{-9}\, n^2 < \nu_f^{-3} >^{-1} \frac{g_e}{g_n} \int \frac{\epsilon(\bar{\nu})\, d\bar{\nu}}{\bar{\nu}} \qquad (1\text{-}4)$$

where n is the refractive index of the medium, g_e/g_n is the ratio of the degeneracies in the lower and upper states, respectively, $<\nu_f^{-3}>^{-1}$ is the reciprocal mean cube of the emission maximum and the integration is carried out over the entire absorption band. The stringent conditions under which this equation holds, i.e. broad bands with a small Stokes' shift and for a strongly allowed transition, make the equation of limited use in practice, where large Stokes' shifts for emission are frequently observed e.g. in the cases of $\left[Cr(urea)_6\right]^{3+}$ [13] and Rh(III) phosphorescence,[14] and d-d bands are invariably weak. The treatment has, therefore, only any real use when absorption and emission bands are coincident, in which case the approximate form

$$k_r \sim 5 \times 10^{-9}\, \bar{\nu}^{-2} \epsilon_{max}\, \Delta\bar{\nu} \qquad (1\text{-}5)$$

gives an order of magnitude estimate of k_r.

Crosby[15] has questioned the usefulness of the Strickler-Berg formula in estimating radiative lifetimes for heavy metal systems due to mixing of the states in the absorption bands, and has formulated a model based on SOC considerations in which the phosphorescence is considered to 'borrow' intensity from fully-allowed transitions due to the loss of spin and orbital identity between the two states caused by SOC. He has used this model to predict radiative lifetimes for several Ru(II) and Os(II) complexes.[15]

The effect of SOC on heavy metal atoms can be illustrated using the equation below, which relates the extent of coupling between two states to the oscillator strength of a transition and is derived from perturbation theory:-[16]

$$f(N \leftarrow G) = \frac{4}{9} \frac{f(M \leftarrow G)}{W_M - W_G}^2 \frac{\bar{\nu}(N \leftarrow G)}{\bar{\nu}(M \leftarrow G)} \xi^2 \qquad (1\text{-}6)$$

where f( ) is the oscillator strength, G represents the ground state, M and N are the two excited states, $W_M - W_G$ is the energy separation of the G and M states, $\bar{\nu}$( ) is the frequency of the transition, and ξ^2 represents the SOC term. In the case of light atoms such as carbon, ξ = 30 cm^{-1}, and negligible mixing of the state occurs. In the case of 3d transition-metals, ξ is of the order of 150 to 800 cm^{-1} and mixing will occur, but the states still retain their identity to a large extent. For 4d elements, ξ becomes very large (500 to 1,800 cm^{-1}), and on going to 5d elements is enormous (e.g. Pt $\simeq$ 10,000 cm^{-1}).[6] These values predict considerable mixing when substituted in the equation (1-6). Crosby[17] points out that the complete Hamiltonian for a system always contains a term of the form $\Sigma(\xi_{ri})\ \underline{l}_i.\underline{s}_i$ which is insignificant in the case of light atoms, but as ξ becomes large these terms may become dominant, so that spin and orbit labellings of states are meaningless, a situation he considers to exist for 4d elements. Although this may well be the case, it is convenient to designate spins and orbital labels to states although these must not be taken as stringent assignments in view of the previous arguments.

1.3 Photochemical Aspects of Transition-metal Excited States

From a knowledge of the band irradiated, it may be possible to make predictions about the type of photochemistry observed. This approach assumes that the type of state initially populated is the reactive species, no intersystem crossing (ISC) to other configurations occurs, and that the transitions are purely of one type. A further complicating factor is that photoreaction

involving a redox mechanism may lead to substitution-type products, as in the case of the photoaquation of $[Rh(NH_3)_5I]^{2+}$ [18]

$$[Rh(NH_3)_5I]^{2+} \xrightarrow[H_2O,I^-]{h\nu(LMCT)} [Rh(NH_3)_4]^{2+} + NH_3 + \cdot I$$

$$\cdot I + I^- \longrightarrow I_2^-$$

$$[Rh(NH_3)_4]^{2+} + I_2^- + H_2O \longrightarrow \underline{trans}\text{-}[Rh(NH_3)_4(H_2O)I]^{2+} + I^-$$

or

$$[Rh(NH_3)_4]^{2+} + \cdot I + H_2O \longrightarrow \underline{trans}\text{-}[Rh(NH_3)_4(H_2O)I]^{2+}$$

$$[Rh(NH_3)_5I]^{2+} \xrightarrow[H_2O]{h\nu(LF)} \underline{trans}\text{-}[Rh(NH_3)_4(H_2O)I]^{2+}$$

However, redox photoreactions can often be identified by the production of a radical transient, for example in the above case, I_2^-.

LF band excitation has been used extensively in Cr(III) systems,[19] where SOC is minimal. LF theory predicts promotion of electron density from the t_{2g} orbitals, which in Oh symmetry point toward the edge of the octahedron to an e_g orbital which are directed towards the ligands, resulting in bond labilisation, while nucleophilic attack at the empty t_{2g} orbital may occur. This statement describes the conditions for photosubstitution, which is indeed the characteristic photochemistry of Cr(III) complexes.[20] A more detailed theoretical treatment has been undertaken by a number of groups[21,22,23] based on the antibonding (both σ^* and π^*) character of the excited electronic states, as given by the LF approach to predict the actual ligand labilised in complexes of varying symmetry and the intricate mechanism involved. In one case,[21] photochemical yields are predicted, whereas the other treatments are qualitative.

LMCT transitions lead to redox reactions as expected, producing reduction of the metal centre, as in the well-documented case of Co(III) photochemistry.[24] The photoreactions are frequently studied by chemical scavenging of the primary radicals produced, and the situation is often complicated by secondary

radical reactions as in the case of $[Co(NH_3)_5I]^{2+}$ [25]

$$[Co(NH_3)_5I]^{2+} + h\nu \xrightarrow[H^+]{} Co^{2+} + I^{\cdot} + 5NH_4^+$$

$$I^{\cdot} + I^- \longrightarrow I_2^-$$

$$I^- + [Co(NH_3)_5I]^{2+} \xrightarrow[H^+]{} Co^{2+} + I_2 + 5NH_4^+$$

$$I_2^- + [Co(NH_3)_5I]^{2+} \xrightarrow[H^+]{} Co^{2+} + I_3^- + 5NH_4^+$$

$$I^{\cdot} + I^{\cdot} \longrightarrow I_2$$

$$I_2^- + I_2^- \longrightarrow I_3^- + I^-$$

$$I^{\cdot} + I_2^- \longrightarrow I_3^-$$

Oxidation of the metal core follows irradiation of the MLCT bands. This situation is uncommon as it requires a reducing metal and an oxidising ligand to be energetically accessible to near-u.v. light.

Finally, ligand-centred transitions, as expected, induce reactions typical of the ligand and are therefore of no real interest from an inorganic point of view. One example is that of $[Ru(bipy)_2(\underline{cis}\text{-}4\text{-stilbazole})_2]^{2+}$ [26]

$$[Ru(bipy)_2(\underline{cis}\text{-}4\text{-stilbazole})_2]^{2+} \rightleftharpoons [Ru(bipy)_2(\underline{trans}\text{-}4\text{-stilbazole})_2]^{2+}$$

This classification of reactions is a somewhat oversimplified view but gives the photochemist a framework from which to assign the type of state responsible for the observed photoreaction. A more detailed study of transition-metal photochemistry yields further insight into the nature of the states involved.

The independence of photosubstitution yield of Oh Cr(III) complexes on excitation wavelength throughout the LF bands suggests that these reactions occur from a common state, that is, the lowest excited state of a given spin multiplicity. Complexes such as $[Cr(NH_3)_5X]^{2+}$ [19] (X = Cl, Br) have been shown to exhibit two reaction modes:-

$$[Cr(NH_3)_5X]^{2+} \xrightarrow{h\nu} \begin{cases} \xrightarrow{\phi_{NH_3}} [Cr(NH_3)_4(H_2O)X]^{2+} + NH_3 \\ \xrightarrow{\phi_{X^-}} [Cr(NH_3)_5(H_2O)]^{3+} + X^- \end{cases}$$

ϕ_{NH_3} is constant throughout the range of excitation, whereas ϕ_{X^-} shows an approximately 50-fold increase (0.005 to 0.3) on going toward the CT absorption bands, suggesting a small but finite CT component to the d-d bands, from which they 'borrow' intensity. This example also illustrates that photochemical reactions are not simply accelerated thermal reactions, but can lead to unique products.

The intermixing of excited states in heavy-metal systems caused by SOC, mentioned earlier, is elegantly demonstrated by the effect of ligand substitution upon the photochemical reactivity of $[Ru(NH_3)_5X]^{2+}$,[27] where X is a series of substituted pyridines. Excitation into the MLCT band in aqueous acidic solution produces two substitution products, which are considered to originate from a common excited LF state.

$$[Ru(NH_3)_5py]^{2+} + H_2O \xrightarrow[(405\ nm)]{h\nu} \begin{cases} \rightarrow [Ru(NH_3)_5H_2O]^{2+} + py \\ \rightarrow [Ru(NH_3)_4(H_2O)py]^{2+} + NH_3 \end{cases}$$

(py = pyridine)

Substitution of the aromatic ring causes the total quantum yield to vary from 0.003 to 0.02 and it is suggested that aromatic substitution by electron-withdrawing groups lowers the energy of the (unreactive) CT state below that of the LF state to give reduced reactivity. The implications of this example are that SOC is so large that inhibition of inter-state transitions is effectively removed, so that relaxation to the (photoreactive) lowest excited state is rapid. Subtle alterations can induce re-ordering of the CT and LF states, thereby altering the reactivity of the complex. This possibility implies the potential of complexes with designated reactions.[28]

1.4 Energy Transfer Techniques as a Probe of Excited State Properties

As indicated above, photochemical reactions are not especially 'clean', particularly in cases where there is considerable overlapping of absorption bands, and it is desirable to examine specific reaction pathways individually. This is made possible by intermolecular energy transfer techniques in which a well-characterised molecule acts either as a donor (sensitisation) or acceptor (quenching) of electronic energy. Sensitisation techniques are used to selectively populate a specific excited state, including those not reached by direct irradiation, which enable its role to be assessed by comparison of the sensitised and direct photochemical yields. In addition, quenching experiments yield quantitative information about intramolecular deactivation steps as well as the nature of the excited state. Quenching can be used to completely suppress an excited state to facilitate a more detailed study of other processes.

Sensitisation studies often use well-defined organic triplet donors, such as biacetyl, napthalene, etc.,[29] although inorganic complexes[30] are sometimes used as donors. The use of the latter may be somewhat ambitious as many inorganic systems are not well-understood in fluid solution at ambient temperature due to the general lack of photophysical data under these conditions.

The technique is most effective when sensitisation by a series of donors is investigated involving a systematic variation in donor energy, thereby allowing results to be correlated with specific states. An excellent illustration has been reported for the sensitised solvation and phosphorescence of $[Cr(CN)_6]^{3-}$ in dimethyl-formamide at ambient temperatures.[31] Energy transfer from high energy donors causes both photosolvation and phosphorescence,

whereas low energy donors promote only phosphorescence, implying that a higher state is photoactive, while the lower one is responsible for phosphorescence. An estimate of the positions of the states may also be obtained by comparison of the donor energies with the manifestations of the two states. This can be useful in cases where the excited state is either distorted or inactive in the absorption spectrum of the molecule. Comparison of the sensitised (ϕ_s) and direct photochemical yields (ϕ_d) can also give insight into the intramolecular processes involved in a system, such as ISC, for the ratio of ϕ_d to ϕ_s indicates the population efficiency of the reactive state.

Sensitisation techniques are of limited use in some cases as population of more than one state may be allowed by spin selection rules, and often the energy separation of these states is not enough to allow selective population.[29] In these cases, quenching studies in which the complex acts as the donor rather than the acceptor are more fruitful.

The over-riding mechanism by which either process occurs in solution is collisional energy transfer, which is characterised by the bimolecular quenching rate constant, k_q. This process is often diffusion-controlled, with the diffusion-controlled rate constant, k_d, being given simply by the modified Stokes-Einstein equation

$$k_d = 8kT/3000\eta \qquad (1\text{-}7)$$

where η is the viscosity of medium, k is the Boltzmann constant and T is the absolute temperature. The experimental quenching constant k_q can be found by use of the Stern-Volmer equation,[4] which is derived by consideration of the quenching mechanism as an additional competing deactivation process of the excited level:

$$\frac{\phi^o}{\phi} = 1 + K_{sv}[Q] \qquad (1\text{-}8)$$

where Q is the quencher concentration, ϕ^o is the photochemical yield in the absence of quencher, ϕ is the observed yield and K_{sv} is given by

$$K_{sv} = k_q \tau \qquad (1\text{-}8a)$$

where τ is the phosphorescence lifetime of the complex under the experimental conditions used. The energy transfer efficiency, α_{et} is given by

$$\alpha_{et} = k_q/k_d \qquad (1\text{-}9)$$

is often well below unity, especially when transition-metal complexes act as quenchers, and this has been attributed to a number of factors, including the nature of the metal, the ionic charge, the orbital nature of the excited states involved, the nature of the solvent and the geometry of the complex.[29] Kinetic schemes produced for energy transfer[32] consider the formation of an "encounter complex" from which the quenching process competes with diffusional separation of this moiety and explains the efficiency of the process

$$*D + A \underset{k_{-d}}{\overset{k_d}{\rightleftharpoons}} \underset{\text{encounter complex}}{[*D....A]} \xrightarrow{k_q} D + *A$$

in terms of this competition. The systematic variation of the properties of the complex leads to quantitative information about the nature of the excited states involved. There are three major ways in which energy may be transferred to the quencher:-

(i) Electronic energy transfer, which involves the exchange of excess energy by physical processes to produce relaxation of the donor with no chemical change. This process often results in acceptor luminescence or excited state absorption by acceptor molecules, and correlation of k_q with the excited state energy of the quencher confirms this process. The mechanism is favoured

when a transition-metal complex, acting as either donor or acceptor, either has a high redox potential, or is abundant in LF states, such as chromium(III), when spin and energy transfer conditions are favourable.

(ii) Electron transfer is a chemical process which involves the transfer of an electron from the donor to the acceptor state, causing chemical change and, as might be expected, is prevalent when CT states are involved, provided that both donor and acceptor have favourable redox potentials. The back reaction is often very favourable so that no net reaction is apparent. However, either correlation of k_q with redox potential of the acceptor or the detection of oxidised transients indicates the presence of this mechanism. In the case of $[Ru(bipy)_3]^{2+}$, the redox potentials are such that quenching by oxidation or reduction of the complex is possible, depending upon the nature of the quencher.[33]

(iii) Exciplex formation, in which the quencher and excited molecule form an excited state complex which is a new entity with its own deactivation pathways back to the ground state. This mechanism is rarely found for transition-metal complexes, and is very hard to detect. It has been postulated for the quenching of $[UO_2]^{2+}$ luminescence[34] by aromatic quenchers, in which both physical and chemical quenching are postulated, even when normal energy processes are thermodynamically impossible.

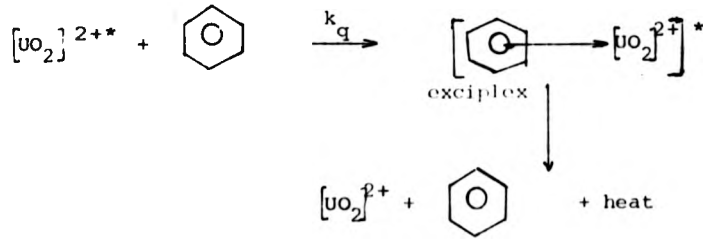

The most conclusive evidence for exciplex formation is the production of a unique emission spectrum. Dynamic processes have, so far, been the only type of quenching discussed. However, the trivial case of static quenching sometimes occurs, which involves complexing between the ground state quencher and donor. This mechanism is of no real use as a probe of excited states, and can be detected by changes in the ground state absorption spectrum of the donor. It is clear that the detection of a quenching mechanism indicates the nature of an excited state and can provide information about the energy and redox potential of that state as well as yielding an insight into the intramolecular processes involved in deactivation.

Photochemistry is only one of a number of possible deactivation processes involved in dissipating energy from an excited state; emission spectroscopy provides an important tool in the study of these other deactivation pathways.

1.5 Emission Spectra of Luminescent Transition-metal Complexes

By analogy with the absorption bands, emission spectra can be considered in terms of the spins of the states involved. Broadly speaking, emission due to a 'spin-allowed' transition is termed fluorescence and 'spin-forbidden' emission is termed phosphorescence. Although these terms will be used in the following discussion, the effects of SOC,as discussed earlier, makes these terms no more than useful labels for the heavier metal atoms.

The specific type of emission observed is given by the rule proposed by Demas and Crosby,[35] *viz*.

Figure 4

Potential energy diagram illustrating the significance of a Stokes' shift.

(a) NEGLIGIBLE STOKES' SHIFT

(b) LARGE STOKES' SHIFT

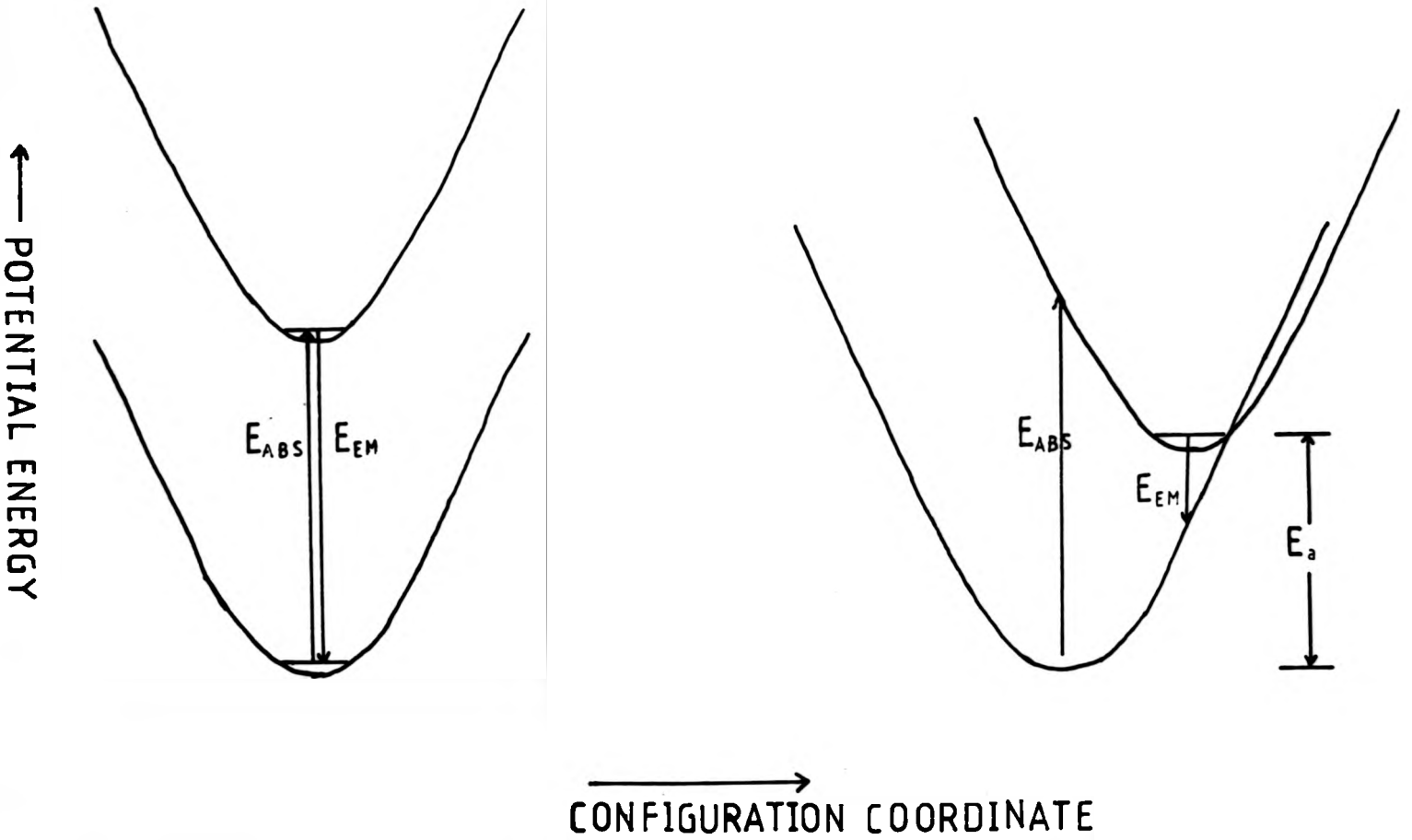

'In the absence of photochemistry from upper excited states, emission from a transition-metal complex with an unfilled d shell will occur from the lowest electronic state in the molecule or from those states which can achieve a significant Boltzmann population relative to the lowest excited state'.

This rule covers, without exception, all of the data so far collected for d^3 and d^6 complexes as indicated by the insensitivity of emission maxima to excitation wavelengths. These are the only two systems for which extensive studies have been undertaken, probably because they provide a substantial variety of luminescent complexes, which are thermally and photochemically stable with their emission in a readily accessible region of the spectrum (300-1,100 nm). Emission has been reported[36] for other electron systems,and recent developments in the luminescence of Pt(II)[37] and Pt(0)[38] promise to extend studies to d^8 and d^{10} systems respectively.

At first sight, one might expect the emission spectrum to be the exact mirror-image of the absorption band, and it should therefore be reasonably easy to classify. However, in practice, both large Stokes' shifts and the overlapping of absorption bands lead to a far more complicated picture,and it is often necessary to consider the shape, lifetime, quantum yield, temperature dependence and possible sensitisation of the emission before an assignment can be made. The emission of $\left[Ru(bipy)_3\right]^{2+}$ provides a prime example, having been assigned to five different types of transition, namely (i) $\pi^* \rightarrow$ d charge transfer (CT) fluorescence,[39] (ii) $d^* \rightarrow$ d phosphorescence,[40] (iii) $d^* \rightarrow$ d fluorescence,[41] (iv) CT phosphorescence[42] and (v) phosphorescence from the $\perp r$ component of the triplet CT level.[43]

The implications of an observable Stokes' shift, which is the difference between the emission and absorption maxima, can be understood from the diagram opposite (Figure 4). From this, it is

apparent that a negligible shift implies little change in the geometry of the excited state from that of the ground state, whereas a large Stokes' shift implies considerable distortion of the molecular moiety (i.e. the complex-solvent aggregate).

The nature of the distortion can be explained in terms of the changes in the position of the potential energy curves for the system, which represent the total energy of a molecule in solution, and therefore include a contribution from its solvent environment. Excitation of a molecule causes a change in the molecular geometry, and is followed by the slower process of solvent relaxation to the new geometry. Deactivation of this state then occurs back to the ground state, followed by solvent relaxation back to the original solvent orientation.[4]

A Stokes' shift, therefore, is a combination of two inter-related factors, as the greater the molecular distortion, the greater the solvent reorientation, both of which will cause movement of the potential energy minima. On moving into a rigid matrix or crystalline medium, a reduction in the Stokes' shift can be expected due to the 'freezing out' of solvent rotations, whereas in fluid solution, the distortion is expected to be larger, assuming solvent relaxation ($\tau \sim 10$ ps) occurs in a time comparable with the lifetime of the excited state.

The consequences of a large distortion are important, as the greater the distortion, the more invalid equation (1-4) becomes for estimating the radiative rate constant, and the corresponding absorption band merely represents a 'Franck-Condon' state of the upper level, rather than the thermally equilibrated position of this state. The importance of these principles have been described by Adamson[44] who proposes the existence of these 'thermally equilibrated, excited' or 'thexi' states to explain the photochemistry of Cr(III) and Co(III) complexes.

Figure 5

Absorption (298 K) and emission (78 K) spectra of 0.03 M $[Cr(urea)_6](ClO_4)_3$; D - quartet-doublet absorption (from ref. 13).

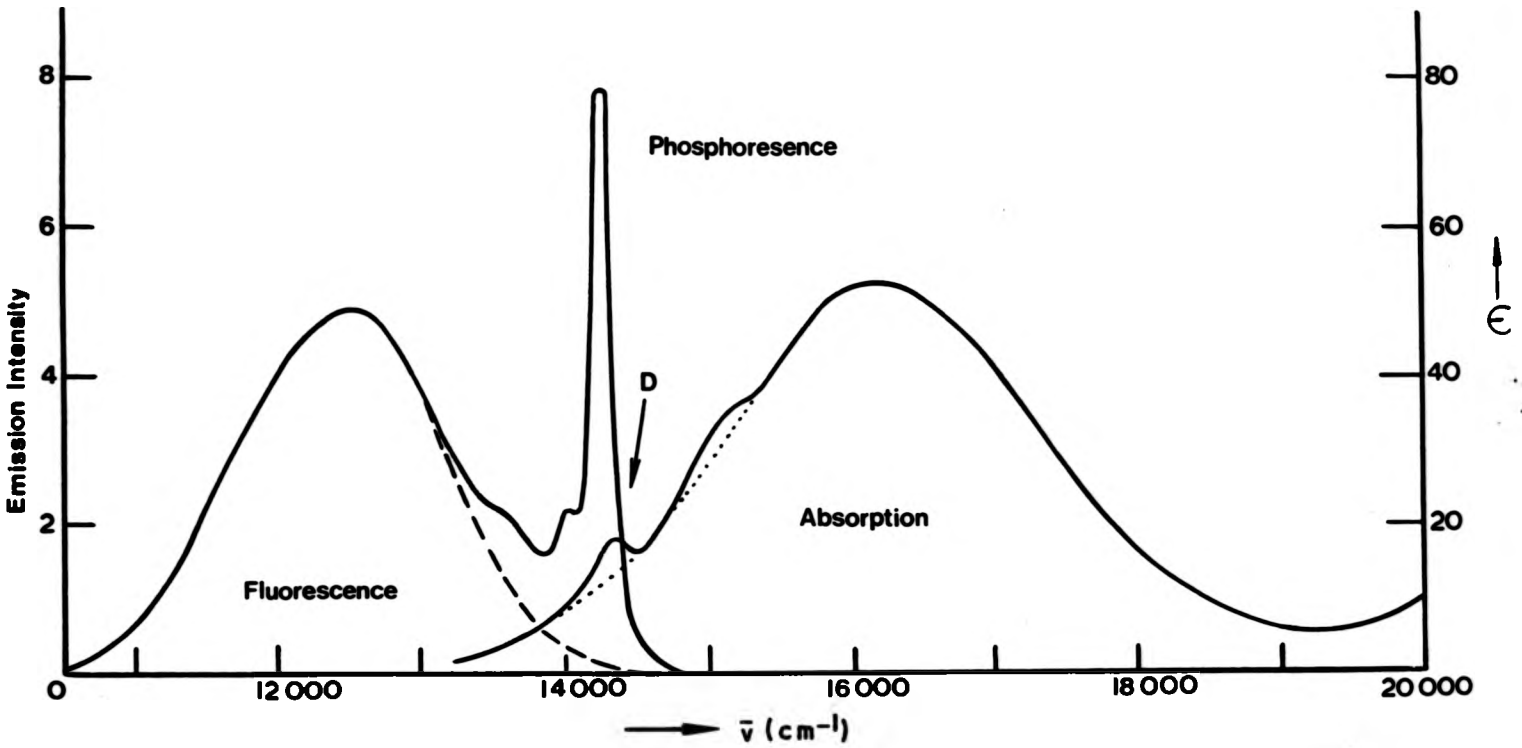
Emission Intensity
8
6
4
2
0
12 000
14 000
16 000
18 000
20 000
$\bar{\nu}$ (cm^{-1})
80
60
40
20
ϵ
Phosphoresence
D
Absorption
Fluorescence

The existence of both large and small Stokes' shifts is amply illustrated by the low temperature absorption and emission spectra of $[Cr(urea)_6]^{3+}$,[13] shown opposite (Figure 5). The phosphorescence spectrum overlaps the weak doublet band (D), whereas the fluorescence spectrum shows a large shift ($\sim$ 3,700 cm^{-1}) and resembles the broad, structureless shape of the absorption band. A rationale for these shapes is provided by Figure 4: the sharp, undistorted phosphorescence spectrum contains few vibrational components, whereas the fluorescence spectrum envelops a multitude of vibrational transitions which are evidently not resolved even at low temperature.

The extent of vibronic coupling between two states can also be estimated from a knowledge of Stokes' shifts.[16] A small shift implies weak coupling of the emitting and ground state, and therefore only high-frequency vibrational modes, such as O-H, should be important as deactivation routes. A large shift implies strong coupling of the states, and low-frequency heavy-atom vibrational modes may facilitate deactivation. Weakly coupled states would, therefore, be expected to be more susceptible to deuteration effects than in the strongly coupled case. It is also noticeable from Figure 4 that,where extensive vibronic coupling is apparent, there is the possibility of an accessible temperature-activated (E_a) reverse-population mechanism between the two states. The assignment of the vibronic coupling mode can be attempted in cases where vibronic structure is observed in the emission spectrum and, preferably, the absorption spectrum as well. The spacing of the structure can then be measured and correlated with absorption bands in the infra-red spectrum, as in the case of $[Cr(diethylenetriamine)_3]^{3+}$.[4,5]

The emission spectrum,when reasonably sharp, plays an important role in illustrating the location of the O-O position of an excited level, a result of considerable importance to photochemical studies. Unfortunately, many emission spectra are measured in a low temperature rigid matrix, whereas photochemistry is studied in fluid solutions at room temperature,and therefore correlations between the two are of limited use due to the difference in environmental factors, as discussed earlier.

Fluorescence is rare amongst transition-metals, and has only been observed for a few chromium(III) complexes at low temperature with general features as described earlier.

Phosphorescence is more prolific and has been characterised for a number of different types of excited state, and can be divided into two broad classifications, namely light and heavy atom phosphorescence.

Light atom phosphorescence has been observed only for chromium(III) and is typically sharp, the excellent matching with the doublet absorption band making identification easier. At low temperatures, vibronic structure is often apparent on the long wavelength side of the spectrum, with consequent sharpening making the no-phonon line easily distinguishable. The phosphorescence yield is low (< 0.01), suggesting that radiationless pathways are important. In a growing number of cases, phosphorescence emission can also be observed at room temperature.[46]

Heavy atom phosphorescence is dominated by spin-orbit states and, in accordance with Crosby's rule,[35] occurs predominantly from the lowest excited state. The nature of the lowest manifold is dictated by the central metal atom, the ligand and the solvent environment, as demonstrated in the cases of iridium(III),[28] ruthenium(II)[47] and rhodium(III).[48]

Three types of phosphorescence have so far been observed for d^6 systems:-

(i) ^{3}(d-d) phosphorescence, which has been reported for Rh(III)[49] complexes, where the LF splitting is small and the oxidation potential of the metal ion is high, giving rise to high energy CT states. The emission is rarely seen at room temperature and is characteristically broad and structureless with a low quantum yield. The spectral position is a function of the average LF strength experienced by the central ion and the enhancement of quantum yield on elimination of high frequency vibrations from the co-ordination sphere suggests weak vibronic coupling with the ground state. The assignment has been made on the basis of the energy, the band shape (which resembles that of d^3 fluorescence) and the lifetime. The existence of a large 'apparent Stokes' shift' is explained by the weakness of the relevant absorption band.

(ii) ^{3}(d-π^*) CT phosphorescence, which has been reported for ruthenium(II) and osmium(II) complexes[15] which are easily oxidised leading to the CT states lying below the d-d states. The emission is intense and highly structured, and is still observable at ambient temperatures. The spectrum is often dominated by a single vibrational progression, assigned to skeletal vibrations of the metal-ligand framework, and lies on the edge of a strong absorption band, which is assumed to be the ^{3}CT absorption. The existence of an isotope effect for both solvent and ligand deuteration suggests weak vibronic coupling mechanisms are active. The quantum yield is exceedingly high, and can be 'tuned' by variation of ligand substituents.

(iii) $^3(\pi-\pi^*)$phosphorescence, which is exhibited by Rh(III)[48] complexes such as $[Rh(phen)_3]^{3+}$ which fulfil the requirements of a large LF splitting and a metal ion which is difficult to oxidise. This situation pushes the d-d and CT states above the ligand states, causing ligand phosphorescence which resembles that of the free ligand.

This survey highlights the possibility that complexes can be engineered to possess a predetermined sequence of states of known types by careful choice of the central metal ion, the ligand and the environment in which the complex is placed, a situation also found previously for photochemistry. Subtle alterations can be effected by means of ligand substitution and environmental modification, while coarse tuning involves changes in the central metal ions. This property has great potential in the use of transition-metal complexes as photosensitisers as well as enabling examination of the properties of different types of states by emission techniques.

1.6 The Nature and Theory of Intramolecular Non-radiative Processes

Since luminescence from complexes rarely occurs with unit efficiency, there must be other modes of deactivation competing for the excitation energy. Photochemistry has been discussed, and this is one possibility,but many luminescent complexes are photochemically inert at ambient temperatures and this explanation for low luminescence efficiency at low temperatures is untenable. The lack of any other chemically or visibly detectable processes implies that the competing deactivation processes are mainly intramolecular and cause regeneration of the ground state species with the excess energy being dissipated as heat by various pathways.

There are three main classes of intramolecular non-radiative relaxation:-

(i) Vibrational relaxation of an excited species. This is confined to one electronic excited state and occurs by collisional interaction of the surrounding medium. Although this is not strictly an intramolecular process, the intimate contact of a complex with its environment qualifies it for inclusion in this category.

(ii) Internal conversion from one electronic state to another state of the same multiplicity, which takes place between co-energetic vibronic levels of the two states.

(iii) ISC between states of different multiplicity which occurs (a) between isoenergetic vibronic levels in the forward direction and (b) from the vibrationally relaxed level to the co-energetic crossover point of the two states in the reverse process when this is energetically feasible.

Vibrational relaxation is assumed to be rapid compared with the other two processes ($\sim 10^{-12}$ s), although in some cases ISC rates of greater than 10^{10} s^{-1} are evident from phosphorescence risetime measurements.[1] The theoretical treatment of non-radiative rate constants by Englman and Jortner[50] considers the rate constant of forward crossing from state i to state j as the sum over all levels of the individual transition probabilities, k_{ij}, each determined by matrix elements for the coupling of the states, which include both electronic factors, C and Franck-Condon factors, S_{ij}:-

$$k_{ij} = \langle \psi_j | V_{ij} | \psi_i \rangle \qquad (1\text{-}10)$$

$$V_{ij} = C.S_{ij} \qquad (1\text{-}11)$$

The values of k_{ij} are dependent upon (i) ΔE, the difference in the zero point energies of i and j and (ii) ΔQ, the displacement of one potential minimum relative to the other along an appropriate co-ordinate, both in a complex fashion, although two

simplifying cases are envisaged, i.e. (i) weak coupling, corresponding to a small ΔQ, and (ii) strong coupling, when ΔQ is large. These conditions are analogous to the small and large Stokes' shifts, E_s, described earier and this fact is used to define the conditions for the two cases. Strong coupling implies

$$E_s >> 2\langle\bar{\nu}\rangle \tanh \langle\bar{\nu}\rangle/2kT \qquad (1\text{-}12)$$

where $\langle\bar{\nu}\rangle$ is the mean vibrational energy in the molecule, k is the Boltzmann constant, and T is the temperature, implying a strong temperature dependence which is related to the energy difference between crossing point and the minimum of the state i. The strong coupling limit applies for E_s > 10,000 cm^{-1} and, in general, is expected only to apply to relaxation via photochemical rearrangement. The weak coupling case ($E_s \leq$ 4,000 cm^{-1}) is given by $E_s \sim 2\langle\bar{\nu}\rangle$, and is expected to apply for interstate crossing. At low temperatures

$$k_{ij} = \frac{C^2(2\pi)^{\frac{1}{2}}}{h(\bar{\nu}_{\cdot\cdot} \Delta E)^{\frac{1}{2}}} \exp -\frac{\gamma \Delta E}{\bar{\nu}_M} \qquad (1\text{-}13)$$

where $\bar{\nu}_M$ is the energy of the highest frequency vibrational modes and γ is given by

$$\gamma = \frac{\log \frac{\Delta E}{\bar{\nu}_M \Delta_M}}{2} - 1 \sim 1 \qquad (1\text{-}14)$$

where ΔM corresponds to ΔQ.

Equation 1-13 implies that the rate constants are temperature insensitive and includes a deuterium effect, qualitatively predicted earlier, since $\bar{\nu}_{\cdot\cdot}$ considers high frequency vibrational modes such as O-H and C-H.

Emission yield and spectral data give only restricted information about non-radiative processes, but when complemented with lifetime measurements, a far greater insight ensues. The distinction between the emission lifetime, τ, and quantum yield, ϕ, is indicated by the definitive equations:-

$$\phi = k_r [M]/I \qquad (1\text{-}15)$$

$$\tau = 1/(k_r + k_{nr}) \qquad (1\text{-}16)$$

where k_r represents the radiative rate constant of the emitting level, $[M]$ the population and k_{nr} the sum of non-radiative rate constants for the emitting level, and I is the intensity of the excitation, under which the quantum yield measurements are performed.

The assumption that the measured emission lifetime represents one emitting level has been proven invalid for d^6 systems, in which two distinct cases are found:-

(i) The emission lifetime is an average of the lifetimes of a manifold of closely spaced emitting levels of the same configuration which are in thermal equilibrium and decay collectively with first-order kinetics, e.g. ruthenium(II) and osmium(II).[5] In this case:

$$(\tau)^{-1} = \sum_{i=1}^{n} (k_{r_i} + k_{nr_i}) \qquad (1\text{-}17)$$

(ii) The emitting levels are of different configurations and decay with multi-exponential kinetics, representing the sum of the individual decays, e.g. in iridium(III) complexes.[51] In this case

$$\tau = \sum_{i=1}^{n} A_i(\tau_i) \qquad (1\text{-}18)$$

where τ_i is defined by equation (1-16) and A_i is a constant representing the contribution of the level to the overall decay.

The emission lifetime and the emission yield may be affected by ligand or solvent or both, which can act as 'acceptor' modes of the vibronic energy. These pathways are distinguished by environmental modification. Changes in lifetime with solvent suggest a solvent contribution as an acceptor of vibronic energy, whereas an increase in lifetime with the 'bulk' of the ligand

suggests the participation of metal-ligand vibrations as acceptor modes, as these vibrations are expected to become more rigid with increasing bulk. Ligand modification must be considered carefully, as it may cause changes in positions of the excited levels or change the symmetry of the molecule, in which case simple correlations with changes in non-radiative rates are inappropriate.

The temperature dependence of an emission process is indicative of the presence of one or more thermally activated radiationless pathways above the emitting level. That this process if often a major deactivation route is suggested by the numerous emissions which occur only at low temperatures and the change in lifetimes of the order of 1,000 on going from ambient to liquid nitrogen temperatures. The position of the higher levels are deduced from the activation energies, E_a, of the processes, whilst their importance is indicated by the size of the associated frequency factor. Information about the nature of the higher deactivating levels can be gained by measuring temperature dependences of luminescence under different environmental conditions, as mentioned above , or by correlation with activation energies for photochemical reactions, if this is suspected to be the deactivation route.

1-7 A General Model for Luminescence

In order to interpret the effect of environmental perturbations on the individual rate constants, it is necessary to be aware of the processes represented in the measured parameters, i.e. the lifetime and quantum yield. This information can be obtained from the derivation of these experimentally measurable quantities from a general model of a luminescent system which may then be applied to specific cases where relevant approximations can be made.

Figure 6

Jablonski diagram depicting a general energy-level scheme for luminescence.

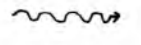
non-radiative transitions

radiative transitions

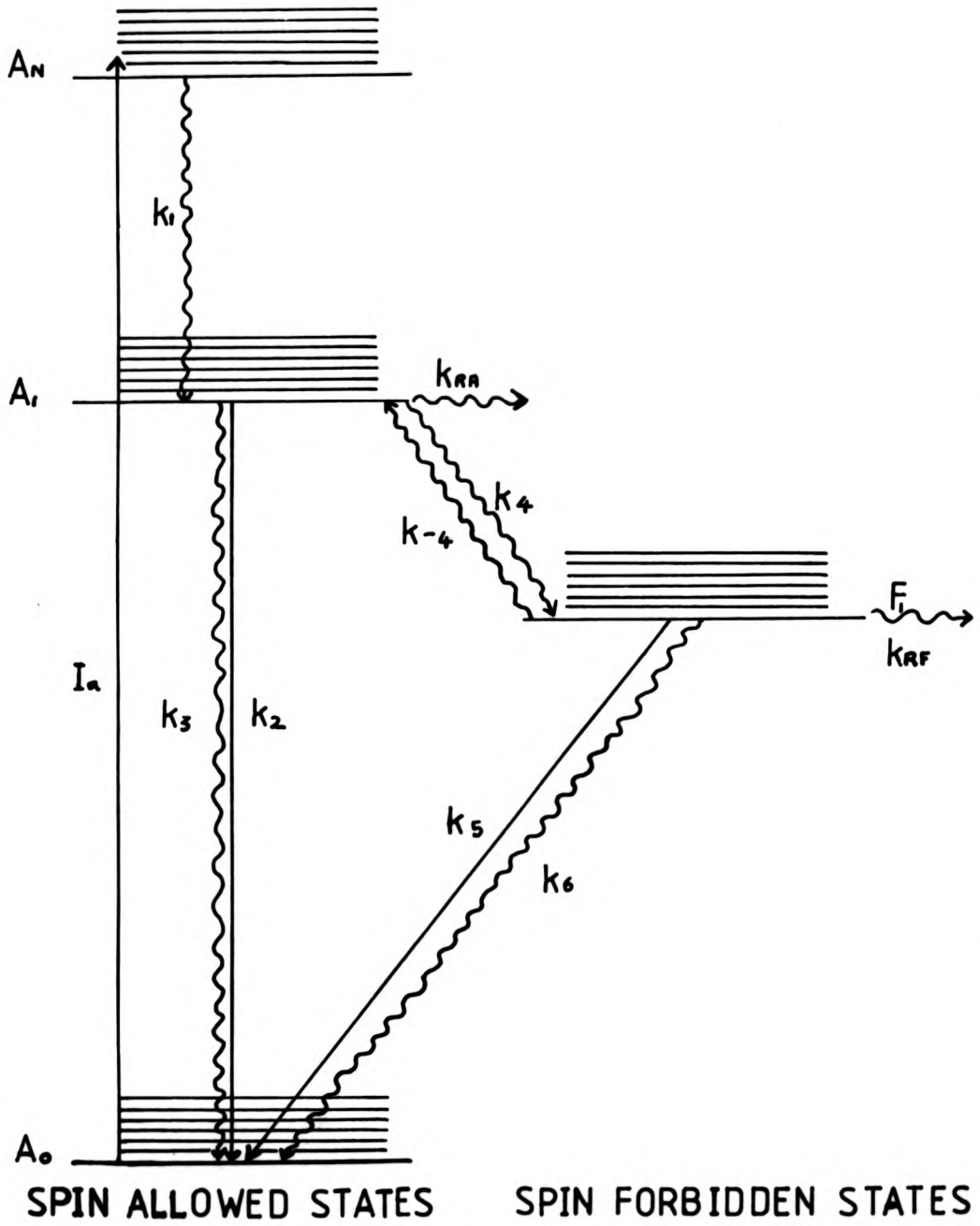
A_N
k_1
A_1
k_{RR}
k_4
k_{-4}
F_1
k_{RF}
I_a
k_3
k_2
k_5
k_6
A_0
SPIN ALLOWED STATES
SPIN FORBIDDEN STATES

A general energy level scheme is represented by a Jablonski diagram in Figure 6. The separation of spin-allowed and spin-forbidden states is for clarity, and is not meant to depict the real situation. The model assumes that vibrational relaxation and internal conversion are fast compared with the other deactivation rates, so that only the lowest excited states need be considered. k_2 and k_5 represent fluorescence and phosphorescence, respectively, whilst k_3 and k_6 are the sum of the intramolecular non-radiative rates for the two levels. k_{RA} and k_{RF} represent the photochemical pathway for A_1 and F_1 respectively, and k_4 depicts ISC between the two levels, k_{-4} representing the thermally activated reverse process.

Neglecting back-ISC, k_{-4}, the relevant rate equations are:-

Pathway	Rate
$A_O + h\nu \rightarrow A_n$	I_a
$A_n \rightarrow A_1$	$k_1[A_n]$
$A_1 \rightarrow A_O + h\nu_F$	$k_2[A_1]$
$A_1 \rightarrow A_O$ + heat	$k_3[A_1]$
$A_1 \rightarrow F_1$	$k_4[A_1]$
$A_1 \rightarrow$ photochemistry	$k_{RA}[A_1]$
$F_1 \rightarrow A_O + h\nu_P$	$k_5[F_1]$
$F_1 \rightarrow A_O$ + heat	$k_6[F_1]$
$F_1 \rightarrow$ photochemistry	$k_{RF}[F_1]$

The pertinent rate equationsfor depopulation of A_1 and F_1 are:-

$$d[F_1]/dt = -(k_5 + k_6 + k_{RF})[F_1] + k_4[A_1] \qquad (1\text{-}19)$$

$$d[A_1]/dt = I_a - (k_2 + k_3 + k_4 + k_{RA})[A_1] \qquad (1\text{-}20)$$

For continuous illumination, as used in the spectroscopic measurement of quantum yields, a steady state approximation, $d[F_1]/dt = d[A_1]/dt = 0$ is valid. Therefore,

$$0 = -(k_5 + k_6 + k_{RF})\, F_1 + k_4 [A_1] \qquad (1\text{-}21)$$

$$0 = I_a - (k_2 + k_3 + k_4 + k_{RA})\, [A_1] \qquad (1\text{-}22)$$

It then follows:-

$$[A_1] = I_a/(k_2 + k_3 + k_4 + k_{RF}) \qquad (1\text{-}23)$$

$$[F_1] = k_4 I_a/ (k_2 + k_3 + k_4 + k_{RA})(k_5 + k_6 + k_{RF}) \qquad (1\text{-}24)$$

Now, by definition,

$$\phi_P = k_5 [F_1]/I_a = k_4 k_5/ (k_2 + k_3 + k_4 + k_{RA})(k_5 + k_6 + k_{RF}) \qquad (1\text{-}25)$$

Similarly,

$$\phi_F = k_2 [A_1]/I_a = k_2/(k_2 + k_3 + k_4 + k_{RA}) \qquad (1\text{-}26)$$

where ϕ_P and ϕ_F are the quantum yields of phosphorescence and fluorescence, respectively. The intersystem crossing yield, ϕ_{ISC}, is defined as:-

$$\phi_{ISC} = k_4/(k_2 + k_3 + k_4 + k_{RA}) \qquad (1\text{-}27)$$

and therefore

$$\phi_P = \phi_{ISC}\, k_5/(k_5 + k_6 + k_{RF}) \qquad (1\text{-}28)$$

$$\phi_F = k_2 \phi_{ISC}/k_4 \qquad (1\text{-}29)$$

Unfortunately, this treatment cannot be extended to define equations for the measured luminescence lifetimes, which are measured using a high energy pulse of negligible duration and results in the following modification of equation (1-22), equation (1-21) remaining unchanged.

$$d[A_1]/dt = -(k_2 + k_3 + k_4 + k_{RA})\, [A_1] \qquad (1\text{-}30)$$

The two differential equations (1-19) and (1-30) can be solved completely, using the assumption $[F_1] = 0$ and $[A_1] = [A_1]_0$ at $t = 0$.

$$[F_1] = \{k_4 [A_1]_0/(k_A - k_F)\} \left[e^{-k_F t} - e^{-k_A t}\right] \qquad (1\text{-}31)$$

where $k_A = k_2 + k_3 + k_4 + k_{RA}$, $k_F = k_5 + k_6 + k_{RF}$. The second term of this equation represents the "grow-in" of the phosphorescence, whilst the first term gives its decay,

$$\text{and} \quad [A_1] = [A_1]_o \, e^{-k_A t} \tag{1-32}$$

Since $k_A >> k_F$, at $t > 1/k_A$, then equation (1-31) reduces to

$$F_1 = (k_4 [A_1]_o \, e^{-k_F t}/k_A = [F_1]_o \, e^{-k_F t} \tag{1-33}$$

where $[F_1]_o = \phi_{ISC}[A_1]_o$ = initial population of F_1. The lifetime of F_1 (τ_P) is defined in the expression $F_1 = [F_1]_o \, e^{-\tau_P t}$. By analogy

$$\tau_P = 1/k_F = 1/(k_5 + k_6 + k_{RF}) \tag{1-34}$$

For fluorescence, a similar treatment reveals

$$\tau_F = 1/k_A = 1/(k_2 + k_3 + k_4 + k_{RF}) \tag{1-35}$$

Combining equations (1-34) and (1-28) gives

$$\phi_P/\tau_P = \phi_{ISC} k_5 \tag{1-36}$$

This expression relates the experimental quantities, ϕ_P and τ_P to ϕ_{ISC}, assuming k_5 can be estimated from the $A_o \rightarrow F_1$ absorption band. Alternatively, excitation into the $A_o \rightarrow F_1$ band effectively makes $\phi_{ISC} = 1$, and the ratio ϕ_P/τ_P will yield k_5. Unfortunately, $A_o \rightarrow F_1$ is often very weak as it is a doubly forbidden transition, making this method impracticable, and introducing large errors in the computation of k_5 from its intensity.

The inclusion of back-ISC into the rate equations introduces some complications:-

$$d[F_1]/dt = -(k_5 + k_6 + k_{RF} + k_{-4})[F_1] + k_4 [A_1] \tag{1-37}$$

$$d[A_1]/dt = I_a - (k_2 + k_3 + k_4 + k_{RA})[A_1] + k_{-4}[F_1] \tag{1-38}$$

Applying the steady state approximation,

$$[F_1] = k_4 I_a/(k_T . k_S - k_{-4} k_4) \tag{1-39}$$

$$[A_1] = I_a k_T/(k_T . k_S - k_{-4} k_4) \tag{1-40}$$

where $k_T = k_5 + k_6 + k_{RF} + k_{-4}$, $k_S = k_2 + k_3 + k_4 + k_{RA}$ and ϕ_P and ϕ_F are now given by:-

$$\phi_P = k_5[F_1]/I_a = k_4k_5/(k_T.k_S - k_{-4}k_4) \quad (1\text{-}41)$$

$$\phi_F = k_2[A_1]/I_a = k_2k_T/(k_T.k_S - k_{-4}k_4) \quad (1\text{-}42)$$

The rate equations for flash techniques become:-

$$d[F_1]/dt = -k_T[F_1] + k_4[A_1] \quad (1\text{-}43)$$

$$d[A_1]/dt = -k_S[A_1] + k_{-4}[F_1] \quad (1\text{-}44)$$

Differentiation produces:-

$$d^2[F_1]/dt^2 = -k_T\, d[F_1]/dt + k_4\, d[A_1]/dt \quad (1\text{-}45)$$

$$d^2[A_1]/dt^2 = -k_S\, d[A_1]/dt + k_{-4}\, d[F_1]/dt \quad (1\text{-}46)$$

By substitution of equations (1-43) and (1-44) into (1-45) and (1-46), two simultaneous differential equations are obtained, which can be solved to give the following expressions:-

$$[F_1] = k_4[A_1]_o\ (e^{-\lambda_1 t} - e^{-\lambda_2 t})/(\lambda_2 - \lambda_1) \quad (1\text{-}47)$$

$$[A_1] = [A_1]_o\ ((\lambda_2 - k_S)\, e^{-\lambda_1 t} + (k_S - \lambda_1)\, e^{-\lambda_2 t})/(\lambda_2 - \lambda_1) \quad (1\text{-}48)$$

By analogy with equation (1-31).

$$\lambda_1 = (\tau_P)^{-1} = \tfrac{1}{2}\left[(k_T + k_S) - \sqrt{(k_S - k_T)^2 + 4k_4k_{-4}}\ \right] \quad (1\text{-}49)$$

Although this equation is quite sophisticated, there are two limiting conditions which may be considered:-[52]

(i) The steady state limit, which becomes valid after the exciting flash has decayed when $k_4 >> k_5 + k_6 + k_{RF}$ and is essentially the application of the steady state assumption to A_1, resulting in the inequality $4k_4k_{-4} << (k_S - k_T)^2$. In this case, equation (1-49) reduces to:-

$$(\tau_P)^{-1} \simeq k_T - (k_4k_{-4}/(k_S - k_T)) \simeq k_5 + k_6 + k_{RF} + (1 - \phi_{ISC})k_{-4} \quad (1\text{-}50)$$

Equation (1-36) is still valid, and ϕ_{ISC} is given by equation (1-27).

(ii) Thermal equilibration, which is only valid if Boltzmann equilibrium is attained in a time short compared with the lifetimes of the excited states, as implied by $k_4 >> k_2 + k_3$ and $k_{-4} >> k_5 + k_6$. Equation (1-49) now becomes:-

$$(\tau_P)^{-1} \sim (k_F + k_A K)/(1 + K) \qquad (1\text{-}51)$$

imilarly, $\phi_P = k_5/(k_F + k_A K)$ (1-52)

therefore $\phi_P/\tau_P = k_5/(1 + K)$ (1-53)

By comparison of equations (1-36) and (1-53), $(1 + K)^{-1}$ has become the equivalent of ϕ_{ISC}. Reminiscing:

$$\phi_{ISC} = k_4/(k_2 + k_3 + k_4 + k_{RA}) \qquad (1\text{-}27)$$

and

$$(1 + K)^{-1} = k_4/(k_{-4} + k_4) \qquad (1\text{-}54)$$

k_{-4} has replaced $(k_2 + k_3 + k_{RA})$ as the competitive process to ISC. This highlights the difference between the two treatments. The steady-state limit assumes k_{-4} to be an inefficient pathway, and occurs in competition with k_5 and k_6 after ISC is complete. The equilibrium limit assumes k_{-4} to be directly competitive with k_4 and precedes deactivation by k_5 and k_6.

k_{-4} and K both show a similar Boltzmann dependence on temperature, with K containing a degeneracy term:-

$$K = (g_{A1}/g_{F1})\, e^{-\Delta\epsilon/k_T} \qquad (1\text{-}55)$$

$$k_{-4} = k'_{-4}\, e^{-\Delta\epsilon/k_T} \qquad (1\text{-}56)$$

where g_{A1} and g_{F1} are the degeneracies of A_1 and F_1 respectively, and k'_{-4} is the limiting back-ISC rate. $\Delta\epsilon$ is the energy level gap between the two levels, k is the Boltzmann factor and T is the temperature.

The choice of limit used in practice is arbitrary as neither extreme is likely to be encountered individually over an entire temperature range used. A rough guide, however, can be obtained from considering equation (1-56); k_{-4} will only be significantly competitive with k_4 (= k'_{-4}) over an entire temperature range if $kT >> \Delta\varepsilon$. This implies that the equilibrium limit will only apply if the level splitting is small compared with kT at the lowest temperatures of the range studied. Crosby[53] has used the equilibrium limit to define the splittings of the emitting manifold $\left[Ru(bipy)_3\right]^{2+}$ between 0 and 100 K ($\Delta\varepsilon \leq 60$ cm^{-1}), whereas Van Houten and Watts[54] have used the steady state limit to cover the luminescence behaviour between 273 and 280 K ($\Delta\varepsilon \sim 3{,}500$ cm^{-1}), the finer splittings being indistinguishable.

Equation (1-50) can be represented in general terms as

$$(\tau_p)^{-1} \quad k_r + k_{nr} + Ae^{-E_A/RT} \qquad (1\text{-}57)$$

for the steady state limit, where k_r = radiative rate constant (k_5), k_{nr} = temperature insensitive radiationless rate constants ($k_6 + k_{RF}$) and $A = (1-\phi_{ISC})k_{-4}$, which represents the limiting back-ISC rate efficiency. This generalisation has assumed that the only temperature-activated pathway is back-ISC, which may well not be the case, when k_{RF} is important, as it must have an activation energy ascribed to it, otherwise spontaneous reaction would result on population of the state, the extent of which would be governed by the relative magnitude of k_{RF} as a degradative pathway. k_6 often contains environmentally dependent factors, as mentioned earlier, which may well be influenced by temperature. Perhaps the most concise representation of equation (1-50) is :-

$$(\tau_p)^{-1} = B + \Sigma A_i \, e^{-\Delta\varepsilon_i/k_T} \qquad (1\text{-}58)$$

where $B = \Sigma_i$ temperature-independent radiative and non-radiative pathways, and A_i = the limiting rate constant for the temperature-activated processes.

Crosby[51] has used a generalised form of equation (1-51) to include the case for a set of n thermally equilibrated levels:-

$$(\tau_p)^{-1} = \Sigma k_i g_i e^{-\Delta\varepsilon_i/kT} \; / \; \Sigma g_i \, e^{-\Delta\varepsilon_i/kT} \qquad (1\text{-}59)$$

where k_i is the sum of the radiative and non-radiative rate constants for the ith level of degeneracy, g_i, excluding back-intersystem crossing.

Temperature dependence (Arrhenius) measurements are only one method of obtaining information about non-radiative rates, and give no insight into individual temperature-independent pathways. The advent of picosecond lasers[1] enables measurements of the risetime of the luminescence to be made, and hence to gain information about ϕ_{ISC}. Low temperature studies[52] have the advantage of "freezing out" diffusional and, in some cases, temperature-dependent deactivation pathways, which simplifies equation (1-50):-

$$(\tau_p)^{-1} = k_5 + k_6 \qquad (1\text{-}60)$$

but makes correlation with the ambient temperature situation dubious.

Intermolecular energy transfer techniques, which have been discussed in the context of photochemistry, apply equally well to ϕ_p and τ_p, and can yield invaluable information about the emitting level and the intramolecular processes.

Information for individual systems can lead either to simplification or to further complications of the general model in specific cases. The model does, however, provide a reference from which individual systems can be discussed.

CHAPTER 2

SELECTED SYSTEMS

2-1 Chromium(III) - a 'light atom' ($3d^3$) System

Since the first report of luminescence from a chromium(III) complex in 1961,[55] the subject has received constant attention in attempts to relate this to the photoreactive state and the photochemical mechanism, which have been encouraged by the realisation that photochemistry may produce synthetic pathways to novel compounds. Unfortunately, the photochemical yields are somewhat less than unity ($\sim$ 0.1 to 0.2), and it is hoped that a better understanding of the competitive photophysical processes and the nature of the photoreactive state may lead to the design of complexes where photochemical pathways are more efficient.

Excitation is frequently employed in the visible and near ultra-violet regions where the typical chromium(III) absorption spectrum (Figure 3) displays d-d bands, which are reasonably well separated from the higher energy charge-transfer bands, due to the reluctance of chromium(III) to undergo either oxidation or reduction. Since SOC is minimal and need only be considered as a perturbing influence, allowing the spin forbidden d-d bands to borrow intensity from the higher energy (allowed) CT bands, spin and orbital labels can be considered meaningful for these systems.

According to LF theory, the promotion of an electron from a t_{2g} to an e_g orbital for the d^3 system in octahedral symmetry produces a set of doublet and quartet states as described earlier for Reinecke's salt. Whilst the state labels only apply to the octahedral case, complexes of lower symmetry are treated as distortions of the octahedral framework caused by the unequal LF strengths, so that the basic result of a set of quartet and doublet states still prevails. The independence of the luminescence yield on wavelength indicates that Crosby's rule[35] applies, and only the lowest lying states of different configurations need be

considered. Where small splittings occur, as in the case of ^2E and $^2T_1$ (Figure 2), the levels are assumed to be thermally equilibrated as the phosphorescence obeys first-order kinetics. The chromium(III) system, therefore, is analogous to the general model expounded earlier with A = quartet, F = doublet, and the same equations can be expected to apply. Both fluorescence and phosphorescence are shown to be possible, although in practice fluorescence is rarely observed.

2-1.1 The identification of the photoreactive state (doublet vs. quartet)

The main aim of any photophysical study is to evaluate the radiative and non-radiative rate constants and to predict the effect of environment on these parameters. Of particular interest is the nature and effect of environment on the photochemical pathway. The independence of photochemical yield on irradiation wavelength throughout a band suggests that a low-lying thermally equilibrated excited state is involved, and as the photochemical reactions are essentially photosubstitution, an LF reactive state is indicated. On first inspection, the doublet state seems the most likely candidate as this is the longer lived state, and gives the most opportunity for photoreaction to be competitive. Schläfer[56] estimates the quartet lifetime as $\sim 10^{-7}$s at room temperature, which would require a quartet photoreaction rate of at least 10^7 s^{-1} to be competitive with the non-radiative quartet rate, whereas the doublet lifetime (10^{-3} s) allows more opportunity for reaction. Even a rate of 10^5 s^{-1}, however, is much greater than that of the ground state, and Schläfer explains this anomaly as due to a negative LF contribution to the activation energy in the excited state. The doublet state was therefore believed to be responsible

for the photoaquation of both $[Cr(H_2O)_6]^{3+}$ and $[Cr(NH_3)_6]^{3+}$ upon d-d excitation by Plane and co-workers.[57,58] The doublet was thought of as the equivalent of a 'hot' ground state for which reaction is 100% efficient, and the photochemical yield to reflect the ISC yield. One consequence of this view would be a predicted enhancement of photochemical yield on irradiation directly into the (very weak) doublet absorption band.

Adamson, however, contests this view, as he found no evidence for such an enhancement throughout an extensive study of acido-pentammine complexes.[59-63] He noted a slight wavelength dependence for the photoaquation of Reinecke's salt,[62] suggesting the presence of a competitive photoreaction. This suspicion was confirmed by the isolation of two products for the photoaquation of $[Cr(NH_3)_5NCS]^{2+}$,[63] following ligand field band irradiation at ambient temperatures.

$$[Cr(NH_3)_5(NCS)]^{2+} + H_2O \longrightarrow \begin{cases} [Cr(NH_3)_5(H_2O)]^{3+} + NCS^- & \phi_{NCS^-} \\ [Cr(NH_3)_4(H_2O)(NCS)]^{2+} + NH_3 & \phi_{NH_3} \end{cases}$$

Aquation of NCS^- is the reaction observed thermally, whereas that of NH_3 is peculiar to photochemical excitation.

This illustrates that photochemistry is not just an accelerated thermal reaction as previously proposed. The wavelength dependence not only of the individual photochemical yields but also their ratio ϕ_{NH_3}/ϕ_{NCS^-} varies from 23:1 (on irradiation of the quartet band) to 8:1 (on direct irradiation of the doublet band). This implies that two different excited state precursors to photoreaction are involved, with the quartet being the major contributor, a view which has been stated[64] and expounded by Adamson.[20,65,66] His principal evidence is the existence of a large Stokes' shift for quartet fluorescence[13] which is indicative of a highly distorted state, suggesting

instability and hence reactivity. Irradiation into the quartet band produces a highly excited vibrational state which then undergoes relaxation in two successive stages.[20] The first stage involves vibrational relaxation (to the lowest quartet state), i.e. within the ground state framework of the complex, followed by the slower diffusion controlled process of geometrical rearrangement to the thermally equilibrated or 'thexi' state configuration. The latter process, he suggests, can be thought of as a series of 'solvent jumps',[44] the rate of which are controlled by the diffusion rate in the medium, and are therefore affected by solvent viscosity and temperature. During the period between jumps, the complex is in a quasi-rigid lattice with reasonably well-defined vibrational states, which change on each solvent jump. This process, therefore, can be viewed as a progression through a series of potential wells towards thermal equilibration.

At lower temperatures and high viscosity the solvent relaxation process will be inhibited and it is most likely that ISC, assumed to be temperature-independent, will be competitive, and population of the doublet state from the initially populated isogeometric Franck-Condon quartet state is feasible, giving rise to the possibility of phosphorescence. At elevated temperatures, thermal relaxation proceeds rapidly ($\sim$ 0.02 ns /solvent molecule)[44] and complete thermal equilibration followed by non-radiative relaxation from the 'thexi' state is envisaged. In this case, ISC to the doublet state, which is considered to occur in competition with this process, will be minimal, allowing for the possibility of fluorescence and photoreaction from the relaxed quartet state explaining Schläfer's[13] observation that the ratio of fluorescence to phosphorescence intensity from $[Cr(urea)_6]^{3+}$ increased on the warming of the glass from 90 K to 130 K, the fluorescence

Figure 7

Simplified energy-level scheme depicting the relaxation pathways of a chromium(III) complex excited into the first (Franck-Condon) quartet state (Q_{FC}); Q_O - quartet ground state; D_O - lowest (emitting) doublet state; Q_T - first 'thexi' quartet state. The ladders represent radiationless processes of either a vibronic or vibrational nature.

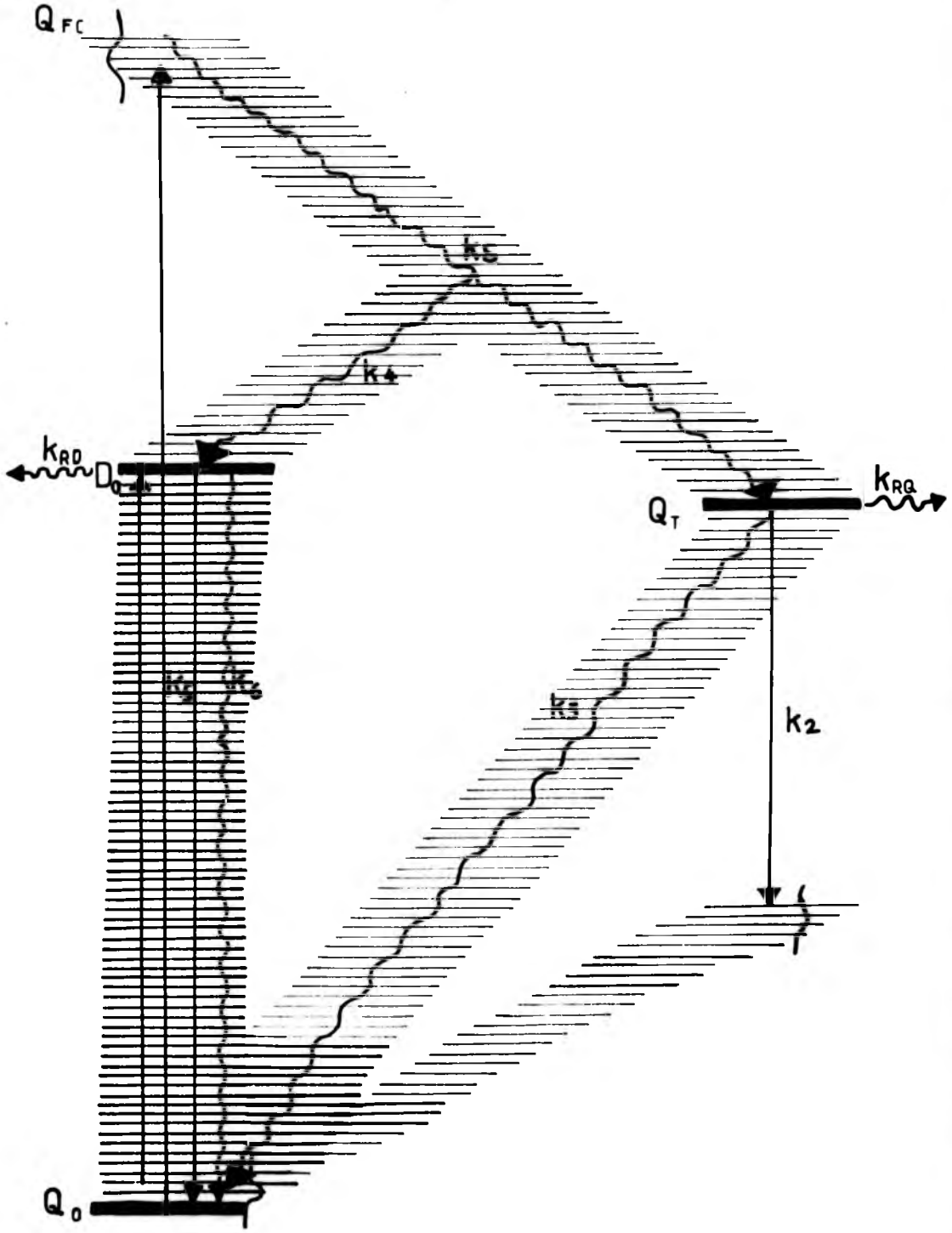
Q_{FC}
k_6
k_4
k_{RD}
D_{0-1}
k_{RQ}
Q_T
k_5
k_3
k_2
Q_0

disappearing on further warming. The situation is depicted in Figure 7, for which the parameters have the same meaning as in the general model described earlier. The various ladders represent radiationless processes of either a vibronic or vibrational nature. k_S represents the relaxation rate of the quartet state and includes both vibrational and solvent terms. This rationale, therefore, explains the temperature dependence of phosphorescence and fluorescence in terms of thermal quenching of ISC by the competitive solvent relaxation pathway. Such a model, while explaining the observed temperature dependence of fluorescence and phosphorescence noted by Schläfer[56] contradicts Schläfer's argument that fluorescence is caused by back-ISC to the quartet from the doublet state, a mode which also accounts for the thermal quenching of the phosphorescence.

The distortion of the quartet state invalidates attempts to estimate its intrinsic lifetime from absorption band measurements as used by Schläfer,[50] and Adamson predicts a lifetime of ca. 10^{-3} s [64] which allows ample time for competitive photoreaction. The quartet state is also thermodynamically favourable as it contains an even more negative LF contribution[67] to its activation energy than does the doublet state.

Support for the quartet state intermediate has come from many photoreaction quenching studies. The first conclusive report was on the quenching of the Reineckate ion (R) photoaquation by $[Cr(CN)_6]^{3-}$ at 208 K in methanol under LF irradiation.[68] It was found that while phosphorescence quenching of R obeyed Stern-Volmer kinetics and could be complete, the photoaquation yield approached a limiting value ($\sim 5 \times 10^{-3}$) which was 40% of the absolute yield. Having verified that $[Cr(CN)_6]^{3-}$ only quenches the doublet state of R,[69] Chen and Porter[68] reached the inescapable conclusion that the unquenchable part of the photoaquation occurs directly from the

quartet state, whereas the quenchable part occurs *via* the doublet state which they assumed returned to the (reactive) quartet state by back-ISC. Although no proof is given of the doublet state being inert, they postulate that the quenchable part of the photoreaction occurs *via* back-ISC to the quartet, *i.e.* the quartet state is effectively completely responsible for the photoreaction.

The report of room-temperature phosphorescence from a number of chromium(III) complexes[46] stimulated more quenching studies of this type, from which the same general conclusion was drawn that phosphorescence and photoreaction occur from different states.[70-72] These important points are nicely illustrated by two cases.

Wasgestian[73] examined the quenching of both the phosphorescence and photosolvation of $[Cr(CN)_6]^{3-}$ in dimethylformamide at 298 K under LF irradiation. The doublet and quartet splitting for this complex is large ($\sim$ 13,900 cm^{-1}) and the two states are not expected to be in good thermal communication. Five important points were illustrated by this study.

(i) The doublet lifetime is 6 ms, yet photochemistry still occurs, suggesting that there is no quenching of the doublet.

(ii) The phosphorescence is strongly quenched by water, whereas the photosolvation is only slightly affected in water ($\phi \sim 0.12$) compared to DMF ($\phi \sim 0.08$).

(iii) The phosphorescence is efficiently quenched by molecular oxygen (90%) but the photoreaction is unaffected.

(iv) The phosphorescence and photoaquation yields show different temperature dependences, a feature also noted by Adamson for Reineckate ion.[62]

(v) Anthracene photosensitisation results only in sensitised phosphorescence (*i.e.* not in any photosolvation).

In a separate study, Balzani[31] has studied the photosensitised aquation of $[Cr(CN)_6]^{3-}$, using a series of energy transfer donors for which transfer to both doublet and quartet are allowed, finding that photoreaction occurs only for donors of energy above $\sim$ 22,000 cm^{-1}, whilst all the donors are more energetic than the ^2E state (13,000 cm^{-1}).

There seems little doubt, therefore, that the quartet state is involved as a precursor to photoreaction, but the proposal that part of the reaction is by back-ISC from the doublet state is less certain. A number of temperature studies on chromium(III) phosphorescence have cited this pathway, but these have been performed mainly in crystalline samples at ambient temperatures,[74] or at low temperatures[75-78] where diffusional modes, such as photoreaction are lost, or over a restricted temperature range in solution.[46] The results have either been qualitative[84,78] or when quantitative, no rigorous curve-fitting procedure has been used for determination of the activation energy. In all cases, the observed activation energy has been correlated to the quartet-doublet splitting obtained from the absorption and emission spectra, and no account of the distorted quartet position has been taken which will reduce this splitting. It is, therefore, uncertain that back-ISC is the major temperature activated pathway from the doublet state under photochemical conditions, although it may well be the case when this pathway is 'frozen out' by using crystalline samples at low temperature. If back-ISC does contribute to the photochemical yield, then one would expect a 'delayed' reaction from this route, but with the same products as the prompt reaction, assuming both to occur from the lowest 'thexi' state. This simple model predicts a single product (or group of products) for a given complex under any irradiation wavelength. However, there are several cases where two clearly defined pathways involving different

In a separate study, Balzani[31] has studied the photosensitised aquation of $[Cr(CN)_6]^{3-}$, using a series of energy transfer donors for which transfer to both doublet and quartet are allowed, finding that photoreaction occurs only for donors of energy above $\sim$ 22,000 cm^{-1}, whilst all the donors are more energetic than the ^2E state (13,000 cm^{-1}).

There seems little doubt, therefore, that the quartet state is involved as a precursor to photoreaction, but the proposal that part of the reaction is by back-ISC from the doublet state is less certain. A number of temperature studies on chromium(III) phosphorescence have cited this pathway, but these have been performed mainly in crystalline samples at ambient temperatures,[74] or at low temperatures[75-78] where diffusional modes, such as photoreaction are lost, or over a restricted temperature range in solution.[46] The results have either been qualitative[84,78] or when quantitative, no rigorous curve-fitting procedure has been used for determination of the activation energy. In all cases, the observed activation energy has been correlated to the quartet-doublet splitting obtained from the absorption and emission spectra, and no account of the distorted quartet position has been taken which will reduce this splitting. It is, therefore, uncertain that back-ISC is the major temperature activated pathway from the doublet state under photochemical conditions, although it may well be the case when this pathway is 'frozen out' by using crystalline samples at low temperature. If back-ISC does contribute to the photochemical yield, then one would expect a 'delayed' reaction from this route, but with the same products as the prompt reaction, assuming both to occur from the lowest 'thexi' state. This simple model predicts a single product (or group of products) for a given complex under any irradiation wavelength. However, there are several cases where two clearly defined pathways involving different

states are present. Examples of these are (i) the possibility of reaction from two quartet states, produced by the splitting of the $^4T_2$ state under lower symmetry, which has been postulated for complexes of low symmetry such as $[Cr(H_2O)_5CN]^{2+}$ [79] and $[Cr(en)_2NH_3Cl]^{2+}$ [80] and (ii) the participation of a higher CT ligand-localised state which has been demonstrated for (trans-$[Cr(tfpd)_3]$ [81] by the presence of a photodecomposition mechanism at 254 nm irradiation. In the case of $[Cr(bipy)_3]^{3+}$, [82] all the photoreaction is thought to occur from the doublet state, on the basis that 97% of the reaction is quenched in parallel with the phosphorescence and back-ISC (E_a > 80 kJ mol^{-1}) would have to occur with unitary efficiency in order for this reaction to be accounted for by the quartet state.

Definite evidence for the direct photoreaction of the doublet state has also been provided by Adamson[83] for $[Cr(en)_3]^{3+}$ by monitoring of the risetime of the photochemical transient due to a 530 nm, 20 ns pulse from a Nd laser which results in a change of the optical density of a monitoring beam. The results show a prompt increase (< 10 ns) attributed to direct reaction from Q, the 'thexi' state (ϕ_Q = 0.15), and a slower increase which grows in with the lifetime of the emission and shows the same temperature dependence which is assigned to direct reaction from the doublet state (ϕ_D = 0.85).

2-1.2 The nature and efficiency of ISC from the quartet state

There seems little doubt that both the quartet and doublet states can give rise to photochemistry under LF irradiation. Intuitively, the photoreaction yield from the doublet state will be a reflection of the population of this state, and hence of the ISC efficiency, which will be controlled by the ISC rate.

According to Adamson,[44] this process occurs in competition with solvent relaxation as mentioned earlier, and its temperature dependence, due to the inhibition of the solvent relaxation rate at low temperatures, should be measurable. Equation (1-36) gives $\phi_P/\tau_P = \phi_{ISC}\, k_5$; however, the measurement of ϕ_P and τ_P under the same conditions would be tedious as well as complicated from an instrumental viewpoint. The problem can be alleviated by measurement of the initial emission intensity, I_o, by extrapolation of the time dependent emission decay curve to zero time. Since I_o is proportional to $\phi_{ISC}\, k_5$, the temperature dependence of I_o reflects that of $\phi_{ISC}\, k_5$. This procedure has been used by two sets of workers with conflicting results:-

(i) Adamson[84] has produced activation energies for the range 273 K to 303 K which he attributes to ϕ_{ISC}, assuming k_5 to be constant. The values range from 18.8 kJ mol^{-1} for $[Cr(en)_3]^{3+}$ in H_2O to -9.6 kJ mol^{-1} for Reinecke's salt in H_2O. He explains these results as due to individual solvation effects. In the case of Reineckate ion, solvation does not occur in a specific manner and the negative activation energy reflects the enhancement of ISC with temperature. The positive activation energy shown by $[Cr(en)_3]^{3+}$ is suggested to reflect a highly structured solvation shell which has a complicated temperature dependence.

(ii) Castelli and Forster[85] have measured I_o over a much wider range (120-300 K) for $[Cr(CN)_6]^{3-}$, $[Cr(en)_3]^{3+}$ and $[Cr(acac)_3]$ in crystalline and noncrystalline media. Contrary to Adamson,[84] they find no temperature dependence for $[Cr(en)_3]^{3+}$ in an alcohol-water medium over the entire temperature range which includes T_g, a result which suggests that ISC occurs either before thermal relaxation or after, but not in direct competition with thermal relaxation. The results for $[Cr(CN)_6]^{3-}$ are complicated by a

temperature dependence of k_5, due to vibronic coupling of the doublet state with the ground state. However, an abrupt change in I_o at 230 K in an alcohol-water solution may be due to solvent relaxation.

It therefore seems that the question of whether ISC is prompt,or occurs in competition with or after solvent relaxation, is far from being answered satisfactorily. Kane-Maguire[86,87] has suggested that ISC occurs by successful competition with thermal equilibration, but considers that this latter process is not solvent restricted, i.e. is prompt. This conclusion is reached from studying the quenching of the photoracemisation of (+)D-$[Cr(en)_3]^{3+}$ in aqueous solution at 298 K by OH^-, which acts as a specific doublet quencher, and has been investigated under LF irradiation. He observed a reduction in the percentage of reaction quenched from 57% between 436 and 495 nm to 38% at 514.5 nm, the total photochemical yield remaining constant at 0.4. The results are explained in terms of a crossover point (ca. 500 nm) between the doublet and quartet states, above which (436 to 495 nm) the doublet quenching (and therefore population) increases, suggesting ISC to be competitive with thermal equilibration as the doublet population would be independent of excitation wavelength if ISC occurred after thermal equilibration, assuming the quartet to be populated at all excitation wavelengths. If solvent relaxation were a competitive pathway, then the activation energy for the phosphorescence yield (population of the doublet state) should be minimal below the crossover point,and rise above the crossover point where ISC and solvent relaxation are competitive. He finds that the activation energy is almost constant ($\sim$ 43.5 kJ mol^{-1}) at 460 and 515 nm, and suggests that an alternative mechanism for successful competition of ISC must be sought. Kane-Maguire[87]

proposes a model based on SOC in which the doublet and quartet states are combined to give a single potential energy surface with two minima through which ISC can occur rapidly at vibrational relaxation rates ($\sim 10^{12}$ s^{-1}). This explanation seems dubious as SOC is not expected to be particularly effective for a 3d complex. Adamson[88] points out that the activation energies may well not be a reflection of the ISC efficiency since the phosphorescence yield will also be affected by competitive relaxation pathways from the doublet state, and he suggests that the activation energies reflect the barrier to chemical reaction from the doublet rather than the ISC rate.

Castelli[89] has repeated Kane-Maguire's[86] experiment, using the I_o method to determine the phosphorescence yield variation with wavelength, at ambient temperature. He reports the same findings, but on plotting the ratio of I_o for $[Cr(en)_3]^{3+}$ in 80% glycerol-water (v/v) and water against excitation wavelength, he finds that the ratio increases with increasing excitation wavelength, and by comparison with the dependence of I_o in H_2O suggests that, as the viscosity is increased, the change in I_o with wavelength is decreased, a result which, in contradiction to Kane-Maguire, suggests a solvent dependence of ϕ_{ISC}.

Measurements of the rate of ISC by monitoring the risetime of phosphorescence have been undertaken by a number of groups[85,90,91] but only limiting values ($\sim 10^{11}$ s^{-1}) could be obtained in all but two cases,[92,1] one of which has been challenged.[91] Picosecond studies by Pyke and Windsor[1] have given the risetime of the transient absorbance of trans-$[Cr(en)_2(NCS)_2]^+$ (16 ± 3 ps), Reinecke's salt (22 ± 2 ps) and $[Cr(NCS)_6]^{3-}$ (16 ± 2 ps) in H_2O. The insensitivity of the risetime to the species studied is indicative of prompt ISC from the initially populated Franck-Condon state,

since ISC from the relaxed state may be expected to depend on the separation of the two states which will be a function of the complex. The observation of a slight solvent deuterium effect on the risetime may hint at competitive solvent relaxation. The rate at which ISC occurs is indicative of a vibrational relaxation rate rather than ISC, and suggests intimate contact between the doublet and quartet states, giving support to Kane-Maguire's[87] model. If the ISC rate does occur from the Franck-Condon state, then no inference of the 'thexi' state lifetime is possible. The 'thexi' model would then predict a longer fluorescence lifetime due to a reduction in ISC, than that indicated from the measured ISC rate, assuming ISC to be the main deactivation pathway.

Unfortunately, fluorescence is rare amongst chromium(III) complexes, as the quartet usually lies above the doublet state. However, when the quartet state is lower, fluorescence has been observed, predominantly at low temperatures, although two cases of room temperature fluorescence have been reported.[93,94] The first of these was for $[Cr(bipy)_3]^{3+}$ in dimethylsulphoxide[193] and has been questioned by later reports[82,95] which attribute it to an unknown luminescent impurity. The room temperature luminescence of trans-$[Cr(en)_2F_2]^{+}$ [94] at 785 nm in water at 298 K appears to be genuine fluorescence, as it shows an appreciable Stokes' shift and mirrors the quartet absorption band. Although the result can be regarded as preliminary and no lifetime has yet been measured, it promises to provide important information about the quartet state.

The measurement of the fluorescence lifetime of $[Cr(urea)_6]^{3+}$ at low temperature has been hindered by the presence of multi-exponential decays. Dingle[96] suggested that the decay was composed of two parts due to prompt and delayed fluorescence with

lifetimes of 50 μs and ∿ 350 μs respectively at < 25 K. Forster[97] has shown that the multiexponential decay is due to emission from multiple sites in the rigid matrix as indicated by the disappearance of non-exponentiality on melting the solution. The lifetimes of the phosphorescence and fluorescence in solution (H_2O/MeOH/ethylene glycol) at 180 K are identical (25 ns) and the fluorescence is assigned as 'delayed'. The prompt fluorescence lifetime was estimated as < 10^{-9} s but, to date, no accurate fluorescence lifetime values exist. Present indications, therefore, suggest that ISC occurs before complete thermal equilibration of the quartet state, but the role of solvent relaxation is ambiguous and the situation is complicated by (i) a lack of direct photophysical measurements, due to the absence of fluorescence date and (ii) an incomplete understanding of the detailed mechanism of the relaxation process.

The actual mechanism of the population of the 'thexi' quartet and doublet states may be uncertain, but measurements of the ISC efficiency, ϕ_{ISC}, can indicate the significance of the process and give the initial relative populations of the doublet and quartet states. As mentioned earlier, $\phi_{ISC}\ k_5$ can be found by measuring, I_o, the initial emission intensity, but this method, as with the determination of ϕ_P/τ_P by conventional means, requires the calculation of k_5 from the weak doublet band in the absorption spectrum and can introduce large errors. One other method is the selective quenching of the the doublet state as mentioned previously. By assuming the energy transfer efficiency is unity and the quenchable percentage of the photoreaction is a direct indication of the ISC efficiency, Bolletta et al.[98] have estimated the ISC efficiency for a number of chromium(III) complexes, ranging from $[Cr(bipy)_3]^{3+}$ (100%) to $[Cr(phen)_3]^{3+}$ (20%). These results, however, are also prone to uncertainty in cases where the overall

photochemical yield is low, as any error in measuring the quenched yield will become magnified on taking the ratio of quenched to unquenched yields. Similarly, the unquenched fraction indicates the population of the quartet state.

2-1.3 Non-radiative deactivation of the 'thexi' quartet state

The initial population of the quartet and doublet states are an important consideration, but equally important are the deactivation pathways open to a molecule when excited to either of these states and the nature of these states.

The notable lack of fluorescence from the quartet state makes direct observation of this state difficult, and hence little is known about the nature of the direct non-radiative pathways back to the ground state, k_3, other than can be inferred from the two observable radiationless routes of ISC and photoreaction. It is assumed that k_3 accounts for any energy not removed by either of these last two processes. Forster[52] has suggested that k_3 may be sensitive to environment, as he notes a hundred-fold decrease in the phosphorescence quantum yield when the lowest quartet level is irradiated for a solution of $[Cr(3\text{-bromoacac})_3]$ in $[Al(3\text{-bromoacac})_3]$ compared with irradiation into higher quartet states. He suggests that this may be due to successful competition of k_3 with ISC for this state. This result, which is not found for the same complex in glassy solutions, may suggest an environmental dependence of k_3. However, the result can be viewed with scepticism as it is assumed that the quartet level is given by the quartet absorption band of the complex which neglects distortion of the quartet state.

The problem of defining the position of the 'thexi' quartet state when no fluorescence occurs is one of considerable importance in discussing the photophysics of this state. Adamson[20] has provided a formula for the position of the 'thexi' state, $E(L^o)$, based

on correlations of the emission maxima for fluorescent complexes with the position of the quartet absorption band.

$$E(L^{O}) = 1.11\ \bar{\nu}_{0.05} - 0.88 \qquad (2\text{-}1)$$

where $\bar{\nu}_{0.05}$ is the frequency at which the quartet absorption band is equal to 5% of its maximum absorbance on the red side of the spectrum. Further, by correlation of the gap between the quartet and doublet, E(L) - E(D), with the luminescence observed, he suggests a criterion by which the luminescence can be predicted.

$E(L) - E(D) < -470\ cm^{-1}$ fluorescence only

$-140 < E(L) - E(D) < 760\ cm^{-1}$ both types of emission

$1{,}000\ cm^{-1} < E(L) - E(D)$ phosphorescence only

2-1.4 Photochemical implications of the 'thexi' quartet state

While direct observations of the excited quartet state are rare, there is no doubt that this state suffers considerable distortion, which is expected to be reflected in the rates and mechanism of the deactivation processes occurring from this state, particularly the photoreactive process.

The first attempt to predict the nature of this distortion resulted in Adamson's two semi-empirical rules[64] which are applicable to non-octahedral complexes.

(1) Consider the ligands to lie in pairs at the ends of three mutually perpendicular axes. That axis having the weakest average crystal field will be the one labilised, and the total quantum yield will be about that for an Oh complex of the same average field.

(2) If the labilised axis contains two different ligands, then the ligand of greater field strength preferentially aquates. This may be due to a type of trans effect.

The introduction of these rules resulted in numerous photochemical studies[99] to elucidate their correctness, and the mechanistic and the theoretical implications.

The underlying implication of stereoretentive reaction was shown by Balzani et al.[100] to be false, as shown by the photoaquation reaction:-

$$[Cr(NH_3)_5Cl]^{2+} + H_2O \longrightarrow$$

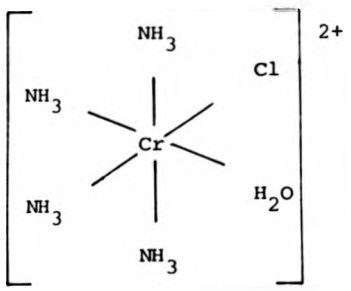

cis

This result is rather ambiguous since it suggests either that the photoreaction involves stereochemical change or that Adamson's rules[64] are incorrect in predicting the leaving group. In order to clarify the situation, Kirk[101] studied trans-$[Cr(en)_2Cl_2]^+$ which allows a greater insight since the Cl-Cl axis is the only one likely to be labilised.

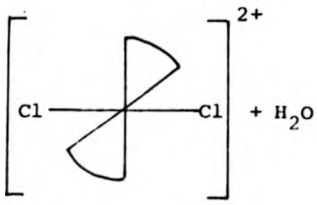

trans

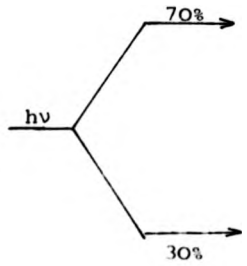

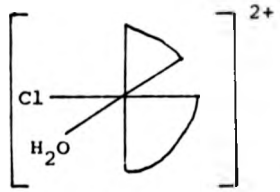

cis

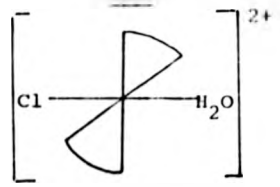

trans

As can be seen, the major product is caused by stereochemical change, a result which he finds also for similar $[CrA_4X_2]^+$-type complexes. He notes[19] that Adamson's rules[64] only predict the nature of the leaving group and suggests that the rules can be presented in a modified form as:-

(1) The reaction mode of a mixed ligand complex can be predicted as preferential substitution of the strong σ-donating ligand on the axis of overall weakest σ-donating strength.

(2) The entering ligand will occupy a position <u>trans</u> to the leaving ligand.

(3) If <u>trans</u> entry is difficult, then the photochemical yield is low.

The replacement of ligand field strength by σ-donating strength is to incorporate the results of Pyke and Linck for $[Cr(en)_2F_2]^+$ [102]

$$[Cr(en)_2F_2]^+ \longrightarrow [Cr(enH)(en)F_2]^{2+}$$

a result which is explained by the strong π-bonding nature of the fluorine, which will be stabilised by the transition from the π non-bonding ground state to the σ* quartet state.

These rules imply that stereochemical change is a necessary prerequisite for photoreaction and only one exception has been noted.[103]

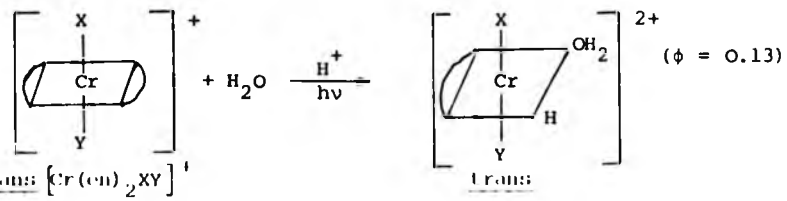

<u>trans</u> $[Cr(en)_2XY]^+$ <u>trans</u>

which has since been disputed.[104] The necessity for stereochemical change has been demonstrated by the introduction of bulky ligands, such as cyclam, which will hinder stereomobility[105] and lead to a severe reduction in reaction and in the specific case of <u>trans</u>-$[Cr(cyclam)Cl_2]^+$,[106] no reaction was found. This last result

suggests that the primary step is not merely dissociative but may either be associative or that the dissociative mechanism is concerted, with collapse into another geometry. The latter case would, however, be expected to yield a mixture of isomers rather than a specific cis-product. The possible intermediates are depicted below.[19]

Dissociative mechanism:-

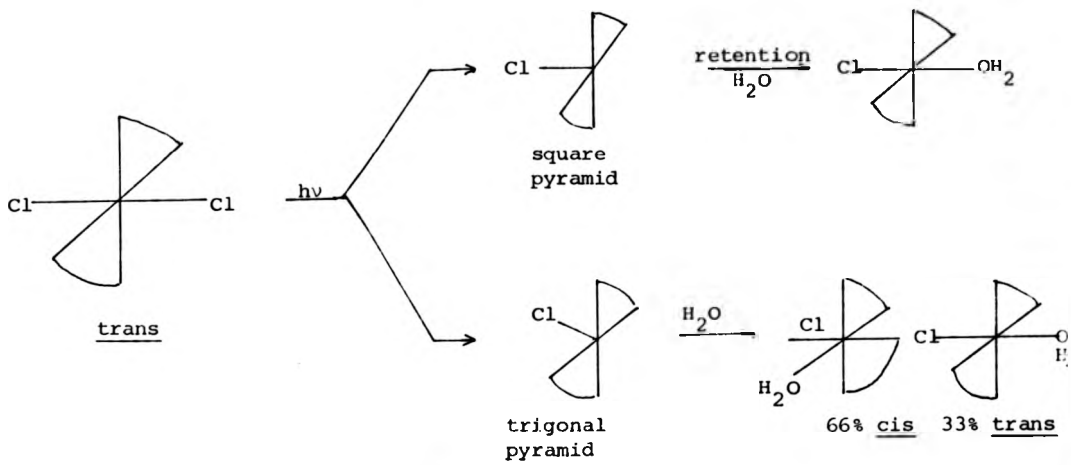

Associative mechanism:-

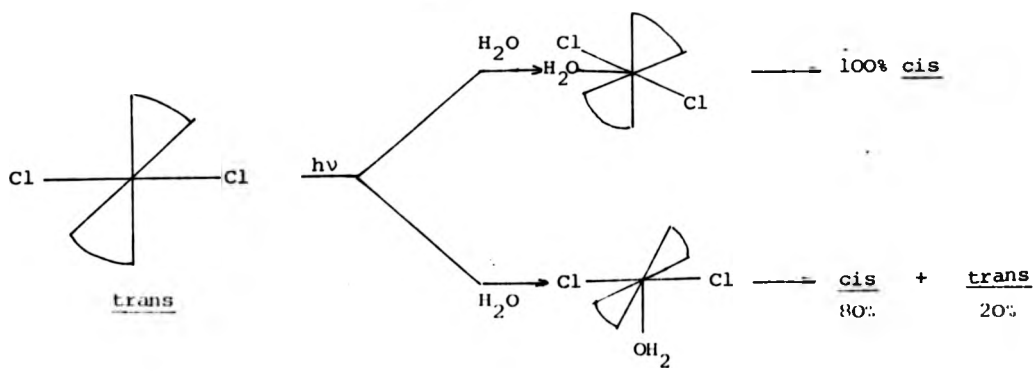

From these possibilities, Kirk[19] suggests that an associative mechanism involving trans attack is most likely, although there is perhaps a need for more experimental data in order to determine whether the stereospecificity is due to the distortion of the quartet state or whether it simply reflects the thermodynamic stability of the cis- over the trans-isomer.

A number of theoretical models have been proposed in order to predict the photoproducts of the reaction,[21-23] and in some cases the actual photochemical yield[21] and the stereochemistry of the reaction.[107] All the models use the basic concept that the one electron promotion from the ground state of a chromium(III) complex involves a change from a π to a σ^* orbital, but differ in their calculation of the effects of this transition, mainly using LF theory. Zink[21] considers the ordering of the d orbitals for the relevant complex and predicts the effect on π and σ bonding by the redistribution of electronic charge caused by the transition. He suggests that in the cases where π-bonding is significant, then the 'π-strengthening' effect of the transition may well overcome the 'σ^* antibonding' effect, as in the case of $\left[Cr(en)_2F_2\right]^+$ mentioned earlier. Other reports, however, consider that σ^* effects are the over-riding factor in all cases.[103,108] Van Quickenbourne and Ceulemans[23] have developed a treatment which considers the contribution of such ligands to the orbital energy, and assumes that bonding interactions cause the ligand basis orbitals to be stabilised to the same extent as the metal orbitals are destabilised. This model has been developed[107] to predict the stereochemistry in terms of a three-step dissociative model, (i) loss of ligand,(ii) stereochemical change, (iii) attack by the entering molecule. This model has been questioned[109,110] using the cases of <u>trans</u>-$\left[Cr(en)_2(NH_3)F\right]^{2+}$, $\left[Cr(NH_3)_5F\right]^{2+}$, <u>trans</u>-$\left[Cr(en)_2F_2\right]^{2+}$ for which aquation of the group <u>trans</u> to F^- occurs in apparent contradiction to the LF model which would predict aquation of an ammine on the equatorial axis. Van Quickenbourne and Ceulemans,[107] however, point out that this case can be explained in terms of their treatment. The electronic excitation is localised over the x, y and z planes, and the metal-ligand bond weakening is proportional to the spectrochemical strength of the interaction.

For an axial (xy) ligand, this amount so $1/4(10D_q(L))$, but $1/8(10D_q(L))$ for an equatorial (z) ligand. Since $D_q(NH_3) > D_q(F)$, this model does correctly predict the leaving group. While their model has explained this apparent anomaly, they point out that these models only function if the basic assumptions made are correct. These are:-

(1) The photoreaction occurs predominantly from the lowest quartet state and only the major product can be predicted.

(2) A dissociative mechanism is assumed.

Although this model covers most of the cases so far investigated, it remains far from complete but is becoming more sophisticated as apparent exceptions are incorporated into it. Adamson,[44] however, considers that LF theory may be totally inappropriate in treating the distorted 'thexi' state, since LF theory makes the approximation of treating the ground and excited states as having the same symmetry and experiencing the same intensity of LF. It has been shown that the quartet state, however, is considerably distorted, and may even exhibit a totally different symmetry, which would make an LF treatment inappropriate. Even so, the LF models have been shown to predict correctly the products of photoreaction in many cases, and there is a need for more work to unify further the situation.

2-1.5 Properties and deactivation modes of the doublet state

In contrast to the quartet state, the doublet state has been thoroughly investigated through its phosphorescence.

The high resolution phosphorescence spectrum has been investigated in either single crystals or glasses at low temperatures to reveal fine structure which can be attributed to the vibrational modes of the ground state which deactivate the doublet state. The study of these modes also gives an insight into

M-L vibrations which are often i.r. and Raman inactive, and provide a discrimination between internal and lattice vibrations of complex ions.[111]

The small Stokes' shift implies the doublet state has very similar geometry to the ground state complex, although in some cases the intense O-O band resolved in the phosphorescence spectrum at low temperatures suggests distortion from a pure geometry,[36] which may be due to a type of Jahn-Teller effect, and indicates possible strong mixing of the quartet and doublet states. This has been demonstrated in the case of a series of chromium-sulphur chelates[112] which show a broad diffuse emission spectrum even at 4 K with a Stokes' shift of $\sim$ 500 cm^{-1}, and is attributed to SOC. This conclusion is verified by the similarity of the lifetimes of these complexes ($\sim$ 200 to 300 μs) with those of other Cr(III) complexes at 77 K, suggesting both the radiative and non-radiative constants of the doublet state show a ξ^2 dependence. While the doublet state is strongly coupled to the quartet state, it is expected to be only weakly coupled to the ground state so that only high frequency deactivational modes will be important in the latter case. It is important, however, to note that chemical reaction from the doublet state will also exhibit strong coupling.

A useful probe into the coupling strength comes from measurements of the deuteration effect of ligand and solvent on lifetime (τ) and quantum yield (ϕ). Large deuterium effects have been reported for (τ) $\left[Cr(ND_3)_6\right]^{3+}/\left[Cr(NH_3)_6\right]^{3+}$ ($\sim$ 20),[113] and (ϕ) $\left[Cr(D_2O)_6\right]^{3+}/\left[Cr(H_2O)_6\right]^{3+}$ ($\sim$ 6)[114] at 77 K in crystalline media, but a negligible deuteration effect (for both ligand or solvent) for several chromium ammines[115] is found at room temperature.

The inference is that,at low temperatures, the doublet state undergoes direct deactivation to the ground state, while at ambient temperatures there is an over-riding presence of a strongly coupled temperature-activated process. This process, which may be either back-ISC or photoreaction, is expected to be the major deactivation route at ambient temperatures from the large thermal effect on lifetime and quantum yield ($\sim$ 100) on going from 77 to 293 K.

In cases where a low-temperature limiting lifetime is reached, this can be used to estimate the limiting rate of ISC to the ground state, k_6^o, as from equation (1-60).

$$(\tau_P^o)^{-1} = k_5 + k_6^o \qquad (2-2)$$

k_5 can be estimated from the doublet absorption band, k_6^o is found to be a function of the individual system[52] and cannot be predicted from any general model: it is found to be sensitive to environment in the cases $[Cr(D_2O)_6]^{3+}$, $[Cr(CN)_6]^{3-}$ and insensitive for others, e.g. $[Cr(acac)_3]$.[52] k_6^o has also been found to be sensitive to ligand substitution in the case of β-diketonate derivatives,[116-118] and is attributed to the π-bonding in these systems whereby the d-electron delocalisation causes k_6^o to increase. Finally, k_6^o has been shown to be dependent upon the nature of the anion for $[Cr(urea)_6]^{3+}$ crystals.[78]

k_6^o is evidently unpredictable, and can be expected to become more intractable as the temperature is raised and diffusional processes come into play.

The temperature dependences of the phosphorescence lifetime and quantum yield have been subjected to a number of studies over varying temperature ranges, as mentioned earlier, and the accumulated data treated by different methods, although all illustrate a clear dependence of the temperature-activated process on environment. Targos and Forster[77] investigated the temperature

dependence of a series of substituted $[Cr(acac)_3]$ complexes in different environments over the temperature range 83 to 223 K, and analysed the temperature profile in terms of the equation:-

$$\tau^{-1} = \tau_o^{-1} + S_1 \exp(-E_1/RT) + S_2 \exp(-E_2/RT) \qquad (2\text{-}3)$$

where τ_o is the low temperature, limiting lifetime, E_n are the activation energies and S_n are the frequency factors for the two temperature-activated processes. Typical values are $S_1 = 10^3\ s^{-1}$, $S_2 = 10^{13}\ s^{-1}$, $E_1 = 3$ kJ mol^{-1} and $E_2 = 30$ kJ mol^{-1}, and τ_o = 450 μs. A similar treatment for the quantum yield gave similar values for the parameters showing the two phenomena to be quenched in parallel and indicating no change in ϕ_{ISC} or k_5. They attributed the low-energy pathway to k_6 and the higher energy rate to back-ISC, k_{-4}. In a later report, dealing with the temperature dependence of chromium(III) phosphorescence in crystalline hosts over the range 80 to 300 K, Forster[76] suggests only one temperature-activated process is dominant, namely k_{-4}. Although the activation energies are smaller than the quartet-doublet gap by a factor of between 2 and 5 for the set of crystals, they do follow the same overall trend of the splitting. Perhaps what is more significant is that the difference between the splitting and the activation energy is approximately constant ($\sim$ 2,500 cm^{-1}) for all cases, and may be indicative of the quartet state distortion, which would make the assumption of back-ISC feasible. A point in favour of assignment to k_{-4} is the fact that the largest activation energy is $\sim$ 32 kJ mol^{-1} for $Cr^{3+}.KAl(SO_4)_2.12D_2O$, a value which is of the same order as that quoted by Adamson[84] for the activation barrier to photochemistry for the doublet state in solution where one would expect photochemistry to become easier. The trend of activation energy and quartet-doublet splitting has also been noted by other workers[74,78] on a qualitative basis.

The activation data obtained from temperature studies of chromium(III) complexes in solution are less precise, due to the restricted temperature range (273 to 373 K) under which the experiments have generally been performed.[46,88,84,119] A number of points do, however, emerge:-

(i) The activation energies for a series of ammine complexes do not follow the same trend as the quartet-doublet splitting,[46] and the difference between the two varies from 4,000 to 8,000 cm^{-1}.

(ii) There is a definite solvent-dependence for the activation energy. In the case of Reinecke's salt,[88] the activation energies vary from 40 to 55 kJ mol^{-1} and obey a Barclay-Butler plot.

(iii) The solvent-dependence of the measured lifetime does not reflect the solvent dependence of the activation energy,[84,88,119] suggesting that other factors are involved.

(iv) In the case of $[Cr(CN)_6]^{3-}$ which has a very large doublet-quartet splitting so that back-ISC may be discounted, a temperature dependence is still found with an activation energy of between 25 and 40 kJ mol^{-1}, depending upon solvent.[119] This is considered to be due to activation of a combination of CN stretching with either Cr-C-N bonding or Cr-C stretching vibrational modes.

While the exact values of these activation energies are open to error, as mentioned earlier, the trends seem to be genuine. The obvious point is that the activation energy of the high-temperature route is between 30 and 60 kJ mol^{-1} for most cases, regardless of environment or nature of the complex, and this is always much lower than the quartet-doublet splitting (> 2,000 cm^{-1}). Therefore, either all the temperature-activated processes have similar activation energies or only one temperature-activated mechanism is dominant. The latter case is shown to be true at high temperatures for individual complexes by the correlation of the activation data

in different solvents to a Barclay-Butler plot[88] of ln A *vs.* E_A, where A is the frequency factor and E_A is the activation energy. This plot relates the increased entropy (ln A) to bond-weakening in the transition state (E_A), giving closer vibrational spacing. The linear relationship for the data indicates the presence of only one mechanism.

There are three possibilities for this 'universal' mechanism: (i) back-ISC, k_{-4}, (ii) non-radiative decay to the ground state, k_6, and (iii) photochemical reaction, k_{RD}. k_6 has been invoked to explain the results for $[Cr(CN)_6]^{3-}$,[185] but a strong coupling model to the ground state was involved, which implies that the doublet state is distorted. As k_{-4} is unlikely for this complex, perhaps a more likely route might be k_{RD}, for which a bond-breaking and -making mechanism could incorporate the Cr-C-N vibrational mode.

k_{-4} has been assigned as the temperature-activated term in most cases,[76,80,46] but while the pathway seems possible at low temperatures, the lack of correlation of the activation energy with the quartet-doublet splitting for fluid solutions, which shows no solvent dependence in the case of Reinecke's salt[88] suggests that k_{RD} may be the dominant pathway, the activation energy being about half of the thermal reaction activation energy for this particular case. This suggestion has been extended to include other chromium(III) ammines,[84] and Adamson has proposed two semi-empirical rules to predict the room-temperature lifetime of chromium(III) complexes, assuming k_{RD} to be the dominant process controlling the lifetime at room temperatures.

(1) For complexes with six equivalent Cr-L bonds, the emission lifetime in room-temperature fluid solution decreases with decreasing ligand field strength.

(2) If two different kinds of ligands are co-ordinated, the emission lifetime will be relatively short (<1 μs) if that ligand which is preferentially substituted in the thermal reaction lies on the weak field axis of the complex.

While these rules appear to be correct for the set of ammine complexes studied, it remains to be seen whether they will be correct on a more general basis. In particular, rule 2 suggests that the solvent dependence of the emission lifetime is connected with thermal reactivity in these solvents.

The assumption of k_{RD} as the dominant process, however, seems unlikely in the cases of crystalline complexes, where the activation energy for k_{RD} would be expected to substantially increase. In this case, k_{-4} is most probably the dominant pathway and the activation energy represents the crossing point of the doublet and quartet state potential curves. If this is true, then it is interesting to note that the activation energies for k_{-4} and k_{RD} are of a similar magnitude, assuming that the activation energy for k_{-4} is of the same order in crystalline as in a solvent environment. Why then does only one process appear to be dominant in solution at room temperature? This might be due to the two being so similar that they become hard to differentiate, but the Barclay-Butler plot for Reineckate[88] necessitates that both have a similar environmental dependence, which would be an even more remarkable coincidence. Adamson[88] suggests that k_{-4} is suppressed at high temperatures, but may become dominant at low temperatures. However, inspection of the temperature profile of a number of chromium(III) complexes in glassing solvents between 273 and 200 K[120] shows only one temperature-activated process is dominant throughout the region. Perhaps the only universal explanation is that the potential surfaces of the doublet, the

doublet reaction products and the quartet share a common crossover point, although this does not take into account changes in the quartet energy with LF strength.

Further information can be obtained from environmental effects on the room temperature lifetime. Wasgestian[119] has correlated the lifetimes of $[Cr(CN)_6]^{3-}$ in different solvents with the Dimroth solvent parameter, E_T, which is a measure of solvent polarity. This plot can also be performed (see Chapter 4) with reasonable success for the Reineckate data of Adamson,[88] which indicates that the lifetime diminishes as the solvent polarity increases and suggests that a vibronic mode involving a change in dipole is active as a deactivation mechanism. It has also been shown that the lifetime is prolonged by the presence of bulkier ligands[121] which may be due either to the restriction of metal-ligand vibrations, or the shielding of solvent molecules from the central metal ion. A comprehensive study of solution medium effects in $[Cr(bipy)_3]^{3+}$ and $[Cr(phen)_3]^{3+}$ [122] has shown, however, that there is no effect of solvent polarity or deuteration on the phosphorescence lifetimes of these complexes, suggesting solvent has little effect on the rate of deactivation, k_6, of the doublet state, although solvent dependence has recently been reported by Kane-Maguire.[115] This is considered to reflect the insulation of the metal ion from the solvent by the bulky ligands, so that any metal-ligand vibronic deactivation is not enhanced by solvent polarity, a result reflected in the abnormally long lifetimes of the two complexes ($[Cr(phen)_3]^{3+}$ = 360 μs, $[Cr(bipy)_3]^{3+}$ = 63 μs) in deaerated water at 298 K. The increase in size of the phen over the bipy ligand also causes a lengthening for reasons mentioned earlier. The addition of anions to aqueous solutions of the complexes causes an increase in the lifetimes which is

attributed to a reduction of both k_6 and k_{RD}, due to restriction by the anion of both the metal-ligand vibration and the freedom of the water molecule to participate in reactions. In accordance with this model, $[Cr(bipy)_3]^{3+}$ shows a ten-fold increase in lifetime (over the value in H_2O), whereas $[Cr(phen)_3]^{3+}$ only shows a two-fold increase in 11.7 M $HClO_4$, the bipy derivative being less rigid and therefore more susceptible to environmental changes. While the effect of solvent on lifetime is minimal, the phosphorescence intensity decreases substantially in non-aqueous solvents, and this is attributed to a decrease in the ISC efficiency, ϕ_{ISC}, the extent of which can be obtained for $[Cr(bipy)_3]^{3+}$ by systematically quenching the phosphorescence in aqueous solution by addition of the non-aqueous solvent, and the curve extrapolated to 100% non-aqueous solvent, assuming $\phi_{ISC} = 1$ for the aqueous system. The results are in the order

$$H_2O < CH_3CN < CH_3OH < DMF$$

where $\phi_{ISC} \sim 0$ for DMF. The decrease in ϕ_{ISC} is accompanied by an increase in photoreaction through the quartet state. From the quenching of the photoreaction of $[Cr(bipy)_3]^{3+}$ in a 0.2 mole fraction DMF in aqueous solution by acid, it is suggested that both the quartet and doublet states have a common seven-co-ordinate reactive intermediate which incorporates a solvent molecule into the complex. The situation is rationalised by considering the solvent to be incorporated in 'inter-ligand pockets' of the complex in the ground state. When excited, the quartet state distortion results in lengthening of the metal-ligand bonds and the appearance of a vacant t_{2g} orbital, both allowing easier access to the solvent molecule which can act as a Lewis base to form the seven-co-ordinate intermediate. The doublet state, however, is not distorted and has no vacant t_{2g} orbital, and this hinders formation of the intermediate, although it may be formed <u>via</u> the higher doublet state which does have a vacant t_{2g} orbital. This explains the

difference in rate for the two photoreactions. Reaction from the ground state is almost impossible, due to the large configuration and energy changes needed. This mechanism rationalises the solvent dependence of ϕ_{ISC} by correlation with the Gutmann donor number of the solvent, which is a measure of the Lewis basicity of the solvent molecule. This view is further substantiated by a similar ordering for the solvent shifts of the extinction coefficients of the absorption bands ($\epsilon_{max}^{DMF} = 3/2 \times \epsilon_{max}^{H_2O}$).

This model, therefore, is consistent with a 'common' pathway for k_{-4} and k_{RD}, and explains the solvent dependence in terms of the donor ability of the solvent, when the metal is 'shielded' from solvent variations of k_o. While this model remains to be tested on a more general basis, it would certainly rationalise many of the results so far reported, and brings together the two conflicting sets of arguments for back-ISC and photoreaction. It also serves to illustrate the complexities which may be encountered for an 'apparently simple' three-level system which promises to be the subject of further study for some time.

2-2 Ruthenium(II), Osmium(II) and Platinum(II). Systems Exhibiting Heavy Atom Luminescence

2-2.1 The photochemical implications of the excited state

The properties of luminescent ruthenium(II) polypyridyl complexes such as $[Ru(bipy)_3]^{2+}$ and $[Ru(phen)_3]^{2+}$ have resulted in these complexes and their analogues being the recipients of considerable attention in reference to solar energy conversion schemes and their use as versatile and powerful sensitisers. These properties are:-[123]

(i) Solubility in aqueous solutions

(ii) Strong absorption in the visible region

(iii) Photostability at room temperature

(iv) Luminescence in a convenient region ($\sim$ 580 nm) while remaining reasonably energetic.

(v) Strong luminescence at room temperature with a lifetime of $\sim$ 0.7 μs for $[Ru(bipy)_3]^{2+}$, which is not particularly sensitive to oxygen.

In addition, the excited state is exceedingly versatile and can undergo both oxidative and reductive quenching, depending upon the nature of the acceptor, as well as an energy transfer mechanism.[124]

$$*[RuL_3]^{2+} + Q \longrightarrow [RuL_3]^{3+} + Q^- \quad \text{oxidative quenching}$$

$$*[RuL_3]^{2+} + Q \longrightarrow [RuL_3]^{+} + Q^+ \quad \text{reductive quenching}$$

$$*[RuL_3]^{2+} + Q \longrightarrow [RuL_3]^{2+} + Q^* \quad \text{energy transfer}$$

It is these electron-transfer processes which are of interest in the solar energy applications for these systems. The redox potentials in aqueous solution for $[Ru(bipy)_3]^{2+}$ are:-

$$[Ru(bipy)_3]^{3+} + e^- \longrightarrow *[Ru(bipy)_3]^{2+} \quad E^o = -0.84 \text{ eV}$$

$$*[Ru(bipy)_3]^{2+} + e^- \longrightarrow [Ru(bipy)_3]^{+} \quad E^o = +0.84 \text{ eV}$$

Therefore the excited state, which is both a strong reductant and reasonable oxidant, should be capable of reducing water to hydrogen,[125]

$$*[Ru(bipy)_3]^{2+} + H_2O \rightleftharpoons [Ru(bipy)_3]^{3+} + \tfrac{1}{2}H_2 + OH^-$$

it being regenerated at moderate to high pH

$$[Ru(bipy)_3]^{3+} + OH^- \rightleftharpoons [Ru(bipy)_3]^{2+} + \tfrac{1}{2}O_2 + \tfrac{1}{2}H_2O$$

or alternatively,[126]

$$2*[Ru(bipy)_3]^{2+} \rightleftharpoons [Ru(bipy)_3]^{3+} + [Ru(bipy)_3]^{+} \quad E_o = 1.7 \text{ eV}$$

$$[Ru(bipy)_3]^{3+} + OH^- \rightleftharpoons [Ru(bipy)_3]^{2+} + \tfrac{1}{2}H_2O + \tfrac{1}{4}O_2$$

$$[Ru(bipy)_3]^{+} + H^+ \rightleftharpoons [Ru(bipy)_3]^{2+} + \tfrac{1}{2}H_2$$

In practice, however, the photo-catalytic reduction does not occur, due to an intrinsic barrier to the electron-transfer process, making it too slow to compete with the decay of the excited state.[127] A monolayer analogue of $[Ru(bipy)_3]^{2+}$ has been reported to cleave water successfully,[127] but this result was not repeatable using a purified sample[128] and the reaction was attributed to an unknown impurity. Interest has also been centred on the possibility of the electron-transfer process producing a reduced species which stores the energy as chemical energy which is then released upon oxidation either as heat or by the cleavage of water to produce hydrogen and oxygen. This approach, however, also has drawbacks as $[Ru(bipy)_3]^{3+}$ and $[Ru(bipy)_3]^{+}$ are even stronger oxidants and reductants, respectively, than the excited state, so that the back electron-transfer process is favourable and no net reaction occurs.

$$[Ru(bipy)_3]^{3+} + e^- \longrightarrow [Ru(bipy)_3]^{2+} \quad E^o = +1.26 \text{ eV}$$

$$[Ru(bipy)_3]^{2+} + e^- \longrightarrow [Ru(bipy)_3]^{+} \quad E^o = -1.26 \text{ eV}$$

Attention has, therefore, been focused on preventing this back reaction either by competitive scavenging of $[Ru(bipy)_3]^{3+}$ [129] or the reduced substrate[130] or by isolation of the oxidised complex from the reduced substrate.[131] A particularly promising system has been the scavenging of $[Ru(bipy)_3]^{3+}$ by cysteine or ethanolamine (D) in the electron-transfer reaction with paraquat.[129]

$$[Ru(bipy)_3]^{2+} + h\nu \rightleftharpoons {}^*[Ru(bipy)_3]^{2+}$$

$${}^*[Ru(bipy)_3]^{2+} + PQ^{2+} \rightleftharpoons [Ru(bipy)_3]^{3+} + PQ^{+}$$

$$[Ru(bipy)_3]^{3+} + D \longrightarrow [Ru(bipy)_3]^{2+} + D^{+} \text{ (irreversible reaction)}$$

This causes a build up in the PQ^+ concentration, which is used to drive the cleavage of water in a secondary cell compartment at a platinised (Pt) electrode.

$$PQ^{+} - e^{-} \longrightarrow PQ^{2+}$$

$$H^{+} + e^{-} \longrightarrow \tfrac{1}{2}H_2$$

This method also produces an appreciable photocurrent ($\sim$ 200 μA), although the system is only 5% efficient in terms of current produced per photon. Promising results have also been obtained by using hydrophobic analogues of $[Ru(bipy)_3]^{2+}$ in which the reactive core is 'shielded' by the hydrophobic sheath [131] formed by substitution of large aliphatic groups into the bipyridyl rings. These complexes have higher oxidation potentials than the parent compound and undergo an electron-transfer reaction with triethylamine in dry acetonitrile at an almost diffusion-controlled rate to produce permanent conversion to $[Ru(bipy)_3]^{+}$ in relatively high yield (> 0.35). The product, which is stable over a period of days in acetonitrile is rapidly converted back to the starting material in the presence of water. The formation of this product suggests that the hydrophobic sheath retards the

back reaction to such an extent that the triethylamine radical cation undergoes further reaction, so that the reverse transfer reaction is prevented. For this system to be of practical use, however, an efficient secondary electron-acceptor is needed to regenerate $[Ru(bipy)_3]^{2+}$. The indirect use of $[Ru(bipy)_3]^{2+}$ as a sensitiser has also been considered, with particular reference to the sensitisation of TiO_2 semi-conductor electrodes.[125,132] In this system, the $[Ru(bipy)_3]^{2+}$ may be either chemically attached to the n-type semi-conductor or be incorporated into the electrolyte. On irradiation, the excited $*[Ru(bipy)_3]^{2+}$ ejects an electron into the conduction band of the semi-conductor, which then flows through an external circuit to a platinum electrode where reduction of water to give molecular hydrogen occurs. The resultant $[Ru(bipy)_3]^{3+}$ is reduced back to the starting material by hydroxide ions with the production of molecular oxygen. The results for this type of system are promising, but the technique is far from perfect.[123] The complex has also been used with an Fe^{2+}/Fe^{3+} couple in a photogalvanic cell[133] which consists of a thin layer of electrolyte ($\sim 10^{-2}$ cm) trapped between two electrodes, one of which is semi-transparent to allow solar radiation to enter the cell, causing photochemical reaction in the electrolyte. The high-energy products then diffuse to the electrode where they react, driving electrons round an external circuit. In the case of the iron-ruthenium system, the pertinent equations are:-

$$[Ru(bipy)_3]^{2+} \xrightarrow{h\nu} *[Ru(bipy)_3]^{2+}$$

$$*[Ru(bipy)_3]^{2+} + Fe^{3+} \rightleftharpoons \underset{B}{[Ru(bipy)_3]^{3+}} + \underset{Y}{Fe^{2+}}$$

$$B + e^- \longrightarrow [Ru(bipy)_3]^{2+}$$

$$Y - e^- \longrightarrow Fe^{3+}$$

electrode reactions

Unfortunately, the back reaction makes this system impracticable. A further experiment has been the sensitisation of the isomerisation of norbornadiene (NBD) to quadricyclane (Q) by $[Ru(bipy)_3]^{2+}$.[134] This occurs with 100% efficiency but NBD does not absorb above 300 nm, which indicates the need for a sensitiser. The product (Q) undergoes catalysed conversion back to the ground state with release of excess energy (1.088 kJ/gm). Although $[Ru(bipy)_3]^{2+}$ does sensitise the

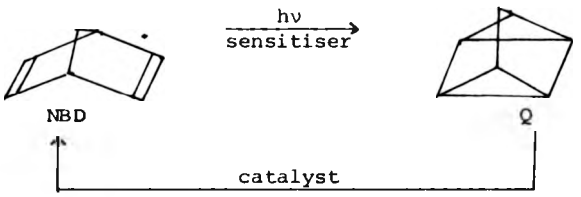

release of ∿1.088 kJ/gm

reaction, the yield is low ($< 2 \times 10^{-3}$).

It is apparent that $[Ru(bipy)_3]^{2+}$ and $[Ru(phen)_3]^{2+}$, which undergoes similar reactions, and their derivatives are potentially very useful both to the photochemist as powerful sensitisers and to solar energy conversion schemes. Similarly, osmium(II) polypyridyl complexes, which are the 5d analogues of the ruthenium(II) systems, have recently attracted attention.[126] These complexes are much shorter lived than their ruthenium(II) analogues (∿ 19 ns for $[Os(bipy)_3]^{2+}$ in H_2O at room temperature)[135] and emit at much longer wavelengths (∿ 670 nm).[135] This would seem to make these complexes less useful than the equivalent ruthenium(II) complexes, but this is compensated for by a larger reduction potential and,more important, by a reduced back electron-transfer reaction.

$$^{*}[Os(bipy)_3]^{2+} + e^- \longrightarrow [Os(bipy)_3]^{+} \qquad E^{o} = +0.59\ V$$

$$[Os(bipy)_3]^{3+} + e^- \longrightarrow {}^{*}[Os(bipy)_3]^{2+} \qquad E^{o} = -0.96\ V$$

It has been shown in the case of quenching by acidopentammine complexes of cobalt(III) that $[Os(bipy)_3]^{3+}$ is formed with unitary limiting yield, whereas the equivalent ruthenium(II) reaction only gives a limiting yield of 0.52[136] due to a competitive back reaction:-

$$^{*}[M(bipy)_3]^{2+} + [Co(NH_3)_5X]^{n+} \underset{k_2}{\overset{k_1}{\rightleftharpoons}} [M(bipy)_3]^{3+} + [Co(NH_3)_5X]^{(n-1)+}$$

$$[Co(NH_3)_5X]^{(n-1)+} \xrightarrow{k_3} [M(bipy)_3]^{3+} + Co^{2+} + 5NH_3 + X^{(n-3)+}$$

when M = Os, $k_3 \gg k_2$

M = Ru, $k_2 \simeq k_3$

The potential of these two sets of complexes has stimulated further investigation of other luminescent transition-metal complexes as suitable photosensitisers, having the characteristics of an intense, room-temperature luminescence in fluid solution with a reasonable lifetime and a broad absorption band. Among those studied have been iridium(III) and chromium(III) complexes, and more recently platinum(II) has come into focus, with the report[37] that the neutral bis(8-hydroxyquinolinato)Pt(II) complex has an intense luminescence (ca. 660 nm) in room temperature solution, an appreciable lifetime (~ 3 μs in dimethylformamide) and a broad absorption spectrum, although it is susceptible to oxygen. This observation promises to promote further work on this and other luminescent platinum(II) systems, for which only preliminary reports exist.[137]

Figure 8

Absorption and emission spectra of $[Ru(phen)_3]^{2+}$ (full line) and $[Os(phen)_3]^{2+}$ (broken line) in 9M $LiCl/H_2O$ at 298 K. The emission spectra are merely qualitative and are not related.

2+

9M

erely

2-2.2 The absorption and emission spectra of these systems

The efficient use of these luminescent complexes as sensitisers requires an understanding of the donor states involved. These can be investigated by means of emission and, when observable, excited state absorption spectroscopy. The chemistry of ruthenium(II) ($4d^6$) and osmium(II) ($5d^6$), as expected from their position in the periodic table, are closely related, and their luminescence behaviours have been treated in a parallel manner, with much of the information acquired from ruthenium(II) systems being applied to the analogous osmium(II) systems. The latter, being heavier, is expected to experience a greater contribution from SOC, and this has been used to explain the quantitative differences between the two systems. The effect of SOC is immediately apparent in the absorption spectrum of osmium(II) systems, where the more intense bands, and hence greater resolution, are attributed to greater mixing of 'forbidden' states caused by SOC (see Figure 8). The absorption spectrum of $\left[Pt(QO)_2\right]$ (Figure 9) shows even more intense and structured bands, indicative of the enhanced SOC effect in this heavy metal complex ($5d^8$).

The emission spectra of the bipyridyl complexes of ruthenium(II) and osmium(II) are identical to those of the 1,10-phenanthrolene complexes shown (Figure 8), except for a red shift of ~ 450 cm^{-1} [43] in the case of ruthenium(II) and ~ 530 cm^{-1} for osmium(II). There is also a striking resemblance between the osmium and ruthenium analogues in both emission and absorption, giving evidence for treating both osmium and ruthenium as similar systems, although there are detailed differences.

Figure 9

Absorption and emission spectra of $[Pt(QO)_2]$ in MeOH at 298 K. The two spectra are not related.

in

ed.

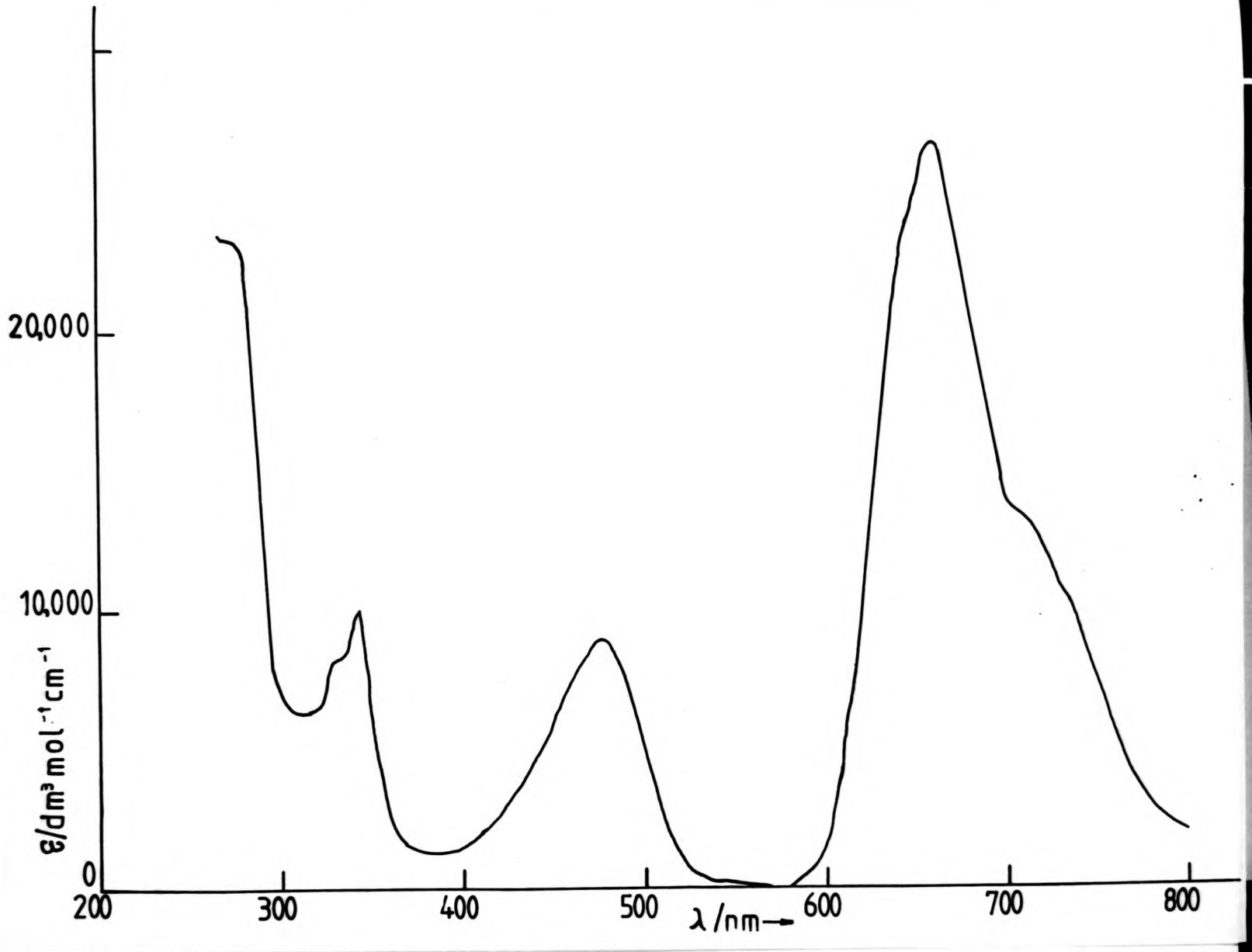

The emission spectra of all three systems are broad and almost structureless at room temperature, but the higher resolution obtained at 77 K reveals the presence of a prominent vibrational progression, superimposed on the single electronic transition, for all three cases.[137,41,138] The spacings are given below:-

COMPLEX	SPACING (cm^{-1})
$[Ru(phen)_3]^{2+}$	∿ 1300
$[Ru(bipy)_3]^{2+}$	∿ 1300
$[Os(phen)_3]^{2+}$	∿ 730
$[Os(bipy)_3]^{2+}$	∿ 730
$[Pt(QO)_2]$	∿ 1220

These spacings are indicative of low frequency vibrations such as metal-ligand vibrations. In the case of ruthenium(II), this vibration has been assigned as a Ru-N skeletal vibration of the complex by comparison with the infra-red spectra of the free and complexed ligand.[43] A similar assignment can be reasonably assumed for the other two systems.

2-2.3 The nature of the luminescence in ruthenium(II) and osmium(II) systems

The nature of the ruthenium emission has been extensively investigated and has borne a number of different assignments[39,40,43,41] since its first report.[39] These assignments have been made on consideration of the low-temperature emission and absorption spectra and the pertinent question has been the nature of the low intensity tail at the red edge of the lowest energy absorption band which overlaps the emission and is assumed to give rise to the state causing luminescence. Comparison with the absorption spectrum of the free ligand reveals that this band lies at lower

energy than the π-π^* bands,[41] and must be either a d-d or charge transfer type transition. Crosby et al.[41] suggested a d-d transition on the assumption that an observed absorption peak at 18,550 cm^{-1} for $[Ru(bipy)_3]^{2+}$ corresponds to the $^1A_1 \rightarrow {}^1T_1$ (d-d) transition. This assignment, however, was in disagreement with other studies of this complex from which estimates of the octahedral splitting of > 21,000 cm^{-1} were predicted,[10,139] putting this d-d transition closer to the u.v. region, and Crosby later reassigned the luminescence to a CT type transition. Further evidence for this assignment comes from a study of a series of substituted complexes of the type $[Ru(bipy)_2X]^{2+}$.[141] It was found that there was a good correlation between the shift of the CT band and the luminescence spectrum, but the shifts are not large, as would be expected from the large changes in LF strength employed if these were d-d bands. The band is assigned as $d \rightarrow \pi^*$ due to the ease with which ruthenium(II) is oxidised, the possibility of $\pi^* \rightarrow d$ being dismissed on the grounds that the transition would be of higher energy due to the low oxidation state of the ruthenium core.[141] The assignment of luminescence as fluorescence or phosphorescence should be made on the basis of the emission lifetime, as the emission intensity may lead to incorrect assignments.[39,41] Demas and Crosby[42] found the lifetime of a series of ruthenium(II) complexes containing polypyridyl ligands at 77 K to be between 0.5 and 10 μs, which is longer than expected for fluorescence, but not long enough for phosphorescence. There are three possibilities which may explain this result:-

(i) The luminescence is orbitally-forbidden, but spin-allowed.

(ii) The luminescence is a low quantum yield, spin-forbidden transition ($\tau_M = \tau_o \phi$)

(iii) The luminescence is a heavy atom-perturbed spin-forbidden transition.

As none of the complexes studied exhibit a particularly high symmetry, the first proposal seems unlikely and the quantum yields are typically high, discounting the second possibility. The third possibility, therefore, seems most plausible, so that the luminescence is assigned as $^3(d \rightarrow \pi^*) \rightarrow {}^1A_1$, and explains the absence of fluorescence due to the enhancement of ISC caused by SOC, the lowest energy absorption band being assigned $(d \rightarrow \pi^*)$. A similar conclusion has been reached by Lytle and Hercules[43] who consider the emission to occur from the low-lying perpendicular polarised component of the charge transfer triplet to the singlet state at 77 K. The measured polarisation, P, of the emission at 77 K is + 1/7[142] for $[Ru(bipy)_3]^{2+}$, and since

$$P = (3 < \cos^2\theta > -1)/(< \cos^2\theta > + 3) \qquad (2\text{-}4)$$

where θ is the angle between the absorption and emission oscillators, so that when $P = + 1/7$, $\theta = 45^{\circ}$ and the absorption and emission oscillators are in the same plane. This result, however, is ambiguous as it does not distinguish between a linear (z) - planar (z,x) interaction and a planar-planar (x,y) interaction of the absorption and emission oscillators respectively. In D_3 symmetry, the two possibilities for the emitting CT triplet are $^3A_2$ and $^3E_1$ which borrow intensity by SOC from the allowed singlet transitions $^1A_1 \leftarrow {}^1E$ (x,y), $^1A_1 \leftarrow {}^1A_2$ (x,y,z). However, $^3A_2$ is a planar (x,y) oscillator and can only borrow intensity from $^1A_1 \leftarrow {}^1E_1$, whereas ^3E is a three-dimensional (x,y,z) oscillator and can also gain intensity from $^1A_1 \leftarrow {}^1A_2$. The increase of polarisation under the $^1A_1 \leftarrow {}^1A_2$ band (21,000 cm^{-1}) suggests that the ^3E triplet is the emitting state and the transition is assigned $^3E \rightarrow {}^1A_1$, and incorporates the assignment of Lytle and Hercules.[43]

Crosby,[143] however, contests this 'classical' outlook and has developed a conflicting model, in which SOC plays the major rather than a perturbing role, based on a number of experimental investigations of the ruthenium(II) and osmium(II) systems. The invariance of the quantum yield throughout the entire absorption spectrum[15] indicates that the lowest-lying states are populated with unitary efficiency and hence k_{ISC} is estimated to be $> 10^{11}\ s^{-1}$, which is comparable with the rate of vibrational relaxation. This suggests that SOC is operative to such a large extent in these systems that the identities (spin and orbital labels) of the different states are almost lost. The success of a SOC model[15] to predict the intrinsic lifetimes of the ruthenium(II) and osmium(II) systems, in which SOC is represented as a matrix element connecting the emitting triplet and 'perturbing' singlet states gives further insight into this effect. The pertinent expression is:-

$$1/\tau_o = K \quad E_T^{\,3}/E_S \quad |M_{SO}|^2/(E_T-E_S)^2 \quad \varepsilon(E_S) \qquad (2\text{-}5)$$

where E_T is the energy of the emitting state above the ground state, E_S is the energy of the perturbing singlet state, $|M_{SO}|$ is the SOC matrix element, K is a constant and $\varepsilon(E_S)$ is the molar extinction coefficient at energy E_S. τ_o is the intrinsic lifetime, which can be estimated from the equation

$$\tau_o = \phi_{ISC} \cdot \tau/Q \qquad (2\text{-}6)$$

where τ is the measured lifetime and Q is the quantum yield at 77 K, and ϕ_{ISC} is assumed to be unity. The resultant calculated values of $K|M_{SO}|^2$ for the complexes studied showed that this parameter was remarkably constant for both the ruthenium system, with an average value of 3.11×10^{-7} mol cm l^{-1} μs^{-1} and the osmium system (7.87×10^{-7} mol cm l^{-1} μs^{-1}), these values giving excellent agreement between the calculated and predicted intrinsic lifetimes for the relevant complexes. This suggests that SOC is a

Crosby,[143] however, contests this 'classical' outlook and has developed a conflicting model, in which SOC plays the major rather than a perturbing role, based on a number of experimental investigations of the ruthenium(II) and osmium(II) systems. The invariance of the quantum yield throughout the entire absorption spectrum[15] indicates that the lowest-lying states are populated with unitary efficiency and hence k_{ISC} is estimated to be $> 10^{11}$ s^{-1}, which is comparable with the rate of vibrational relaxation. This suggests that SOC is operative to such a large extent in these systems that the identities (spin and orbital labels) of the different states are almost lost. The success of a SOC model[15] to predict the intrinsic lifetimes of the ruthenium(II) and osmium(II) systems, in which SOC is represented as a matrix element connecting the emitting triplet and 'perturbing' singlet states gives further insight into this effect. The pertinent expression is:-

$$1/\tau_o = K \quad E_T^{\,3}/E_S \quad . |M_{SO}|^2/(E_T-E_S)^2 \quad \varepsilon(E_S) \qquad (2\text{-}5)$$

where E_T is the energy of the emitting state above the ground state, E_S is the energy of the perturbing singlet state, $|M_{SO}|$ is the SOC matrix element, K is a constant and $\varepsilon(E_S)$ is the molar extinction coefficient at energy E_S. τ_o is the intrinsic lifetime, which can be estimated from the equation

$$\tau_o = \phi_{ISC} \cdot \tau/Q \qquad (2\text{-}6)$$

where τ is the measured lifetime and Q is the quantum yield at 77 K, and ϕ_{ISC} is assumed to be unity. The resultant calculated values of $K|M_{SO}|^2$ for the complexes studied showed that this parameter was remarkably constant for both the ruthenium system, with an average value of 3.11×10^{-7} mol cm l^{-1} μs^{-1} and the osmium system (7.87×10^{-7} mol cm l^{-1} μs^{-1}), these values giving excellent agreement between the calculated and predicted intrinsic lifetimes for the relevant complexes. This suggests that SOC is a

function of the central metal ion rather than the ligand structure, and the success of this formula indicates that the basic assumption of only one perturbing singlet state is justified, which is in direct conflict with the interpretation of the polarisation studies described earlier. It is interesting to note that the increase in $K|M_{SO}|^2$ on going from ruthenium(II) to osmium(II) (2.5) is not as large as predicted by theory (7.5). This may be due to either a higher degree of covalency in these systems, causing greater delocalisation of the d electrons on to the ligands, and so effectively reducing ξ, the SOC constant, or because the S-O interaction is so great that the ^{3}CT level is split to such an extent that not all the components are thermally accessible at 77 K, so that the assumption that the radiative rate constant receives contributions from all three components of the triplet at this temperature is erroneous and the τ_o calculated from equation (2-6) would be longer than that obtained from equation (2-5), although this does not appear to be the case for the three osmium(II) complexes studied. The model does, however, predict the slight increase in the radiative lifetimes of the osmium(II) complexes over those of the equivalent ruthenium(II) species. This would not be expected from the increase in $K|M_{SO}|^2$, but this is compensated for by a larger energy gap between the emitting triplet and perturbing singlet, so producing the slight increase. The decrease in $K|M_{SO}|^2$ parallels that of the non-radiative rate constant, k_q, for ring-phenylated analogues of $[Ru(phen)_3]^{2+}$ and $[Ru(bipy)_3]^{2+}$,[144] and it is suggested that this model can also be used to predict the radiationless rates by substitution of the radiative terms by a term for the vibronic coupling of the non-radiative pathway from the ^{1}CT to the singlet ground state, implying that the non-radiative process is the inverse of the

radiative pathway, i.e. SOC of the emitting triplet state with the perturbing singlet followed by radiationless relaxation to the ground state.

2-2.4 The Crosby model for ruthenium(II) and osmium(II) low temperature luminescence

Temperature studies on ruthenium(II) and osmium(II) complexes between 77 K and 4 K[145,146] have indicated that luminescence occurs from a set of thermally equilibrated excited levels at 77 K, and it is suggested that the emitting CT triplet label merely indicates that there are three emitting levels of CT origin, each spin-orbit coupled to the perturbing singlet state. The temperature dependence between 77 and 4.2 K of decay times for both osmium(II) and ruthenium(II) show similar trends[57,143] and give the unexpected result that the measured lifetime at 4.2 K exceeds the intrinsic lifetime calculated at 77 K by factors between 4 and 15, while the quantum yield decreases,[53] suggesting a manifold of emitting levels. Crosby[53] has used the general equation (1-59) to fit this data, assuming that (i) thermal equilibration is fast compared with depopulating processes, (ii) each of the levels is capable of coupling with the ground state either radiatively or radiationlessly, and these pathways are controlled by first-order kinetics with temperature-independent rate constants, (iii) the manifold of luminescing states is populated from higher excited states with near unit efficiency at all temperatures, and this efficiency is independent of excitation wavelength. A minimum of three levels are needed to produce a good fit to the experimental data and the observed lifetime, τ, is given by the equation:-

$$\tau = (1+ 2e^{-\Delta\varepsilon_1/KT} + e^{-\Delta\varepsilon_2/KT}) / (k_1 + 2k_2 e^{-\Delta\varepsilon_1/KT} + k_3 e^{-\Delta\varepsilon_2/KT}) \quad (2\text{-}7)$$

where k_i represents the sum of radiative and non-radiative processes for the ith level, and $\Delta\varepsilon_i$ is the energy gap between (i+1)th and

TABLE (2-1) Energy Gaps, Rate Constants and Exchange Integrals for the Lowest Excited States of Ruthenium(II) and Osmium(II) Complexes in Polymethylmethacrylate Film for the Range 4 - 80 K

Complex	$\Delta\varepsilon_1$ (cm^{-1})	$\Delta\varepsilon_2$ (cm^{-1})	$\tau_1=1/k_1$ (μs)	$\tau_2=1/k_2$ (μs)	$\tau_3=1/k_3$ (μs)	$K(a_1,a_2)$	$K(e^+,a_2)$	$K(a_1,a_2)/K(e^+,a_2)$	Ref.
$[Ru(bipy)_3]SO_4$	10	80	220	19	0.5	47	67	0.70	143
$[Ru(bipy)_3]Cl_2$	10.1	61.2	183.1	18.8	0.58	36	63	0.57	53
$[Ru(4,4'\text{-}ph_2bipy)_3]Cl_2$	9.5	60.1	165	18	0.7	36	59	0.61	143
$[Ru(4,4'\text{-}me_2bipy)_3]Cl_2$	9.2	64.2	152	18.8	0.58	38	57	0.66	53
cis-$[Ru(CN)_2(bipy)_2]$	11.2	32.5	62.5	9.7	1.8	19	75	0.25	143
$[Ru(phen)_3]I_2$	8.9	53	380	41	12	31	56	0.55	5
$[Ru(4,7\text{-}me_2phen)_3]Cl_2$	8.5	30.4	271.2	43.7	3.06	18	53	0.33	147
$[Ru(4,7\text{-}ph_2phen)_3]Cl_2$	8.6	30.1	230	22.9	2.56	18	53	0.33	147
$[Ru(5,6\text{-}me_2phen)_3]Cl_2$	8.5	53.1	377	45.0	1.13	32	53	0.6	147
$[Os(phen)_3]I_2$	23	63	33	5.1	0.5	-	-	-	5

first levels. The second level has been given a two-fold degeneracy on the basis of the theoretical model which has been proposed to allow symmetry labels to be attached to these levels. The values of these parameters are tabulated opposite (Table 2-1) for a number of ruthenium(II) and one osmium(II) system, although a splitting of $\sim$ 100 cm^{-1} for $\Delta\varepsilon_2$ has been reported for a number of osmium(II) complexes with π-conjugated ligands.[146]

All the complexes studied show a similar splitting pattern in that $\Delta\varepsilon_1$ is small ($\sim$ 10 cm^{-1}) and almost constant for a given ligand system, whereas $\Delta\varepsilon_2$ is larger (30 to 100 cm^{-1}) and more susceptible to change in both ligand substituent and counter ion. Both $\Delta\varepsilon_2$ and $\Delta\varepsilon_1$ are larger for the osmium(II) system, as expected from the enhanced SOC effect. The levels are ordered in decreasing lifetime, with the longer lived level lying lowest (15 to 300 μs), the second level being 5 to 10 times shorter lived, and the highest level having a lifetime of the order of a microsecond. The osmium system, as expected, has the same ordering but with significantly reduced lifetimes.

These results have been used to develop an electron coupling model for CT transitions of these d^6 complexes,[143,53,147,148] in which the lowest excited state produced by promotion of an electron from the d^6 core to a π^*-antibonding orbital of the ligand system is split by weak electrostatic coupling to the strongly spin-orbit coupled ground state of the resultant d^5 core. This model is contrary to that employed by Fujita and Kobayashi[142] in which SOC causes finer splitting of the gross splittings produced by electrostatic forces.

For $(nd)^6$ systems with D_3 symmetry,[148] CT transitions from the ground state ($^1A_1$) to the $\pi^*(a_2)$ or $\pi^*(e)$ antibonding orbitals

of the ligands leaves the oxidised metal core in one of several possible states whose energies can be calculated by treating the system as a d^5 LF problem. The final CT states are then calculated by introducing the perturbation of the optical electron in one of the π^* ligand orbitals into the Hamiltonian of the system. Consideration of the electrostatic interaction between the core and the excited electron produces the final splitting of the CT state functions and energies of the excited d^6 complex ion. The case of $[Ru(bipy)_3]^{2+}$ produces typical results for this treatment[143]. The promotion of the optical electron to the ligand system produces a d^5 ruthenium(III) core whose ground state is the strongly spin-orbit coupled E' in the D_3^* double group. The optical electron with spin E' interacts with the lowest unoccupied orbitals of the ligand system, which transform as either a_2 or e in D_3 symmetry, through their direct product. The final symmetries of the microstates are found by allowing these states to interact with the metal core by the direct product of the two systems. Reduction of this product in the D_3^* symmetry group produces the final set of states $\Gamma d\pi^*$. The two possibilities are either

$$\Gamma d\pi^* = (E') \text{ core} \times (E' \times a_2) \text{ ligand} = A_1 + E + A_2$$

or

$$\Gamma d\pi^* = (E') \text{ core} \times (E' \times e) \text{ ligand} = A_1 + A_2 + E + E + E$$

The temperature data suggest that a three-level manifold is lowest, and this is assumed to be $d \rightarrow \pi^*$ (a_2), so that the three emitting levels are A_1 (forbidden), A_2 (z allowed) and E (x,y allowed). The ordering of these levels is assumed to be A_1 lowest, then E, then A_2, superficially, by comparison with the calculated lifetimes of the three states and, more rigorously, from a full mathematical treatment of the system.[148]

The splittings of these three states, which are dependent both on SOC and electrostatic interactions of the optical electron on the ligand system with the d^5 core, are given by the exchange interactions $K(e^+,a_2)(1-k_1^2)$ for the A_1-E splitting and $2k_1^2K(a_1,a_2)$ for the A_1-A_2 splitting where k_1^2 is related to spin-orbit coupling, $K(e^+,a_2)$ is the exchange integral representing the non-classical electrostatic interaction between the promoted electron residing in the $\pi^*(a_2)$ ligand orbital and an electron in a d orbital of e symmetry and $K(a_1,a_2)$ is the exchange interaction between the promoted electron and one occupying the d orbital extending along the principle symmetry axis of the complex. Assuming a value of 0.85 for k_1^2 [148] in both $[Ru(phen)_3]^{2+}$ and $[Ru(bipy)_3]^{2+}$ systems, the experimental splitting (Table 2-1) can be rationalised in terms of the two exchange integrals, which can be calculated from these splittings. The smaller splittings, and hence exchange integrals, for the phenanthrolene series can be attributed to greater delocalisation of the promoted electron by the larger π-structure of this ligand. It also seems reasonable that $K(e^+,a_2)$ should be greater than $K(a_1,a_2)$ since the e orbital of the metal core is in the x,y plane of the ligands whereas the a_1 orbital is directed along the z axis. The case of 4,7-substitution on the phenanthrolene ring produces a remarkable effect, while 5,6-substitution gives no appreciable change (Table 2-1). This is explained by the $\pi^*(a_2)$ orbital being more sensitive to 4,7- than to 5,6-substitution, a result indicated by studies of the analogous iron(II) system.[149] However, this study would also predict a marked effect for 4,4'-substitution into the bipyridyl ring, which is not observed (Table 3-1). This implies that k_1^2 may also vary as well as the two exchange integrals, which restricts the validity of the treatment to systems for which

k_1^2 has been determined experimentally from e.p.r. data for the oxidised complex. It is, however, apparent from the rate constants that the phenanthrolene system is less susceptible to quenching, reflecting the enhanced rigidity of this ligand.

The excitation of the optical electron to produce a ruthenium(III) core might be thought to involve geometrical change, but only a small Stokes' shift is observed for the luminescence, and the report of little change in bond lengths on complete oxidation of the ruthenium(II) system[150] indicates this not to be so.

Further experimental tests of this model have been hindered by the diffuseness of the peaks of the emission spectra even at 4.2 K ($\sim$ 300 cm^{-1}),[147] but the doubly degenerate E(x,y) level should be split by the application of an external magnetic field along the principal symmetry axis. The application of a 75 kG field to $[Ru(bipy)_3]^{2+}$ in this direction at 1.65 K[151] produces a distinct change in the emission band shape with a concomitant decrease in the measured luminescence lifetime. The result is explained by the splitting of the E state into two components, which reduces the gap between the A_1 and E levels so decreasing the lifetime. The study of circularly polarised luminescence induced by an external magnetic field can also be explained by similar reasoning within the context of this model. Further evidence for this three-level model comes from a study of the lower-temperature luminescence spectra of $[Ru(bipy)_3]SO_4$ between 10 and 1.65 K[151] which shows the 'grow-in' of a new spectrum, red shifted by 400 cm^{-1} at 1.65 K which is attributed to the A_1 state, while analysis of the temperature dependence of the spectra yield an A_1-E splitting of 10.2 cm^{-1} in good agreement with that obtained from lifetime measurements (Table 2-1).

This model, therefore, offers an excellent interpretation of the low-temperature luminescence properties of these ruthenium(II) systems, and may be extended to include their osmium(II) analogues,[148] although the enhanced effect of SOC will make these systems quantitatively quite different. Crosby[5] further suggests that the variation of the splittings of these levels, and hence the measured lifetime of the complex, with ligand substitution as well as a total shift of the manifold to produce a shift in the emission spectrum, can be utilised to produce fine tuning of the emission properties of the system to specified requirements, course tuning being provided by total change of the ligand or central metal ion.

2-2.5 The luminescence and photochemistry of Ru(II) at elevated temperatures (> 273 K)

The chemical implications of this model are that the excited state cannot be viewed as a simple triplet, but as a cluster of three closely spaced levels which represent the $d^5\pi^*$ configuration in which an electron has been essentially transferred to the ligand system of the complex. This excited state possesses both oxidising and reducing sites

$$\left[Ru(bipy)_3\right]^{2+}(d^6) \xrightarrow{h\nu} \left[Ru^{III} \quad (bipy)_3^{-}\right]^{2+}(d^5\pi^*)$$

and both types of electron-transfer reaction have been reported at ambient temperatures.[152,153] However, chemical quenching is performed at ambient temperatures whereas this model has been developed for 77 K and it is possible that a number of other levels may be thermally populated, for instance, the higher $d\pi^*(e)$ manifold, at ambient temperatures. There is, therefore, an obvious need for further emission studies at elevated temperatures in order for reasonable comparison with photo-

chemical studies to be made. While little more than the emission lifetime has been reported for osmium(II) complexes at room temperature,[154] a more detailed analysis of ruthenium(II) luminescence has been undertaken. Lytle and Hercules[43] studied the temperature dependence of the lifetime and quantum yield of $[Ru(bipy)_3]Cl_2$ between 80 and 285 K in an EPA glass. They fitted their lifetime data to an equation of the form:-

$$1/\tau_M = k_{1r} + k_{1q} + k_{2q} \exp(-\Delta E/kT) \qquad (2\text{-}8)$$

where k_{1r} is the radiative and k_{1q} the non-radiative rates for the combined levels of the low-lying CT 'triplet' and k_{2q} represents the temperature activated radiationless pathway from this state (see equation (1-57)), although they reported the presence of a small temperature activated pathway below 200 K. Lytle and Hercules[43] considered the activation energy which they calculated from the high temperature data (> 310 K) and varied from 800 cm^{-1} in water to 3,100 cm^{-1} in ethanol:methanol, to represent the gap between the emitting CT triplet state and the perturbing singlet state, while the frequency factor is attributed to the limiting non-radiative decay of the singlet to the ground state, as no fluorescence could be detected.

Van Houten and Watts[55] have shown the existence of a deuterium effect on quantum yield (Q) and emission lifetime (τ_{D_2O}) by both ligand and solvent deuteration of $[Ru(bipy)_3]^{2+}$ (τ_{D_2O}/τ_{H_2O} = 1.8, $\tau_{bipy\text{-}d8}/\tau_{bipy}$ = 1.2) in aqueous solution at 298 K and by ligand deuteration at 77 K (1.2). The radiative lifetime (τ_M/Q) is found to be constant and the deuterium effect is attributed to the non-radiative pathway which is suggested to contain a contribution from a weak coupled charge-transfer-to-solvent state.

They also report an inexplicable 20% reversible decrease in intensity of the entire absorption spectrum on deaeration of the aqueous solution at 298 K, but this has not been seen by other groups studying the same system,[156] although the quenching of the emission quantum yield and lifetime by molecular oxygen is well known.[156] The temperature dependence between 273 K and 373 K of Q and τ_M for these systems[54] were explained using equation (2-8) for τ_M and $Q = k_{1r}\tau_M$ for Q. This treatment yields an activation energy of $\sim$3,600 cm^{-1} with $k_{2q} = 10^{13}$ s^{-1} for both aqueous and deuterated systems, and the deuterium effect of both ligand and solvent is manifest in k_{1q} which varies from 1.222 x 10^6 s^{-1} for aqueous $[Ru(bipy)_3]^{2+}$ to 4.07 x 10^5 s^{-1} for $[Ru(bipy\text{-}d^8)_3]^{2+}$ in deuterated solvent. While these equations are essentially the same as those employed by Lytle and Hercules,[43] the model on which they are based is vastly different. k_{1r} and k_{1q} refer to the average values of the radiative and non-radiative rate constants respectively, over the three levels of the Crosby[143] model which, because $k_T >> 61$ cm^{-1} (their splitting) at ambient temperatures are assumed to be indistinguishable in this region, k_{2q} refers to the sum of the rate constants for both radiative and non-radiative return to the ground state of an additional level situated $\sim$ 3,600 cm^{-1} above the triplet manifold. Justification for retaining this triplet manifold when there is the possibility of an extra 36 d-π^* states and 9 states of d-d orbital parentage within thermal reach ($\sim$ 3,000 cm^{-1}), stems from the observation that $[Ru(bipy)_3]^{2+}$ is photoinert at room temperature and k_{1q} shows a deuterium effect, suggesting that weakly coupled radiationless transitions are the dominant deactivation mode. It is unlikely that these processes will be enhanced from higher levels, and since

most of these levels probably lie more than $\sim$ 200 cm^{-1} above the low lying triplet manifold, the Boltzmann factors favour decay from this triplet manifold. Further evidence for this weakly-coupled mechanism being charge-transfer-to-solvent is given by major changes occurring in both the shape of the luminescence spectrum and the radiative lifetime at the glassing point of the complex in EPA, and the presence of this diffusional deactivation mode is thought to explain the difference between the lifetime predicted by the Crosby[143] model ($\sim$ 3 μs) and the observed lifetime (0.78 μs) at 298 K. The higher energy additional level, which may also represent a cluster of levels, shows no deuteration effect, indicating a strongly coupled, thermally activated radiationless pathway. This pathway is dominant above $\sim$ 330 K and is responsible for dissipating 95% of the excitation energy at 360 K, where photochemistry of the complex occurs. This implies that this pathway is photochemical and a detailed study of the photochemistry of $[Ru(bipy)_3]^{2+}$ in 0.1 M HCl between 313 and 368 K has been undertaken.[157] The photolysis produces an initial colour change from yellow-orange to red-orange, attributed to the formation of a thermally unstable mono-dentate bipyridyl complex, $[Ru(bipy)_2OH(bipyH)]^{+}$ followed by production of the stable photoproduct by total displacement of the bipyridyl ligand which produces total bleaching of the visible absorption region, with a quantum yield, ϕ_P, of between 10^{-3} and 10^{-5}, depending upon conditions. The temperature dependence of ϕ_P was fitted to the equation

$$\phi_P=(P_P A e^{-(\Delta E+\Delta Ea^*)/k_T})/(k_1+A e^{-(\Delta E+\Delta Ea^*)/k_T}+k_{2q}e^{-\Delta E/k_T}) \quad (2\text{-}9)$$

where ΔE, k_1 ($=k_{1r}+k_{1q}$) and k_{2q} were obtained from their luminescence work,[54] P_P is the probability of product formation, and A is the combination of k_{2q} with the reaction rate from the

higher level : ΔEa^* is the activation energy of the photoreaction from this level. The results indicate that ΔEa^* is $\sim$ 2,000 cm^{-1} for the protonated ligand, and $\sim$ 1,600 cm^{-1} for the deuterated form, with P_pA ranging from $\sim 2.5 \times 10^{13}$ s^{-1} to $\sim 4 \times 10^{12}$ s^{-1} for the two cases respectively. This study implies the presence of a ligand substitution type reaction as found for chromium(III) complexes[19] and this analogy has led to the classification of this higher level as either the $^3A_2$ or ^3E d-d state, which are produced by the splitting of the octahedral d^6 $^3T_1$ state by the reduced D_3 symmetry.

In conclusion, the excited state model for ruthenium(II) systems typified by $[Ru(bipy)_3]^{2+}$ can be thought of as a set of three low-lying CTTL states, the spin and orbital labels of which have limited meaning due to the magnitude of SOC, which are responsible for the luminescence characteristics of the system at low temperature (77 K). At ambient temperatures, diffusional modes become active with some CTTS character being imparted to these low-lying levels, indicated by the observed solvent deuteration effects, and a higher (3,600 cm^{-1}) d-d photoactive triplet state participates in the deactivation mechanism. At elevated temperatures (> 330 K), this level is the predominant deactivation mode,and ligand substitution reactions with an activation energy of $\sim$ 2,000 cm^{-1} occur from this state. While similar conclusions may be drawn about the low-temperature luminescence of osmium(II) systems, the lack of detailed emission studies at ambient temperatures, makes any further analogy merely speculative. Further insight into the positions of higher excited states comes from the excited state absorption (ESA) spectrum of the triplet manifold (^3CT) at 298 K in aqueous solution. This shows two peaks at 360 nm (27,780 cm^{-1}) and 430 nm (23,255 cm^{-1})

for $*[Ru(bipy)_3]^{2+}$ and peaks at 360 nm (27,780 cm^{-1}) and 460 nm (21,740 cm^{-1}) for $*[Os(bipy)_3]^{2+}$.[126] These peaks have been attributed to $^3CT \rightarrow {}^3\pi-\pi^*$ transitions from their similarity with the ESA of the bipyridine anion, although a previous report,[158] in which no peak at 430 nm was observed, considers a $^3CT \rightarrow {}^3d-\pi^*$ transition more likely for $*[Ru(bipy)_3]^{2+}$.

Quenching studies of $[Ru(bipy)_3]^{2+}$ reveal that both dynamic electron transfer, as mentioned earlier, and energy transfer[159] processes are possible, and while the ^3CT state is certainly responsible for the electron-transfer processes, it may be possible that the LF state gives rise to the observed energy-transfer mechanism. However, when energy-transfer has been found, the results show that the donor level is at 17,200 cm^{-1},[159] which is the ^3CT energy, and it seems more likely that the quenching mechanism is decided by the nature of the quencher with the quenching action being depicted as a competitive deactivation pathway with the LF state for the ^3CT level energy. If this is the case, then the design of a complex with an enhanced ^3CT-LF splitting and a hydrophobic sheath combined with a high reduction potential will allow most efficient sensitisation of an appropriate quencher.

2-2.6 The nature of the luminescence in platinum(II) systems

The luminescence of platinum(II) systems has received comparatively little attention, although it has been long known.[160] The luminescence of the square-planar (D_{4h}) complexes has been reported, mainly in the solid state at cryogenic temperatures with little more than the luminescence spectrum being given. Interest has been centred on identification of the luminescence, which is thought to be either CT or d-d phosphorescence, although the large

SOC effect may make these terms of limited use.[30]

The square-planar ligand field of platinum(II) complexes splits the five degenerate d orbitals into two sets;[36] the lower manifold consists of the four orbitals d_{z^2}, d_{xz}, d_{yz} and d_{xy}, the exact ordering of which is subject to uncertainty, and a higher level due to the $d_{x^2-y^2}$ orbital although its exact position with respect to the ligand and metal π orbitals is less certain in cases where these are apparent. The situation is exemplified by $[Pt(CN)_4]^{2-}$ whose absorption spectrum consists of a series of intense CT bands situated in the u.v. region, with a less intense band being apparent on the red edge of the first intense band (35,600 cm^{-1}) which is considered to be the absorption band from which the emission gains intensity. The absorption spectrum has been subject to a number of interpretations in which this weak band has been given the label $d_{z^2} \rightarrow \pi^*$, $d_{xy} \rightarrow \pi^*$ and $d \rightarrow \pi(p_z)$ where $\pi(p_z)$ is the π-bonding 6 p_z metal orbital.[36] The emission spectrum exhibits an apparent Stokes' shift of 12,600 cm^{-1} and it has been suggested that a low-lying level not apparent in the absorption spectrum must be responsible for this emission. A band has been detected in the excitation spectrum at 28,000 cm^{-1} which, although a Stokes' shift of 5,000 cm^{-1} is still apparent, is attributed to the inverse singlet-triplet transition assigned to the double banded luminescence spectrum. The 35,600 cm^{-1} band is therefore designated the analogous singlet-singlet transition.[36] A shift of 1,800 cm^{-1} of the emission maximum with variation of counteranions for $[Pt(CN)_4]^{2-}$ shows the emissive state to contain a considerable amount of z character[161] which has resulted in the luminescence being labelled as $d_{z^2} \rightarrow \pi(p_z)$ phosphorescence, although polarisation studies indicate that the emission spectrum contains a considerable xy contribution, and

it has been suggested that the emission may contain contributions from a number of closely spaced levels.[36] The situation for low field complexes such as $[PtCl_4]^{2-}$ [162] is less confused, with good separation of the d-d and CT bands being apparent. The solid state emission spectrum at 77 K, although still showing a large Stokes' shift (5,000-8,000 cm^{-1}), is less sensitive to counterion effects, and polarisation studies of the emission show at least 70% is xy polarised, consistent with a small z axis contribution to the populated orbital. The emission has been assigned $d_{x^2-y^2}\,(^3A_{1g}) \rightarrow d_{xy}\,(^1A_{1g})$, although the possibility of a distorted excited state as indicated by the large Stokes' shift has been considered.

The emission lifetimes at 77 K bave been reported for a number of platinum(II) complexes with ligands of σ or π character.[137] In accordance with the above discussion, the σ bonding complexes are ascribed to d-d luminescence while the π-donor ligands of high LF strength, such as bipyridyl and pyridine, are considered to exhibit d-π*luminescence. While most of the lifetimes are >20 μs, indicative of phosphorescence, the π-ligand complexes exhibit a much longer lifetime (50 to 500 μs) than the σ bonding ligands (1 to 10 μs), which is suggested to be caused by the larger effect of SOC on the metal-centred states. It is also noted that the cis isomers show a shorter lifetime than their trans counterparts. A comparison of the relative quantum yields and lifetimes for changes in counterion of $[Pt(NCS)_4]^{2-}$ indicates that the effect is mainly due to changes in the non-radiative rate, k_n, assuming ISC to the emitting state to be unity, and is related to the vibrational coupling of the counterion through hydrogen bonding to the chromophore rather than ion-ion coupling. Changes in the molecular geometry of cis and trans forms are thought to

affect the radiative rate, k_r, as well as k_n, but no quantitative correlation could be made. It is, therefore, concluded that both k_r and k_n are determined by the molecular environment. Preliminary temperature dependence studies between 77 K and 278 K indicate that all of the complexes show a relatively small effect ($\sim$ 20 fold) on lifetime between these extremes with the quantum yield (ϕ) showing a similar dependence in all but the trans forms of neutral complexes, such as trans-$[Pt(gly)_2]$, trans-$[Pt(NH_3)_2Cl_2]$ and trans-$[Ptpy_2Cl_2]$ for which ϕ is relatively unaffected, indicating that k_r is temperature-sensitive in these cases. The temperature-dependence of the other complexes is attributed to k_n through enhanced vibrational coupling with the lattice at higher temperatures.

Preliminary reports of luminescence of platinum(II) complexes[161,36] in glassy solution indicate that there are major differences from the crystalline state. The luminescence from $[Pt(bipy)Cl_2]$, $[Pt(bipy)(en)]Cl_2$ and trans-$[Pt(gly)_2]$ in frozen methanol (77 K) shows a change from the diffuse solid state emission spectrum to a highly structured emission with three or four prominent peaks. In the case of $[Pt(bipy)Cl_2]$ and $[Pt(bipy)(en)]Cl_2$, the emission spectrum shows a distinct shift causing overlap with the red tail of the first absorption band, although trans-$[Pt(gly)_2]$ shows an enhanced Stokes' shift of 5,600 cm^{-1}. The spacing of these peaks for the bipyridyl complexes is $\sim$ 1,300 cm^{-1}, which is the same as for $[Ru(bipy)_3]^{2+}$ [41] reported earlier, and it has been suggested that the emission may be CT in nature, indicating a possible crossover of the lowest-energy excited state in going from solid to solution for the low LF case of trans-$[Pt(gly)_2]$. Further similarity is indicated by the report of room temperature luminescence from $[Pt(QO)_2]$ [37] in dimethylformamide, which

shows a blueshift of the emission maximum of ∿ 1,000 cm^{-1} on going to liquid nitrogen temperatures, which may be due to the presence of a number of thermally equilibrated emitting levels, the excess splitting being caused by the enhancement of SOC in this system. The effect of SOC is illustrated by the exceedingly fast ISC rate of << 8 ps for population of the emitting level or manifold in [Pt(porphyrin)],[163] indicating an assumption of unitary efficiency for this process to be valid. Quenching studies on the excited state of $[Pt(QO)_2]$ [164] have revealed the presence of a dynamic electron-transfer mechanism, indicative of a charge-transfer state, and the redox potential of the excited state has been estimated as -0.95 V, suggesting a strong reducing power.

2-2.7 The photochemistry of platinum(II) complexes

The photochemistry of platinum(II) complexes may also give some insight into the nature of the emitting level, assuming both photoreaction and emission to occur from the same state, but the marked effect of platinum(II) luminescence on environment makes any real quantitative comparison restricted to cases where both phenomena are studied under parallel conditions. Irradiation of these complexes has been found to give either ligand substitution reactions, cis/trans isomerisation or oxidation-reduction processes,[165,56] depending upon the nature of the ligands and the conditions. The large Stokes' shift observed for the emission has been interpreted in terms of a tetrahedrally distorted excited state, giving greater ligand lability and an associative mechanism for the case of ligand-substitution reactions. The photochemistry of $[PtCl_4]^{2-}$ in aqueous solution is restricted to photoaquation, but the

quantum yield shows a marked dependence on irradiation wavelength, with excitation at 254 nm in the CTTM band giving a yield of 0.9, whereas irradiation in the LF region produces a yield of only 0.17.[166] This result is explained in terms of two photoreactive states, a lower LF state (^3E_g) and a higher CTTM($\pi_{Cl} \rightarrow \sigma^*_{Pt}$) $^1B_{1g}$ state, the sensitisation of the LF state photoreaction by $[Ru(bipy)_3]^{2+}$ [167] and biacetyl[168], making the possibility of a 'hot' ground state reaction unlikely. Studies of photoisomerisation reactions have revealed that the cis form is predominantly photosensitive, with the trans form being almost inert.[165] This result is the reverse of that found for luminescence where the trans forms are longest lived,and this may be indicative of a photochemical non-radiative pathway. For the case of cis-$[Pt(gly)_2]$, sensitisation studies have shown that the excited state has a geometry significantly distorted from the ground state[169] in line with the emission studies noted earlier. In fact, the Stokes' shift is so large that the molecule may well assume a totally different geometry in the excited state. The photochemistry of the polypyridyl complexes of platinum(II) in fluid solution has not been subject to full investigation, but preliminary reports indicate the complexes to be relatively inert, although the presence of oxygen quenching adds support to a CT assignment.[20]

From the discussion, it is apparent that a great deal more work of both a photophysical and photochemical nature needs to be undertaken before a complete understanding of this rather confused picture can be attempted. It is hoped that the findings reported in this work will help clarify the situation.

2-3 The Luminescence of the Uranyl Ion ($[UO_2]^{2+}$)

2-3.1 Spectroscopic studies of the absorption and emission spectra of $[UO_2]^{2+}$

The luminescence of $[UO_2]^{2+}$ has received continuous interest[2,170] stimulated by both its proposal as a chemical actinometer[171] and the nuclear implications of the species in general. It is, therefore surprising that this subject, which was first investigated in 1852,[172] is still relatively confused compared with the more recently studied inorganic systems, and this can be attributed to both its inherent complexities and the need to eliminate adventitious impurities toward which the uranyl moiety is extremely reactive.

X-ray diffraction data have shown that the uranyl ion is linear with short bonds (1.749 Å) which are thought to be covalent, indicating a significant contribution from π-bonding and displays a co-ordination number of 4,5 or 6 depending on the other ligands.[170] This interpretation has been extended to solution studies, and the presence of weak 'forbidden' fundamental vibrations in both the Raman and infra-red spectra which may be caused by an angular UO_2 molecule, have been explained by the interaction of the electric fields of the solvent and ligand environment.[1] The solvated $[UO_2]^{2+}$ molecule is, therefore, assumed to have $D_{\infty h}$ symmetry. The ground state configuration of the free uranium atom is $5f^3 6d^1 7s^2$ and combination of these one-electron atomic orbitals with the 2p-orbitals of the oxygen atoms in the $D_{\infty h}$ point group produces a set of MO orbitals for the uranyl ion[173] and yields a ground state configuration of $(1\sigma_u^+)^2(1\sigma_g^+)^2(1\pi_u)^4(1\pi_g)^4$, giving a totally symmetric $^1\Sigma_g^+$ ground state. This treatment gives the U-O bond as a triple bond, comprised of one σ and two π linkages. The π-bonding is attributed

to the 6d metal orbital[173-175], whereas the origin of the weaker σ bonding is less certain but is thought to be due to the 5f metal orbitals[173,174] from both magnetic susceptibility measurements, by which the temperature-independent paramagnetic components of the overall diamagnetic susceptibility of the uranyl complexes is accounted for,[173] and theoretical arguments.[174] However, the 6d orbital is also thought to participate in σ bonding[175] which may also explain the observed magnetic behaviour. The nature of the bonding to the co-ordinating ligands is also uncertain with the extent of the 5f orbital participation being disputed[174] and the 6f[176] and 6d[173] orbitals also being considered to contribute.

The absorption spectrum of the uranyl ion is very susceptible to environment, to the extent that it has been suggested by one set of workers[177] that the ligand geometry plays a major role in the positioning of the absorption bands, indicating that account must be taken of the total complex geometry rather than the central $D_{\alpha h}$ symmetry of the uranyl moiety as used above. However, the photochemical properties of these systems are predominantly those of the uranyl species and the preceding discussion is still valid.[170] The absorption spectrum of the hydrated uranyl ion, $\left[UO_2(H_2O)_6\right]^{2+}$, taken in a non-complexing aqueous perchlorate medium to prevent hydrolysis, shows complicated vibronic structure in the weak low-energy, unresolved absorption band between 330 nm and 500 nm, with a series of progressively stronger bands towards higher energy. The luminescence spectrum overlaps the low-energy band slightly, and is also highly structured, extending from 450 to 600 nm.[172] The most rigorous investigation of these spectra has been presented by Bell and Biggers[172,178] who used a non-linear

least squares computer fit to resolve the entire absorption spectrum into 24 bands and the luminescence spectrum into 6 bands. In accord with a model proposed earlier by McGlynn and Smith,[173] they initially assigned the first 13 bands into three series representing three components (21,329 cm^{-1}, 24,107 cm^{-1} and 27,731 cm^{-1}) of a low-lying triplet state, $^3\Pi_\mu$, $(1\sigma_u^+)^2(1\sigma_g^+)^2(1\pi_\mu)^4(1\pi_g)^3(\delta\mu)^1$ split by the high degree of SOC (1481.9 cm^{-1}) and gaining intensity from two higher-energy perturbing singlet states. The luminescence was considered to occur from the lowest level of this state due to the excellent agreement between the positions of the resolved emission bands and the first series of bands in the absorption spectrum. In a later, more complete, report[178] they considered the above triplet to account for the first twelve bands, with the next seven being due to another excited triplet state $^3\Delta_u$ (25,800 cm^{-1} to 34,000 cm^{-1}), also proposed by McGlynn and Smith,[173] with the other five bands representing five perturbing high-energy singlet states whereas only two singlets had been previously assumed.[172,173] A closer inspection of the six bands in the luminescence spectrum revealed that five had a spacing of 855 cm^{-1} (the ground state symmetric vibration frequency) while the sixth achieved a spacing of 768 cm^{-1} from the next lower energy band. It was, therefore, suggested that emission occurred from the first two vibrational levels of the lowest component of the excited triplet state $^3\Pi_\mu$ (20,582 cm^{-1}, 21,270 cm^{-1}), although only a minimal contribution (4.66%) is expected from the upper level, to at least the first five vibrational levels of the ground state.

Although the intricate details are open to question, the general model which essentially assumes that the absorption

spectrum arises by transitions from the highest occupied π-bonding molecular orbital (HOMO) to the lowest unoccupied molecular orbital (LUMO) consisting of a uranium 5f orbital is reasonably well accepted, and has been used to explain the quenching of the uranyl ion luminescence by a variety of substrates[179] as the production of a U(V) core coupled with a deficient π-bonding orbital upon excitation implicates both a reducing and an oxidising character for the excited species. The exact nature of the HOMO has been challenged by Jörgenson,[180] who considers it to be a loosely bound π-bonding 2p orbital of oxygen with π_u symmetry rather than a full MO of uranium 6d or 5f and oxygen 2p orbitals. However, while these treatments may differ theoretically, their experimental implications are similar, since McGlynn and Smith's[173] model shows most of the electron density to be distributed on the oxygen atom in the HOMO, and the luminescence can be viewed as an $f \rightarrow \pi$ transition. The assignment of the luminescence to phosphorescence or fluorescence is also controversial, with the above treatment of Bell and Biggers favouring phosphorescence, a result supported by other workers.[181] Other groups, however, envisage the lower energy absorption bands as due to singlet-singlet transitions, indicative of fluorescence.[182] Perhaps the most comprehensive interpretation is that of Jörgensen[180] who suggests that SOC is so large ($\sim$ 2,000 cm^{-1}) that it plays more than just a perturbing role as previously assumed in theoretical treatments, and spin labels are not meaningful, a situation paralleled in the heavier-metal systems mentioned earlier.

2-3.2 Non-radiative relaxation of the excited state of the uranyl ion in an aqueous environment

The characteristic, highly structured luminescence of the uranyl ion is apparent in both solid state and solvated forms[2] and emission studies indicate that both ligand and environment play a major role in non-radiative relaxation pathways of the excited state, especially in solution where the luminescence yield is considerably lower ($\sim$ 0.25 for uranyl sulphate in sulphuric acid at 298 K[2]) than the unitary yield often found in crystals.[2] The nature of these non-radiative processes are certainly chemical, as indicated by the extensive photochemistry of the excited state,[120] but may also be partly physical, as suggested by changes in the luminescence yield with viscosity.[2] The uranyl luminescence is sensitive to temperature,[184] concentration[183] and pH[184] as well as solvent, and care must be taken in defining exact conditions for any results to be meaningful. This is particularly true in aqueous solutions where a number of hydrolysed forms are known to be possible.[2] Lifetime measurements show that the luminescence obeys good first-order kinetics under most conditions, although multi-exponential decays have been reported for some inorganic glasses,[185] attributed to multi-site emission, and some frozen organic solvents,[186] considered to be due to a number of different complexed species. Further insight into the nature of the excited states has come from the report of an ESA spectrum following flash photolysis of an aqueous 0.02 M uranyl perchlorate solution.[170] The ESA which shows vibrational structure with a peak at 590 nm has been shown to be due to the emitting state by the coincidence of the lifetimes of the ESA and the emission ($\sim$ 2.2 μs at 298 K) and by parallel quenching of both phenomena.[187]

The spectrum is assigned to the transition from the $^3\Pi_\mu$ state defined by McGlynn and Smith[173] to a higher lying triplet state because of the highly intense nature of the transition. The higher state is situated at 38,750 cm^{-1} which coincides with the position of the low-energy singlet-singlet transition in the Bell and Biggers[176] model and it is speculated that this level may be degenerate, giving rise to the observed triplet level upon excitation of the $^3\Pi_\mu$ state.[170] The vibronic structure of the ESA gives a spacing of 580 cm^{-1} which can be compared to the spacings of 855 cm^{-1} and 715 cm^{-1} given for the symmetric stretching frequency of the molecule in the ground and first excited state respectively.[178] This suggests that the U-O bond is progressively weakened,[188] a result which is consistent with proposed model of McGlynn and Smith.[173]

The effect of solvent and ligand on the uranyl luminescence has been most frequently studied using isotopic substitution, as demonstrated by the study of $[UO_2(CH_3COO)_2(H_2O)_2]$[189] crystals in which acetate deuteration both at 77 K and 298 K gives an isotope effect of $\sim$ 1.14 whereas deuteration of the water molecules produces an isotopic effect of $\sim$1.6 on the emission lifetime for both these temperatures and suggests that high frequency O-H vibrations provide a more efficient non-radiative deactivation pathway than the lower frequency C-H vibrations, a result also found from the isotope effects of a number of uranyl complexes in frozen solution at 80 K.[190] This latter report gives an isotope effect of $\sim$ 6 for the uncomplexed solvated $[UO_2(H_2O)_6]^{2+}$ species which drops to between 1.2 and 1.8 for anionic complexes, where water molecules are excluded from the ligand sphere. An isotope effect of $\sim$ 1.9 has been reported for $[UO_2(H_2O)_6]^{2+}$ on deuteration of the bulk solvent at 298 K.[188] These results indicate that a weak

coupled deactivation mode is operative, especially in aqueous solution, as indicated by the distinct shortening of the lifetime (1.0 μs for 0.01 M $(UO_2)(ClO_4)_2$) on going to this pure medium from higher acid concentrations (58 μs for 0.01 M $(UO_2)(ClO_4)_2$ in 10 M $HClO_4$).[191] However, the mechanism by which this deactivation process operates is uncertain, and three possibilities have been proposed by Burrows and Kemp[170] in a recent review:-

(i) Physical (intramolecular) deactivation <u>via</u> the O-H stretching modes of co-ordinated water molecules.

(ii) Intermolecular energy transfer from the excited uranyl ion to the vibrational modes of the solvent water molecules.

(iii) Chemical deactivation of excited uranyl ion ($[UO_2]^{2+*}$) by hydrogen abstraction from water.

$$[UO_2]^{2+*} + H_2O \longrightarrow [UO_2H]^{2+} + \dot{O}H$$

While the first explanation is certainly true for the solid state case as exemplified by the uranyl acetate example given earlier, the onset of diffusional modes makes the latter two possibilities also likely and the authors point out that while no e.s.r. signal of $\dot{O}H$ could be detected for photolysis of uranyl perchlorate in an aqueous glass, the uranyl ion has been shown to exchange its oxygen atoms with H_2O^{18} upon irradiation, giving weight to the third possibility, and the failure to observe $\dot{O}H$ may be due to a rapid back reaction between the $\dot{O}H$ and U(V) species. The mechanism, which is essentially that of electron-transfer coupled with proton-transfer, gains support from quenching studies of the uranyl ion by aliphatic alcohols for which a radical intermediate has been detected both at low temperatures (77 K)[182] in glassy alcoholic solution and in viscous solutions at 200 K.[193] Further support for a chemical pathway comes from a recent study of the quenching of 0.01 M $[UO_2]^{2+}$ by water in a series of perchloric

acid and perchlorate solutions.[191] The results indicate that it is the acidic content (H^+) rather than the anion which is effective in prolonging the lifetime of the species in concentrated acid solution. The marked temperature-dependence of the lifetime in a series of acid concentrations between 285 and 323 K has also been studied, and activation energies which increase slightly with increasing concentration of acid between 40 (0.01 M $HClO_4$) and 52 kJ mol^{-1} (1 M $HClO_4$) were found. This compares favourably with the activation energy of 41.2 kJ mol^{-1} given for the 0.04 M uranyl ion transient in 0.23 M $HClO_4$.[183] This temperature-dependence is not found in other heavy metal luminescence systems, such as Eu^{3+}, where energy transfer is known to occur[194] but a similar activation energy ($\sim$ 42 kJ mol^{-1}) is found for the electron-transfer processes of many other metal ions involving co-ordinating water molecules such as Fe(II) to Fe(III), indicating that quenching of the uranyl ion by water is an electron-transfer process. Further, the increase of emission lifetime with increased acid concentration and the retarding of the quenching action in neutral uranyl complexes confirms this view. However, the authors suggest that electron transfer of the form

$$[UO_2]^{2+*} + H_2O \rightleftharpoons [UO_2]^{+} + H^+ + \dot{O}H + e^-$$

is more likely than hydrogen abstraction, a mechanism which was also originally proposed by Kemp et al.[183] This mechanism is favoured because of the necessity of a fast back reaction needed to explain the absence of the $\dot{O}H$ radical, and the authors[191] consider the above mechanism to allow more freedom for back reaction than that of hydrogen abstraction, which they consider to provoke decomposition of the intermediate. The process, which is considered to be intermolecular, as the ligand exchange rate of water is expected to be > 1.25 x 10^6 s^{-1}, the observed ground

state exchange rate at 298 K, has been treated in terms of Marcus Theory,[195] which treats the electron-transfer reaction between two spherical molecules by the equation

$$k = Z \exp(-\Delta G^*/RT) \qquad (2\text{-}10)$$

where k is the bimolecular electron-transfer rate, Z is the bimolecular collisional frequency of the reaction (10^{10} to 10^{11} M^{-1} s^{-1}), T is the absolute temperature, R is the gas constant and ΔG^* is the activation energy of the encounter complex given by the equation

$$\Delta G^* = (\lambda/4)(1 + \Delta G/\lambda)^2 \qquad (2\text{-}11)$$

where λ is the solvent reorientation energy needed to form the encounter complex and ΔG is the standard free-energy change of the reaction calculated, in this case, from the standard redox potential, E_2, of the reaction $\dot{O}H + H^+ + e \rightarrow H_2O$, E_1, the standard redox potential of $[UO_2]^{2+}$ (0.06 eV) and ΔE the change in potential of the ground and luminescent states (2.64 eV) to give:-

$$\Delta G = 0.12 - 0.059\ pH\ (eV) \qquad (2\text{-}12)$$

Using this expression, and by assuming λ to be 42 kJ mol^{-1}, the observed activation energy for the quenching by water, k was calculated as 10^8 M^{-1} s^{-1} ($Z = 10^{11}$) or 10^7 M^{-1} s^{-1} ($Z = 10^{10}$), which is 3 or 4 orders of magnitude larger than that observed experimentally (7.6×10^3 M^{-1} s^{-1}). The theory does, however, correctly predict the quenching rate for chloride ions (5.6×10^9 M^{-1} s^{-1} *cf.* 1.4×10^{10} M^{-1} s^{-1} observed experimentally). They explain the discrepancy in terms of the hindrance of the diffusional process caused by steric effects, as the two molecules are not spherical, and they suggest overlaps of the HOMO of the uranyl ion and the non-bonding oxygen orbital of the water molecule may be required to facilitate forward electron transfer from the water

molecule to the uranyl ion. Similarly, they explain the lengthening of the lifetime in acidic solution as due to the formation of the hydroxonium ion, which stabilises the non-bonding oxygen orbital of the water molecule, making electron abstraction more difficult. Kazakov et al.[196] noted a similar effect for the luminescence intensity in perchloric acid which they attribute to the cleavage of the bonds between the uranyl ion and the water molecules in the secondary co-ordination sphere, thus reducing the number of deactivation routes.

Moriyasu et al.[191] results show that the non-radiative deactivation of the uranyl ion in aqueous solution is not just a simple diffusional electron-transfer process, and hydrogen abstraction cannot be discounted. Additionally, it is hard to see how the reported isotope effect for aqueous solutions at 298 K can be explained by any chemical mechanism other than the latter, and the proposals of significant hydroxonium ion concentration for low acidity solutions (0.01 M → 1 M $HClO_4$) seems unlikely when the water concentration is estimated as ∿ 55 mol dm^{-3}. A theoretical treatment of non-radiative transitions has been used to give support to hydrogen abstraction as the predominant deactivation mode at room temperature by Burrows and Formosinho[197], and has also been proposed by Marcantonatos[198] as the initial step in a deactivation scheme which involves the formation of an emitting exciplex, $[U_2O_4H]^{4+*}$. The scheme is based on studies of the uranyl luminescence in 10^{-2} M HNO_3 at 298 K, in which it was found that plots of ln $I_{L\lambda}$ against ln I_M, where $I_{L\lambda}$ is luminescence intensity at wavelength λ and I_M is the rate of light absorption at 406 nm were curved at 544 nm and at 554 nm for uranyl concentrations above 10^{-2} M but linear at 478 nm for all concentrations. Since no

change in the absorption spectrum was detectable, it was assumed that only the $[UO_2]^{2+}$ species was present, and the following scheme was proposed to explain the curvature:-

$$[UO_2]^{2+} \xrightarrow{h\nu} [UO_2]^{2+*}$$

$$[UO_2]^{2+*} \longrightarrow [UO_2]^{2+} + h\nu(1)$$

$$[UO_2]^{2+*} + H_2O \rightleftharpoons [UO_2H]^{2+*} + \dot{O}H$$

$$[UO_2H]^{2+*} \longrightarrow [UO_2H]^{2+} \xrightarrow{\dot{O}H} [UO_2]^{2+} + H_2O$$

$$[UO_2H]^{2+*} + [UO_2]^{2+} \rightleftharpoons [U_2O_4H]^{4+*}$$

$$[U_2O_4H]^{4+*} \longrightarrow [UO_2]^{2+} + [UO_2]^{+} + H^{+} + h\nu(2)$$

An analysis of this scheme was undertaken to produce relevant kinetic expressions which describe the observed behaviour, based on substitution of the derived expressions for $[UO_2]^{2+*}$ and $[U_2O_4H]^{4+*}$ from a steady-state treatment into the expression $I_{L\lambda} = q\, k_{rU}\left[[UO_2]^{2+*}\right] + k_{rE}\left[[U_2O_4H]^{4+*}\right]$ for the luminescence intensity, where q is an experimental constant. This results in the expression:-

$$\ln I_{L\lambda} = \ln \phi_\lambda + \ln I_M \qquad (2\text{-}13)$$

where ϕ_λ is the experimental quantum efficiency at wavelength λ. At 478 nm, and low I_M, ϕ_λ is considered to contain no contribution from the exciplex, and is given by the intercept of the low intensity 'linear' portion of the curve in the latter case. At high I_M, ϕ_λ features contributions from the exciplex as well as the uranyl ion, which represents a more complicated situation; it is estimated as the intercept of the 'linear' high intensity portion of the curve. Similarly, the more detailed properties of the set of curves can be explained within this model in particular the derivation of an equation for the exciplex concentration shows a dependence on the uranyl concentration, and this is used to explain the onset of curvature at a lower I_M as the uranyl concentration is increased. Further support comes from

self-quenching studies involving variation of the uranyl concentration at a fixed I_M. The results can be fitted to the full expressions for ϕ_λ for the relevant cases, and it is noted that it is the activity rather than the concentration of the uranyl ion which is important. The spectrum of the proposed exciplex is given by the difference of the luminescence spectra at 10^{-2} M and 6 x 10^{-2} M uranyl concentrations, and is shown to have vibrational structure with an $\sim$120 cm^{-1} smaller spacing than the vibrational progression of the $[UO_2]^{2+}$ case, indicating an expected weakening of the U-O bond. A red-shift of the spectrum occurs on lowering the temperature to 207 K, which is considered to support hydrogen involvement in the exciplex. This dual luminescence model has also been used to explain the acidity effect on the uranyl luminescence,[199] the pertinent result being the reversion back to linearity of the ln $I_{L(554)}$ *vs.* ln I_M plot on going from pH 1.94 to pH 2.7. This result is considered to indicate the effective decomposition of the $[UO_2H]^{2+*}$ before it is able to form the emitting complex at lower acid concentration through hydrolysis.

$$[UO_2H]^{2+*} + H_2O \rightleftharpoons [UO_2]^{+*} + H_3O^+$$

This equilibrium suggests that the $[UO_2H]^{2+*}$ species will be stabilised at higher acidities, thereby promoting more efficient formation of the emitting exciplex, which would also explain the lengthening of the emission lifetime at higher acidities, as previously reported.[191] Presumably, the emission is attributed to the exciplex, as no deviation from first-order kinetics was reported, indicating only one type of emission to be involved. However, while this step can be fitted into the previously proposed kinetic scheme to yield an expression for ϕ_λ which explains the observed results, the proton transfer to a water molecule seems

speculative. Marcantonatos[199] explains this as follows

$$\left[O \equiv U = O^{-H}\right]^{2+*} \rightleftharpoons \left[(O \equiv U = O)H\right]^{2+*}$$

$$\left[O \equiv U \equiv O\right]^{+*} + H^{+}$$

However, the lack of direct spectroscopic evidence for an emitting exciplex, such as a distinct change in the luminescence spectrum at the glassing point of an acidic solution, makes this kinetic scheme less convincing as there may well be other schemes which can yield kinetic expressions to fit the observed behaviour or the results may be due to the presence of more than one solvated uranyl species, as indicated by a recent report in which a number of hydrated species were observed for a uranyl concentration between $\sim 2 \times 10^{-4}$ and 2×10^{-3} mol dm^{-3} in 0.1 M KNO_3 at 298 K.[200]

The exact mode of radiationless deactivation is therefore still uncertain, although a chemical electron-transfer type process seems to be predominant at ambient temperatures, while a physical deactivation through the excited vibrational levels of the aquo-ligands is preferred at cryogenic temperatures.[189,190] The temperature-dependence of the emission lifetime has already been noted, and a study of this dependence can yield further information about the nature and importance of this process at different temperatures.

The temperature-dependence of the luminescence intensity of uranyl sulphate in sulphuric acid between 288 and 363 K was studied initially by Vavilov and Leoskin in 1928.[2] This data was supplemented by lifetime data for the full range of 70 to 300 K.[201] The Arrhenius plot showed a smooth curve which levelled out at $\sim$180 K to give a horizontal region at $180 > T > 77$ K. The temperature profile could be directly related to the temperature dependence of the solvent viscosity and indicated a single thermally-

activated process. However, recent studies of uranyl thermoluminescence following X irradiation[201] in this range suggested the presence of several distinct regions, and a more detailed analysis undertaken for uranyl solutions in varying concentrations (5 to 17.5 M) of sulphuric acid,[201] which was rapidly frozen to 77 K by liquid nitrogen showed, on heating, that both the lifetime and luminescence quantum yield followed the thermoluminescence trends, indicating that the previous assumption of a single activation process may be invalid and that the non-radiative pathway is affected by structural changes in the medium. Similar behaviour has also been reported by Bist[202] for 0.2 M uranyl nitrate solutions, although in this case the temperature variation of the fluorescence spectrum was considered to be due to the presence of different complexed uranyl species, the nature of these species being dependent upon the rate of cooling of the solution. However, as mentioned earlier, thermal activation energies of between 40 and 50 kJ mol^{-1} have been reported for aqueous solutions in a limited temperature range (205 to 323 K) which must either represent a higher state through which deactivation occurs non-radiatively to the ground state, not necessarily directly, or an intermolecular process which may be chemical or physical. The former possibility seems unlikely as these activation energies correspond to an energy gap of between 3260 and 4100 cm^{-1} and the next higher level has a spacing of $\sim$ 10,000 cm^{-1} from the excited state. Therefore this activation energy must correspond to direct deactivation from the state and the preceding discussion would indicate this to be a chemical mechanism in aqueous solution.

2-3.3 Chemical quenching of the uranyl ion luminescence by organic molecules

The quenching of the uranyl luminescence by a number of types of organic molecules and inorganic ions have shown that the excited state has a versatile behaviour which is dependent upon the nature of the quenching substrate.[170] The quenching action of aliphatic alcohols has been studied extensively by both Kemp et al. and Matsushima et al.,and their results give a compelling argument for a diffusional hydrogen abstraction mechanism, expounded in the recent review by Burrows and Kemp,[170] the brief details of which are given here. The results show that good Stern-Volmer kinetics are obeyed by the quenching of the luminescence yield, the emission lifetime and the ESA lifetime, and all three are quenched in parallel,indicating a simple diffusional process. The quenching constant (K_{sv}) has been correlated to the quantum yield for photo-oxidation, as determined by the yield of U(IV),implicating a chemical process. Further, isotopic substitution of hydrogen at the weakest bond in the alcohol retards the quenching rate and reduces the yield of U(IV)to a similar extent which, together with the correlation of K_{sv} to the strength of the C-H bond for primary alcohols, implies a hydrogen abstraction mechanism. E.s.r. work has given direct evidence for the $RC\dot{H}OH$ radical for most primary alcohols confirming the mechanism,but results for secondary alcohols indicate that C-C cleavage occurs in preference to hydrogen abstraction. The former process is explained in terms of an electron transfer to the uranyl moiety, although whether this is intermolecular or via a CTTM transition within the uranyl-substrate complex is uncertain. Hydrogen abstraction has also been found by e.s.r. studies to be the predominant mode, in

competition with C-C cleavage, in a number of other aliphatic organic substrates (esters, aldehydes, ketones, etc.).

Recent studies of the ESA of aqueous $[UO_2]^{2+}$ in the presence of a series of aliphatic alcohols by Sergeeva et al.[203] have shown the production of the spectrum of a U(V) species following flash excitation. This gives further evidence of a mechanism involving uranyl reduction and hydrogen abstraction has also been proposed by Marcantonatos[204] for the quenching of the aqueous uranyl luminescence with methanol. He considers the quencher to form a transient exciplex with $[UO_2]^{2+*}$ in which a simultaneous overlap of the π-bonding HOMO and a σ bonding component of the $[UO_2]^{2+*}$ $^3\Pi_\mu$ orbital with the π_{CH_3} orbital of methanol occurs, and the quenching efficiency is determined by both the expansion and energy of the overlapping quenching orbital and the steric conditions needed to form the complex. The overall scheme for the quenching action of aliphatic alcohols can therefore be represented as

$$[UO_2]^{2+} \xrightarrow{h\nu} [UO_2]^{2+*}$$

$$[UO_2]^{2+*} \longrightarrow [UO_2]^{2+} + h\nu$$

$$[UO_2]^{2+*} + RCH_2OH \longrightarrow \underbrace{\left[[UO_2]^{2+*} .. RCH_2OH\right]}_{\text{encounter complex}} \xrightarrow{\text{chemical quenching}} [UO_2H]^{2+*} + R\dot{C}HOH$$

$$\left[\text{encounter complex}\right] \xrightarrow{\text{physical quenching}} [UO_2]^{2+} + RCH_2OH + \text{heat}$$

The physical quenching mode has been proposed for heavier alcohols in which steric hindrance prevents the chemical mechanism[205] in cases where energy transfer is feasible. The quenching action of aromatic molecules is distinctively different from that of the above case as no net photochemical products are formed and no isotope effect has been found. The correlation of K_{sv} with the

polarity of the aromatic molecules as given by the Yakawa-Tsano σ constant of the substituent, for a series of substituted benzenes, indicates an interaction of the excited uranyl moiety with the π-electron aromatic system. Although there is no direct evidence, an exciplex in which charge is transferred from the aromatic π cloud to the uranyl ion has been proposed which may decay either by the reverse reaction or by its own deactivation to the ground state.[206,207]

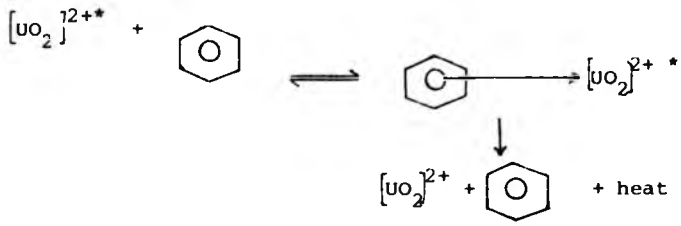

2-3.4 The quenching action of metal ions in the luminescence of the aqueous uranyl ion

The quenching of uranyl luminescence by metal ions has been studied extensively of late.[179,208-211] The pertinent conclusion is that quenching occurs by an intermolecular diffusional process involving electron transfer to the uranyl ion by the quencher unless this is energetically impossible, as in the case of cations, when diffusional energy transfer, sometimes accompanied by sensitised reaction of the quencher, occurs. Evidence for an electron-transfer process has come from correlation of K_{sv} with the oxidation potential of the metal ion,[209,208] the lack of correlation with the atomic weight or magnetic moment of the metal ion[208-210] indicating heavy atom and paramagnetic effects not to be important, and the occurrence of quenching under energetically unfavourable conditions for energy transfer.[209] Direct evidence for the case of electron transfer has been found for the case of quenching by Mn^{2+} ions in aqueous solution.[208]

Flash photolysis of this system produced the characteristic transient of Mn^{3+}, giving definite proof of an electron-transfer mechanism, and indicates that there is complete formation of the oxidised species so that a CT exciplex intermediate can be ruled out. The electron-transfer mechanism can be explained in terms of the MO model of McGlynn and Smith.[173] On excitation, an electron is transferred from the HOMO (π) to the LUMO (5f) orbital of the uranyl ion, leaving a hole in the HOMO (π) to which electron transfer from the quencher occurs. However, this leaves a hole in the HOMO (q) of the quencher and reverse electron transfer from the LUMO (5f) of the uranyl ion to this orbital occurs.[211] The model suggests that electron-transfer will only occur if the HOMO (q) effectively overlaps the two uranyl orbitals at the same time, implying a steric hindrance to the process, and is similar to the model proposed for alcoholic quenching by Marcantonatos,[204] although the consequences differ. The quenching rate, k_q, shows a charge dependence and is most efficient for ions in lower oxidation states, e.g. for Ag^+, k_q is $\sim 4 \times 10^9$ M^{-1} s^{-1} but for Cr^{3+}, $k_q = 3.0 \times 10^6$ M^{-1} s^{-1}. This dependence has been explained in terms of electrostatic repulsion, and the process is thought to be always diffusion-controlled.[179]

Energy transfer has been proven in the cases of $[Co(CN)_6]^{3-}$ and $[Cr(en)_3]^{3+}$ [209] for which sensitised reactions occur, and for Eu^{3+} [174] which shows sensitised luminescence.

2-3.5 The photochemistry of the complexed uranyl ion in solution

As mentioned earlier, the uranyl ion is capable of forming ground state complexes with a number of ligands, especially carboxylic acids, an indication of which is a substantial change in the ground state absorption spectrum which has been attributed

to the presence of CTTM bands.[170] Excitation of these complexes results in the destruction of the carboxylate ligand, although the exact mode depends upon the nature of the acid. The most extensively studied example is that of the uranyl oxalate system[170,2] which finds use as a chemical actinometer. In this case the complex, which is dependent upon pH, is expected to be a 1:2 uranyl:oxalate complex for the pH range 1.7 to 4.5[212] in aqueous solution which has been shown by a number of studies, e.g. a plot of the initial reaction rate against oxalate concentration shows a plateau at a 1:2 ratio with the uranyl ion concentration.[212] These studies have resulted in a comprehensive picture of the photolysis of the system being produced.[212]

$$[UO_2]^{2+} + 2\ C_2O_4^{2-} \rightleftharpoons [UO_2(C_2O_4)_2]^{2-}$$

$$[UO_2(C_2O_4)_2]^{2-} \underset{\text{dark}}{\overset{h\nu}{\rightleftharpoons}} [UO_2^*(C_2O_4)_2]^{2-} \quad (X)$$

$$X \rightleftharpoons [UO_2^*(C_2O_4)] + C_2O_4^{2-}$$

$$X + H_2O \longrightarrow [UO_2]^{2+} + C_2O_4^{2-} + CO_2 + HCOO^- + OH^- \quad (a)$$

$$X \longrightarrow U(IV) + C_2O_4^{2-} + 2CO_2 + 2O^{2-}$$

$$[UO_2^*(C_2O_4)] + H_2O \longrightarrow [UO_2]^{2+} + CO_2 + HCOO^- + OH^- \quad (b)$$

$$[UO_2^*(C_2O_4)] \longrightarrow U(IV) + 2CO_2 + 2O^{2-}$$

The production of U(IV) is exceedingly small, and reactions (a) and (b) are the predominant rate-determining steps, which are expected to proceed via a U(V) ($[UO_2]^+$) intermediate.[211] This indicates that the reaction is essentially a sensitised breakdown of the oxalate ligand produced by a CTTM transition to give a U(V) species which is then reconverted to the U(VI) state.[170]

Studies of other carboxylic acid systems have included:-

(i) benzilic acid,[170] in which the presence of the diphenylketyl radical intermediate has been detected by flash photolysis and e.s.r. studies, indicating a CTTM transition to give oxidative

decarboxylation is involved. The final product is benzophenone; (ii) Lactic acid,[2] citric acid[213]. These differ from oxalate in that U(IV) can be formed in abundance. The nature of the overall product is dependent upon the medium for lactic acid, which gives acetaldehyde and carbon dioxide at high pH and pyruvic acid at low pH. In contrast, citric acid gives acetone and carbon dioxide as overall products for all conditions (pH 1 to pH 3.5), although the yield varies as indicated by ϕ(U(IV)) which varies from 0.03 (pH 1) to 0.99 (pH 3.5). The reaction is expected to go through U(V) and ketocarboxylic acid intermediates, and the absence of a competing reaction is suggested to be due to the increased stability of the chelate ring in the 1:1 uranyl:citrate complex; (iii) Formic acid.[214] This system also shows appreciable formation of U(IV) and is thought to proceed either by direct decomposition of a uranyl:formate complex of unknown composition or by sensitised decomposition of the formate substrate, depending upon the formate concentration in the pH range 1 to 4, with U(IV) and CO_2 being the only two detectable products.

(iv) Acetic acid and its homologues.[170] The e.s.r. work on these systems indicates that α-hydrogen atom abstraction is the main mechanism in concentrated solutions of the substrate, whereas decarboxylation is preferred in dilute aqueous solutions, both mechanisms occurring through a U(V) intermediate involving an intramolecular CTTM transition.

This discussion shows that the excited uranyl ion is very reactive towards a number of substrates, mainly by means of either an intra- or intermolecular CTTM mechanism. This makes it very useful in photosynthesis, but also means extreme care must be taken in purification of reactants to avoid unwanted side reactions and irreproducibility. The basic pattern of a thermally activated

non-radiative pathway combined with temperature-insensitive routes is reminiscent of the general model proposed in the introduction,and this scheme has been used to elucidate further the role of the non-radiative pathway in the excited state chemistry of the uranyl ion, as will be shown later.

2-4 Aims of this work

The preceding introduction has illustrated the potential use of the photo-excited state of many inorganic systems, both in a more general sense as either sensitisers or in direct use in chemical and electrical solar energy conversion schemes, and in the synthesis of novel chemical compounds as well as providing a source of intriguing and unusual chemistry, both through their own photoreactions and the sensitisation of other chemical reactions. One of the most powerful probes into the nature and deactivation of the excited state is the luminescence (when observable) of that level, and this fact has been used in this work to study the properties of the excited states of the previously discussed systems in order to examine the effect of environment on these properties as well as to establish the deactivation modes and their importance in fluid solution at ambient temperatures for these systems, in order to ascertain the nature of the photoreactive state, which may be different from the luminescent state. This last statement underlines the aim of this work as few comprehensive studies of the luminescence of these systems have been reported and, therefore, the correlation between photochemical and quenching experiments in fluid solution at ambient temperatures and luminescence studies undertaken at low temperatures in crystalline or glassy media is uncertain as the possible effects of predominant deactivation through a higher (photoreactive) state and the perturbing influence of diffusional mechanisms (or both) are unpredictable.

The notable lack of photophysical data in fluid solution at ambient temperature can be attributed mainly either to the weakness of the luminescence at this temperature, or to the short emission lifetime. However, the advent of laser flash photolysis

has provided a tool with which this type of study can be attempted, and this work has been aimed at both elucidating the nature of the photophysical pathways predominant at these temperatures through environmental changes and trying to provide a unifying model to describe the luminescent properties of a system over a complete temperature range of 77 to 300 K through studies of the thermal activation of the luminescence lifetime over this range.

Each system which has been studied has its own particular problem to which this work has been addressed:

(i) Chromium(III). The problem in this system centres around the question as to the nature of the thermally-activated non-radiative deactivation of the emitting doublet state. The establishment of either back-ISC or photoreaction as this deactivation mode will allow inference about the nature of the photoreactive state and possible insight into the photochemical mechanism of individual systems.

(ii) Ruthenium(II). The ruthenium(II) luminescence has been thoroughly investigated at low temperatures (4 to 100 K) by Crosby et al.[53] and the resultant three-level model which has been developed is generally accepted. However, at elevated temperatures, this model requires modification. Van Houten and Watts[54] have included a fourth level of higher energy and have considered the low-lying three levels to be indistinguishable at elevated temperatures, and they have therefore treated them as one state. Kemp et al.,[215] however, have reported that the temperature profile of the luminescence can be ascribed to two temperature-activated pathways for studies of the same system ($Ru(bipy)_3^{2+}$ in H_2O and D_2O) over the same temperature range (273 to 373 K), and this work has been continued in order to

elucidate further the nature of the deactivation mode of ruthenium(II) luminescence at elevated temperatures.

(iii) Osmium(II). This system has received little attention, other than by inference, compared to the ruthenium(II) analogue. For low temperatures (4 to 100 K) the same three-level model as for ruthenium(II) has been used to explain the luminescence behaviour, with an enhanced SOC effect causing increased splitting of the levels. The aim of this work has been to extend the study to ambient temperatures to see whether this model still holds or whether the analogy with ruthenium(II) is invalid at ambient temperatures.

(iv) Platinum(II). The luminescence characteristics of $[Pt(QO)_2]$ make it of interest as a potential photosensitiser. However, little is known of the excited state properties of this novel complex, and it is hoped that flash photolysis studies can provide further information about the nature of the luminescence.

(v) $[UO_2]^{2+}$. The excited state of the uranyl ion is extremely reactive, and therefore presents a promising source of sensitised reactions and reactive radical intermediates. The aim of this work has been to consider the nature of the deactivation of the excited state in aqueous and organic media through the environmental effects (particularly concerning isotopic substitution) on the lifetime and thermal activation energy of the non-radiative deactivation of the excited state.

While each individual system shows typical behaviour for that system, they all show a thermally-activated luminescence, and it is hoped to illustrate the importance of temperature studies in elucidating the nature and significance of the deactivation of the excited state for a given temperature.

CHAPTER 3

EXPERIMENTAL METHODS AND MATERIALS

3-1 Instrumentation

3-1.1 Luminescence intensities and spectra

The measurements were performed on a Perkin-Elmer MPF-3 spectrofluorimeter, using a Hamamatsu R666S photomulitplier tube for $\lambda > 600$ nm and an RCA IP28 photomultiplier for $\lambda < 600$ nm. The dark current produced by the red-sensitive photomultiplier was not excessive, and cooling was not considered necessary. This model, which uses right-angle illumination, is a double-beam instrument and consequently the spectra are automatically corrected for lamp intensity fluctuation by feeding the reference lamp signal to the slide wire of the recorder and the sample signal to the sliding contact (pen) so that the voltage change caused by lamp fluctuation on both the slide wire and contact are balanced, which results in a constant pen position, as the pen servo-control monitoring the difference between these two voltages will sense no voltage difference. The spectra were not corrected, either for photomultiplier response or the transmittance and bandwidth of the analysing monochromator, although a reasonably 'flat' photomultiplier response was ensured throughout the relevant region of the emission spectra.

The instrument employs a 150 W xenon lamp as the excitation source which is passed through an excitation monochromator, allowing an excitation wavelength of between 220 and 800 nm to be chosen with a bandwidth of between 1 and 40 nm. The analysing monochromator is identical to the excitation analogue, and activates a photomultiplier whose amplified signal is fed to a chart recorder to give the luminescence spectrum, as described above. The emission or excitation wavelengths can be scanned at preset speeds by means of a motor

Figure 10

Sample cell arrangements used for ambient and low-temperature luminescence measurements.

(a) Aerial view of low-temperature sample cell holder insert for the Perkin-Elmer MPF-3 spectrofluorimeter

(b) Low-temperature sample cell and cooling arrangement

(c) Room-temperature sample cell

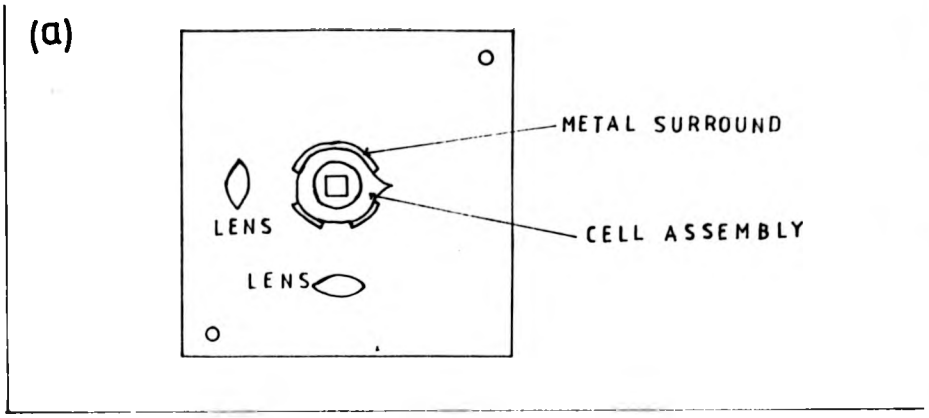
(a)
METAL SURROUND
LENS
CELL ASSEMBLY
LENS

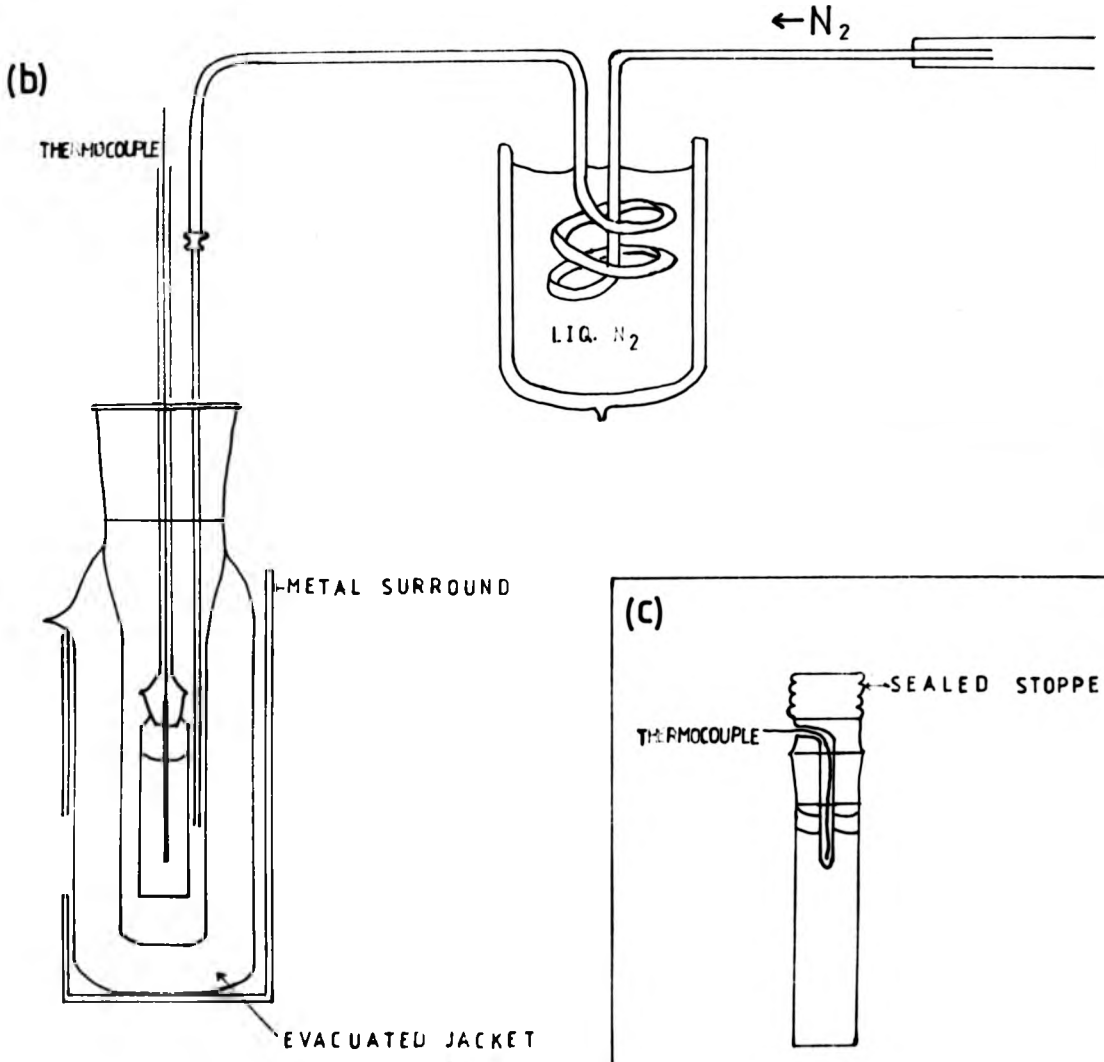
(b)
$\leftarrow N_2$
THERMOCOUPLE
LIQ. N_2
METAL SURROUND
EVACUATED JACKET

(c)
SEALED STOPPER
THERMOCOUPLE

to give either emission or excitation spectra,depending upon whether the emission or excitation wavelength control is engaged. The right-angle illumination mode of the instrument reduces effects from scattered light, sample cell luminescence and the portion of the excitation beam which is transmitted, and gives most accurate measurements when weakly-absorbing solutions are used which reduce inner filter effects caused by re-absorption of the luminescence to give 'front-facing'. For the luminescence spectra in polymer films, the films were mounted across the diagonal of the sample cell to give effectively front-face illumination.

The samples were thermostatted by means of a cell block, supplied with the instrument, through which a coolant was pumped, and the cell faces were prevented from misting by passing a flow of dried nitrogen over them. This set-up allowed temperature variation between 343 and 273 K when a refrigerated 'Churchill' pump unit was used with ethylene glycol as the coolant. The sample cell was sealed with a 'supa-sealed' capped stopper which contained a glass insert to allow the sample temperature to be monitored by means of a thermocouple placed in the insert, with a small drop of liquid paraffin to allow good thermal contact between the glass and the thermocouple (see Figure 10). This method allowed the temperature to be controlled accurately to 0.1 K, but is somewhat tedious in that up to 15 minutes between readings has to be allowed for thermal equilibration and is, of course, useless for very low temperature work, as the coolant will freeze.

A low temperature cell compartment has been designed to replace the existing cell compartment of the spectrofluorimeter, and is shown in Figure 10. The sample cell is placed in an

unsilvered quartz dewar which is surrounded by a metal shroud with appropriate spaces to allow entry of the excitation beam and exit of the emission, and acts as a safeguard against implosion of the dewar,which is cooled by passage of nitrogen through a stainless steel coil immersed in liquid nitrogen and heated by placing a water bath underneath the coil. Stainless steel tubing was chosen in preference to copper as the latter was found to produce contamination of the dewar on prolonged heating. A previous version had two coils, one for heating and one for cooling, but this was found to be inefficient and better control could be gained by controlling the gas pressure and position of the dewar over the coil. With this system, temperature equilibration is quite rapid, but it is more difficult to keep a stable temperature for the one or two minutes necessary to run a full spectrum of the sample, and an error of up to ± 2 K has to be tolerated for some readings, which may be compensated for to some extent by taking a large number of readings. This system, however, is considered to be superior to systems in which the liquid coolant is placed in the dewar, as this will cause scattering of the excitation and emission light resulting in 'noisy' spectra, although it is not as accurate as that developed by Crosby *et al.*[216] for front-face illumination for which an error of ± 0.02 K has been quoted. This method, which was originally developed for solid state samples, has been extended to include polymer films and involves an alternative technique of temperature control which allows temperature variation by means of a small resistance heater wrapped round a copper sample surround. This technique has been used by a number of workers,[4,75] although Harrigan and Crosby[216] have produced the most elegant refinement.

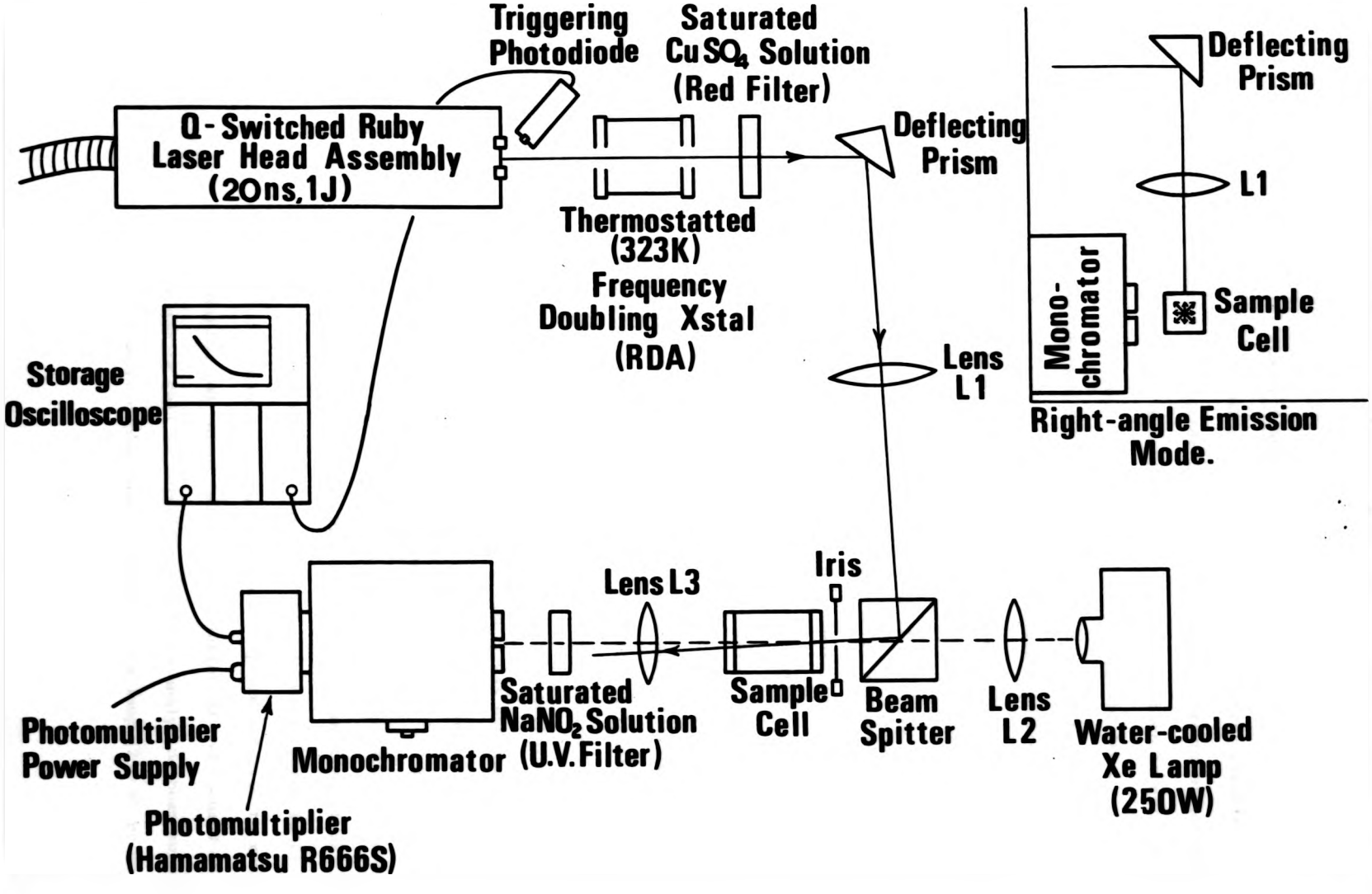

LASER FLASH PHOTOLYSIS ASSEMBLY

3-1.2 Laser flash photolysis

The technique of flash photolysis, first reported by Norrish and Porter in 1949,[217] has had a profound effect on the study of fast reactions. The technique, which is not limited to luminescent compounds, but can be applied to any molecule which absorbs light and is therefore almost universal in its application, is essentially a relaxation method in which an initial high energy pulse of light produces a momentarily large number of molecules in their excited state which absorb a following analysing pulse ('spectroflash') to give an excited state absorption (ESA) spectrum which can either be recorded on a spectrograph or as time dependent kinetics at a pre-set monitoring wavelength by attaching the photomultiplier output to an oscilloscope. In this original form, the limitation of this technique is the duration of the high energy lamp pulse, and although refinements produced lamps which carried the compromise of a short lifetime with high intensity to the micro-second domain, it was not until the production of a laser flash photolysis assembly in 1967[218] that this technique entered the nanosecond time domain. The assembly was essentially the same as the apparatus used for this work (supplied by Applied Photo-physics Ltd.), and is depicted in Figure 11. The red output (694 nm, $\sim$ 1 J/pulse) of the Q-switched ruby laser pulse is frequency doubled by an RDA crystal (thermostatted at 323 K) to give an $\sim$ 75 mJ ultra-violet (347 nm) output which is first passed through a saturated copper sulphate solution to remove any remaining red output before being deflected and focused on to the sample cell in coincidence with an analysing beam supplied from a water-cooled xenon high pressure lamp (250 W) by means of

a beam splitter and iris. Absorption of the laser pulse by the sample results in formation of the excited state in high yield which in turn absorbs the analysing beam resulting in a transient change in the intensity of the latter corresponding to the lifetime of the excited state. The change in the intensity of the beam is monitored at a preset wavelength by the analysing high radiance monochromator and photomultiplier (Hamamatsu R666S) after it has passed through a saturated sodium nitrite solution to remove any harmful laser output. The monochromator allows wavelengths between 0 and 999 nm to be selected with a bandpass of between 1 and 20 nm, and a slit-width of between 1 and 20 mm, and has a light gathering power of > 0.25 so that a reasonable bandwidth can be used to give a satisfactory photomultiplier signal to noise ratio. For the detection of right-angle emission, the arrangement is simplified as shown in Figure 11, and the laser beam is focused directly on to the sample cell. The transient photomultiplier output in both cases is recorded on a Tektronix 7623 storage oscilloscope equipped with 7A15A(y) and 7B50(x) amplifiers, which is triggered by a photodiode placed near to the front face of the laser head so that it 'sees' enough of the laser output to produce a triggering pulse. The resulting presentation is then photographed on to Polaroid Type 46-L film, using a Telford Type A oscilloscope camera, ready for analysis.

This technique, therefore, has essentially replaced the conventional lamp source with a laser to give a high-intensity coherent pulse of very short duration. It should be noted, however, that it is not the laser itself, which can be simply viewed as an optical amplifier inside a conventional Fabry-Perot etalon, which is responsible for this property, but the

Q-switching of the laser action which results in the 'giant' pulse. This statement can be understood by considering the nature of the laser action. The laser head consists of a partially reflecting sapphire front window and a rear total internally reflecting prism which acts as an optical resonator (Fabry-Perot etalon). In between these is placed a reflecting cavity containing a ruby rod (6" x ½") which is in line with these mirrors and a Wingent F12-120 flash tube lying in parallel above the rod. The whole cavity is flooded with circulating water refrigerated at 288 K to allow for good laser action. When the flash-lamp is fired by discharging a bank of capacitors (680 μF) through it (2 kV plus an initial 5 kV triggering pulse), the resultant light is absorbed by the chromium ions in the rod to excite a large number of molecules into the ^4F states from which they spontaneously decay into the ^2E state and gradually phosphoresce back to the ground state. The component of this phosphorescence, travelling normal to the mirrors of the optical resonator, is reflected between the two mirrors and amplified by stimulated emission from the ^2E state on each passage through the laser rod, losing a fraction (1-R) where R is the reflectivity of the front face mirror, during each oscillation. Laser action occurs when amplification and feedback are greater than the light losses within the cavity and a series of high intensity spikes of random intensity and separation are produced, lasting almost the duration of the flash ($\sim$ 1.5 ms) caused by the continuous feedback to the ^2E state throughout the lifetime of the flashlamp. There is, therefore, an obvious need to reduce the number of pulses to make the laser useful, and this is achieved by using a Q-switch where Q refers to the quality factor

of the optical resonator. The purpose of the Q-switch is to lower this factor so that no oscillation occurs during the pumping of the rod so that the gain (population inversion) builds up to a very high value. Once this reaches its peak, the Q-switch is opened and the gain per pass in the laser rod is now extremely high, resulting in a rapid build up of the oscillation with a simultaneous rapid exhaustion of the population inversion to produce the required high-intensity, sharp 'spike' which releases a (1-R) fraction of intensity on each oscillation to give a lifetime of $\sim$ 20 ns. A number of Q-switching methods have been developed, and include (i) mounting one of the two end reflectors on a rapidly rotating shaft so that the optical mirrors are only parallel for a brief moment, (ii) electro-optic switching with Kerr or Pockels cells which produce an electrically induced change in polarisation within the cell to prevent lasing of the polarised stimulated emission, the applied voltage being removed when optimum population inversion occurs, and (iii) a chemical Q-switch placed between the reflector cavity and the rear mirror which is mis-aligned with the reflector cavity to reduce oscillation caused by reflection from the front face of the Q-switch. The latter method, which is the cheapest and easiest, is the one adopted for this work, with the Q-switch consisting of a 1 cm cylindrical cell containing a reversibly bleachable dye (vanadyl phthalocyanine) in nitrobenzene. The concentration of the Q-switch is varied until an optimum pulse is produced (usually $\sim$ 0.3 optical density at 694 nm), a weak solution producing 'double pulsing' and an over-concentrated solution resulting in reduced efficiency and eventually loss of laser action.

Frequency doubling, as mentioned earlier, was produced by an RDA (rubidium dihydrogen arsenate) crystal thermostatted at 323 K and supplied by JK Lasers Ltd. This replaced the original ADP (ammonium dihydrogen phosphate) crystal, and gives a ten-fold improvement in ultra-violet output as well as the need for less critical adjustment, although the hydroscopic nature of the crystal makes it more susceptible to damage. Further changes to the original system have included the replacement of the deflecting mirror by a deflecting prism, which avoids the degradation of the mirror coating by the laser pulse and the change of the 347 nm filter in front of the monochromator which was found to luminesce by a saturated sodium nitrite solution in a 1 cm cylindrical cell which filters 347 nm light. As indicated previously, the apparatus can be used to give either ESA or emission measurements, and the method used for each case is given below.

(i) ESA measurement

As explained previously, the ESA transient is detected by the change in the analysing beam intensity. It is, therefore, imperative to ensure a stable power supply (in this case an iREM E2-X20P) so that fluctuations do not occur over the lifetime of the transient. Similarly, to observe weak, short-lived transients, an intense beam will be needed to reduce the effects of scattered light and provide an adequate photocathode current, and to facilitate this a pulsing unit is connected to the xenon arc lamp which increases the lamp intensity up to a hundredfold, depending on the wavelength, for approximately 1.5 ms. The pulse is flat to within 5% for 400 μs, and is better than 1% over 100 μs. To ensure that the ESA is recorded over the flat part of the pulse, the triggering of the pulsing unit and laser are synchronised.

Figure 12

(a) Circuit diagram for 'off-set' box used in recording weak ESA transients

(b) Low-temperature ESA cell

in

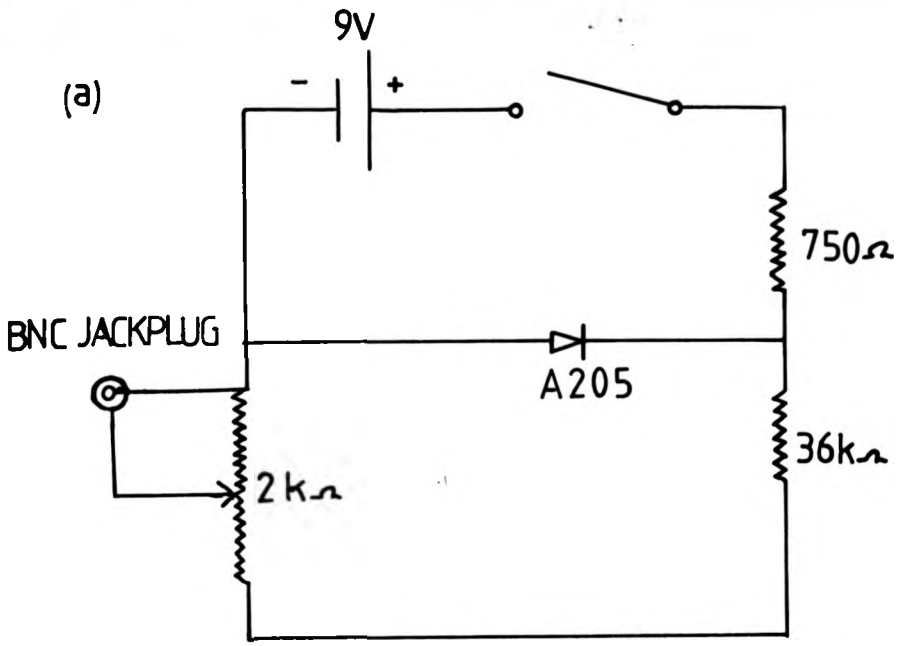
(a)
9V
-
+
750Ω
BNC JACKPLUG
A205
36kΩ
2kΩ

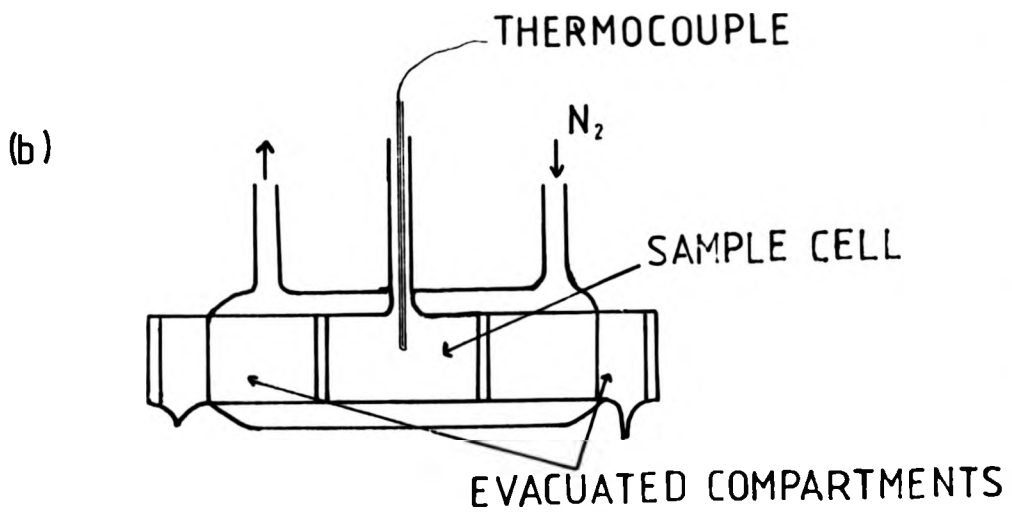
(b)
THERMOCOUPLE
N_2
SAMPLE CELL
EVACUATED COMPARTMENTS

A further restriction to the measurement of weakly absorbing transients is the need to restrict Io, the initial intensity of the analysing light, so that it produces a full-scale deflection on the oscilloscope screen in order that the value of Io can be measured in terms of applied photomultiplier voltage. As the ESA transient intensity is a constant percentage of Io for a given time, then one way of enlarging the ESA transient decay to allow more accurate measurements would be to increase Io. This has been achieved by 'off-setting' the zero-light level off the 'top' of the oscilloscope screen, which means, however, that Io can no longer be determined as the position of the zero-light level is not known. The latter problem has been overcome by using an 'off-set box' which gives a pre-calibrated output voltage which, when applied to the y amplifier of the oscilloscope in place of the photomultiplier output, allows the zero-light level to be brought back on to the screen. This level can now be used to give the 'apparent' Io value and by addition of the applied voltage from the 'off-set box', the true value of Io in mV can be calculated. The circuit diagram for the 'off-set box' is given in Figure 12.

ESA spectra were recorded by measuring the initial intensity of the transient as a function of monitoring wavelength, each reading being taken several times to allow for fluctuation in the intensity of the laser pulse. Frequent checks for photo-decomposition were made by redetermining the lifetime and intensity of the ESA transient at a wavelength chosen at the beginning of the experiment, and when photodecomposition was suspected, the ground state absorption spectrum was recorded to see whether any change had occurred. This was done automatically at the end of the experiment to confirm no change in the spectrum.

Photodecomposition of the sample is always a danger when using high-intensity light sources, and checks were made in all experiments both in emission and absorption modes of the reproducibility of the results and,where anomalies were found, absorption spectra were run in order to test for photo-decomposition.

The sample cell used for normal room temperature work consisted of a 2 cm cylindrical cell (5 cm^3 volume) with optical faces at each end. For low-temperature work, a special cell was designed (Figure 12) which allowed for cooling of the sample using the gas-flow apparatus described in the preceding section and given in Figure 10. The basic design is an ordinary 2 cm cylindrical room-temperature cell to which a cooling jacket has been fitted along with two evacuated chambers to avoid 'misting' of the front and back faces of the cell. Low-temperature ESA measurements are, however,limited to the solution phase, as glassing of the solution often results in the matrix being subjected to micro-cracking on the impact of the laser pulse, resulting in loss of the ESA transient due to the scattering of the analysing light. This problem, therefore, requires that the solution must be re-frozen before each shot. Similarly, glassing solutions which involve expansion of the sample are to be avoided as this will shatter the cell. Temperature studies over a wide range were done using emission measurements where possible.

(ii) Emission measurements

These measurements are easier to make than the ESA measurements, requiring minimal critical 'tuning',and optically pure glasses are unnecessary. In order to conserve film, two traces were recorded on each photograph. This was achieved by storing the first measurement on the oscilloscope and then

changing the polarity of the y axis and adjusting the position of the zero light level to be at the bottom of the oscilloscope, indicated by a marked position on the dial. The second measurement was then recorded as an inverted trace, and the two photographed.

The sample cells used for room-temperature measurement were ordinary quartz fluorimetry cells, and an analogous arrangement to that used for the spectrofluorimeter being adopted for low-temperature work. However, the dewar was constructed of 'pyrex' rather than quartz as the latter was found to luminesce and was inessential for this work as 'pyrex' gives good transmission at 347 nm and above (>80%). Similarly, the quartz cell insert was replaced by cheaper pyrex cylindrical tubes of $\sim$ 1 cm diameter which reduced the probability of the cell shattering when using solvents which give poor glasses and which expand on freezing, as well as reducing costs. Also, copper tubing was used instead of the stainless steel tubing used in the spectro-fluorimeter case as conditions did not need to be so demanding. The same cooling system was adopted, although heating was performed without the water bath surround, by simply using a Bunsen burner. Finer temperature control to obtain a given temperature above 273 K can be obtained by injecting acetone into the dewar to either cool or retard the rate at which the temperature increases, ensuring that the acetone is well removed from the naked flame of the Bunsen burner and the temperature does not exceed the flashpoint of the liquid. As emission (and ESA) measurements are taken over a very short time period (usually < 1 ms) then a greater accuracy in the measured temperature (± 0.2 K) could be gained compared with the fluorimeter. An

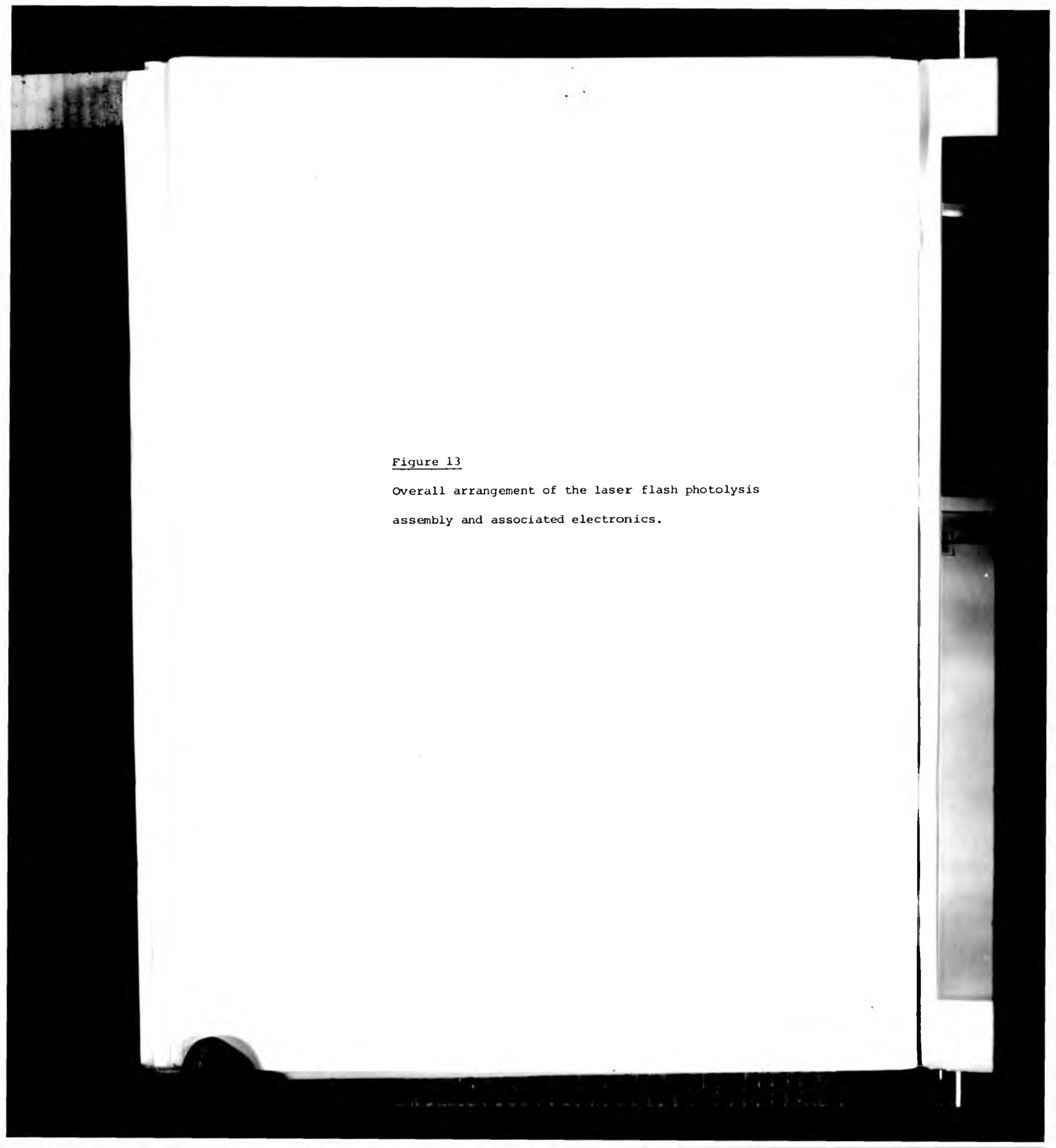

Figure 13

Overall arrangement of the laser flash photolysis assembly and associated electronics.

lysis

lysis

Figure 14

Laser head assembly and optical bench. Arrangement for low-temperature emission measurement.

ement

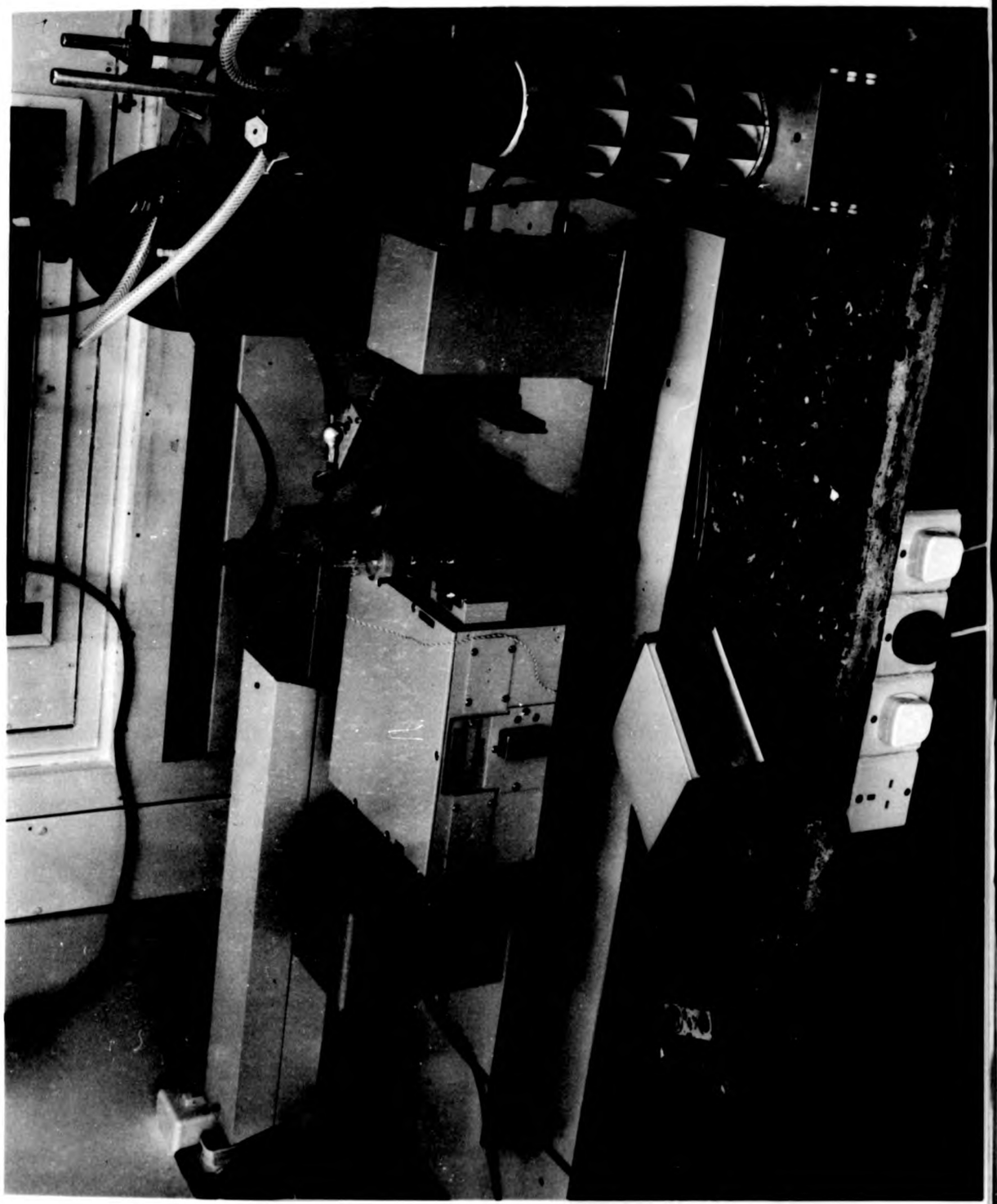

impression of the actual arrangement of the apparatus as well as the general layout of the complete laser equipment can be gained from the photographs in Figures 13 and 14.

As indicated, the results of all the laser experiments were photographed on to Polaroid film which records the results as transparencies, which are then fixed using a 'Polaroid dippit' containing a fixing solution of 0.03 mol dm^{-3} $SnCl_4$ in iso-propanol. The negatives were then enlarged (x 2) on to graph paper, and the transient curves digitised by hand ready for analysis.

3-1.3 Other instrumentation used

Visible and u.v. absorption measurements were made on a Pye-Unicam SP800 spectrophotometer, and the infra-red spectra of the Pt(0) complexes examined were recorded on a Perkin-Elmer 621 infra-red spectrophotometer. The lifetimes of these complexes could not be determined using the ruby laser as no absorption occurs at 347 nm, highlighting the major disadvantage of the laser technique which is the limitation of a fixed exciting wavelength. Tunable dye lasers in which laser action is obtained by pumping a short-lived fluorescent dye with a conventionally pulsed laser have been developed which allow wavelength alterations to be made by changing the organic dye used and give a pulse width of $\sim$ 3 ns,[219] although obviously wavelengths smaller than the pumping wavelength are not possible. For the Pt(0) complexes, however, the difficulty was overcome by using a frequency-quadrupled, Q-switched, neodynium glass laser installed at the University of East Anglia and supplied by Applied Photophysics Ltd., which gives an excitation wavelength of 264.8 nm.

Some preliminary lifetime measurements of $[Cr(phen)_3]^{3+}$ luminescence in dimethyl sulphoxide/water mixtures were made on the single photon counting apparatus built by Dr. F. Palmer at the University of Nottingham. This is a technique allowing very short lifetimes (> 3 ns) to be measured by using a multi-channel analyser to monitor the luminescence decay from the sample excited by a 'chopped' light source over a number of counts (ca. 2,000 to 10,000) depending upon the lifetime of the sample. The multi-channel analyser gradually builds up a decay profile of the luminescence superimposed on the tail of the lamp profile which can be monitored on an oscilloscope, and the luminescence lifetime can be found by deconvolution of the lamp profile using an appropriate computer program. Recently, the effect of inhomogeneous broadening of the laser pulse caused by the slightly different crystal environment of the individual ions resulting in a slight frequency spread of the laser oscillations has been reduced by the mode-locking of the phase of the laser oscillations by a variety of techniques to give an intense picosecond pulse (~ 300 fs in the case of a neodynium glass laser),[320] and lifetimes of the order of picoseconds are now being reported using this type of apparatus.[1] The possibility of using such a laser pulse in combination with the single photon counting technique could well give the opportunity of measuring even shorter lifetimes, providing that suitable instrumentation can be developed.

3-2 Sample Preparation

For work over a wide temperature range, a good glassing solvent is required. A number of these are known, and the most commonly used are organic glasses of ethanol:methanol mixtures,

EPA (ethanol:isopentane:ether 2:5:5) and methanol:water: ethylene glycol mixtures, a comprehensive list being given in the excellent monograph by Murov.[221] However, for this work a single solvent medium is preferred as this is more meaningful in discussing environmental effects, removing the complicating possibility of preferential solvation by one component of the mixed solvent medium. Relatively few of these are known, and aqueous 9 M lithium chloride has been the one extensively used in this work to give an extended temperature range to the aqueous environment while MTHF (2-methyltetrahydrofuran) has been used as a good organic glass, although the selective use of solvents obviously depends upon the solubility of the sample. In the case of the uranyl ion, strongly acidic media were used as good glassing solvents, although it was also found with this ion that both methanol and water give sufficiently good glasses to allow emission lifetime measurements, although these were unsuitable for absorption and other luminescence studies. The uranyl ion was also investigated in a fused silica block, although this technique is restricted on a more general basis as it requires the sample to be able to withstand the high temperatures used to fuse the glass.

Most of the samples used were sensitive to oxygen quenching and required deoxygenation before use. This was achieved by passing argon gas through them for twenty minutes, the gas having previously been saturated with the solvent by passing it through a chamber containing the solvent, thereby ensuring no change in concentration of the sample. This method of 'degassing' was used because of the ease with which it can be implemented, and it was found to be just as effective as the other popular freeze-pump-thaw method in which the sample is placed on

a vacuum line, frozen, and pumped to remove the air from the line. The sample is then allowed to thaw and re-equilibrate its residual oxygen with the dead-space. The procedure is then repeated two or three times to ensure all the oxygen is removed. To prevent oxygen re-dissolving into the solution during experiments, the samples were either sealed or a constant flow of argon was passed over the top of the sample.

A more recent innovation has been the use of polymer matrices[222] which give the distinct advantages of (i) optical clarity, (ii) the possibility of investigation of the luminescence over a much wider temperature range, (iii) absence of the complications caused by transition through the glassing point of the solvent, (iv) strengthening of the luminescence intensity in many cases due to restriction of diffusional deactivation modes, giving better resolution of the luminescence spectra at ambient temperatures, (v) in the case of luminescence spectra, removal of the perturbing influence of peaks from the vibrational Raman spectrum of the solvent. (The Raman spectrum can be distinguished from the luminescence spectrum by changing the excitation wavelength which will cause a parallel shift in the Raman spectrum), and (vi) relatively easy preparation.

It is necessary for the polymer to have a negligible absorption in the excitation region and little or, preferably, no luminescence. The polymer which has been most widely used is polymethylmethacrylate (PMM), which is transparent to well below 330 nm, although early reports of no luminescence[223] have been contradicted by more recent studies[224] which show a luminescence spectrum between 400 and 500 nm with an excitation maximum at $\sim$ 360 nm. However, for strongly luminescent complexes, the effect is considered negligible,

a vacuum line, frozen, and pumped to remove the air from the line. The sample is then allowed to thaw and re-equilibrate its residual oxygen with the dead-space. The procedure is then repeated two or three times to ensure all the oxygen is removed. To prevent oxygen re-dissolving into the solution during experiments, the samples were either sealed or a constant flow of argon was passed over the top of the sample.

A more recent innovation has been the use of polymer matrices[222] which give the distinct advantages of (i) optical clarity, (ii) the possibility of investigation of the luminescence over a much wider temperature range, (iii) absence of the complications caused by transition through the glassing point of the solvent, (iv) strengthening of the luminescence intensity in many cases due to restriction of diffusional deactivation modes, giving better resolution of the luminescence spectra at ambient temperatures, (v) in the case of luminescence spectra, removal of the perturbing influence of peaks from the vibrational Raman spectrum of the solvent. (The Raman spectrum can be distinguished from the luminescence spectrum by changing the excitation wavelength which will cause a parallel shift in the Raman spectrum), and (vi) relatively easy preparation.

It is necessary for the polymer to have a negligible absorption in the excitation region and little or, preferably, no luminescence. The polymer which has been most widely used is polymethylmethacrylate (PMM), which is transparent to well below 330 nm, although early reports of no luminescence[223] have been contradicted by more recent studies[224] which show a luminescence spectrum between 400 and 500 nm with an excitation maximum at $\sim$ 360 nm. However, for strongly luminescent complexes, the effect is considered negligible,

and PMM matrices have been used by Crosby et al.[53] for low-temperature studies of ruthenium(II) complexes and by Forster[52] for thermal quenching studies of chromium(III) luminescence. In this work, however, cellulose acetate has been used as the polymer film for which no luminescence could be detected even at excitation wavelengths of ∿ 240 nm: it is also transparent at 347 nm and below. The films were mounted at an angle of 45° to both the excitation and detection system to allow front-face illumination in the case of both emission spectra and lifetime measurements. For low-temperature work, the acetate film was placed in a cell containing 9 M LiCl which afforded good thermal equilibration with the surrounding dewar with no leaching of the film by the solution being apparent. Unfortunately, polymer matrices can only be used when a common solvent, in this case acetone, for both polymer and compound can be found, although a small addition of water (1 to 2 %) can be tolerated without significant 'clouding' of the film, and care must be taken not to allow crystallisation of the sample in the matrix. The films were made by adding AnalaR acetone to a small amount of cellulose acetate powder (May and Baker Laboratory Grade) with stirring, until a solution with the consistency of treacle was obtained (2 to 3 hours). A solution of the sample in acetone (∿ 20 cm^3) is then added, and the doped solution stirred to give a homogeneous distribution of the sample until it becomes treacle-like again. The doped solution is then poured into a crystallising dish until there is a 3-5 mm thick layer, and the solvent is allowed to evaporate overnight. The resultant film is then cut into 1 cm strips ready for use, and pumped on a vacuum line for twenty-four hours, both to 'degas' the film

and remove any excess solvent trapped in the film. The polymer film, however, is of little use in ESA measurements, but this has been overcome by Ohno and Kato[225] who built up a polymer rod of PMM by adding successive doped layers of the polymer solution, allowing each one to set before further addition. This technique also overcomes any cracking that may be caused by a laser pulse, as occurs when solvent glasses are used.

The optical density of the sample used was varied, depending on the nature of the experiment. For fluorimetry, a weakly absorbing solution (< 0.01) is preferred, as this eliminates 'inner filter' effects caused either by total absorption of the exciting light at the front of the cell or re-absorption of the luminescence, which can result in distortion of the luminescence spectrum,[4] although this is sometimes not possible when the luminescence is weak. In contrast, laser measurements require a good optical density ($\sim$ 0.9) at 347 nm to allow for absorption of the laser pulse.

As mentioned in the previous chapter, the uranyl ion is extremely sensitive to impurities,and special precautions were taken with this system. These included the cleaning of the sample cell in chromic acid (or, if necessary, permanganic acid) to remove organic impurities which the uranyl ion was able to leach from the glass. For the quenching experiments of the uranyl ion by perchloric acid, discussed later, the acid was accurately weighed into volumetric flasks containing a standard weight of uranyl nitrate, and the solutions then made up. A dry-box was used when making up the deuterated analogues of the aqueous solutions, and the flasks stoppered and sealed with 'parafilm' before removing them from the dry-box. The lifetimes

were measured by flashing these solutions whilst in the volumetric flasks. A dry-box was used in handling most deuterated solvents throughout this work.

The silicate glass doped with $[UO_2]^{2+}$ was made in the ceramics workshop of the Department of Physics in the University.

3-2.1 Solvent purity

Most organic solvents used were of spectroscopic grade and were used without further purification. However, pyridine (AnalaR grade) and nitromethane (B.D.H. Laboratory Grade) were also used. Two organic solvents received further purification.

(i) Acetone. AnalaR grade acetone was refluxed under nitrogen with K MnO_4 overnight, and then distilled under nitrogen. The lifetime of the excited uranyl ion (0.2 mol dm^{-3}) in this solvent was then measured. The procedure was then repeated until a constant lifetime was recorded for two consecutive purifications (1.37 μs at 298 K).

(ii) MTHF. MTHF (puriss grade, Koch-Light Laboratories) was purified by 'trap-to-trap' distillation over Na/K alloy on a vacuum line to remove any oxidised impurities caused by prolonged storage.

For aqueous media, fresh singly or doubly distilled water was used except for $[UO_2]^{2+}$ and $[Cr(phen)_3]^{3+}$. For these cases, doubly distilled water was refluxed with alkaline permanganate to constant emission lifetime of dissolved uranyl ion (1.9 μs for 0.2 mol dm^{-3} $[UO_2]^{2+}$ solution at 298 K), using the same procedure as described for acetone. Lithium chloride (Hopkins and Williams Laboratory Grade) was twice recrystallised from distilled water and dried in a vacuum oven (393 K) to remove water of crystallisation, and cooled in a vacuum desiccator

over P_2O_5 before use. Sodium fluoride and sodium perchlorate were of AnalaR grade.

The inorganic acids used for $[UO_2]^{2+}$, namely H_2SO_4 (sp. gr. 1.86), $HClO_4$ (sp. gr. 1.7, 11.7 M) and H_3PO_4 (sp. gr. 1.75) were of AnalaR grade.

All deuterated solvents were used without further purification and were of 'gold label' standard (> 99.79%D for D_2O) with the exception of the D_2O used in the $[UO_2]^{2+}$ studies which was purifed under nitrogen by the method described for water, with the permanganate being made alkaline with sodium metal to avoid contamination by OH^- through using NaOH. A constant lifetime of 3.3 μs for 0.2 mol dm^{-3} solution at 298 K was achieved.

3-3 Sample Syntheses

$[Cr(phen)_3]ClO_4{}_3$, $[Cr(terpy)_2]ClO_4{}_3$ and $[Cr(bipy)_3]ClO_4{}_3$ were prepared according to the general principle of Brauer[226] by addition of a solution of the ligand in deaerated methanol to a deaerated solution of chromous chloride in an inert atmosphere followed by air or H_2O oxidation to the chromic state.

(i) $[Cr(terpy)_2]ClO_4{}_3$. The reaction vessel consisted of a three-necked 250 cm^3 round-bottomed flask, the middle neck being stoppered and used to facilitate addition of reactants. The other two necks were used as inlet and outlet ports to allow a continuous stream of oxygen-free (chromous-scrubbed) nitrogen to be directed through the contents of the flask, the outgoing gas then being used to 'degas' further reactants. 2.5 cm^3 of 1 M hydrochloric acid (AnalaR grade) were placed in the flask and thoroughly degassed (1 hour). 0.26 gm of chromium metal (B.D.H. Laboratory Grade) was then added, and allowed to dissolve

to give a blue chromous chloride solution with the evolution of hydrogen (12 hours) before rapid addition of 20 cm^3 of deaerated doubly distilled water. A thoroughly deaerated solution of 0.5 gm of 2,2',2"-terpyridyl (Koch-Light 'puriss' grade) in 40 cm^3 of methanol (spectroscopic grade) was then rapidly added and the resultant orange-yellow solution shaken. The solution was then bubbled with air to give the chromic form and $[Cr(terpy)_2]ClO_4{}_3$ was then precipitated by addition of a solution of 1 gm of $NaClO_4$ (AnalaR grade, sg. gr. 1.7). The precipitate was filtered off and recrystallised from doubly distilled water, and the crystals were washed with cold MeOH. A sample sent for microanalysis gave good agreement between the theoretical figures (in brackets) and the measured percentages of C, H, N and Cl present. C, 42.82 (44), H, 3.01 (3.4), N, 9.99 (10), Cl, 13 (12.43).

(ii) $[Cr(bipy)_3]ClO_4{}_3.\frac{1}{2}H_2O$ This was prepared by the same method as above, with the 0.5 gm of 2,2',2"-terpyridyl being replaced by 2.35 gm of 2,2'-bipyridyl (B.D.H. AnalaR grade). The purity was checked by u.v. absorption and emission lifetimes and spectra.

(iii) $[Cr(phen)_3]ClO_4{}_3.2H_2O$ This compound was prepared using the same principle but a rather different method to the above complexes. The solutions used were all 'degassed' and sealed in separate flasks using 'supa-seal' stoppers and were then placed in an oxygen-free dry-box. The solution of 9 gm of 1,10-phenanthroline (B.D.H. AnalaR grade) in 40 cm^3 of spectroscopic grade methanol was then added to a solution of chromous chloride (0.8 gm of chromium metal (B.D.H. Laboratory Grade) in 40 cm^3 of 1 M HCl (AnalaR grade)) which gave a yellow-green solution. The solution was then stirred for ten minutes

before adding 125 cm^3 of 1M HCl containing 7.2 cm^3 of 100 vol. H_2O_2 to oxidise the solution to give $[Cr(phen)_3]Cl_3$. $[Cr(phen)_3]ClO_4{}_3$ was precipitated by adding 300 cm^3 of saturated $NaClO_4$ solution and the solid filtered off, washed successively with cold H_2O, cold methanol, chloroform, absolute ethanol and ether. The sample was then recrystallised and tested for purity by u.v. absorption and emission spectra measurements. However, while these measurements gave excellent agreement with literature values, the lifetime in water was substantially less (∿ 120 μs) than that reported by Henry (360 μs)[121] at 295 K in a deaerated aqueous solution. The sample was, therefore, further purified by repeatedly extracting any excess ligand with chloroform from an aqueous solution until the absorption spectrum of the chloroform extract showed no presence of ligand (20 to 30 times). The recrystallised sample then gave a lifetime of 270 μs at 295 K in a deaerated aqueous solution and further extraction or recrystallisation produced no further lengthening of the lifetime. This lifetime is in good agreement with other reports of the lifetime[227,228] except for that of Henry,[121] and was therefore considered acceptable, although the discrepancy with this case is disconcerting.

Reinecke's salt ($NH_4[Cr(NH_3)_2(NCS)_4].H_2O$) was prepared by a standard method.[226]

The following compounds were prepared either by Dr. S.R. Allsopp or by Professor O. Traverso, using standard methods.

COMPLEX	AFTER.....
$[Cr(NH_3)_6]NO_3{}_3$	Ref. 229
$[Cr(en)_3]Cl_3$	Ref. 226
$NH_4{}_3[Cr(NCS)_6]$	Ref. 226
$[Ru(phen)_3]Cl_2.6H_2O$	Ref. 230
$[Ru(bipy)_3]Cl_2.6H_2O$	Ref. 230
$[Os(phen)_3]I_2.3H_2O$	Ref. 231
$[Os(bipy)_3]I_2.3H_2O$	Ref. 231
$[Pt(QO)_2]$	Ref. 37
$[(PPh_3)_2.Pt(tetracyanoethylene)]$	Ref. 232
$[(PPh_3)_2.Pt(fumaronitrile)]$	Ref. 232
$[(PPh_3)_2.Pt.O_2]$	Ref. 232
$[(PPh_3)_2.Pt.C_2H_4]$	Ref. 232
$[(AsPh_3)_2.Pt(fumaronitrile)]$	Ref. 232

The uranyl ion was used in the form of $[UO_2]NO_3{}_2.6H_2O$ (B.D.H. AnalaR grade) without further purification.

3-4 Analysis of Results

3-4.1 Emission spectra

The relative emission yields at different temperatures were calculated by integration of the entire emission spectrum recorded at the various temperatures. The area under the spectrum was measured using a planimeter (Allbrit compensating planimeter), and an average over five readings was taken for each spectrum. This method was considered to be more accurate than the two alternative techniques involving either calibrated weighing of the spectrum or 'counting of the squares'. The values of the ln (area) and $(\text{temperature})^{-1}$ were then transferred to a computer file ready for further analysis as described in detail in a later section.

Figure 15

Typical oscilloscope traces obtained from:

(a) emission of $[Ru(phen)_3]^{2+}$ in 9M $LiCl/H_2O$ at 289 K (λ_{em} = 580 nm).

(b) ESA of 0.2M uranyl nitrate in H_2O at 298 K (λ_{abs} = 585 nm)

(a)

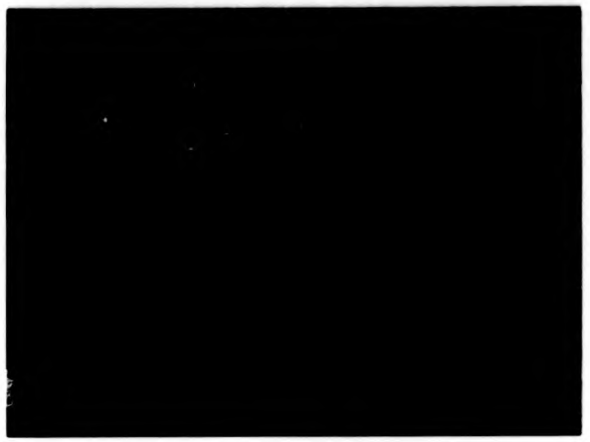

(b)

(a)

(b)

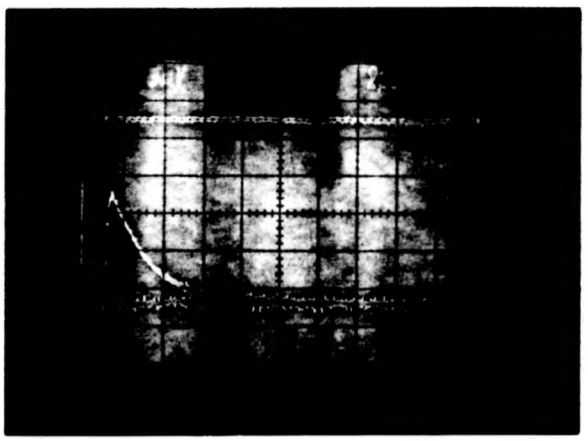

3-4.2 ESA and emission lifetime measurements

Typical ESA and emission oscilloscope traces are given in Figure 15. The digitised form of these traces, obtained from the graphical enlargement of the traces (x 2) were analysed by computer techniques for normal first-order kinetics according to the equations

either $F = C \exp(-k_{obs}t)$ for emission work

or $I_t = I_o \exp(-k_{obs}t)$

where F is the emission intensity at time t (in seconds), C is a constant of integration, and k_{obs} is the first order rate constant in s^{-1}. I_t is the transmitted intensity of the analysing beam at time t and I_o is the initial intensity of the analysing beam measured in terms of the photomultiplier voltage. The pertinent computer program (V1EOX) utilised a subroutine (VBO1A) which involves a least-squares approximation to the relevant function. Initial estimates for k_{obs} were obtained by inspection of the transient decay, and C was made equal to the initial emission intensity, whereas I_o was calculated accurately and fed into the program. For the emission decays of the uranyl ion in the silicate glass block, which were distinctly non-exponential, the data was fitted to the equation

$$F(t) = A \exp(-k_1 t) + B \exp(-k_2 T)$$

where A and B are pre-exponential constants and k_1 and k_2 are first-order rate constants. The initial estimates for A and B were both taken as half the initial emission intensity. k_1 was estimated from inspection of the transient decay and k_2 was made equal to $k_1/10$. The program used to fit this data (V12EX) involved a modified version of VBO1A) which gave a 'least squares' fit to the equation. Details of these and

the other programs mentioned, along with the input and output form of the data and results respectively are given in Appendix I.

3-4.3 Analysis of Arrhenius-type data

The results in the form of either k_{obs} or ϕ_{rel} and T(K) are collected on to data files ready for analysis by one of three methods, depending on the form of the Arrhenius plot.

(i) A simple linear Arrhenius plot, i.e.:-

$$k_{obs} = A \exp(-E_A/RT)$$

For this case, the data can be analysed either by a simple linear least-squares method (WLSSRA) or by using an appropriate version of VBOlA (SEXP) in cases when the scatter of points is not excessive. For the latter case, estimates for A and E_A can be found from a rough hand plot. All points were given an equal weighting and the relevant programs can be found in Appendix I.

(ii) A plot of the form

$$k = A \exp(-E_A/RT) + B$$

This type of plot is easily recognisable by a low-temperature horizontal plateau corresponding to the B term. However, over a restricted higher temperature range, the form of the equation is not readily detectable and should be used only when a linear plot is definitely invalid rather than by analogy with other plots for the same system. The fitting procedure involves a version of VBOlA (VHEXP) which gives the best-fit values of A and B (in s^{-1}) and E_A (in kJ mol^{-1}) along with the standard deviation of these parameters, as well as a comparison of the observed and fitted points. In order to obtain 'reasonable' fits for these curves, it was necessary in many cases to apply extra weighting to the low-temperature

plateau points to ensure the curve passed through this region. This will obviously affect the standard deviation of the B parameter and, to a much lesser extent, the errors in A and E_A. The value of B and its error were, however, to some extent obvious from these curves in many cases, and the errors quoted can be regarded as reasonable estimates rather than a rigorous standard deviation. Estimates of E_A and A were obtained from the slope and intercept of the high temperature portion of the curve, respectively. It is interesting to note that it is the correct ratio rather than the approximate correct values which give convergence on the exact values of the variables.

(iii) An Arrhenius plot of the form

$$k = A \exp(-E_A/RT) + B \exp(-E_B/RT)$$

This type of plot is most easily recognisable by the presence of two distinct regions with different slopes, usually apparent over a large temperature range. The data are fitted using another modified form of VBOlA (DBEXP) and A and B are estimated from the intercepts of the two regions, whereas E_A and E_B are given by the slopes of these regions, and further details are given in Appendix I.

The choice of the analysis procedure can be clear-cut but, especially in the case of restricted temperature ranges, the curves may be ambiguous, particularly between the second and third cases. In these situations it should be borne in mind that the appropriate fit is the simplest form to which the data can be fitted, as any curve can be fitted to the sum of a set of exponentials provided enough are used. An indication of correct use of the second case is that when the third possibility is used, the second exponential is reduced to zero.

For other types of plot, a simple linear least-squares program (WLSSRA) was used to produce a straight line fit where a linear relationship between parameters was apparent.

CHAPTER 4

CHROMIUM(III)

RESULTS AND DISCUSSION

4-1 Results of temperature-dependence studies

The temperature dependence of the emission from several chromium(III) complexes have been investigated in a variety of solvents, using the experimental method previously described. The temperature range covered was as wide as possible, restrictions being imposed by either poor transmission of the solvent glass or boiling of the solvent and, in some cases, either degradation of the complex or anomalous behaviour which will be discussed in detail later. The emission was monitored at the relevant maximum emission wavelength (Table 4-1), either determined by fluorimetry or by reference to the literature. In the case of $[Cr(terpy)_2]^{3+}$, the emission maximum was set at 800 nm, which was the wavelength giving maximum emission intensity as monitored by flash photolysis, as no report of the luminescence spectrum could be found, and the Perkin-Elmer MPF-3 spectrofluorimeter does not allow measurement above 800 nm. A wide bandpass (20 nm) was used in most cases to allow a detectable emission over the maximum temperature range, and as no emission wavelength dependence of the luminescence lifetime was found,or has indeed been reported for any chromium(III) complex, indicating, as expected, a common phosphorescing (doublet) state for all emission wavelengths. Similarly, no concentration dependence of the emission lifetime has been found, affording direct correlation of our results with those of other workers.

A similar form of temperature dependence was exhibited by all but two of the cases investigated, which showed a distinct change at T_{η} for the system (see Figure 16). The overall pattern is that described by equation (1-58) derived from the general model (Chapter 1), i.e.

Figure 16

Temperature dependence of luminescence lifetime of chromium(III) complexes. X-experimental points; full line-computer fit to equation 4-1. (Individual parameters are given in Table 4-1)

(a) $[Cr(NH_3)_6]^{3+}$ in 9M $LiCl/H_2O$

(b) $[Cr(en)_3]^{3+}$ in 9M $LiCl/H_2O$

(c) $[Cr(bipy)_3]^{3+}$ in 9M $LiCl/H_2O$

(d) $[Cr(bipy)_3]^{3+}$ in CA film

(e) $[Cr(phen)_3]^{3+}$ in 9M $LiCl/H_2O$

(f) $[Cr(phen)_3]^{3+}$ in MeOH

(g) $[Cr(phen)_3]^{3+}$ in CH_3CN

(h) $[Cr(phen)_3]^{3+}$ in nitroethane

(i) $[Cr(phen)_3]^{3+}$ in CA film

(j) trans- $[Cr(NH_3)_2(NCS)_4]^-$ in MTHF

(k) trans- $[Cr(NH_3)_2(NCS)_4]^-$ in CA film

(l) $[Cr(terpy)_2]^{3+}$ in 9M $LiCl/H_2O$

(m) $[Cr(terpy)_2]^{3+}$ in CA film

(n) $[Cr(NCS)_6]^{3-}$ in CA film

ifetime of
points;

e 4-1)

(b)

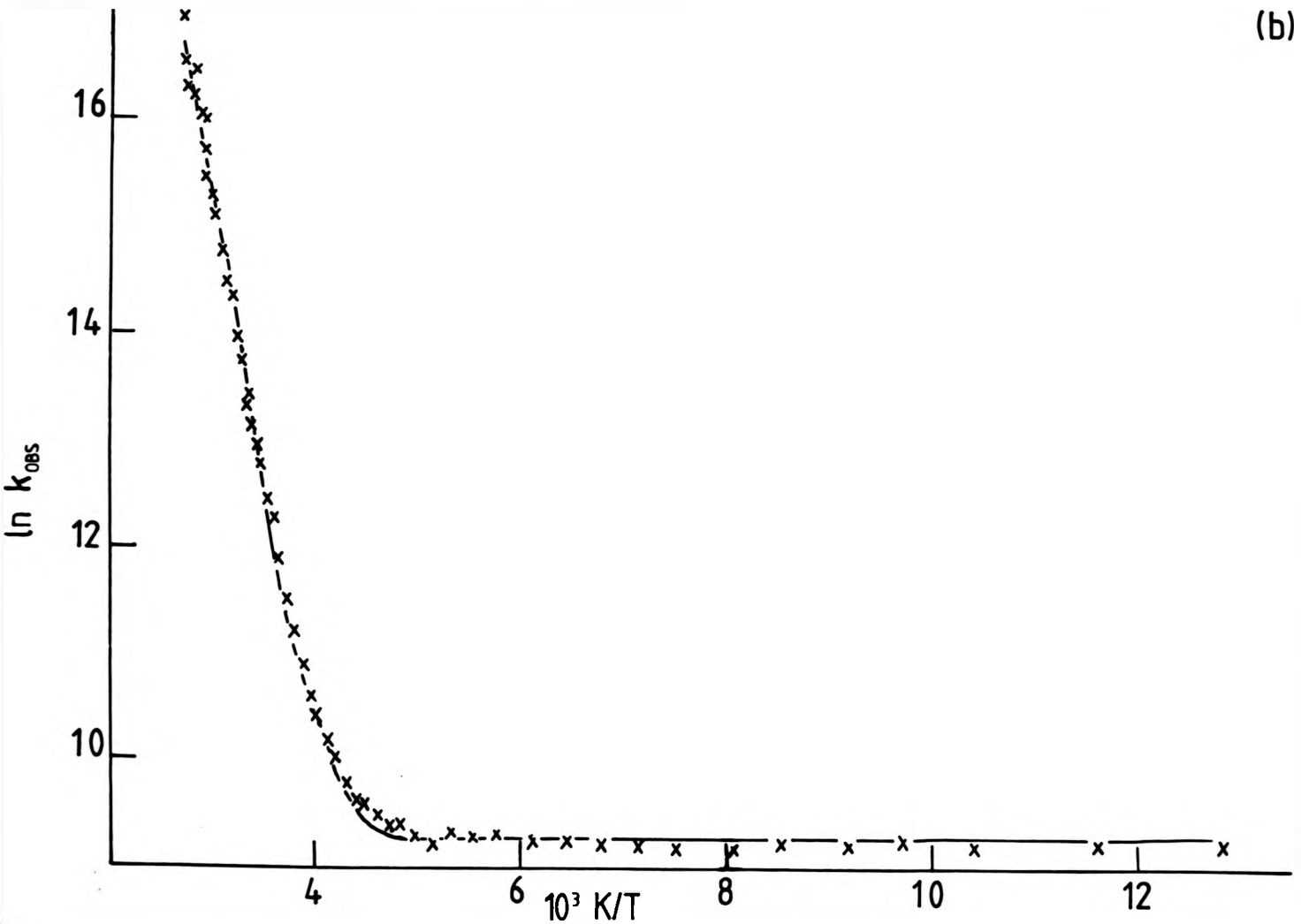

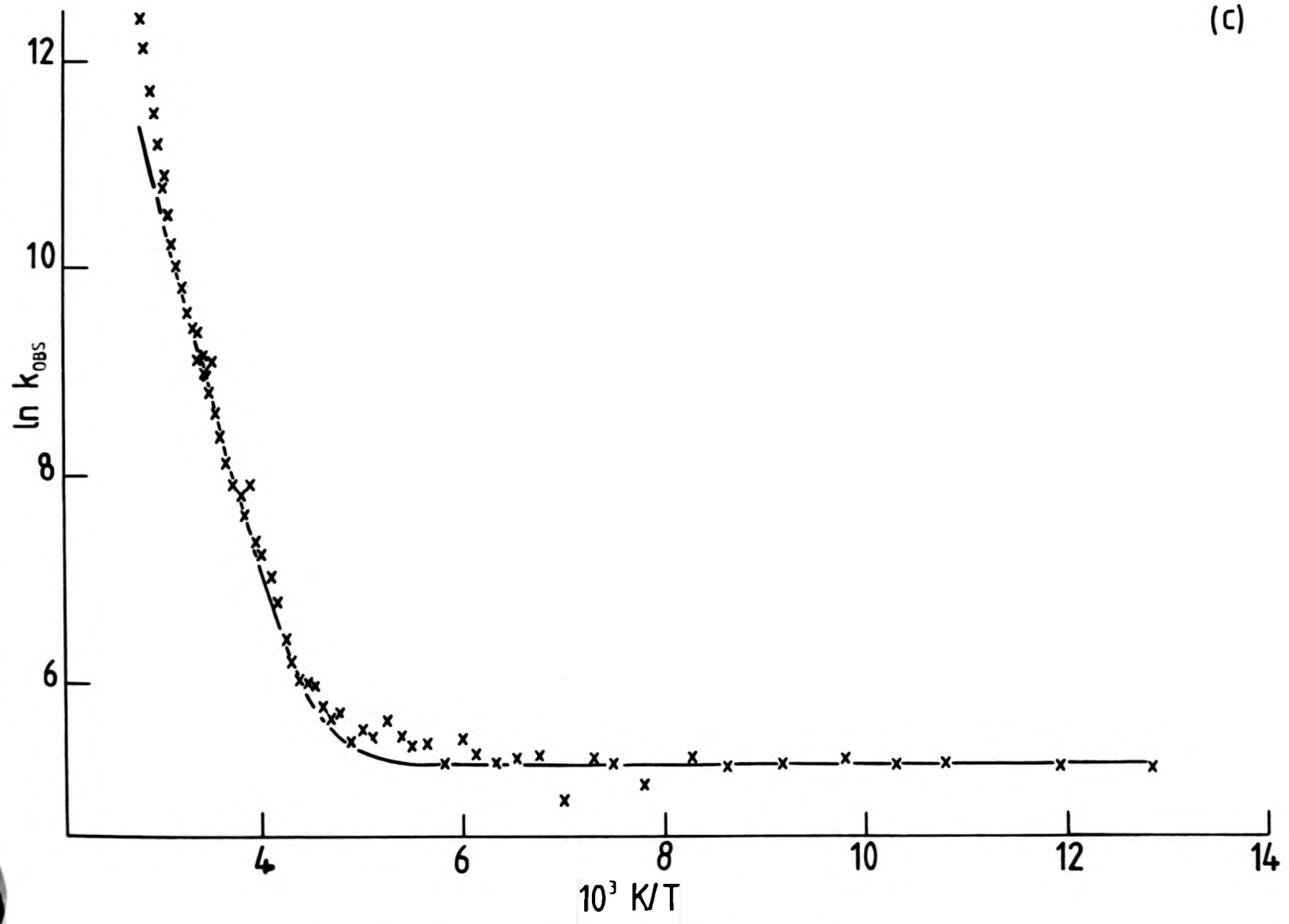
(c)
12
10
8
6
ln k_{OBS}
4
6
8
10
12
14
10^3 K/T

(d)

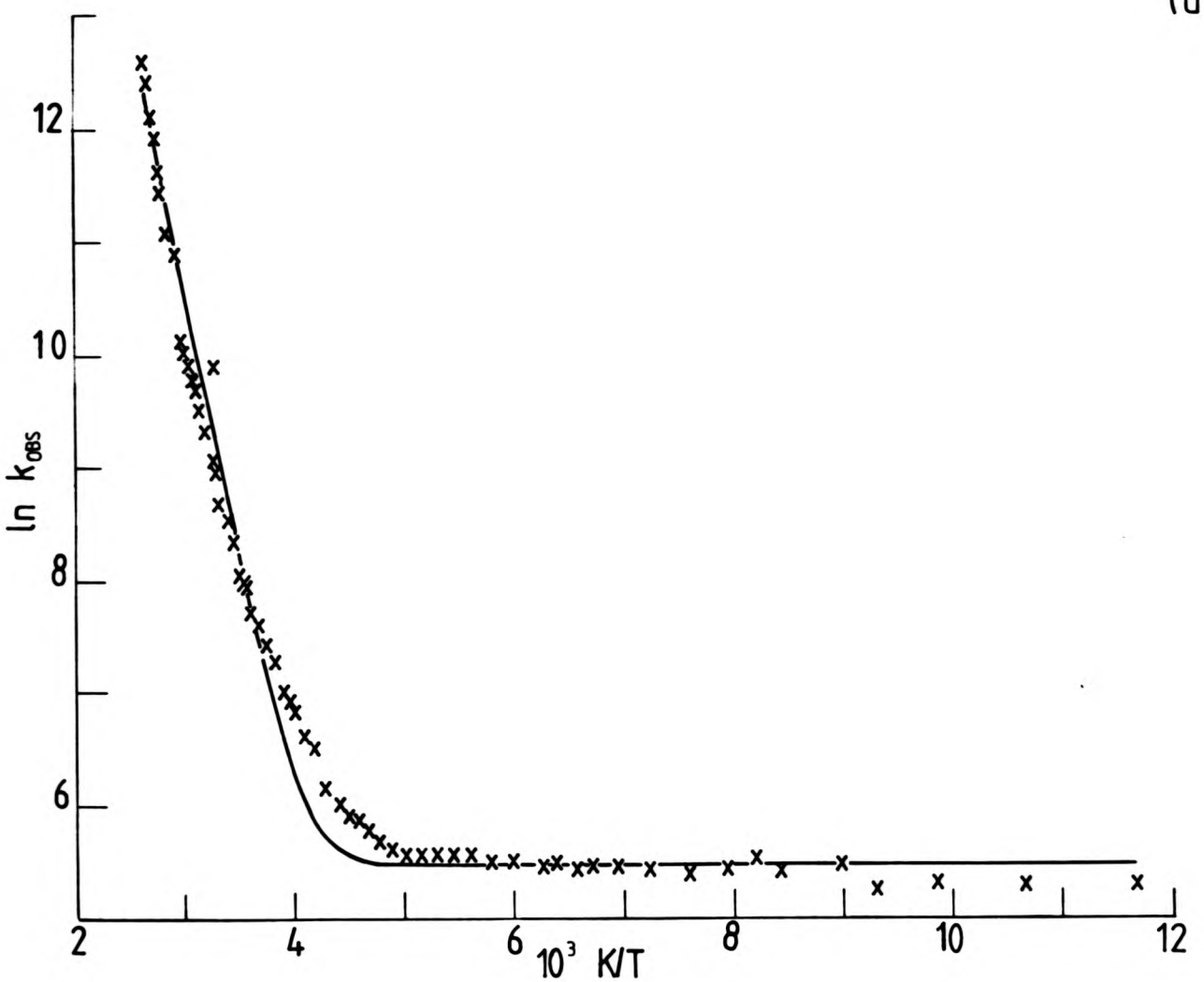

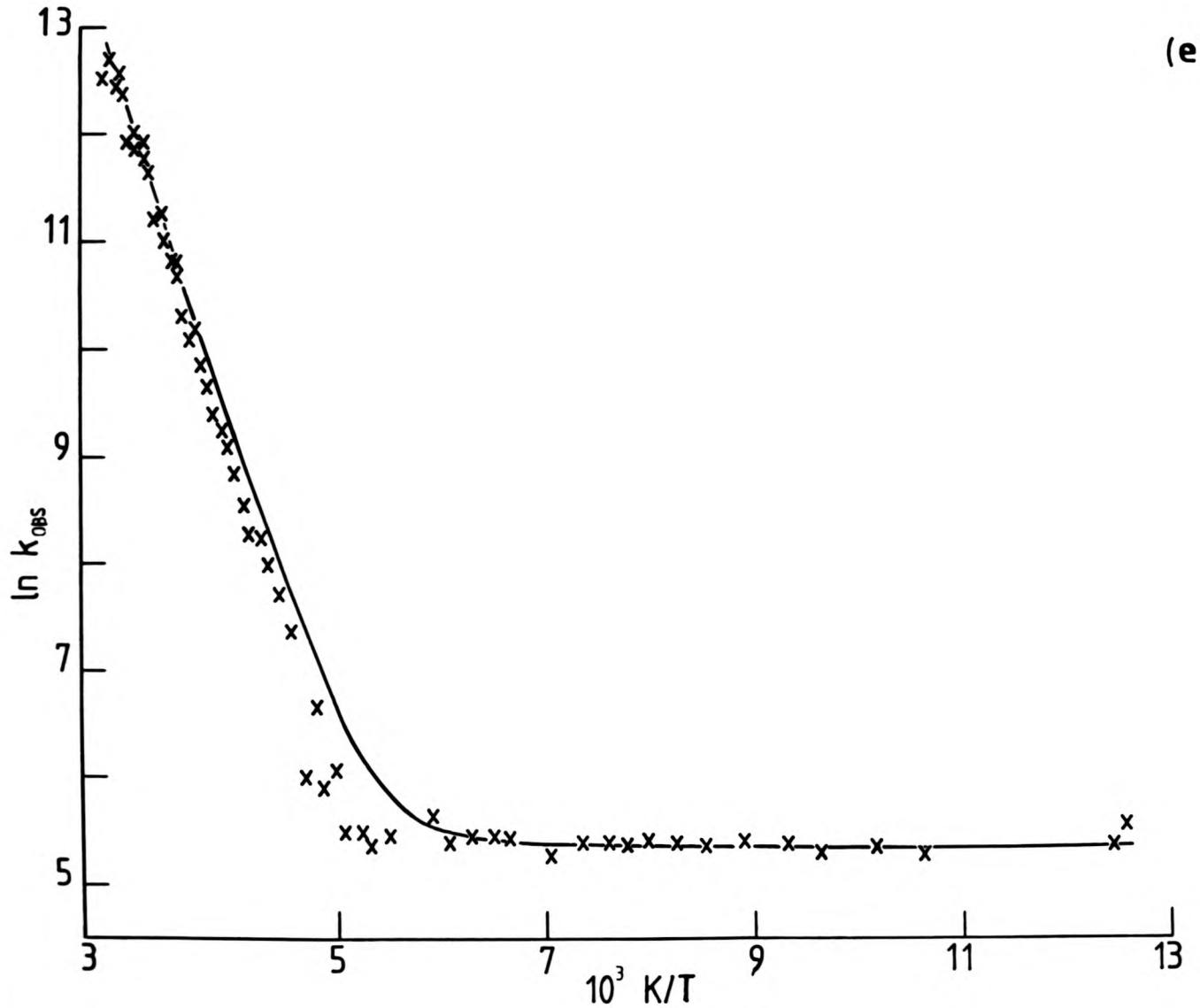
(e)
13
11
9
7
5
ln k_{OBS}
3
5
7
9
11
13
10^3 K/T

(f)

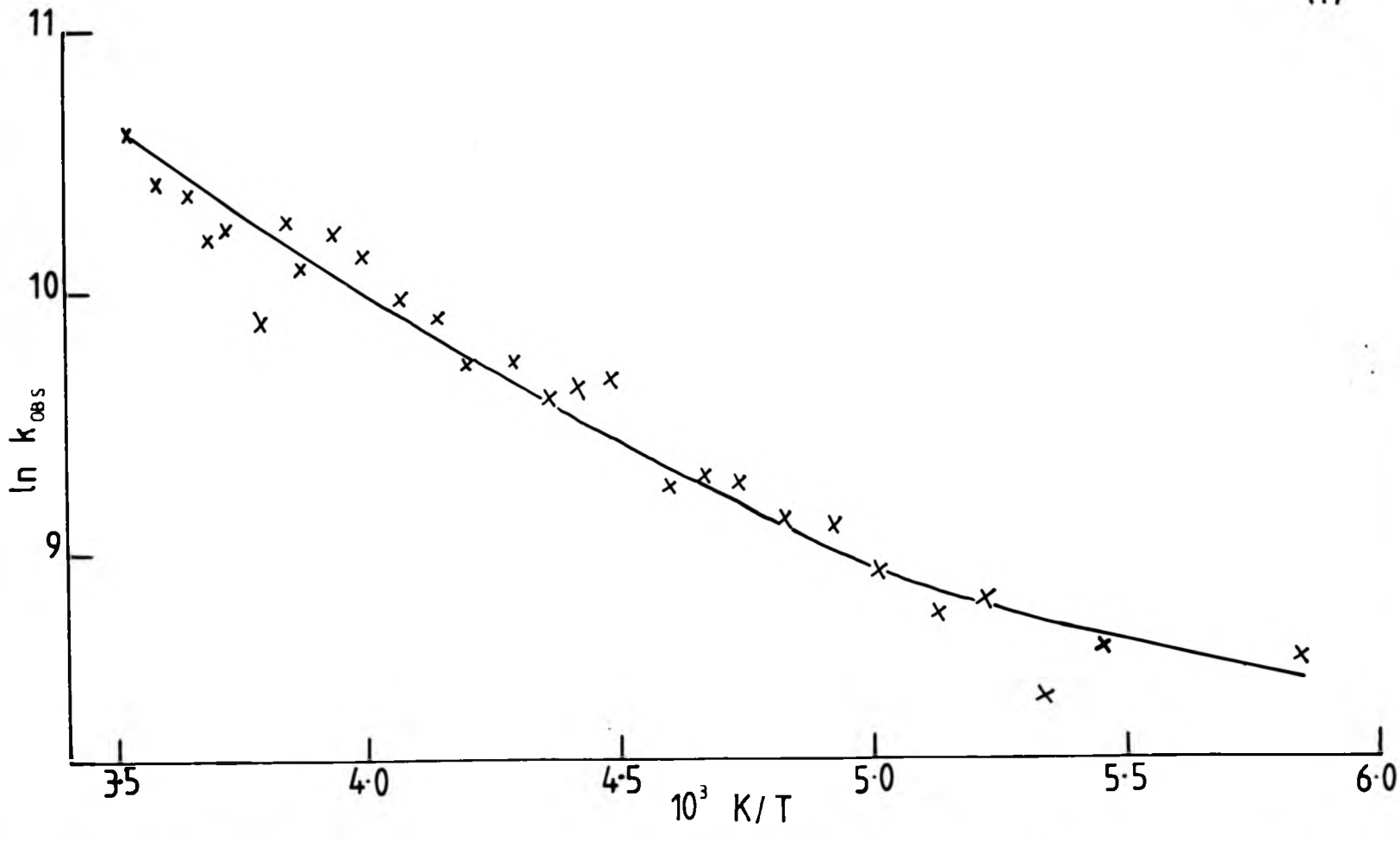

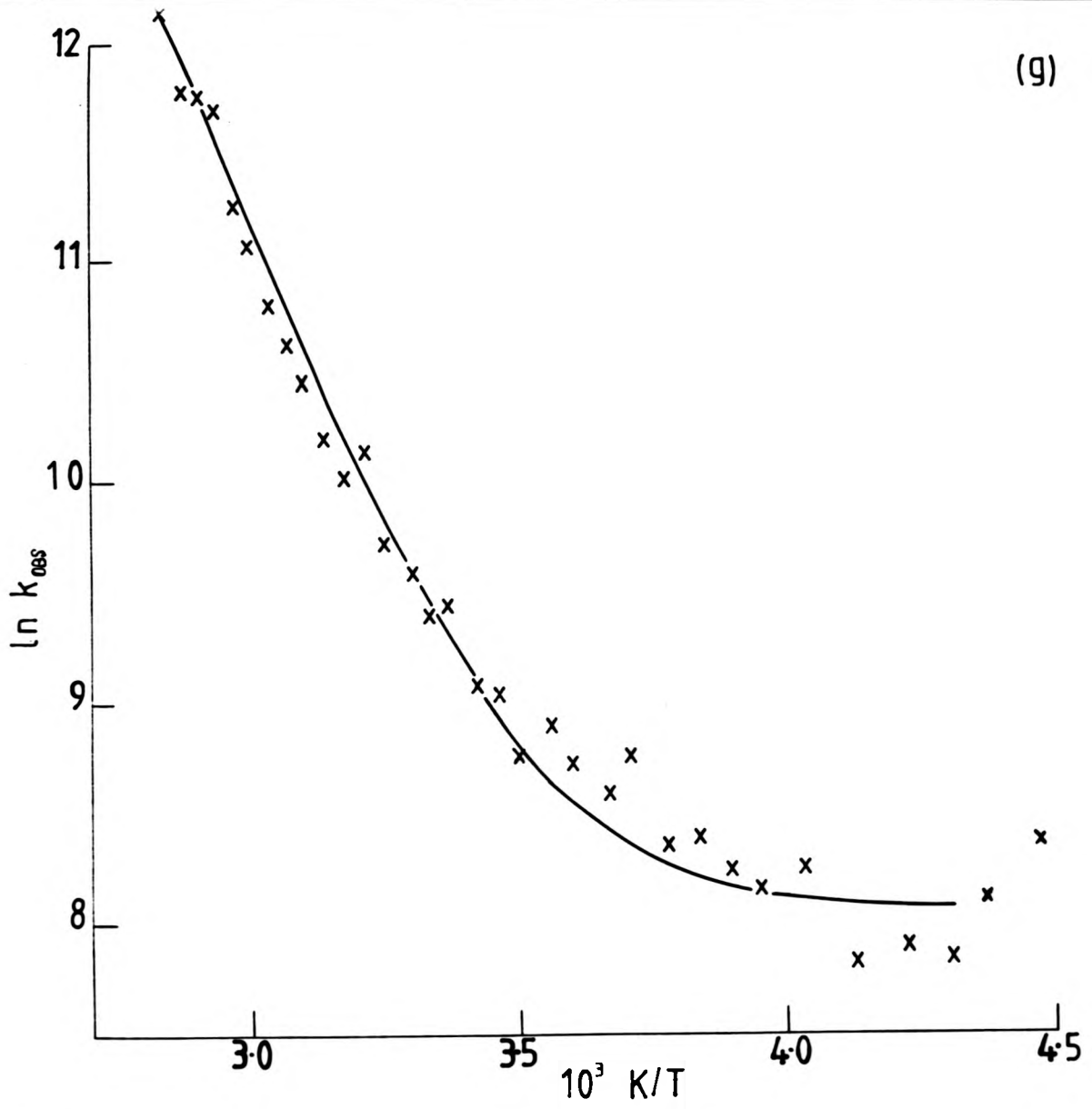
(g)
12
11
10
9
8
ln k_{obs}
3·0
3·5
4·0
4·5
10^3 K/T

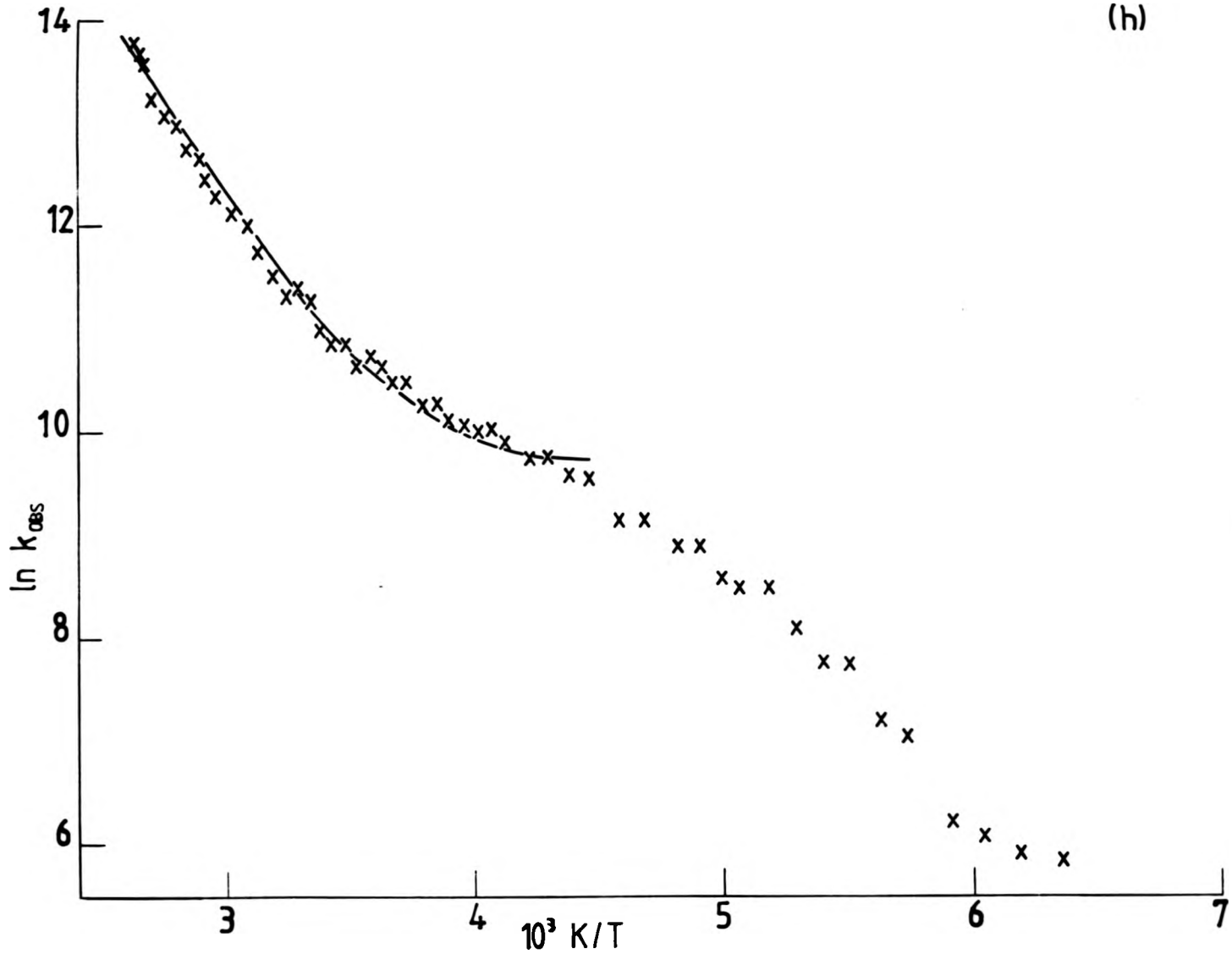
(h)
14
12
10
8
6
ln k_{obs}
3
4
5
6
7
10^3 K/T

(i)

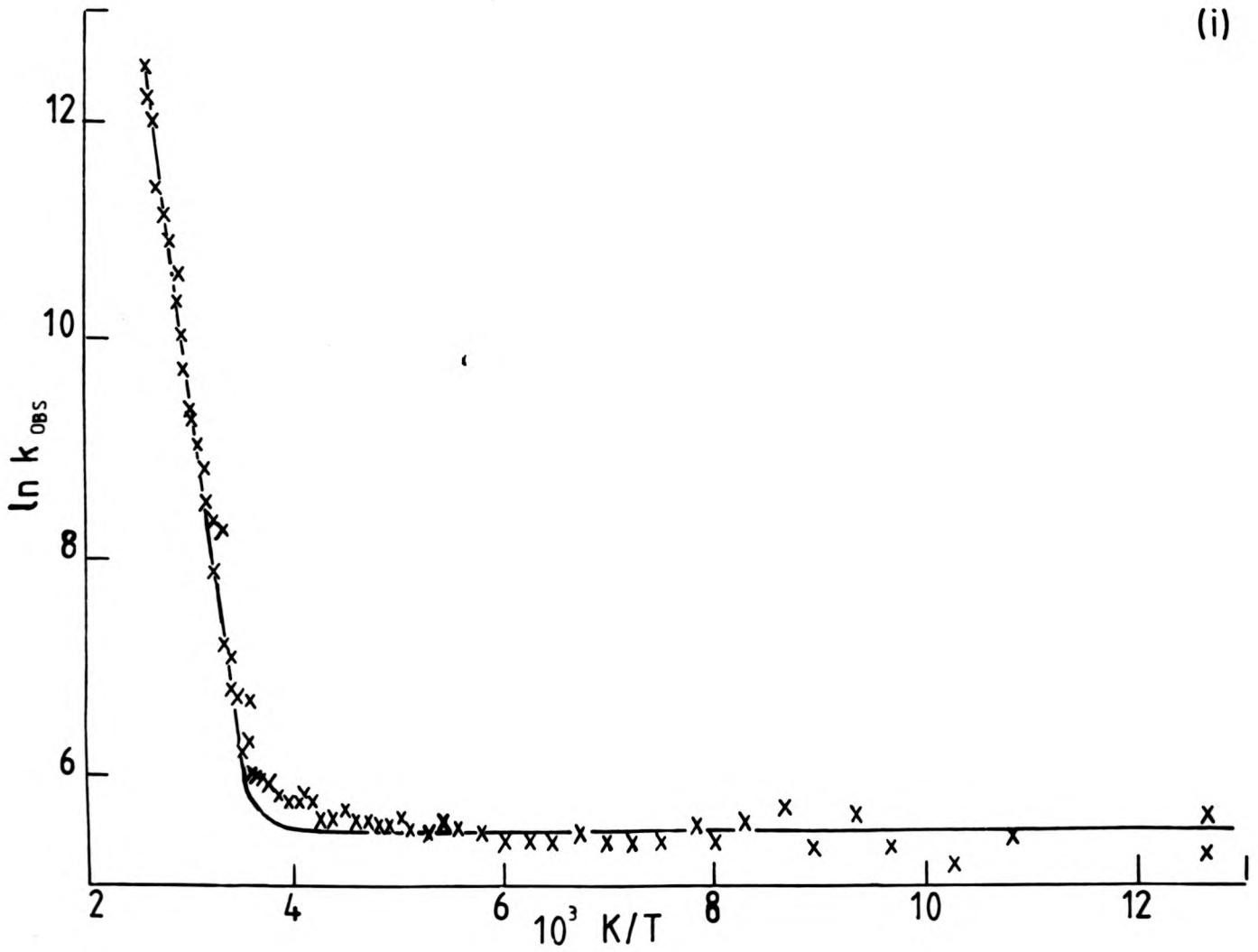

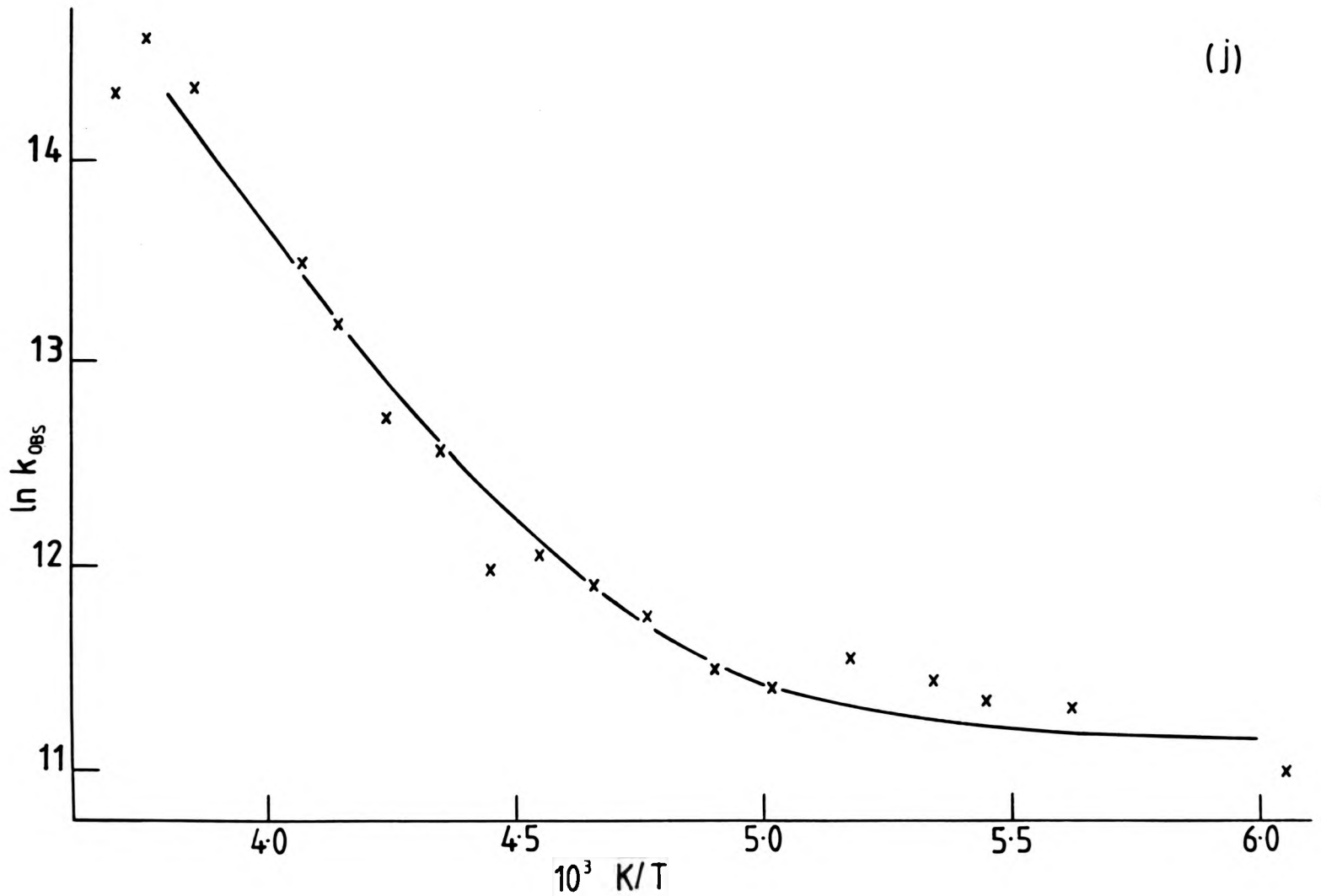
(j)
14
13
12
11
ln k_{OBS}
4·0
4·5
5·0
5·5
6·0
10^3 K/T

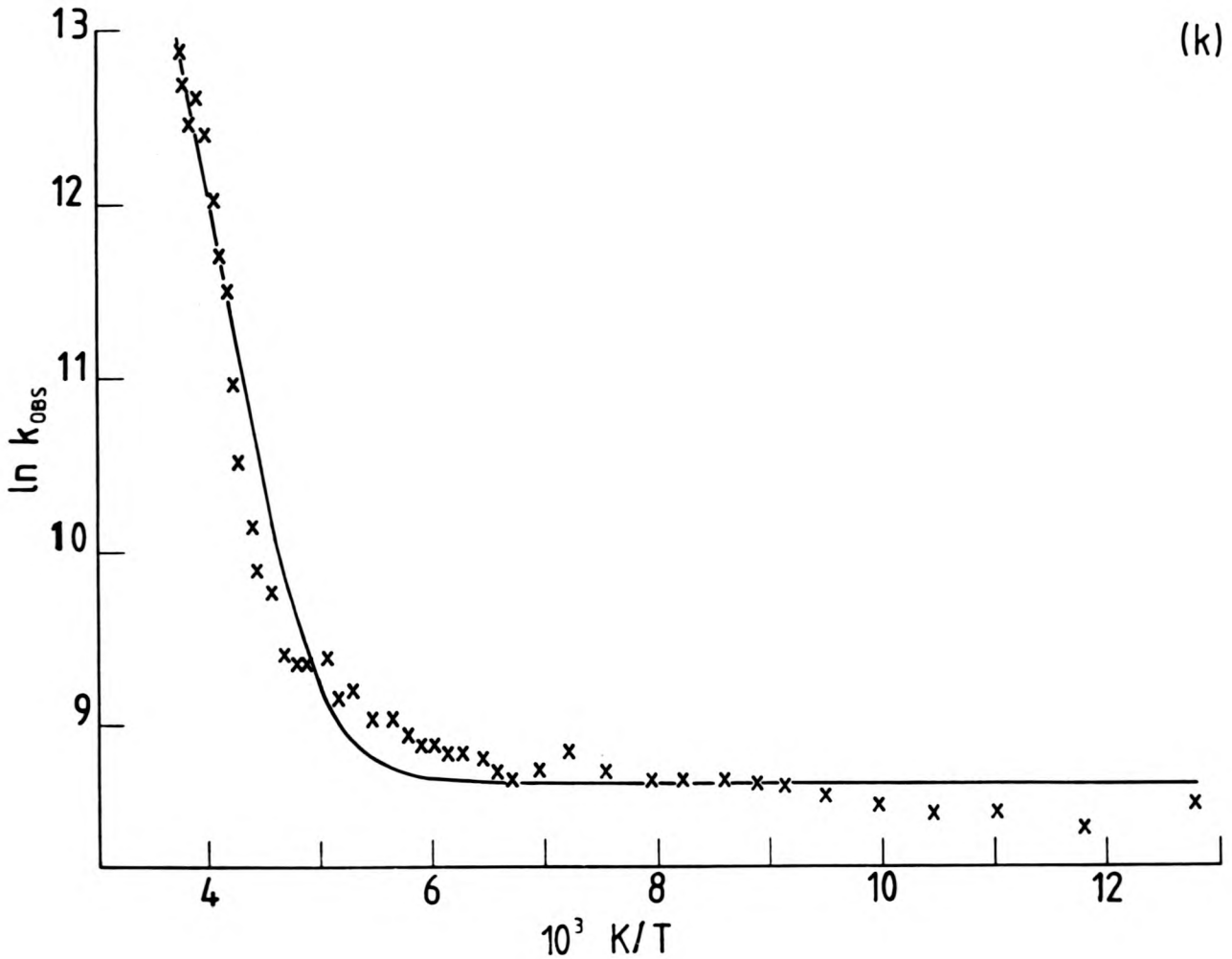
(k)
13
12
11
10
9
ln k_{OBS}
4
6
8
10
12
10^3 K/T

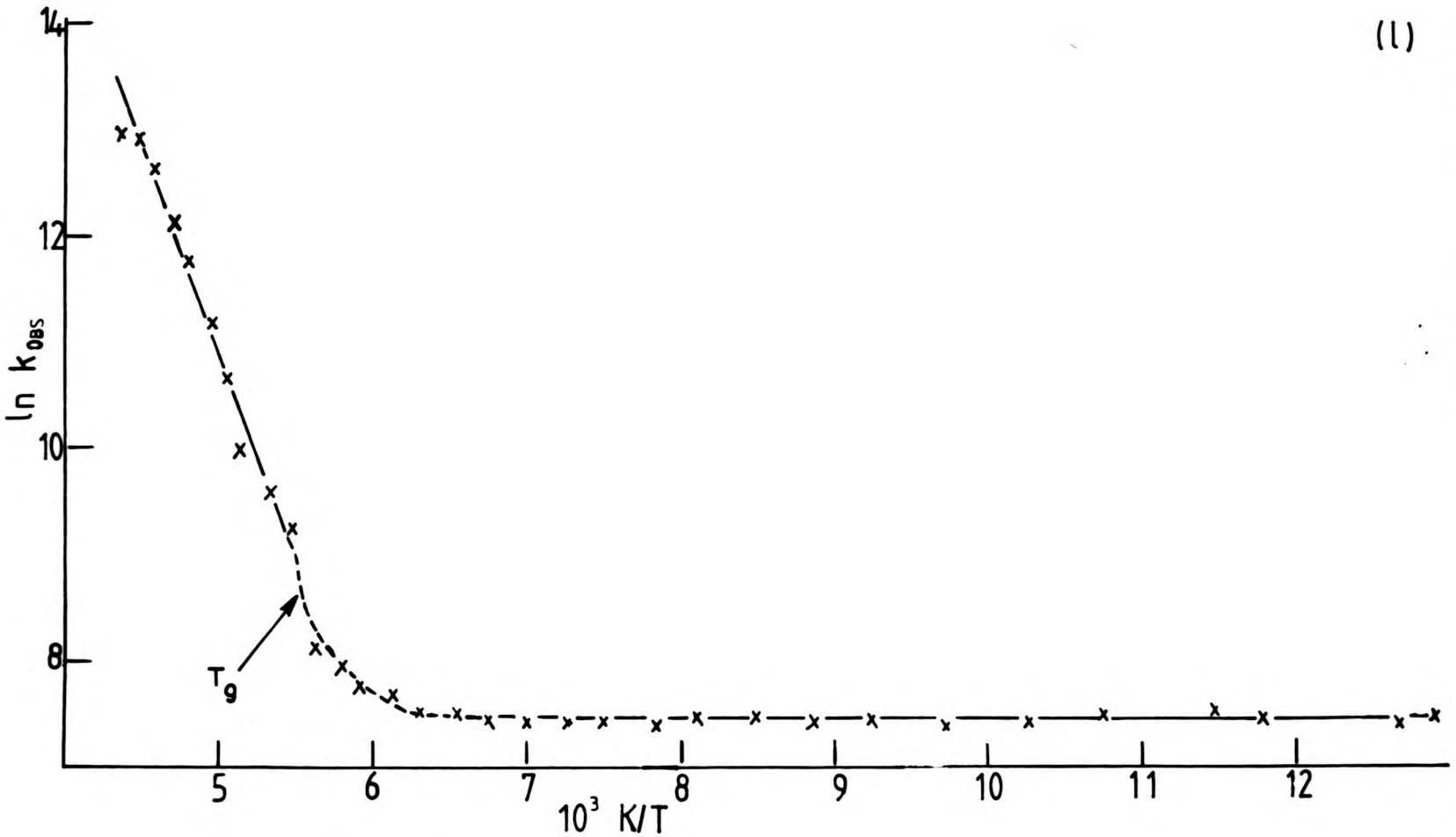

(l)

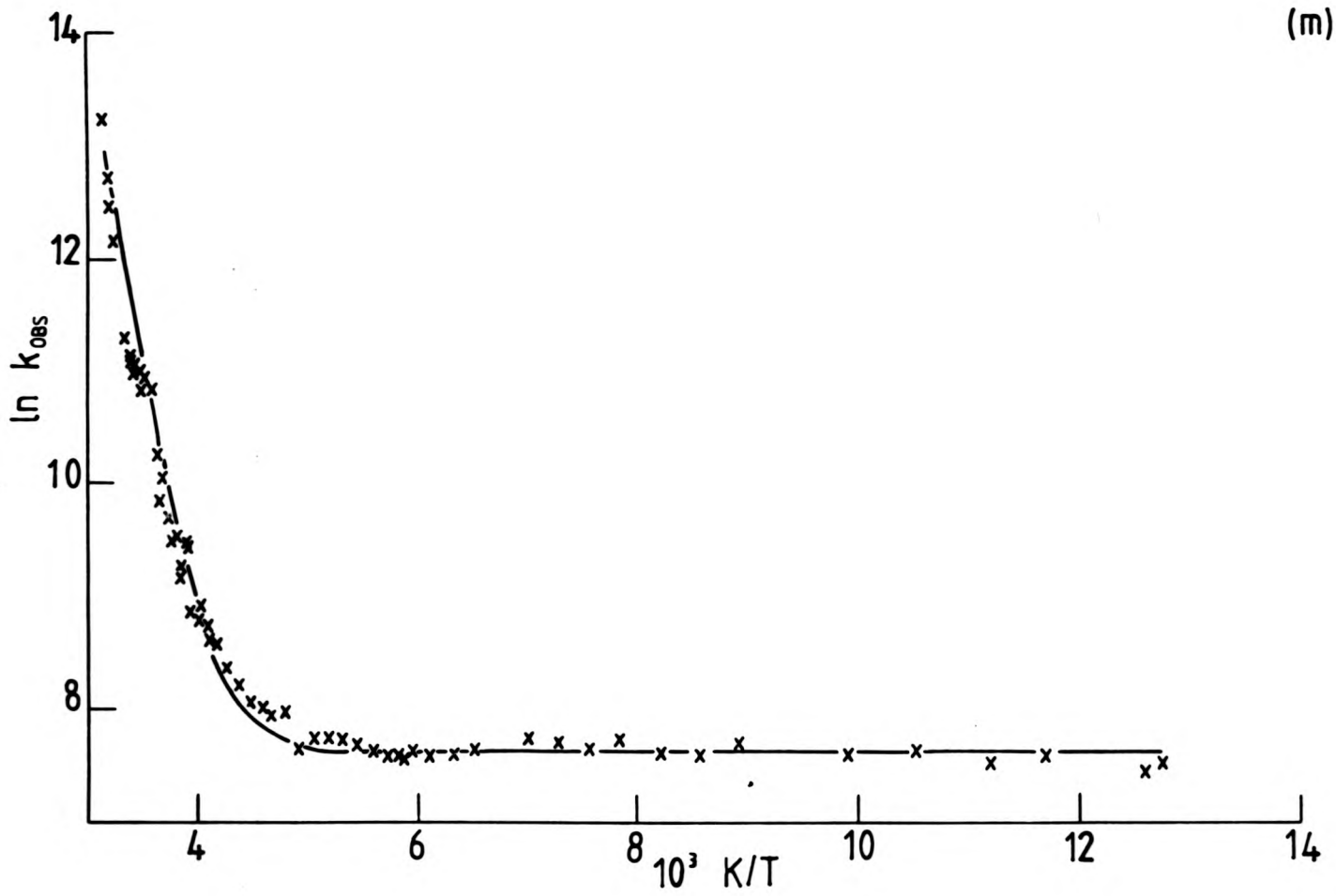
(m)
14
12
10
8
ln k_{OBS}
4
6
8
10
12
14
10^3 K/T

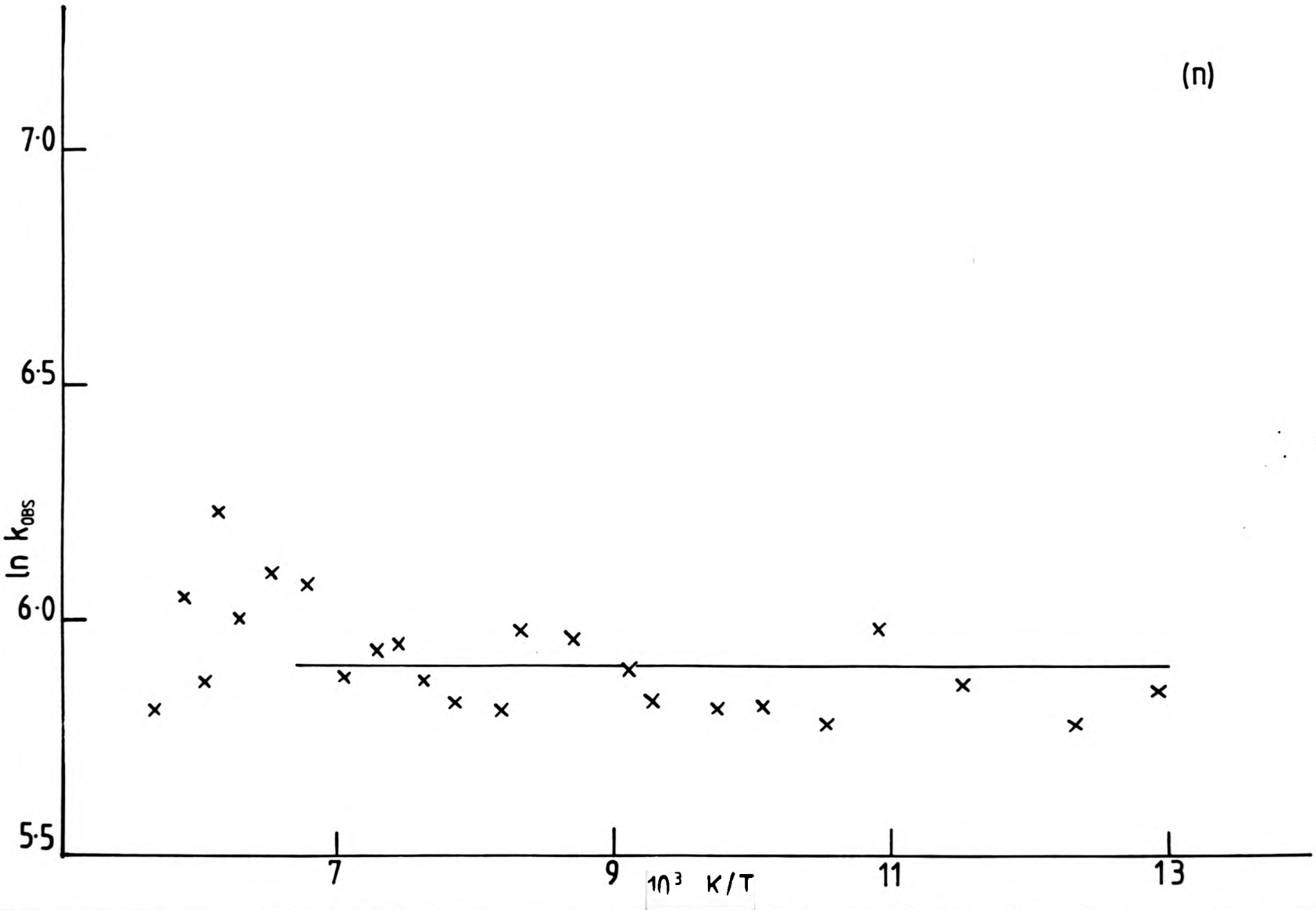
(n)
7·0
6·5
6·0
5·5
ln k_{OBS}
7
9
11
13
10^3 K/T

$$k_{obs} = A \exp(-E_A/RT) + B \qquad (4\text{-}1)$$

where B represents the sum of the temperature-independent radiative and non-radiative rate constants, A is the limiting rate of the temperature-activated pathway of activation energy, E_A. R is the gas constant (8.3142 J mol^{-1} K^{-1}) and T is the absolute temperature. The values of A, B and E_A resulting from computer-fitting the observed data to this expression are given in Table 4-1, with the fitted curves and experimental data points being given in the Arrhenius plots of Figure 16. The experimental data is also given more accurately in tabulated form in Appendix II.

Table 4-1 also gives the results of fitting equation (4-1) to the digitised forms of graphical data given by other workers for the thermal quenching of chromium(III) luminescence in crystalline as well as polymeric and solvent media for which either no activation parameters have been given, or a rigorous curve-fitting routine has not been adopted. Of particular interest is the analysis of the data given by Targos and Forster[77] for which the authors preferred a two-exponential expression (equation (2-3)). However, as shown in Figure 17. equation (4-1) has been found to provide a better explanation of the observed trends than equation (2-3), although the relatively few data points (typically 12 to 15) lead to large standard deviations in the activation parameters (Table 4-1). The fitted curves to these sets of data have not been given (to conserve space), but are typical of the standard shown for the experimental data produced from this work (Figure 16). Figure 17 also illustrates the importance of correct presentation of the data. This figure shows the Arrhenius data in the form given by the authors, and it is not

Figure 17

Temperature dependence of the luminescence lifetime of 0.1% $[Cr(acac)_3]$: $[Al(acac)_3]$ crystals. X-experimental points from ref. 77; dotted line - fitted expression from ref. 77; full line-computer fit to equation 4-1.

nce lifetime

s.

ted line -

ne-computer

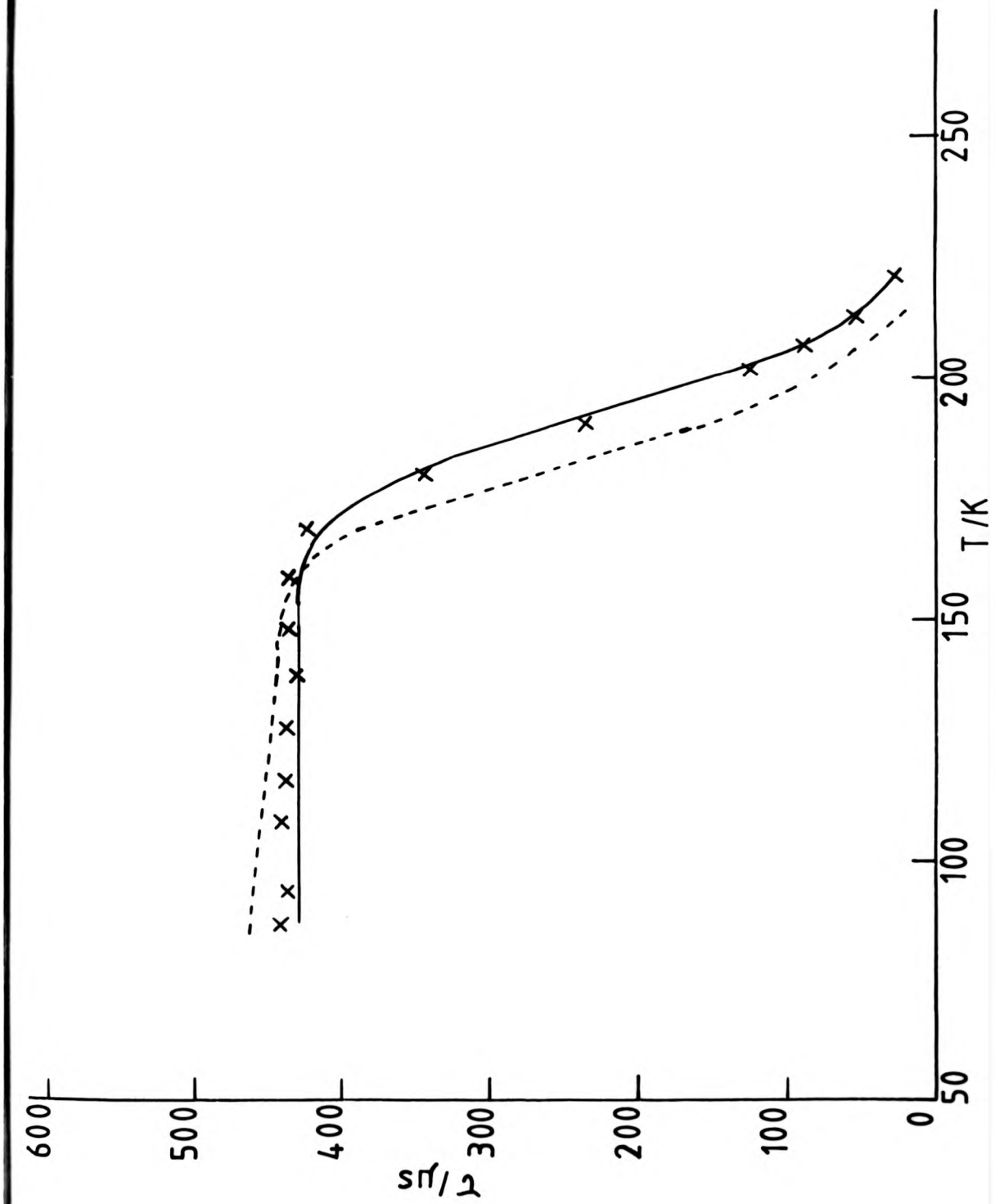

easily interpretable as a form of equation (4-1) to which the data has been shown to be a good fit. However, if this data were presented in the correct Arrhenius form, then the presence of one or more temperature-activated pathways would be more discernible.

Table (4-1) also contains activation parameters reported for related chromium(III) systems (although in most cases over a restricted temperature range) in order to facilitate comparison between the results of this work and related studies, so that any general trends can be noted and discussion of these results in the context of a general model for the luminescence from chromium(III) systems can be made.

4-2 Discussion of the Arrhenius plots obtained from this work

A perusal of these plots shows that all the plots have a similar form, as noted earlier, and reach the low-temperature plateau region either just above or around T_g in the case of 9 M $LiCl/H_2O$ solutions ($1/T_g = 5.5 \times 10^{-3}\ K^{-1}$) with the exception of $[Cr(terpy)_2]^{3+}$ in 9 M $LiCl/H_2O$) which shows a discontinuity in the region of the phase transition. The absence of this behaviour in cellulose acetate film shows that this is due to the phase transition itself rather than any inherent deactivation mode within the complex. Similarly, the complicated behaviour exhibited by $[Cr(phen)_3]^{3+}$ in nitroethane can also be attributed to a phase transition. Unfortunately, the loss of emission intensity in this solvent below T_g (cf. acetonitrile and methanol) due to poor glassing made studies at lower temperatures impossible for these systems, and the limiting value of B is therefore uncertain (see Table 4-1). However, these last two cases illustrate the presence of a

Table 4-1 Measured, fitted* and reported activation parameters for the thermal quenching of the luminescence from chromium(III) complexes in solution, polymeric and crystalline environments

COMPLEX	MEDIUM	$10^{-2}B/s^{-1}$	$10^{-10}A/s^{-1}$	E_A/kJ mol^{-1}	ΔE_{SPEC} [a]	λem(nm) [b]	τ_{298}(μs) [c]	REFERENCE
	H_2O	-	-	43.30	75.4		- [d]	87
	H_2O	-	-	43.69±1.2	(49.3)		- [d]	46
	H_2O	-	1.07×10^3	41.9			2.07	84
$[Cr(NH_3)_6]^{3+}$	9 M LiCl/H_2O	(1.9±0.9)x10^2	(1.3±0.7)x10^3	41.6±1.6		654	1.47	This work(Fig.16a)
	D_2O	-	-	45.37±1.2			- [d]	46
	D_2O	-	2.9×10^3	45.2			2.9	84
	DMF	-	-	53.39±1.2			- [d]	46
	DMSO	-	-	58.78±1.2			- [d]	46
$[Cr(MeNH_2)_6]^{3+}$	H_2O	-	-	39.03±1.2	71.8		- [d]	46
	DMF	-	-	49.56±1.2			- [d]	46
	H_2O	-	-	43.5	82.6		- [d]	87
	H_2O	-	-	44.05±1.2	(58.1)		- [d]	46
	H_2O	-	1.07×10^3	41.9			2.07	84
†$[Cr(en)_3]^{3+}$	9 M LiCl/H_2O	1.09±0.88)x10^2	(1.41±1.1)x10^3	41.6±2.4		677	1.37	This work(Fig.16b)

† (continued on next page)

Table 4-1 (page 2)

	D_2O	-	2.1×10^4	49.0			1.85	84
	DMF	-	-	44.89±1.2			- [d]	46
	DMSO	-	-	48.72±1.2			- [d]	46
	MeOH-H_2O-glycol	$(1.110\pm0.002)\times10^2$	$(1.57\pm0.45)\times10^4$	47.3±0.63			1.23	Fitted from ref. 120
$[Cr(tn)_3]^{3+}$	MeOH-H_2O-glycol	$(9.18\pm0.09)\times10^1$	$(1.72\pm0.37)\times10^2$	37.99±0.47			2.59	Fitted from ref.120
	H_2O	-	-	34.7	99.4		- [d]	95
	H_2O	-	-	31.48±1.2	(65.6)		- [d]	46
	H_2O	-	0.36	29.31			38	84
	H_2O (0.4 M HCl)	-	-	32.32±1.2			- [d]	46
$[Cr(bipy)_3]^{3+}$	9 M LiCl/H_2O	1.87±0.04	0.18±0.05	29.9±0.7		727	95.1	This work (Fig. 16c)
	DMF	-	-	28.61±1.2			- [d]	46
	DMSO	-	-	33.16±1.2			- [d]	46
	MeCN	-	-	15.5			- [d]	84
	CA film	2.3±0.2	$(1.05\pm0.25)\times10^1$	40.8±0.7		727	130.1	This work (Fig. 16d)

(continued)

Table 4-1 (page 3)

	H_2O	-	-	17.96±1.2	120.9		- [d]	46
	9 M LiCl/H_2O	2.1±1.4	0.11±0.04	24±1.0		735	17.1	This work (Fig. 16e)
$[Cr(phen)_3]^{3+}$	MeOH	38±4	$(7.2\pm3.5)\times10^{-4}$	12.4±1.0		735	19.2	This work (Fig. 16f)
	MeCN	32±2	$(3.7\pm3.3)\times10^{2}$	49.3±2.6		735	85.9	This work (Fig. 16g)
	$EtNO_2$	161±8 [h]	1.8±0.4	31.4±0.7		735	13.8	This work (Fig. 16h)
	CA film	2.5±0.6	$(6.2\pm4.1)\times10^{4}$	68.6±2.1		735	1265.2	This work (Fig. 16i)
	H_2O	-	7.2	31.8	76.6		5.21	84
trans-$[Cr(en)_2(NCS)_2]^{+}$	H_2O	-	-	25.62±1.2	(50.2)		- [d]	46
	DMSO	-	-	34.72±2.4			- [d]	46
	H_2O	-	4.0×10^{5}	41.9±2.5	71.8		5.53×10^{-3}	88
	H_2O	-	4.3×10^{5}	41.9	(40.3)		5.14×10^{-3}	84
	D_2O	-	1.6×10^{5}	37.7			2.54×10^{-3}	84
trans-$[Cr(NH_3)_2(NCS)_4]^{-}$ [e]	MeOH-H_2O-glycol	$(3.76\pm0.64)\times10^{1}$	$(6.12\pm1.03)\times10^{4}$	41.51±0.33			3.09×10^{-2}	Fitted from Ref. 120
	MTHF	$(6.9\pm0.1)\times10^{2}$	$(9.6\pm7.6)\times10^{1}$	29.1±1.7			.13	This work (Fig. 16j)
	MeCN	-	5.8×10^{4}	44.0			8.90×10^{-2}	84
	MeCN	-	2.5×10^{5}	47.7±0.8			9.19×10^{-2}	88
	CA film	$(5.8\pm0.2)\times10^{1}$	$(2.6\pm1.3)\times10^{1}$	29.7±1.1			.62	This work (Fig. 16k)

(continued)

Table 4-1 (page 4)

$[Cr(CN)_6]^{3-}$ f	MeOH-H_2O-glycol	2.88±0.8	14.1±1.4	30.54±0.21	161.9	1.60	Fitted from Ref.120
	Glycerin-H_2O	-	-	46.9	(137.4)	- d	75
	Formamide-MeOH	-	-	15.9		- d	75
$[Cr(terpy)_2]^{3+}$	9 M LiCl/H_2O g	$(1.7\pm0.1)\times10^{1}$	$(1.76\pm0.97)\times10^{2}$	31.6±1.7	800	.197	This work (Fig.16l)
	CA film	$(2.05\pm0.09)\times10^{1}$	$(1.69\pm0.63)\times10^{2}$	40.3±0.9	800	6.76	This work (Fig.16m)
$[Cr(NCS)_6]^{3-}$	MeOH-H_2O-glycol	2.43±0.08	$(3.47\pm0.11)\times10^{4}$	39.19±0.06	56.3	2.13×10^{-2}	Fitted from Ref.120
	Glycerin-H_2O	-	-	14.2	(32.92)	- d	75
	Formamide-H_2O	-	-	29.3		- d	75
	MeCN	-	3.2×10^{6}	49.4		1.43×10^{-2}	84
	CA film	3.65±0.2	-	-		- d	This work (Fig.16n)
$[Cr(acac)_3]$ †	EtOH	$(2.17\pm0.09)\times10^{1}$	$(2.1\pm1.1)\times10^{-4}$	8.2±0.7	65.8	12.7	Fitted from Ref.77
	n-PrOH	$(2.04\pm0.24)\times10^{1}$	$(4.1\pm4.8)\times10^{-3}$	11.2±1.5	(39.3)	21.4	Fitted from Ref.77
	n-BuOH	$(2.10\pm0.08)\times10^{1}$	$(7.8\pm8.8)\times10^{-3}$	13.4±1.5		2.85	Fitted from Ref.77
	n-C_5H_9OH	$(2.07\pm0.13)\times10^{1}$	$(8.1\pm6.8)\times10^{-4}$	10.1±1.1		7.17	Fitted from Ref.77
	n-$C_6H_{11}OH$	$(2.04\pm0.15)\times10^{1}$	$(8.2\pm13.9)\times10^{-3}$	13.4±2.2		2.71	Fitted from Ref. 77

† continued on next page

Table 4-1 (page 5)

	$\underline{n}$-$C_7H_{13}OH$	$(2.28\pm0.06)\times10^{1}$	$(4.2\pm8.6)\times10^{4}$	26.3 ± 2.5		9.7×10^{-5}	Fitted from Ref. 77
	$\underline{n}$-$C_8H_{15}OH$	$(2.17\pm0.09)\times10^{1}$	$(9.2\pm4.2)\times10^{-4}$	7.15 ± 0.58		1.94	Fitted from Ref. 77
	isopentane-3-methylpentane	$(2.31\pm0.05)\times10^{1}$	$(4.8\pm0.9)\times10^{-6}$	3.7 ± 0.24		76.4	Fitted from Ref. 77
	PMM	$(2.17\pm0.02)\times10^{1}$	$(3.0\pm0.8)\times10^{-5}$	7.1 ± 0.4		51.9	Fitted from Ref. 52
	ether-isopentane-alcohol	-	$(3.16\pm0.76)\times10^{-5}$	3.60 ± 0.22		13.5	Fitted from Ref. 77
	MeOH-H_2O-glycol	2.62 ± 0.10	$(8.26\pm0.90)\times10^{3}$	32.63 ± 0.17		6.35×10^{-3}	Fitted from Ref. 120
	$Al(acac)_3$	$(2.30\pm0.01)\times10^{1}$	$(2.54\pm0.47)\times10^{1}$	28.4 ± 0.3		0.374	Fitted from Ref. 52
	Crystalline	$(7.82\pm0.76)\times10^{1}$	$(1.54\pm3.33)\times10^{-1}$	17.22 ± 0.34		0.674	Fitted from Ref. 77
$[Cr(acac)_3]$	50% in $Al(acac)_3$	$(4.27\pm0.4)\times10^{1}$	$(1.39\pm0.99)\times10^{-3}$	9.5 ± 1.0		3.28	Fitted from Ref. 77
	10% in $Al(acac)_3$	$(2.23\pm0.06)\times10^{1}$	$(1.36\pm0.97)\times10^{2}$	31.4 ± 1.2		0.235	Fitted from Ref. 77
	0.1% in $Al(acac)_3$	$(2.34\pm0.05)\times10^{1}$	$(7.70\pm1.43)\times10^{2}$	35.4 ± 0.34		0.208	Fitted from Ref. 77
	5% in $AlCl_3.6D_2O$	$(2.36\pm0.62)\times10^{1}$	$(4.03\pm4.74)\times10^{-4}$	6.24 ± 1.24	25.1	3.06	Fitted from Ref. 76
Cr^{3+}	2% in $NaMgAl(C_2O_4)_3.9H_2O$	$(1.16\pm0.04)\times10^{1}$	$(8.88\pm2.82)\times10^{-1}$	14.69 ± 0.33		4.23×10^{-2}	Fitted from Ref. 76
	5% in $K_3\,CO(CN)_6$	$(8.70\pm0.35)\times10^{-2}$	$(7.37\pm1.99)\times10^{-9}$	4.80 ± 0.63		8742.0	Fitted from Ref. 76

(continued)

Table 4-1 (page 6)

* values quoted to ± one standard deviation

[a] refers to the observed quartet (absorption)-doublet(emission) splitting. Values are adapted from ref. 46 except for $[Cr(CN)_6]^{3-}$ which was calculated from data in ref. 119. Bracketed figures represent the 'thexi'-doublet splitting calculated from ref. 20 except for $[Cr(bipy)_3]^{3+}$ which is from data in ref. 93.

[b] refers to the monitoring wavelength used for this work.

[c] lifetimes at 298 K were calculated from the appropriate fitted expression.

[d] phosphorescence intensity study and therefore no lifetime calculation is possible.

[e] for many more solvents, see ref. 88.

[f] activation parameters (and Arrhenius plots) for a number of solvents are given in ref. 119, but values are dubious due to the vestige of curvature in the experimental plots, for which a linear Arrhenius relationship has been assumed.

[g] fitted in two parts due to anomalous behaviour at T_g of solvent (see Fig. 161).

[h] this value of B is not a low-temperature limit due to the presence of a change in the temperature profile at T_g. A value of $\sim 3.65 \times 10^2$ s^{-1} may be more appropriate (see Fig. 16h).

solvent-perturbed deactivation at least for these systems, with the viscosity of the environment having a significant effect on the emission lifetime, which may be indicative of either a diffusion-controlled deactivation mechanism involving the solvent molecules or deactivation through the metal-ligand vibrations of the complex which will be affected by the enhanced rigidity of the 'solvent cage'. However, the latter possibility is unlikely because this effect would then be expected to be seen for all solvent media as the metal-ligand vibrations will be restricted in all cases, although this mechanism may well explain the nature of the overall temperature-activated pathway. This behaviour may, therefore, reflect the effect of viscosity on the temperature-independent non-radiative pathway, although the absence of this behaviour in other cases is puzzling. Possibly the observed behaviour for the cases of $[Cr(terpy)_2]^{3+}$ in 9 M $LiCl/H_2O$ and $[Cr(phen)_3]^{3+}$ in nitroethane can be simply explained by the drastic change in the environment experienced by these complexes on going through this phase transition. However, this would not explain (i) why no effect of phase transition is apparent for other complexes in 9 M $LiCl/H_2O$ and (ii) similar behaviour was not found for $[Cr(phen)_3]^{3+}$ either in acetonitrile or methanol, which gave equally opaque glasses as nitroethane.

4-3 Comments on the Arrhenius parameters tabulated in Table 4-1

The general trends which emerge from this table are:-

(i) The activation energies for a given complex are very sensitive to solvent.

(ii) The activation energies are considerably less than the observed (Franck-Condon) quartet-doublet splitting, ΔE_{SPEC}, and

with the exception of $[Cr(acac)_3]$ and Cr^{3+} lie mainly within the range 30 to 50 kJ mol^{-1}.

(iii) The activation energies for the Cr-N (ammine) systems in H_2O are remarkably constant for both mono- and bidentate ligands with trans-$[Cr(en)_2(NCS)_2]^+$ the only definite exception, although the value for $[Cr(NCS)_6]^{3-}$ is unknown as emission from aqueous solution could not be detected for this system. In contrast, however,there is a noticeable drop in activation energy (by 10 to 15 kJ mol^{-1}) on going to polypyridyl complexes in aqueous media. For these systems, $[Cr(bipy)_3]^{3+}$ and $[Cr(terpy)_2]^{3+}$ show similar activation energies with a similar sensitivity of E_A to solvent as found in the Cr-N (ammine) systems. $[Cr(phen)_3]^{3+}$, while adhering to a general reduction in E_A for aqueous media, shows extreme sensitivity to solvent with E_A varying between $\sim$12 and 69 kJ mol^{-1}.

(iv) The B term, where given, is reasonably constant for a given complex, with the apparent exception of $[Cr(phen)_3]^{3+}$. However, this is probably due to the restricted temperature range for these exceptional systems (see Figure 16), and good agreement between the two low temperature (77 K) values for CA film and 9 M $LiCl/H_2O$ is evident.

4-4 The argument against back-ISC as the thermally activated pathway

Points (i) and (ii) are in general agreement with previous results and the implications have been discussed fully in the Introduction. However, it is worth noting that while the activation energies for these systems are solvent-sensitive, a similar trend in ΔE_{SPEC} is not apparent as this term has been found to be not particularly sensitive to solvent, either for the

systems studied in this work or other reported systems, although a slight solvent-dependence (a few hundred cm^{-1}) for the individual terms in some cases have been reported,[119,88] but this is insufficient to parallel the change in activation energy. Assuming ΔE_{SPEC} to reflect, rather than to predict, the position of the 'thexi' state, then this observation would indicate that the temperature-activated pathway is not back-ISC as there is no parallel behaviour between E_A and ΔE_{SPEC} toward solvent. However, this argument is by no means conclusive as ΔE_{SPEC} may well bear no reflection of the final 'thexi' state position as the doublet and Franck-Condon quartet states both represent the same complex geometry and there seems no reason, therefore, why ΔE_{SPEC} should be sensitive to solvent; indeed, the insensitivity gives weight to the argument that the quartet absorption band represents the 'Franck-Condon' state. However, Adamson's[20] expression (equation (2-1)) suggests a simple parallel between 'observed' and distorted quartet positions which would be expected to be reflected in the value of ΔE_{SPEC}, suggesting the use of this expression for solvent dependence may be inappropriate. Another argument derives from the fact that while the 'thexi' state is distorted, the doublet state is not, and the cross-over point representing back-ISC to the 'thexi' state may well occur through the isogeometric 'Franck-Condon' state, in which case the lack of solvent dependence would rule out this mechanism for the temperature-activated pathway. Conversely, the cross-over point could equally well be at a position of common distortion for the doublet and 'thexi' states, in which case the lack of correlation of E_A with ΔE_{SPEC} is not particularly meaningful.

However, for back-ISC to be the mechanism responsible for this temperature-activated pathway, then the activation energies must represent, at least, the difference in energy between the cross-over point to the 'thexi' state and the doublet state and, in fact, should be larger than this value as the coincidence of the cross-over point with the potential minimum of the 'thexi' state is unlikely. On referring to the bracketed figures for ΔE_{SPEC} in Table 4-1, however, it is apparent that the observed activation energy is considerably lower than the required value, and back-ISC would seem to be an inappropriate description of the temperature-activated pathway. This statement is not surprising in the light of the introductory discussion in Chapter 2-1, but what is remarkable is the result that $[Cr(acac)_3]$ in a crystalline environment also shows an observed E_A much lower than ΔE_{SPEC}, indicating back-ISC to be unimportant even in this environment.

4-5 What is the nature of the thermally-activated non-radiative pathway?

While back-ISC to the quartet state may be unimportant, there is also the possibility of deactivation through other excited states to consider, in particular higher doublet states. The report of ESA spectra for a number of chromium(III) complexes has enabled the position of these states to be evaluated, and the position of the lowest energy absorption band, assigned to the $^2A_{1g} \leftarrow {}^2E$ transition (Δ_D) are given below for a number of complexes.

Figure 18

Barclay-Butler plots for the Arrhenius parameters for the non-radiative decay term for Cr(III) complexes in various media.

(a) $[Cr(CN)_6]^{3-}$ (slope = 0.5 ± 0.2 mol kJ^{-1})

Key: 1-DMF; 2-MeCN; 3-i-PrCN; 4-PhCN; 5-i-PrOH; 6-n-PrOH; 7-EtOH; 8-EtOD; 9-MeOH; 10-MeOD; 11-methylformamide; 12-formamide.

(b) $[Cr(acac)_3]$ (slope = 0.48 ± 0.02 mol kJ^{-1})

Key: 1-100% crystal; 2-50% in $[Al(acac)_3]$; 3-10% in $[Al(acac)_3]$; 4-0.1% in $[Al(acac)_3]$; 5-EtOH; 6-n-PrOH; 7-n-BuOH; 8-n-pentanol; 9-n-hexanol; 10-n-heptanol; 11-n-octanol; 12-ether/isopentane /alcohol; 13-isopentane/3-methylpentane; 14-polymethylmethacrylate; 15-MeOH/H_2O/glycol; 16-$[Al(acac)_3]$.

(c) $[Cr(phen)_3]^{3+}$ (slope = 0.32 ± 0.02 mol kJ^{-1})

parameters

(III) complexes

kJ^{-1})

5-i-PrOH;

; 1O-MeOD;

ol kJ^{-1})

c)$_3$];

[Al(acac)$_3$];

pentanol;

-octanol;

$_3$].

2 mol kJ^{-1})

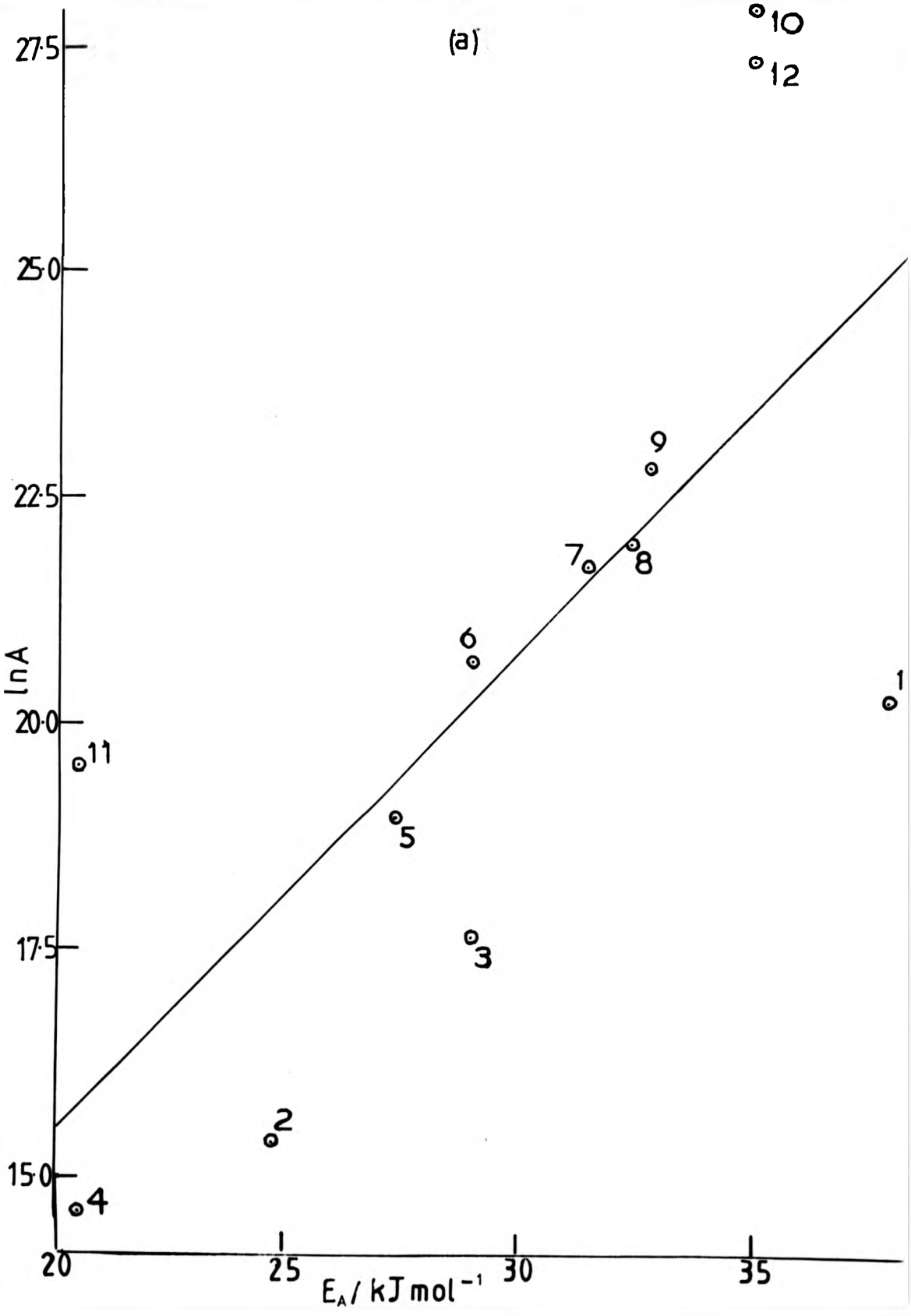

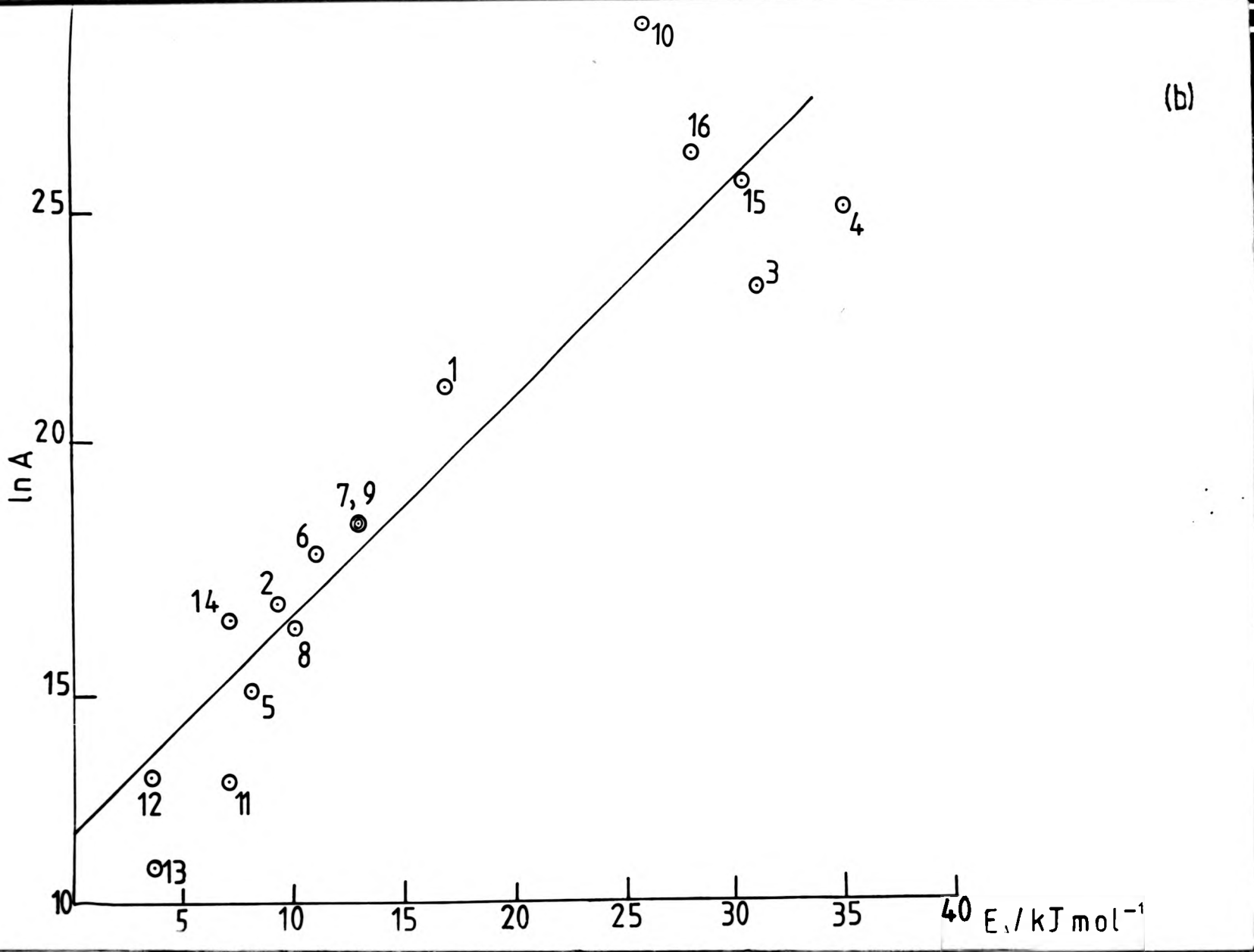
(b)
ln A
25
20
15
10
5
10
15
20
25
30
35
40
E_a / kJ mol^-1
1
2
3
4
5
6
7, 9
8
10
11
12
13
14
15
16

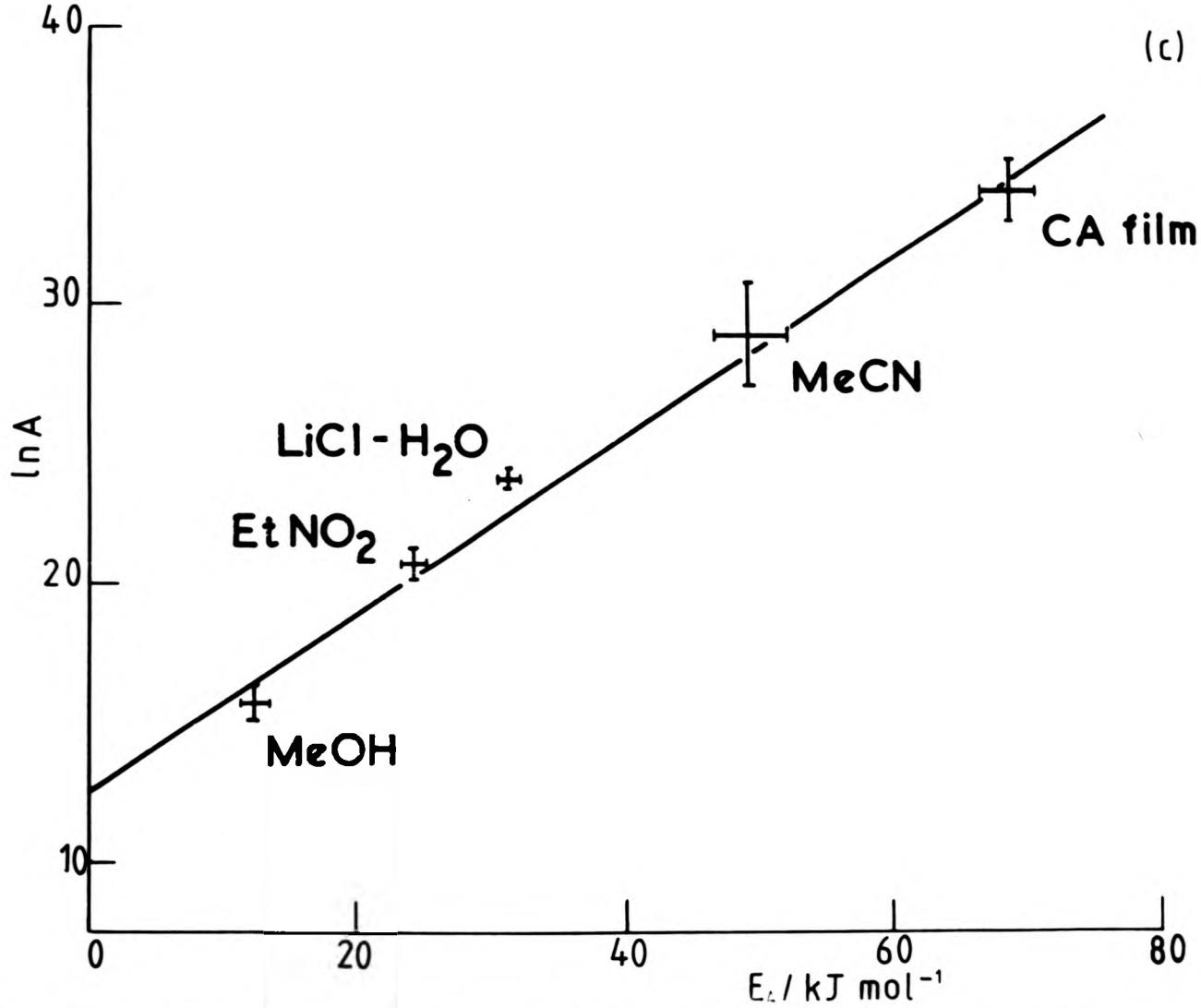
(c)
40
30
20
10
lnA
CA film
MeCN
LiCl - H2O
Et NO2
MeOH
0
20
40
60
80
Ea / kJ mol-1

COMPLEX	Δ_D(kJ mol^{-1})	REFERENCE
trans-$[Cr(NH_3)_2(NCS)_4]^-$	225.9	88
$[Cr(NCS)_6]^{3-}$	222.6	233
$[Cr(acac)_3]$	227	225
$[Cr(bipy)_3]^{3+}$	202.3	82

These values of Δ_D are obviously far too high to explain the observed activation energy for the thermally-activated non-radiative route, k_{TA}, and it can therefore be safely assumed that k_{TA} involves direct deactivation of the doublet state without involvement of any other intermediate states. This, however, does not necessarily indicate direct communication with the ground state. With reference to the general model, this implies that k_{TA} can be assigned to either k_6 or k_{RD}, assuming that k_5 is temperature-independent. That a common mechanism can be used to describe k_{TA} for a given complex has been shown in the case of Reinecke's salt by Adamson,[88] who showed that the Arrhenius data could be fitted to a Barclay-Butler plot, the significance of which has been discussed previously in the Introduction. Similar plots have been performed both for the data referring to $[Cr(phen)_3]^{3+}$ and $[Cr(acac)_3]$ given in Table 4-1, and those of Wasgestian *et al.*[119] for $[Cr(CN)_6]^{3-}$, and the results, along with those of Adamson, are tabulated below, the plots being given in Figure 18.

COMPLEX	SLOPE (mol kJ^{-1})	CORRELATION COEFFICIENT	DATA REFERENCE
trans-$[Cr(NH_3)_2(NCS)_4]^-$	0.41	-	88
$[Cr(CN)_6]^{3-}$	0.5 ± 0.2	0.722	119
$[Cr(acac)_3]$	0.48 ± 0.05	0.927	Table 4-1
$[Cr(phen)_3]^{3+}$	0.32 ± 0.02	0.994	Table 4-1

The poor correlation coefficient for $[Cr(CN)_6]^{3-}$ is not surprising when footnote f of Table 4-1 is taken into consideration, but the two other sytems give pleasing results. This, therefore, suggests that a single, common mechanism for a given complex should be sought, although the need for this mechanism to cover all complexes is questionable and is certainly not required by this result. However, point (iii) of section 3 suggests that the Cr-N (ammines) all adhere to a common mechanism whereas the polypyridyl complexes may pertain to a different (common) mechanism. One other point which emerges from the Barclay-Butler plot of $[Cr(acac)_3]$ (Figure 18b) is that the Arrhenius parameters for both solution and solid state environments can be correlated to this plot, which indicates a common mechanism for all forms of environment, at least for this complex.

The proposed mechanism must obviously incorporate a considerable solvent contribution to explain the noted solvent effects, both on the observed activation energies in this work and those reported in the Introduction (Chapter 2-1). In particular, a mechanism invoking a strong-coupled process is required by the notable lack of any significant solvent deuterium effect at ambient temperature. As k_6 is expected to be weakly-coupled, from the lack of distortion of the doublet state, then k_{RD} would seem to be the obvious choice for the temperature-activated route, a conclusion which was implied on the preceding introduction. This pathway must involve a bond-breaking mechanism to allow for photochemical reaction, but the exact nature of the solvent participation is uncertain, for instance, is the mechanism dissociative or associative? It maywell be that the nature of the participation is the origin

of the markedly differing solvent dependencies of the activation energies for different complexes.

As noted earlier, there seems good reason for treating Cr-N (ammine) and Cr(N-N) polypyridyl complexes as separate cases. Similarly, $[Cr(acac)_3]$ displays unexpected behaviour and warrants special attention. These complexes will therefore be discussed separately, and the role of the thermally-activated pathway in the context of other deactivation processes will be considered and further elucidation of the mechanism of the former process will be attempted.

4-6 Selected complexes

4-6.1 $[Cr(acac)_3]$

The β-diketonate complexes of chromium(III) were amongst the first to be investigated[55] and Forster et al.[116-118] correlated the changes in lifetime for a series of β-diketonate complexes at 77 K with the extent of π-bonding from the low energy, empty π orbitals of these ligands which cause delocalisation of the d electrons and high energy vibrational modes of the ligands are implicated as the principal deactivation route[114] at cryogenic temperatures. This conclusion is substantiated by Table 4-1 which shows the B term for $[Cr(acac)_3]$ to be reasonably solvent insensitive for all but two cases for which no explanation can be offered. This implies that deactivation occurs through intramolecular vibrational modes rather than a process involving solvent participation, a conclusion substantiated by a noted increase in lifetime on methyl substitution of the hydrogen atoms.[116]

This complex does not emit at room temperature which, superficially, seems puzzling (see equation (1-36)) as it is obviously not due to the thermally-activated process which predicts

reasonably long lifetimes. However, Forster et al[85] have reported that ϕ_{ISC} shows a temperature dependence for $[Cr(acac)_3]$ in alcoholic media and polymer film, although ϕ_{ISC} is invariant with temperature in crystalline matrices exemplified by Cr^{3+} in 10% $[Al(acac)_3]$ Further, the temperature-dependence is most marked for the polymer film, indicating the macroscopic viscosity to be unimportant. This thermal quenching of ϕ_{ISC} is consistent with Adamson's proposal of a 'thexi' quartet state[20] for which thermal equilibration competes successfully with ISC at higher temperatures, although the solvent effects indicate that the participation of solvent relaxation to this former process is less certain, and Forster[52] suggests that it is the microviscosity rather than the macroscopic viscosity which must be considered. This statement, therefore requires more detailed consideration of the environment. For instance, a 'rigid' solvation shell may well be more effective in retarding deactivation than a crystalline environment for which large 'sites' may be available for $[Cr(acac)_3]$ in promoting degrading vibrations.

However, in the absence of back-ISC, the expression for the phosphorescence lifetime (equation 1-34)) contains no contribution from any component of the expression ϕ_{ISC}, but requires that, assuming the radiative rate to be temperature-insensitive, the thermally-activated pathway is due either to photochemistry, k_{RD}, or to indirect non-radiative deactivation back to the ground state, k_6. However, the lack of an appreciable increase in E_A on going to crystalline media detracts from the assignment of k_{RD} to this pathway. Similarly, k_6 has been shown to involve deactivation through high-energy ligand vibrational modes and, therefore, a temperature activation can reasonably be expected. k_{RD}, however, must also

involve M-L vibrations, although these will be the low-energy M-L modes rather than higher energy L-H vibrations. If this statement is correct, then k_6 can be regarded as involving a mechanism through which energy transferred to the ligand system is rapidly degraded through the high energy L-H vibrations. However, as the temperature is raised, the M-L bond will become more 'flexible' and will, therefore, become competitive with these vibrations for the excitation energy, and, coupled with the onset of diffusional modes,may well produce photochemistry if the M-L bond becomes considerably weakened. For this treatment, therefore, k_6 and k_{RD} can be regarded as directly competitive processes within a common mechanism. In this particular case, it would seem that either the L-H vibrations are particularly efficient and the M-L bond particularly strong, which would explain the small activation energies in terms of thermal enhancement of the lighter L-H vibrations for which a small activation energy would seem reasonable, or the M-L bond is not very rigid, allowing easier activation of the pathway. The former explanation, however, does not cover the cases where high activation energies are found (Table 4-1) which would suggest that M-L vibrations are involved and would implicate the existence of two alternative mechanisms in this case. While this could still be envisaged to adhere to a Barclay-Butler plot, as a common M-L mechanism is implicated, the best fit has been shown to be a single exponential expression (equation (4-1)); therefore a combination of M-L and L-H vibrations which would be expected for high activation energy cases is unlikely. It would, therefore, seem that the most feasible explanation is thermally-activated deactivation through M-L vibrations which are particularly sensitive to

solvent in some cases, while no detailed explanation of the dependence can be offered, although the microviscosity of the medium could well be important.

4-6.2 Cr-N (ammine) complexes

The parent compounds of this group are $[Cr(NH_3)_6]^{3+}$ and $[Cr(en)_3]^{3+}$ for mono- and bidentate ligands respectively. These compounds and their derivatives have been the subject of extensive studies from a photochemical viewpoint since the first reports on this subject (see Introduction), although few photophysical studies are available. Studies of ϕ_{ISC} for $[Cr(en)_3]^{3+}$ have shown it to be unity in the solid state,[234] but falling to a value of 0.7 in an aqueous environment[98] and a value of 0.4 has been reported for $[Cr(en)_2(NCS)_2]^{+}$. One obvious way in which a photochemical mechanism from the doublet state would be required is if the observed photochemical yield is larger than $1-\phi_{ISC}$. Unfortunately, this is not the case, and the photochemical yield does in fact indicate that ∿25% of the molecules populating the quartet state must either undergo internal conversion to the ground state or undergo cage recombination of the primary photoproducts. This latter mechanism is thought to be relevant, in particular for $[Cr(CN)_6]^{3-}$, by analogy with $[Co(CN)_6]^{3-}$ for which the pathway has been found to be important.[98] Forster[85] has reported no temperature-dependence of ϕ_{ISC} for $[Cr(en)_3]^{3+}$ between 150 and 293 K in any environment which may well be why emission can still be detected at room temperature for these systems and which is in agreement with the above hypothesis.

The large isotope effect on ligand substitution of ∿20 for $[Cr(NH_3)_6]^{3+}$ at 77 K,[113] given in the Introduction indicates

that k_6 is the dominant process at cryogenic temperatures and implicates a weak-coupled deactivation through high energy vibrational modes of the ligand. However, from the Arrhenius parameters given in Table 4-1, it can be calculated that the temperature-activated pathway accounts for 97.6% of the energy dissipated from the doublet state for $[Cr(NH_3)_6]^{3+}$ and 98.6% for $[Cr(en)_3]^{3+}$. Further, the lack of an appreciable isotope effect for either solvent or ligand at ambient temperatures[84] indicates that this is a strong-coupled mechanism, and since back-ISC is unlikely for reasons explained earlier, then a photochemical pathway seems most likely. This route has been preferred by Adamson,[84] who has provided a suitably modified version of his photolysis rules to afford qualitative predication of the room-temperature lifetimes for this series of complexes and, as mentioned in the Introduction, these seem to be quite successful. These rules are based on the principle that the weaker the bond the shorter the lifetime as deactivation is made easier by the less restricted high frequency vibrations. This is, basically, the same assumption made for the model developed in the section dealing with $[Cr(acac)_3]$.

The photoreaction must be the photosubstitution of the ligand by solvent, and some indication of the nature of the participation by the solvent may be found by considering the effect of solvent on luminescence properties of the complex. Wasgestian *et al.*[119] have correlated the lifetime of $[Cr(CN)_6]^{3-}$ at 298 K with the Dimroth paramater, E_T, for the solvent. This parameter is related to the solvent polarity as measured by the solvatochromic shift of the CT absorption band of (4-hydroxy-3,5-diphenyl-phenyl)-2,4,6-triphenyl-

Figure 19

Correlation of $\log_e \tau$ at 296 K with E_T values for trans-$\left[Cr(NH_3)_2(NCS)_4\right]^-$ using the data of ref. 88 (slope = $-(2.7 \pm 0.5) \times 10^{-2}$ kJ^{-1}).

Key: 1-H_2O; 2-MeOH; 3-EtOH; 4-CH_3COOH; 5-i-PrOH; 6-CH_3NO_2; 7-CH_3CN; 8-DMSO; 9-sulpholane; 10-DMF; 11-acetone; 12-CH_2Cl_2; 13-pyridine; 14-$CHCl_3$; 15-tetrahydrofuran.

values for

of ref. 88

; 5-i-PrOH;

pholane;

3-pyridine;

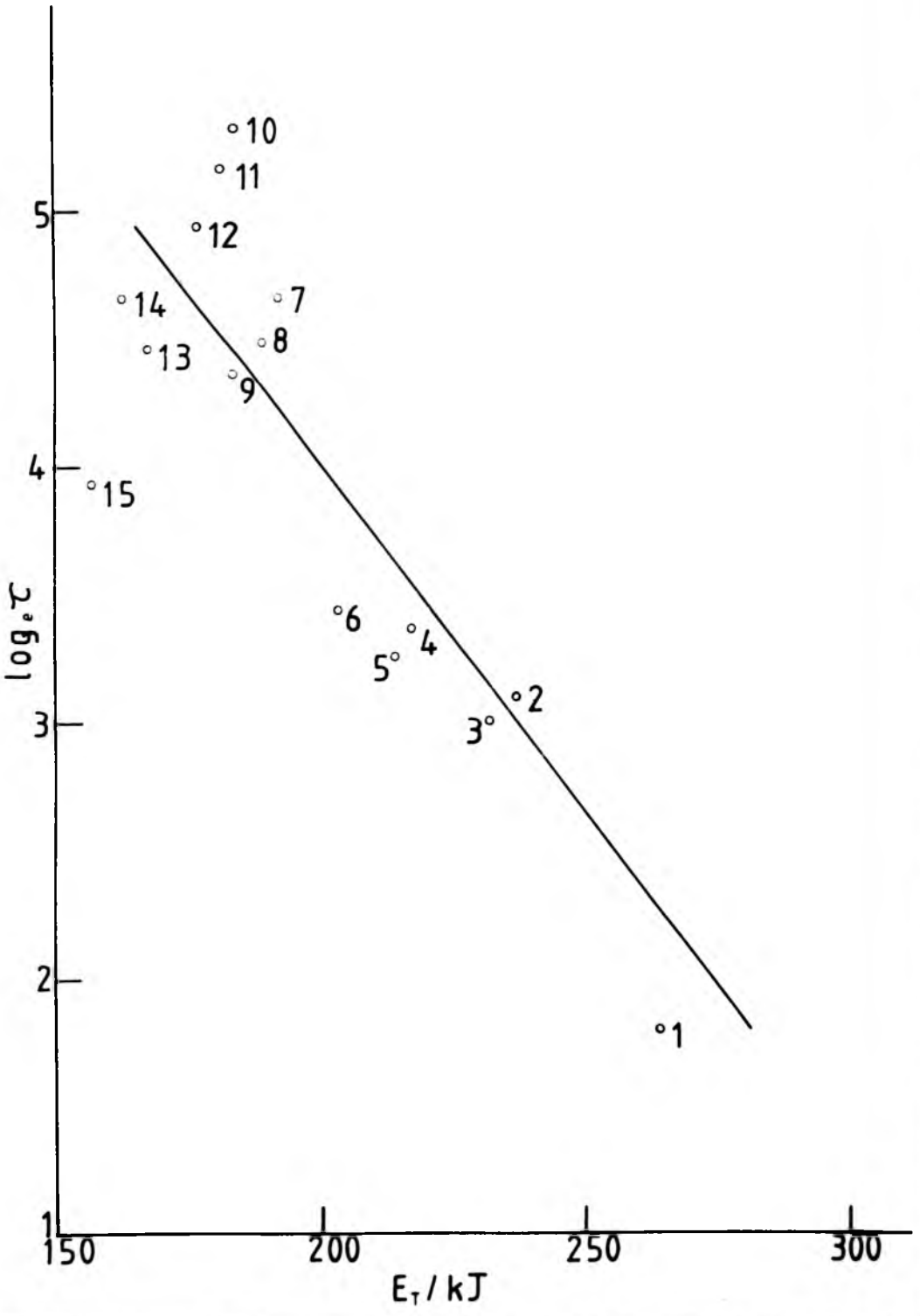

pyridinium-betain. We have also performed this plot for the lifetime data of Reinecke's salt in a number of solvents as given by Adamson,[88] and the result is shown in Figure 19, from which a definite, although approximate, correlation is apparent. Adamson[88] also found no simple correlation between the emission lifetime and macroscopic viscosity of the solvent for this complex, indicating diffusion-controlled processes to be unimportant. The dependence of the emission lifetime on the solvent dipole may reflect either the ease with which a solvent molecule can attack the excited complex, or the solvent enhancement of the M-L vibration, or both. That the dependence is not diffusion-controlled implies the solvent molecules in the solvation shell to be most important. This view is substantiated by the report that the quenching of the emission lifetime of the Reineckate ion in acetonitrile by water obeys Stern-Volmer kinetics of the form[88]

$$\tau_{AN}/\tau = 1 + K_{SV}\, a_w^m \qquad (4\text{-}2)$$

where τ_{AN} is the lifetime in pure acetonitrile, τ is the measured lifetime at a given water activity, a_w. K_{SV} is the Stern-Volmer quenching constant and the exponent m has been found to best fit the observed data with a value of 10, which indicates that there are ten water molecules in the solvation shell. Alternatively, a plot of τ_{AN}/τ against the mol-fraction of water shows a complicated dependence, but indicates that R^- is preferentially solvated by acetonitrile and τ is not affected until a high mol-fraction of water is present. However, both interpretations indicate that the lifetime is dependent upon the composition of the solvation shell rather than the properties of the bulk solvent. Langford[235] has shown that the initial ESA intensity for this complex, and also

trans-$[Cr(en)_2(NCS)_2]^+$ and $[Cr(bipy)_3]^{3+}$ is much more sensitive to solvent than the lifetime, and he has related this to changes in ϕ_{ISC}. However, he has correlated the decrease of the initial ESA intensity (ϕ_{ISC}) with the increasing nucleophilicity of the solvent for trans-$[Cr(en)_2(NCS)_2]^+$ which he considers is indicative of an associative mechanism, involving reaction through the quartet state, as the better the nucleophile, the smaller is ϕ_{ISC}. However, this explanation seems puzzling as the ISC rate, k_4, has been shown to be in the picosecond region, and therefore for the quartet reaction rate, k_{RQ}, to have a significant effect on ϕ_{ISC}, which is the underlying implication in Langford's proposal, then k_{RQ} must be of a similar order of magnitude as the ISC rate (see equation (1-27)). This is highly improbable, and it is more likely that the solvent dependence of the initial ESA intensity lies in the thermal equlibration rate of the quartet 'thexi' state if this quantity does reflect ϕ_{ISC}. However, a more intriguing possibility is that the change in initial ESA intensity is a result of static quenching by the solvation shell,in which case the lifetime dependence on solvent polarity previously noted may be related to the solvating power of the solvent.

It therefore appears that the effect of solvent on the excited state parameters of chromium(III) complexes is very complicated and the explanation of the dependence is imprecise, making predictions about the type of mechanism involved in the doublet photoreaction questionable. Perhaps a more profitable approach would be by studying the equivalent thermal reaction to which the doublet photoreaction has been directly related.

One further point is that it has been shown in the Introduction that reaction from the quartet state may lead to different products than the thermal reaction, and it would therefore be expected that the quartet and doublet state must have different mechanisms for their particular chemical reactions. Whether these mechanisms are totally different, e.g. dissociative and associative, or merely involve a different type of distortion within a common overall mechanism is not clear, but this latter possibility should be borne in mind.

4-6.3 Cr-(N-N) polypyridyl complexes

These complexes are typified by the behaviour of $[Cr(bipy)_3]^{3+}$ and $[Cr(phen)_3]^{3+}$ which both exhibit abnormally long lifetimes of 60 μs and 270 μs in H_2O at 298 K respectively. While the lifetime for $[Cr(bipy)_3]^{3+}$ is in good agreement with that quoted in the literature, that of $[Cr(phen)_3]^{3+}$ is inconsistent with the 360 μs given by Henry and Hoffman,[122] although it is in good agreement with that quoted by other workers,[115] and exhaustive purification of the complex (see Chapter 3) produced no further lengthening in lifetime. These exceptionally long lifetimes have been attributed to both the strengthening of the Cr-N band due to the bulk of the ligand and the ability of the ligand to shield the metal core from the solvent environment. In order to test this hypothesis further, $[Cr(terpy)_2]^{3+}$ was prepared, which was expected to be more rigid than $[Cr(bipy)_3]^{3+}$ and should therefore, exhibit an even longer lifetime. However, the lifetime was found to be < 20 ns at 298 K, with a lifetime of 10 μs being recorded at 77 K. This result is paralleled in the case of the equivalent ruthenium(II) complexes for which $[Ru(bipy)_3]^{2+}$ and $[Ru(phen)_3]^{2+}$ have lifetimes of 612 and 1280 ns respectively, whilst $[Ru(terpy)_2]^{2+}$ [236]

is essentially non-luminescent, and indicates that the terpy ligand is considerably more flexible than first thought. We also found that $[Cr(cyclam)Cl_2]^+$ is quite non-luminescent.

ϕ_{ISC} for $[Cr(bipy)_3]^{3+}$ in H_2O has been evaluated as unity[82] and as a photoreaction has also been observed for this complex then the assignment of the thermally-activated, non-radiative pathway to k_{RD} is almost certain. Henry and Hoffman[122] noted that ϕ_{ISC} was solvent-dependent, becoming negligible in dimethylformamide, as discussed earlier. This result is interesting as Langford et el.[93] have previously reported a fluorescence from $[Cr(bipy)_3]^{3+}$ in dimethylsulphoxide at 298 K which would seem to be reasonable if ϕ_{ISC} is negligible. However, as mentioned earlier, this observation has been disputed by other workers,[82] although Langford[237] insists that it is genuine, as he still detects it on the first laser pulse with highly purified samples, indicating it not to be a photochemical product. An equally peculiar effect was obtained from our work on $[Cr(phen)_3]^{3+}$ in EtOH:MeOH (4:1) in which a short-lived transient at 510 nm was found to grow in place of the expected 735 nm transient as the temperature was lowered, so that at 77 K only a strong emission from the short-lived (< 20 ns) transient was apparent. This result,which is only preliminary, is inexplicable in terms of impurity quenching, but the lack of this behaviour in methanol would suggest preferential solvation by the ethanol,and further work is required to establish the cause of this behaviour, although it gives weight to Langford's[93] observations.

Hoffman and Henry[122] have also claimed that the emission lifetimes of both $[Cr(bipy)_3]^{3+}$ and $[Cr(phen)_3]^{3+}$ are insensitive to the solvent environment. This has been contested

by Kane-Maguire[115] and Adamson,[88] and the results of our work also give an opposite view, with the latter complex being particularly sensitive to environment. However, in agreement with Hoffman and Henry, no solvent isotope effect was detected on the emission lifetime of these complexes in aqueous solution, implying a strong-coupled mechanism.

The case of $[Cr(phen)_3]^{3+}$ deserves comment, in particular the observation that the lifetime is drastically reduced (20 fold) on addition of 9 M LiCl, which would seem to conflict with reports of the lengthening of the lifetime by addition of perchlorate ions (> 1 M $HClO_4$).[122] However, a lengthening of this lifetime in 1 M HCl[82,122] was found which agrees with previous reports, as does the lengthening of the lifetime of $[Cr(bipy)_3]^{3+}$ in 9 M LiCl. This result, therefore, would suggest that while the added anion is effective in prolonging the lifetime of $[Cr(bipy)_3]^{3+}$, which is explained both by the extensive ion-pairing with the cationic complex and the lowering of the activity of the solvent water molecules, thereby restricting deactivation of the doublet state. The case for $[Cr(phen)_3]^{3+}$ is somewhat different in that while the doublet state is quenched by the added anions, this effect is reversed when acid is added, and a prolongation of the lifetime occurs, although the exact mechanism for this is not clear. A further interesting point is that while the thermally-activated non-radiative pathway accounts for 98.6% of the dissipation of doublet state energy in $[Cr(terpy)_2]^{3+}$ even in CA film, and 96% for $[Cr(bipy)_3]^{3+}$, it only accounts for 68% in the case of $[Cr(phen)_3]^{3+}$ and other non-radiative pathways must be significant for the latter case.

As noted earlier, the thermally-activated, non-radiative pathway can be attributed almost certainly to k_{RD}, especially in the case of $[Cr(bipy)_3]^{3+}$, and a seven-co-ordinate intermediate employing an associative mechanism has been proposed.[122] This conclusion is given considerable weight by the report that the pH dependence of the photochemical yield is exactly the same as that for the rate constant of the thermal reaction at 295 K. This indicates that a common, pH-dependent chemical intermediate in both the thermal and photochemical reaction is required, and an associative mechanism is implied by the lack of acid catalysis for both the thermal and photochemical pathways. Similarly, it is hard to see how added anions can affect the breaking of the M-L bond; in fact, the activation energy for 9 M $LiCl/H_2O$ is not significantly different from that for H_2O (see Table 4-1), and this would indicate that the anion is effective in restricting the co-ordination of the solvent. On a more general basis, there seems no reason why the metal-ligand bond distance in the doublet state should be significantly different from that of the ground state and, therefore, it would not be expected to undergo easier M-L bond rupture. The mechanism can therefore be given as:-

$$(^4A)\ [Cr(bipy)_3]^{3+} + h\nu \rightarrow (^2E)\ [Cr(bipy)_3]^{3+}$$

$$(^2E)\ [Cr(bipy)_3]^{3+} + H_2O \rightarrow [Cr(bipy)_3(H_2O)]^{3+} \quad \text{rate determining step}$$

$$[Cr(bipy)_3(H_2O)]^{3+} \rightleftharpoons [Cr(bipy)_3(OH)]^{2+} + H^+$$

$$[Cr(bipy)_3(OH)]^{2+} \rightleftharpoons [Cr(bipy)_2(bipy\text{-})(OH)]^{2+}$$

$$[Cr(bipy)_2(bipy\text{-})(OH)]^{2+} \xrightarrow{OH^-} [Cr(bipy)_2(OH)_2]^{+} + bipy$$

In this scheme, the rate-determining step will compete with the other deactivation steps for the doublet state, namely phosphorescence and non-radiative decay back to the ground state.

However, the phosphorescence yield is $< 10^{-3}$, and the former process has been shown to be unimportant at ambient temperatures and, therefore, perhaps the rate determining step should be represented as an equilibrium

$$(^2E)\ [Cr(bipy)_3]^{3+} + H_2O \rightleftharpoons [Cr(bipy)_3(H_2O)]^{3+}$$

in which the back-reaction allows an energy-wasting mechanism to be involved. Another possibility is

$$(^2E)[Cr(bipy)_2(H_2O)]^{3+} \longrightarrow (^4A)\ [Cr(bipy)_3]^{3+} + H_2O$$

However, the lack of any appreciable photochemistry must be attributed to a mechanism of this type. While an associative mechanism provides an excellent interpretation of the observed trends, this mechanism from a theoretical viewpoint is questionable as the ^2E state is not expected to have any empty t_2 orbitals to facilitate nucleophilic attack by the solvent. However, two arguments have been proposed to overcome this objection. The first is that given by Henry and Hoffman[122] in the Introduction, and considers a reaction through a higher doublet state of a t_2e configuration. Secondly, these polypyridyl complexes are not strictly of Oh symmetry but of a lower (D_3) symmetry, and this results in t_{2g} orbitals which are not equally occupied due to configuration interactions, and therefore the formation of a seven-co-ordinate intermediate should be facilitated.[82]

The extension of this scheme by Henry and Hoffman[122] to predict a common seven-co-ordinate intermediate for both the quartet and doublet states photoreaction based on the initial ESA intensity changes in different solvents is less certain, both for reasons mentioned earlier and the fact that, contrary to their report, the lifetime <u>is</u> sensitive to solvent. The basic supposition that ϕ_{ISC} is determined by the magnitude of

Figure 20

Jablonski diagram for a chromium(III) complex with the general formula $\left[Cr(L\text{-}L)_3\right]^{3+}$. The specific case of $\left[Cr(bipy)_3\right]^{3+}$ is illustrated. Q_0 - ground quartet state; Q_1^{FC} - Franck-Condon excited quartet state; Q_1^{T} - 'thexi' quartet state; D_0 - lowest (emitting) doublet state.

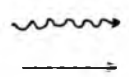

non-radiative transitions

radiative transitions

mplex with

pecific case

round quartet

rtet state;

st (emitting)

itions

ns

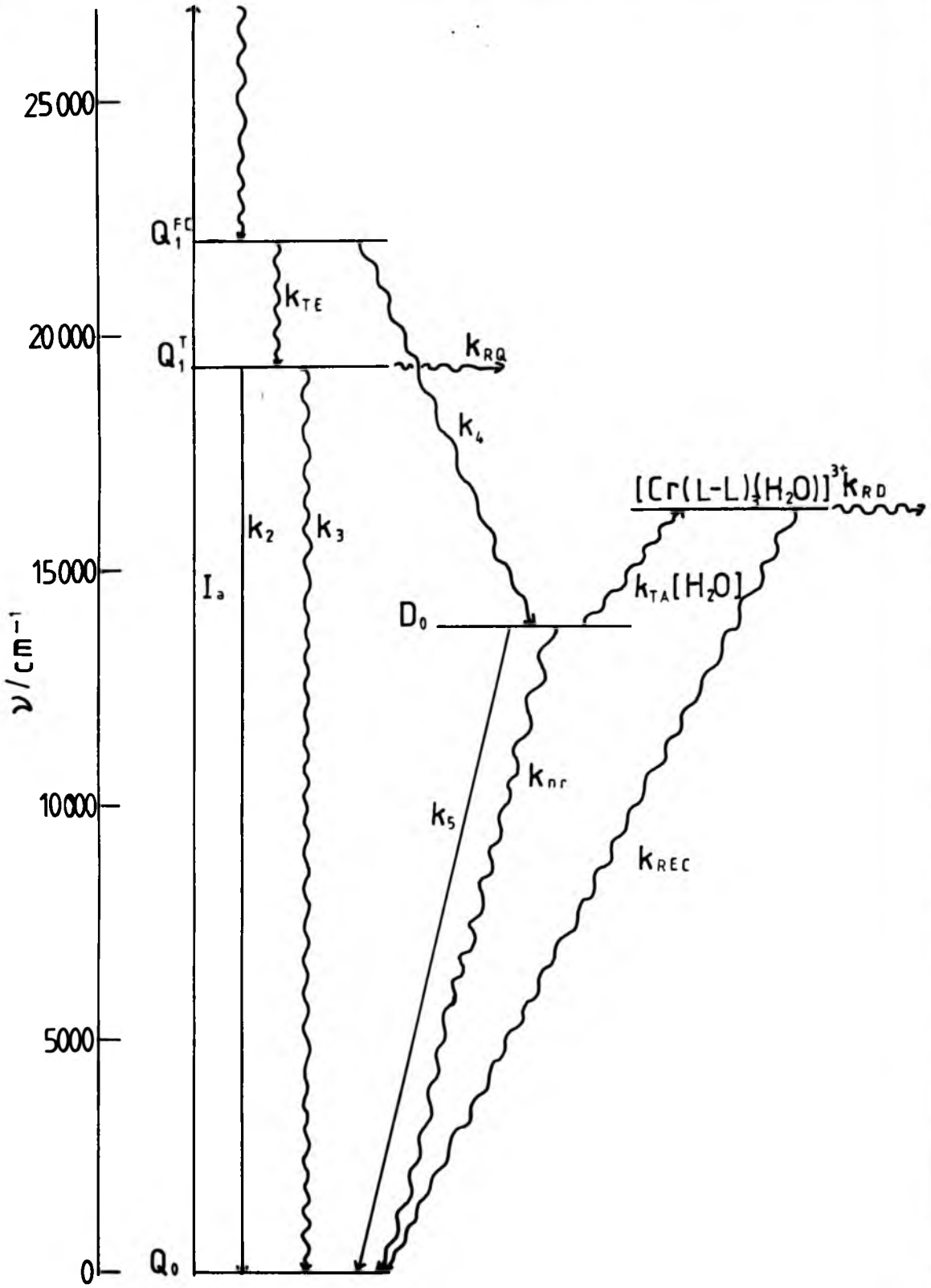

k_{RQ} is purely speculative and cannot be substantiated without values for the fluorescence lifetimes of the quartet state which are not available. From the previous discussion, the most likely competitive process with ISC is the relaxation of the 'thexi' quartet state, and the supposition that ISC is prompt would suggest no indication of the fluorescence lifetime or relaxation rates can be be obtained other than by direct observation of this state. Similarly, while the possibility of an associative mechanism for both states is not unreasonable, a common intermediate would suggest identical photoproducts for both quartet and doublet state reactions, which is inadmissible on a more general basis, although it may apply to this particular type of complex.

4-7 General conclusions for chromium(III) complexes

The Jablonski diagram shown in Figure 20 shows the basic model which has been developed throughout this discussion. On excitation, internal conversion occurs to the lowest quartet state from which ISC occurs in competition with thermal equilibration of the 'thexi' state, the success of the former depending upon both solvent and temperature. The resultant population of the doublet state then gives rise to the characteristic luminescence, but the main deactivation pathway at ambient temperatures is that of doublet photoreaction. However, while this pathway is efficient in removing energy from the doublet state, it is exceedingly inefficient in producing photochemical products as exemplified by the negligible photochemical yield for many complexes. Therefore, the relaxation of the doublet state to the ground state via recombination of the primary photoproducts is the dominant mode.

The activation energy for this route is related to the strength of the M-L bond and shows a dependence on environment which may be related to the ease with which the complex can transform to allow entry of an attacking solvent molecule, in the case of an associative mechanism. The photochemistry from the doublet state has been correlated to the thermal reaction for which an associative mechanism is dominant, exemplified by the case of $[Cr(bipy)_3]^{3+}$.[82] However, while this would be a reasonable explanation for cationic complexes, the case of anionic complexes would require solvent re-orientation before nucleophilic attack, as the nucleophilic moiety of the molecule will be remote from the metal core. For these cases, typified by Reinecke's salt and $[Cr(CN)_6]^{3-}$, a dissociative mechanism may be more appropriate since no viscosity effect is found, i.e.

$$[(L)_5Cr - L]^{3+} \xrightleftharpoons[\text{fast}]{h\nu} [Cr(L)_5\ L]^{3+}$$

$$\text{slow} \downarrow S$$

$$[Cr(L)_5S]^{3+} + L$$

However, this mechanism would necessitate that the recombination process is competitive with both the solvent chelation rate and the diffusion of the ligand away from the excited moiety. This would, therefore, imply that the solvent cage is reasonably inert to both nucleophilic attack of the complex and exchange with the bulk solvent. Although the former cases seems reasonable in the light of the above discussion, the second possibility seems less likely in view of the relatively long lifetime of the doublet state. At cryogenic temperatures, the observed isotope effect indicates that L-H type vibrations are the dominant deactivation mode, and k_{RD} is negligible as expected.

It therefore seems that,although the overall picture is fairly complete, some of the finer details still require further work, but it is hoped that this study has at least put discussion of chromium(III) photophysics on a more quantitative footing.

CHAPTER 5

RUTHENIUM(II)

RESULTS AND DISCUSSION

5-1 Collection and analysis of experimental data

The temperature dependences of the luminescence lifetimes of $[Ru(bipy)_3]^{2+}$ and $[Ru(phen)_3]^{2+}$ have been investigated in both aqueous-based and organic media, all solutions being de-oxygenated as described on p. 127 . Both the luminescence (excitation wavelength = 347 nm) and ground state absorption spectra of all the ruthenium(II) samples used were recorded at room temperature and neither showed any significant change with environment, with the emission spectrum for $[Ru(bipy)_3]^{2+}$ showing a maximum located between 583 and 590 nm, while that of $[Ru(phen)_3]^{2+}$ varied between 573 and 575 nm, clearly showing the emitting level to be almost insensitive to solvation forces, and both emissions were monitored at 580 nm over as wide a temperature range as possible using the method given on p. 123 In the cases of $[Ru(phen)_3]^{2+}$ in CH_3CN and DMF, the onset of photochemistry prevented adequate measurements.

The resultant activation data have been computer-fitted to both a double exponential expression (2EXP)

$$k_{obs} = A_1 \exp(-E_1/RT) + A_2 \exp(-E_2/RT) \qquad (5\text{-}1)$$

and a single exponential expression (VHW)

$$k_{obs} = k_r + k_{nr} + A_1 \exp(-E_1/RT) \qquad (5\text{-}2)$$

Equation (5-2) is the expression used by van Houten and Watts[54] to fit their data for aqueous $[Ru(bipy)_3]^{2+}$ systems between 273 and 373 K, and is reminiscent of the expression produced in the general model (equation (1-57)) as well as that used for analysis of Cr(III) in Chapter 4. Equation (5-1) has been used by Kemp *et al.*[215] to fit activation data for $[Ru(bipy)_3]^{2+}$ over a similar range, and was originally described by Lytle and

Hercules[43] who generalised equations used to rationalise thermally-activated ISC in substituted anthracenes. It is hoped that by illustrating the best fits for both expressions to the experimental data on the same plot, a choice between the two can be clearlymade on a general basis.

The final values of the Arrhenius parameters for both expressions which were reiterated by the computer routine are given in Tables 5-1 and 5-2, for which $B=(k_r + k_{nr})$ in the case of the VHW analysis.

For 2EXP it appears that k_r has been neglected; however, this can be explained in terms of the Crosby[53] model expounded earlier. According to this, the low-temperature luminescence from ruthenium(II) complexes originates from a three-level manifold of emitting states. At temperatures of 70 K and above, at least 90% of the observed luminescence originates from the highest level of this manifold, so that the term A_1 is also given by $A_1=(k_r + k_{nr})$. This illustrates the essential difference between the two schemes, in that VHW represents a simple thermally-activated non-radiative route from a 'single' emitting level, whereas 2EXP considers both the dominant non-radiative route at room temperature and the observed luminescence to be thermally activated. The finer details of these two models will be dicussed later in this chapter.

Tables 5-1 and 5-2 feature activation data produced both for extended temperature ranges (77-370 K) from this work and by co-workers which was analysed in the course of this work (ref. 215), as well as fitted parameters to data reported in the literature by other groups. The fitted curves for both expressions are given along with the original data for the

Table 5-1 Fitted Arrhenius Parameters for the Temperature-dependent Luminescence of $[Ru(bipy)_3]^{2+}$

(a) Water and 9 mol dm^{-3} aqueous LiCl solutions

Medium		Source of fitted data	2EXP analysis $10^{-6}k_{298K}$ /s^{-1}	$10^{-13}A_1$ /s^{-1}	ΔE_1 /kJ mol^{-1}	$10^{-6}A_2$ /s^{-1}	ΔE_2 /kJ mol^{-1}	VHW analysis $10^{-6}k_{298K}$ /s^{-1}	$10^{-6}B$ /s^{-1}	$10^{-13}A_1$ /s^{-1}	ΔE_1 /kJ mol^{-1}
H_2O		Ref. 215	1.724	4.00 (2.01) [a]	46.72 (1.60)	4.27 (2.29)	2.64 (1.25)	0.332	1.37 (0.003)	1.68 (0.33)	43.95 (0.60)
		Ref. 54	1.645	91.8 (58.6)	56.05 (2.00)	7.95 (3.93)	4.12 (1.18)	1.618	1.40 (0.03)	16.85 (5.43)	50.71 (0.97)
		Ref. 43*	-	-	-	-	-	1.671	-	1.2×10^{-5}	10.59
D_2O		Ref. 215	1.062	5.37 (3.41)	47.26 (1.98)	1.05 (1.33)	0.74 (2.94)	1.060	0.77 (0.03)	4.67 (1.22)	46.82 (0.78)
		Ref. 54	0.966	217.4 (65.4)	58.40 (0.94)	11.68 (4.70)	6.52 (0.96)	0.939	0.75 (0.02)	48.3 (11.3)	53.67 (0.70)
9 M LiCl in H_2O	T > 178 K	This work	1.635	6.65 (2.14)	48.99 (0.96)	3.15 (0.17)	1.90 (0.10)	1.505	1.13 (0.03)	0.20 (0.11)	38.38 (1.55)
	T < 143 K	This work	-	-	-	0.69 (0.026)	0.63 (0.03)	-	-	-	-
9 M LiCl in D_2O	T > 178 K	This work	1.018	4.33 (1.83)	47.83 (1.26)	1.62 (0.21)	1.63 (0.26)	0.951	0.69 (0.02)	0.80 (0.31)	42.71 (1.14)
	T < 143 K	This work	-	-	-	0.47 (0.009)	0.66 (0.02)	-	-	-	-
50% H_2SO_4	T > 200 K	Ref. 43	1.60	0.034 (0.018)	32.10 (1.32)	0.80 (0.05)	0.048 (0.0117)	1.593	0.77 (0.002)	0.028 (0.007)	31.63 (0.61)
	T < 120 K	Ref. 43	-	-	-	0.404 (0.005)	0.067 (0.009)				

(continued)

Table 5-1 (continued)

(b) Solutions in non-aqueous solvents

C_2H_5OH	Ref. 215	1.475	80.9 (130.0)	51.92 (4.74)	13.5 (42.1)	6.90 (7.05)	1.444	0.64 (0.006)	24.5 (10.4)	48.40 (1.19)
C_2H_5OH-CH_3OH T > 125 K	Ref. 43	1.38	1.00 (0.18)	40.49 (0.44)	0.64 (0. 4)	0.22 (0.008)	2.349	-	0.54	37.8
CH_3CN	Ref. 215	1.253	71.8 (46.0)	52.09 (1.90)	2.78 (3.50)	3.33 (2.84)	1.227	0.63 (0.03)	39.4 (11.1)	50.31 (0.81)
DMF	Ref. 215	1.215	8.04 (2.47)	47.64 (0.93)	1.42 (0.41)	1.25 (0.62)	1.179	0.78 (0.03)	5.29 (1.20)	46.34 (0.68)
	Ref. 43*						1.06×10^{-5}	-	2.4×10^{-9}	19.14
DMSO	This work	0.968	20.5 (16.9)	51.7 (2.8)	1.77 (8.77)	2.0 (12.6)	0.978	0.79 (0.05)	19.1 (2.70)	51.38 (0.46)
EPA[b]	Ref. 43	-	2.78×10^{-3} (7.04×10^{-3})	26.74 (6.04)	1.01 (0.07)	0.77 (0.09)		0.399 (0.049)	7.09×10^{-7} (4.40×10^{-7})	5.89 (1.47)
Cellulose acetate film	This work	0.744	1.73×10^{-6} (0.78×10^{-6})	9.61 (1.12)	0.50 (0.04)	0.64 (0.07)	0.681	0.22 (0.08)	3.07×10^{-7} (0.41×10^{-7})	4.70 (0.30)
Polymethyl methylacrylate film	Ref. 147*				1.46	0.73				

[a] bracketed figure refers to one standard deviation

[b] ether:isopentane:ethanol mixture (5:5:2)

* author's fitted values

Figure 21

Temperature activation plots for luminescence of $[Ru(bipy)_3]^{2+}$ in various media. Full curves-computer fit to equation 5-1; broken curves-computer fit to equation 5-2 (individual parameters are given in Table 5-1).

(a) H_2O(X) and D_2O(·)

(b) 9M LiCl/H_2O (·) and 9M LiCl/D_2O (X)

(c) ethanol (X) and acetonitrile (·)

(d) DMF (X)

(e) DMSO (X)

scence of

curves-computer

puter fit to

given in

X)

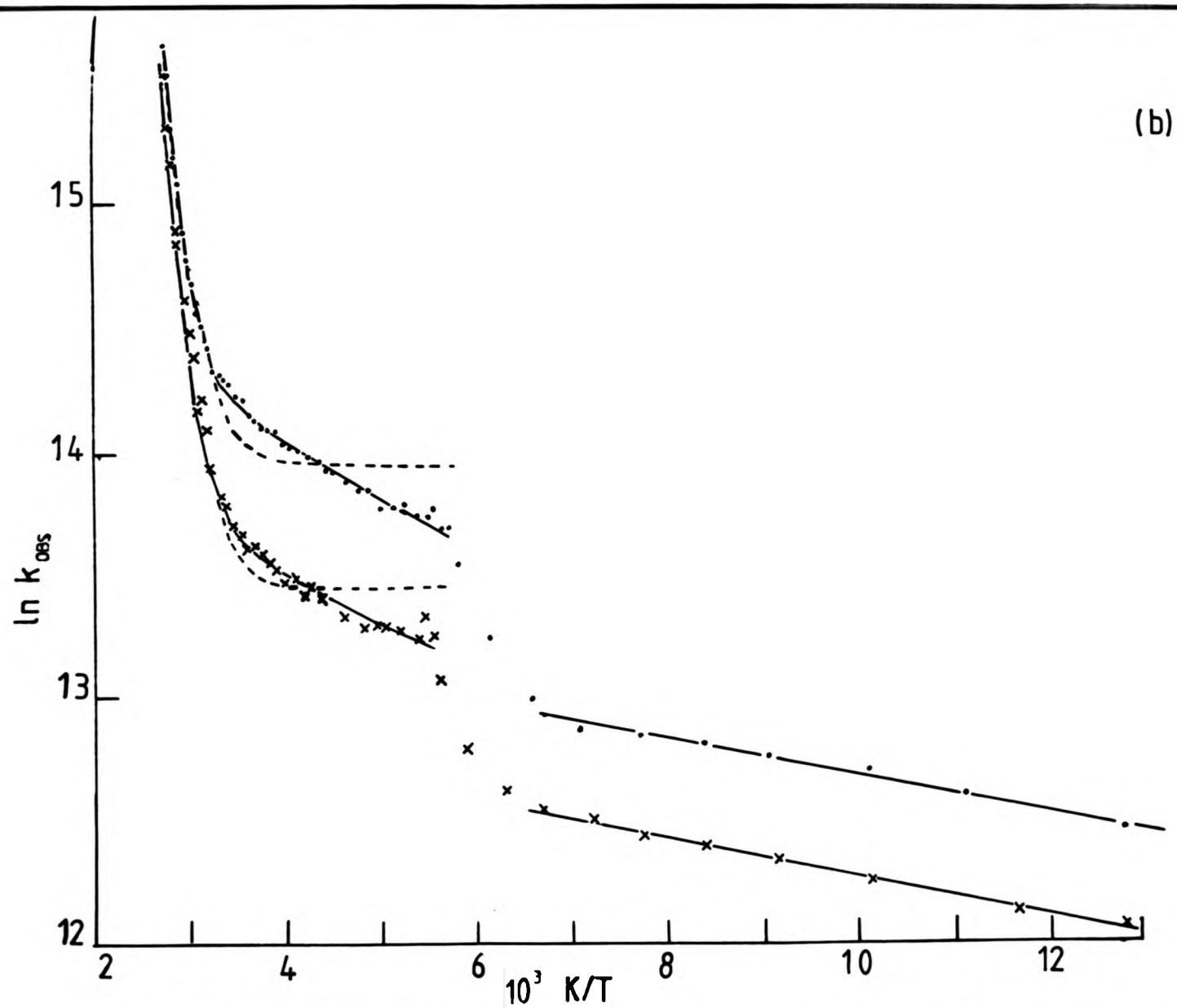
(b)
15
14
13
12
ln k_{obs}
2
4
6
8
10
12
10^3 K/T

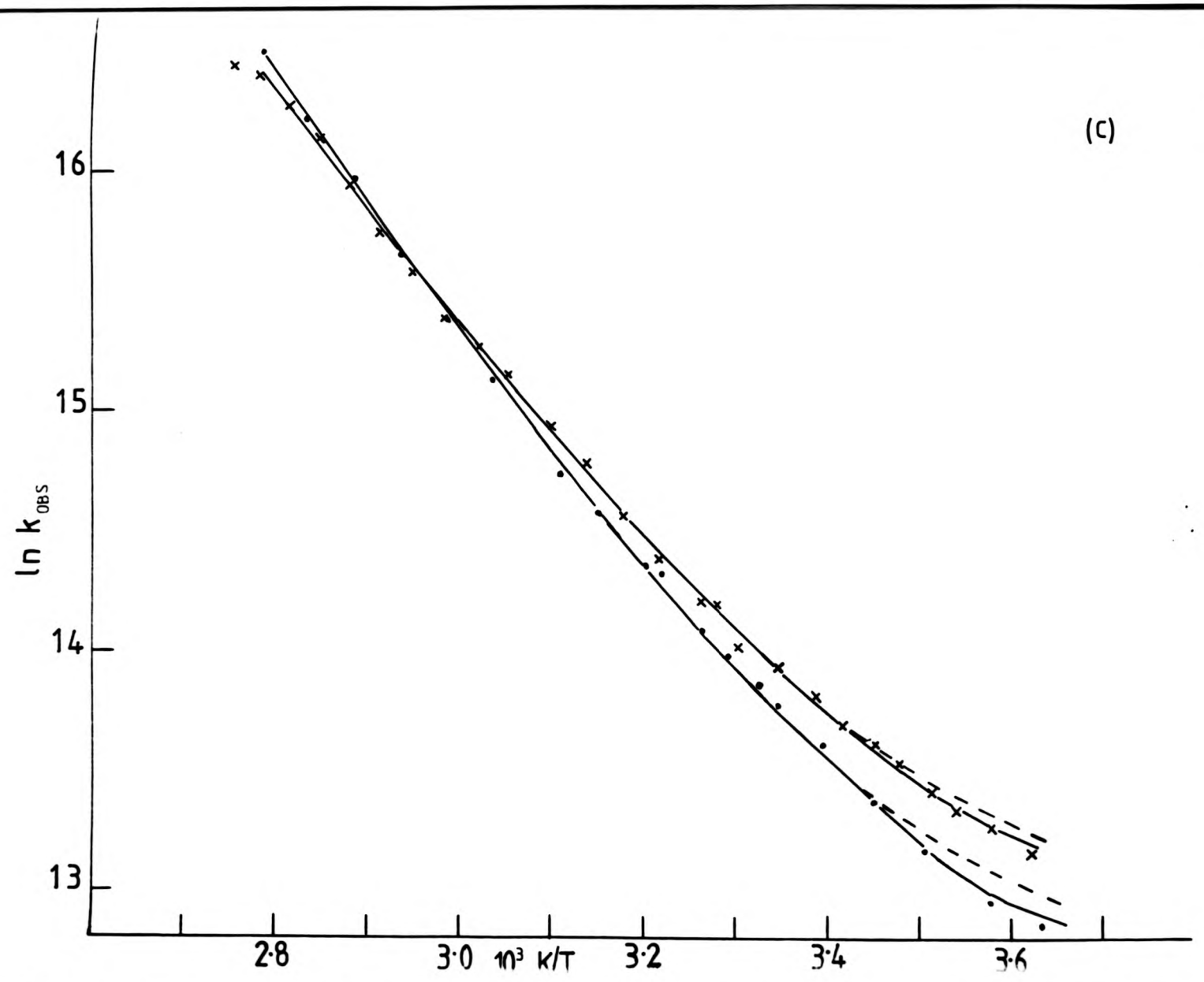
(c)
16
15
14
13
ln k_{OBS}
2·8
3·0
10^3 K/T
3·2
3·4
3·6

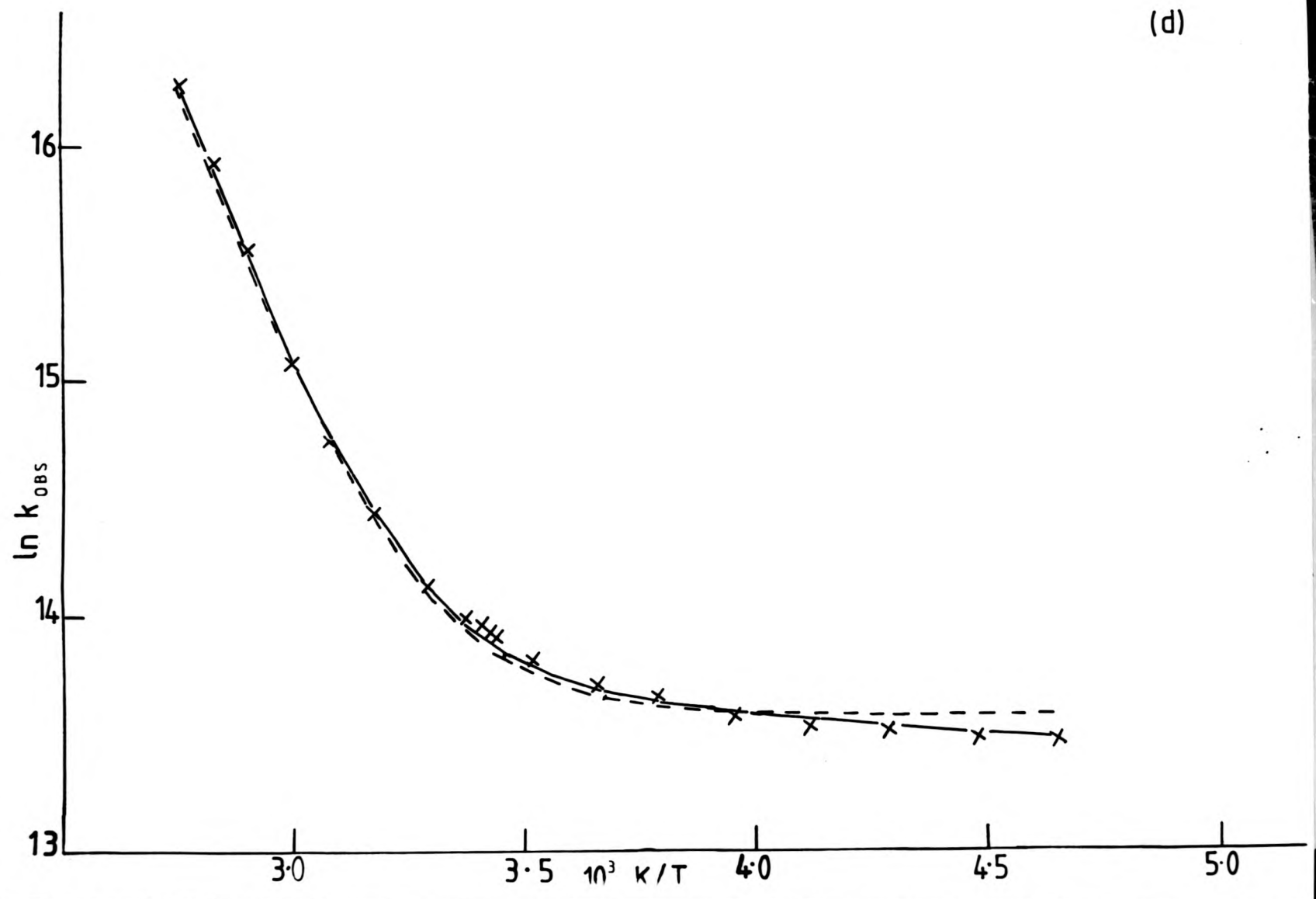
(d)
16
15
14
13
ln k_{OBS}
3·0
3·5
10^3 K/T
4·0
4·5
5·0

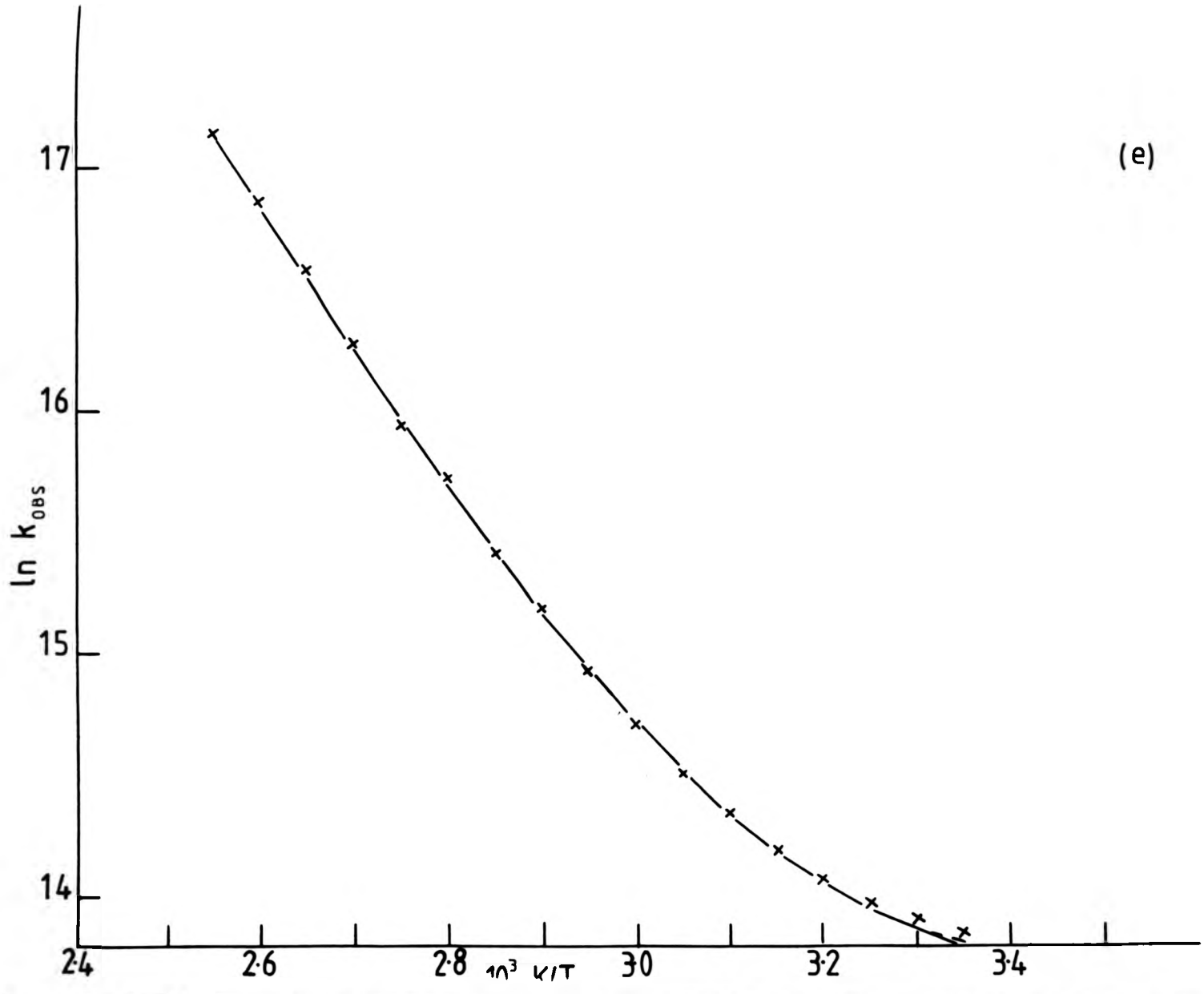
(e)
17
16
15
14
ln k_{OBS}
2·4
2·6
2·8
3·0
3·2
3·4
10^3 K/T

Table 5-2 Fitted Arrhenius parameters for the temperature-dependent luminescence of $[Ru(phen)_3]^{2+}$

Medium		Source of fitted data	2EXP analysis					VHW analysis			
			$10^{-6}k_{298K}$ /s^{-1}	$10^{-13}A_1$ /s^{-1}	ΔE_1 /kJ mol^{-1}	$10^{-6}A_2$ /s^{-1}	ΔE_2 /kJ mol^{-1}	$10^{-6}k_{298K}$ /s^{-1}	$10^{-6}B$ /s^{-1}	$10^{-13}A_1$ /s^{-1}	ΔE_1 /kJ mol^{-1}
H_2O		This work	1.130	2.92 (2.43)[a]	43.45 (2.62)	2.27 (13.16)	4.16 (13.30)	1.118	0.37 (0.06)	2.35 (0.61)	42.77 (0.77)
D_2O		Ref. 215	0.928	9.74 (4.45)	46.98 (1.46)	4.11 (16.7)	6.04 (9.50)	0.917	0.31 (0.04)	7.73 (1.23)	46.24 (0.48)
9 M LiCl in H_2O	T > 178 K	This work	0.781	11.1 (6.93)	48.11 (1.82)	1.09 (0.72)	2.66 (1.30)	0.754	0.276 (0.020)	4.78 (1.96)	45.64 (1.16)
	T < 143 K	This work	-	-	-	0.22 (0.004)	0.46 (0.02)	-	-	-	-
9 M LiCl in D_2O	T > 178 K	This work	0.639	6.41 (1.05)	46.60 (0.47)	0.28 (0.07)	0.74 (0.50)	0.634	0.186 (0.005)	5.46 (0.64)	46.13 (0.33)
	T < 143 K	This work	-	-	-	0.21 (0.05)	0.54 (0.02)	-	-	-	-
C_2H_5OH		Ref. 215	4.50	2.48 (0.44)	38.46 (0.48)	-	-	as 2EXP analysis			
DMSO		This work	0.950	2.39 (0.49)	42.22 (0.59)	-	-	as 2EXP analysis			
Cellulose acetate film		This work	0.343	9.30 x 10^{-6} (7.83×10^{-6})	15.70 (1.92)	0.21 (0.008)	0.40 (0.04)	0.290	0.132 (0.004)	2.14 x 10^{-7} (0.73×10^{-7})	6.46 (0.75)
Polymethyl methylacrylate film		Ref. 147*				0.86	0.63				

[a] bracketed figures refer to one standard deviation

* author's fitted values

Figure 22

Temperature activation plots for luminescence in $[Ru(phen)_3]^{2+}$ in various media. Full curves-computer fit to equation 5-1; broken curves-computer fit to equation 5-2 (individual parameters are given in Table 5-2).

(a) H_2O (X) and D_2O (·)

(b) 9M LiCl/H_2O (X) and 9M LiCl/D_2O (·)

(c) DMSO (left hand side) and ethanol (right hand side)

scence in
curves-
urves-computer
ers are given

·)
(right hand

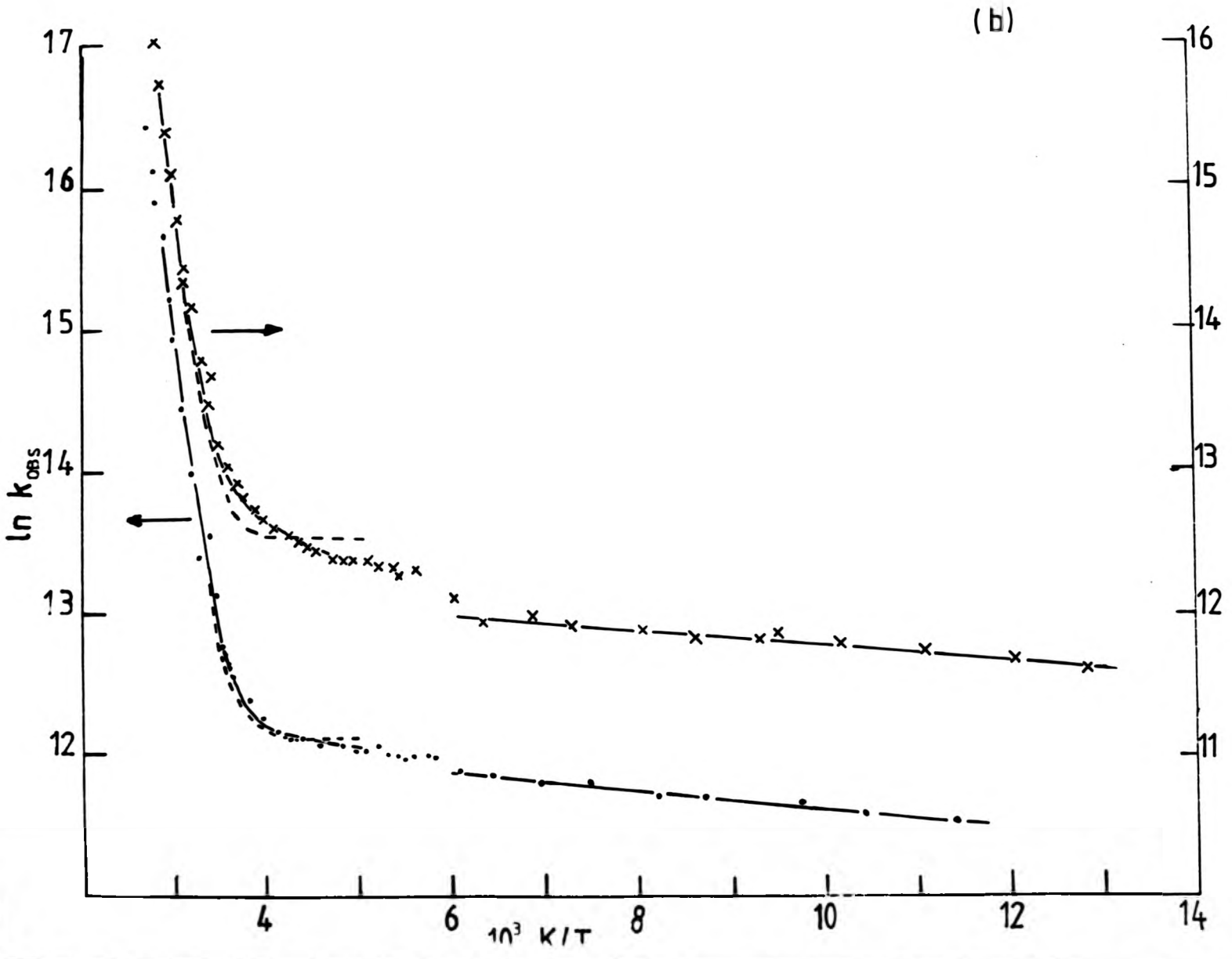
(b)
17
16
15
14
13
12
16
15
14
13
12
11
ln k_{OBS}
4
6
8
10
12
14
10^3 K/T

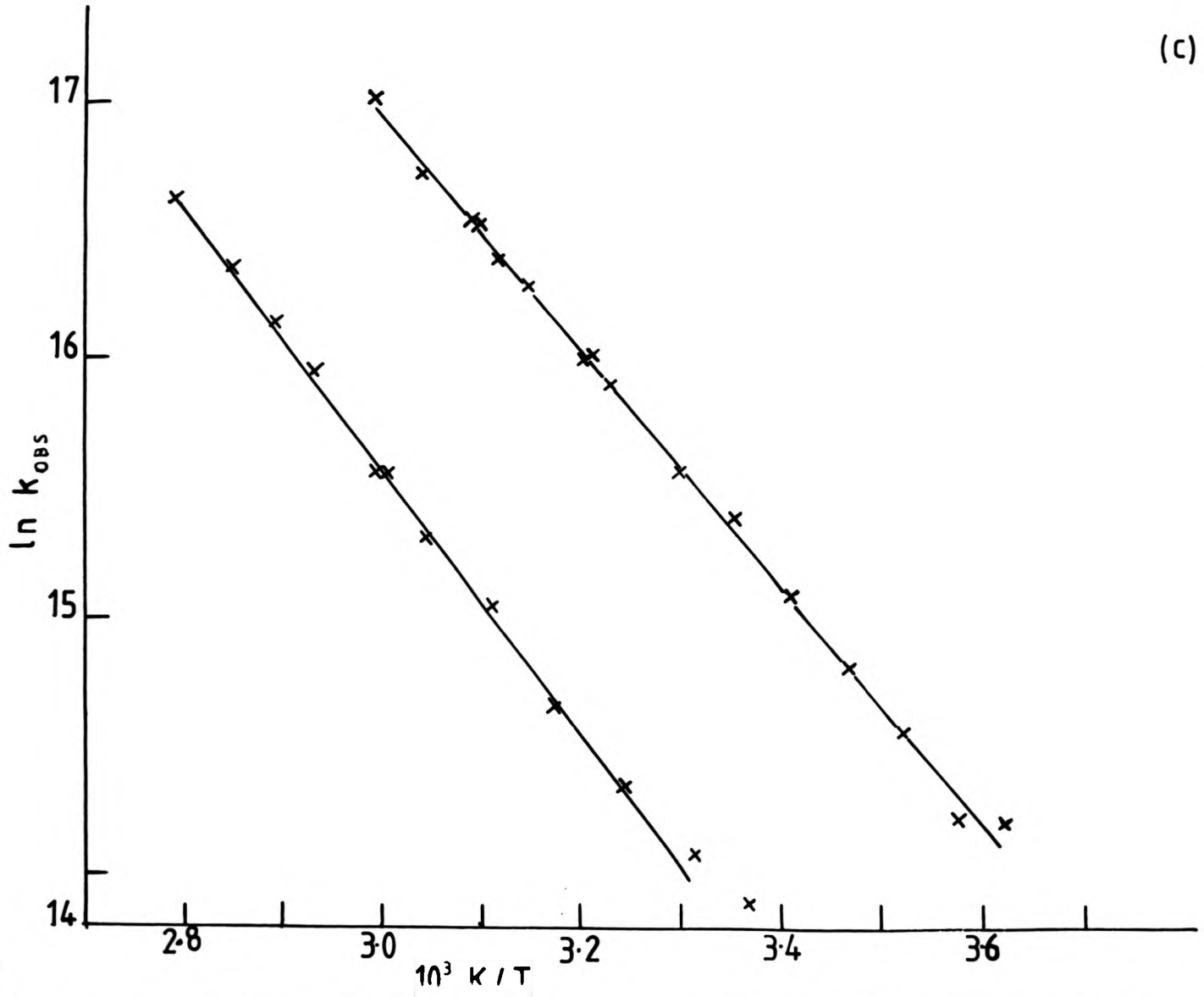
(c)
17
16
15
14
ln k_{OBS}
2·8
3·0
3·2
3·4
3·6
10^3 K / T

first two sets of measurements in figures 21 and 22, the tabulated form of the Arrhenius plots being given in Appendix II, and the results of co-workers are also given here for completeness, as these values have not been reported elsewhere.

5-2 Inferences made from the Arrhenius plots for the luminescence of $[Ru(phen)_3]^{2+}$ and $[Ru(bipy)_3]^{2+}$ in a variety of solvents

The most important point to be made here is that while VHW is an adequate description of the Arrhenius plots at elevated temperatures or over a restricted temperature range (> 273 K), 2EXP is clearly far superior when considering an extended temperature range and gives justification for adopting a more complicated expression to explain the luminescent behaviour of these complexes. In some cases, a single exponential expression is adequate as illustrated by $[Ru(phen)_3]^{2+}$ in DMSO and ethanol (Figure 22c). In the figures shown, the full curves represent the 2EXP fit, while the dotted lines show the deviation from this fit on using a VHW analysis.

It is also noticeable that $[Ru(phen)_3]^{2+}$ produces a much less pronounced curvature than the bipyridyl analogue, indicating a reduced sensitivity to environment, as well as a much longer lifetime for a given temperature. This is probably due to the increased bulk of the ligand which will both shield the complex and reduce the M-L vibrations, an effect discussed in Chapter 4 for chromium(III).

The effect of the phase transition for glassing solvents is marked in all cases, and indicates these complexes to be particularly sensitive to environment. It is apparent, however,

Figure 23

Temperature activation plot for luminescence of $[Ru(phen)_3]^{2+}$ and $[Ru(bipy)_3]^{2+}$ in CA film.

Upper series - $[Ru(bipy)_3]^{2+}$; full curve-computer fit to equation 5-1, broken curve-computer fit to equation 5-2.

Lower series - $[Ru(phen)_3]^{2+}$; full curve-computer fit to equation 5-1, broken curve, computer fit to equation 5-2.

ence of

lm.

-computer

er fit to

-computer

ter fit to

Figure 23

Temperature activation plot for luminescence of $[Ru(phen)_3]^{2+}$ and $[Ru(bipy)_3]^{2+}$ in CA film.

Upper series - $[Ru(bipy)_3]^{2+}$; full curve-computer fit to equation 5-1, broken curve-computer fit to equation 5-2.

Lower series - $[Ru(phen)_3]^{2+}$; full curve-computer fit to equation 5-1, broken curve, computer fit to equation 5-2.

ance of

.m.

computer

er fit to

computer

er fit to

that a significant isotope effect still persists, even in a low-temperature glass, indicating that the contribution of the solvent to the deactivation of the excited state is not diffusional in origin but conforms with the suggestion of a weakly-coupled CTTS deactivation of the low lying triplet manifold, as suggested by van Houten and Watts,[155] and our isotope effect of 1.6 agrees well with that of 1.8 quoted by the latter for $[Ru(bipy)_3]^{2+}$ in D_2O/H_2O at 293 K.

A decisive result is that of the study in polymer film which allows the validity of 2EXP and VHW to be tested over a 300 K range without any interference of phase transitions. The plot (Figure 23) clearly shows 2EXP to be superior, as well as giving unquestionable support to the unusual behaviour in the glassing aqueous media as due to phase transitions by their absence in this polymeric medium and the absence of any discontinuities indicated that when these occur in glassy aqueous media, then the cause lies in phase transitions. Another important result is that of $[Ru(bipy)_3]^{2+}$ in DMF (Figure 21d) which is the only organic medium apart from the polymer film to show clearly the superiority of 2EXP over VHW and suggests that the former expression is universal in its application to these particular complexes.

It is also interesting to note that the range covered by the rate constant is almost invariant ($\sim$ 2.5 to 3 natural log units), regardless of the overall temperature range covered, and suggests that the enhancement of the thermally activated non-radiative route (ΔE_1) is intimately connected with the viscosity of the medium. A notable exception to this last statement is the case of the polymer films (Figure 23) in which $\log_e k$ only traverses one unit over the entire

temperature range (77 to 370 K). This gives weight to the inference that the viscosity of the medium is an important influence, a point also emphasised by the discontinuity observed through the phase transition in the glassing aqueous media, although no correlation between the macroscopic viscosity of the medium and the rate constant at 298 K is apparent.

5-3 Implications of the fitted Arrhenius parameters for the $[Ru(bipy)_3]^{2+}$ (Table 5-1) and $[Ru(phen)_3]^{2+}$ (Table 5-2) systems

The preceding section has indicated that 2EXP is a superior expression to VHW on a qualitative basis; the quantitative aspects of this result can be considered by reference to Tables 5-1 and 5-2. As expected, the effect of using 2EXP instead of VHW is to increase the activation energy of the higher energy process to allow for the presence of a lower-energy activated pathway. While the increase is insignificant in the case of results taken over a restricted temperature range, as illustrated by the appropriate Arrhenius plots, with the difference being almost within the standard deviation of ΔE_1, the values become significantly different over an extended temperature range as indicated by the extreme case of the polymer films (77 to 370 K). For this case, ΔE_1 varies by a factor of between 2.0 and 2.5 for the two expressions. Attention should also be drawn to the fitted parameters for the data given by van Houten and Watts[54] for $[Ru(bipy)_3]^{2+}$ in H_2O and D_2O between 273 and 373 K. These differ significantly from those produced by the author's own procedure for a VHW-type fit (e.g. for $[Ru(bipy)_3]^{2+}$ in H_2O ($A = 10^{13}$ s^{-1}, $\Delta E_1 = 42.6$ kJ mol^{-1}

and B = 1.3 x 10^6 s^{-1}). Similarly, a trial of van Houten and Watts'[54] parameters, using the computer routine adopted throughout this work, simply iterated the values to those quoted in Table 5-1. However, while agreement between the two procedures was reasonable on a point-to-point basis, the residual sum of the squares of the errors indicates the procedure used in this work to provide a rather better overall agreement. The similarity of the values for k_{298K} for the samples used in this work and that of van Houten and Watts[54] is pleasing, but while the analysis of their data provides an alternative set of activation parameters, these do not agree with those obtained from the data of Kemp et al.[215] and are consistently higher for both H_2O and D_2O media. This discrepancy is puzzling, but may be caused by the relatively few data points (12) given by van Houten and Watts[54] which will result in any experimental error in these points being magnified.

As expected, the low-energy term of 2EXP is also susceptible to large errors for data covering a restricted temperature range (> 250 K), since the ΔE_2 term will provide only a relatively small contribution to the overall rate constant over this range, particularly in the case of the phen complex for which ΔE_2 is inherently smaller.

The room-temperature lifetime of $[Ru(bipy)_3]^{2+}$ is relatively insensitive to the presence of anionic (9 M LiCl) and acidic media (50% H_2SO_4). The activation energies for H_2O and 9 M LiCl/H_2O are also very similar, indicating that the latter can be regarded as an extended range of the pure aqueous medium. The case of 50% H_2SO_4, however, shows a marked decrease in both ΔE_2 and ΔE_1, indicating both pathways to be affected by acidity. In contrast, $[Ru(phen)_3]^{2+}$ shows a small but definite

increase in lifetime at 298 K for 9 M $LiCl/H_2O$ compared with the pure aqueous medium (885 to 1,280 ns) and the values of ΔE_2 and ΔE_1 show much more diverse behaviour with the difference in the aqueous media being reflected in both ΔE_1 and ΔE_2, whereas the deuterated systems show the change to be due to ΔE_2 only.

For non-aqueous solvents, the values of both ΔE_1 and ΔE_2 are not significantly different from those obtained in the aqueous environment for $[Ru(bipy)_3]^{2+}$ with the lifetime at 298 K being in general slightly longer in the non-aqueous media. The two notable exceptions are EPA and cellulose acetate film. The former data was obtained from a report by Lytle and Hercules,[43] and fits to all the data obtained from this paper seem to give unusually low values for the activation parameters (see Table 5-1), which may be due to the given data being erroneous, although in this particular case a mixed solvent system has been used and the result may be due to the effect of unusual solvation forces. The unusually low value for ΔE_1 in polymeric film is puzzling as, intuitively, this value would have been expected to become higher due to the enhanced rigidity of this medium, if a vibrational or photochemical deactivation mechanism is operative, as discussed in the chromium(III) system. A similar effect is shown by $[Ru(phen)_3]^{2+}$ in cellulose acetate film, while ΔE_1 is slightly reduced in both ethanol and DMSO, although this may be due to the restricted temperature range making a proper 2EXP analysis impossible

5-4 The development of a model to describe these results, incorporating earlier models

The general implication of this work is that the luminescence behaviour of $[Ru(bipy)_3]^{2+}$ and $[Ru(phen)_3]^{2+}$ requires a model

Figure 24

Temperature activation plots based on the data of ref. 43 for the luminescence of $\left[Ru(bipy)_3\right]^{2+}$ in 50% H_2SO_4 (X) and ethanol-methanol (·). Full curves correspond to computer fitting of equation 5-1.

e data of

$y)_3]^{2+}$ in

Full curves

on 5-1.

involving the presence of two thermally-activated decay routes to give a complete description of the luminescence of these complexes over a full temperature range (77 to 370 K). This work therefore provides a communication between the Crosby[53] low-temperature model and the elevated temperature (> 273 K) work of van Houten and Watts,[54] and gives a convincing argument for the modification of the model proposed by the latter workers to contain the two thermally-activated routes proposed in this work.

While 2EXP gives an equally good interpretation of the results of van Houten and Watts,[54] it also provides an excellent explanation of the data presented by Lytle and Hercules[43] for $[Ru(bipy)_3]^{2+}$ over the range 70 to 240 K, as shown in Figure 24, to give Arrhenius parameters which are in reasonable agreement with those obtained from this work. This is a pleasing result as it provides an alternative set of parameters to those given by the authors for a simple Arrhenius analysis of a VHW-type expression, using a non-iterative method. This gave values of ΔE_1 ranging from 10.6 kJ mol^{-1} in H_2O to 37.1 kJ mol^{-1} in ethanol-methanol and values of A_1 ranging from 2.4 x 10^4 (in DMF) to 5.4 x 10^{12} (in ethanol-methanol) which would indicate the complex to be extremely sensitive to solvent. However, a 2EXP analysis (see Table 5-1) of this data shows that these results are probably erroneous.

The two thermally-activated pathways can be categorised in terms of a high-energy and low-energy route, the former being in the range 40 to 50 kJ mol^{-1} while the latter is usually $\leq$ 4 kJ mol^{-1}, although the exact values are dependent upon the actual environment,and the case of cellulose acetate is an obvious exception which will be discussed later. The high-energy pathway is essentially the same as that found by van

Houten and Watts[54] and there is no evidence in this work to challenge the authors' assignment of this route as due to non-radiative deactivation through a higher state of LF character. This view is substantiated by the report of $[Ru(bipy)_3]^{2+}$ undergoing a photosubstitution reaction at elevated temperatures (313 to 363 K), which is indicative of LF-type behaviour[157] (see chromium(III)). This reaction has a very small quantum yield (5.3×10^{-4} at 363 K), and can therefore be discounted as giving any significant contribution to the activation energy of the higher-energy route, which can therefore be considered at the ^3CT - LF splitting. The activation energy of the photochemical reaction has been estimated as $\sim$24 kJ mol^{-1} [157] greater than this splitting, with reference to the ^3CT level and, presumably, if the temperature were raised sufficiently, then an increase in the value of ΔE_1 of 24 kJ mol^{-1} should occur.

ΔE_2 is much smaller and, as suggested earlier, has been correlated to the deactivation through the A_2 level of the Crosby[53] triplet manifold. The implication, therefore, that more than 90% of the energy goes through the A_2 level at 70 K and above gives a good explanation of why the non-radiative and radiative decay routes of the lower levels of this manifold can be neglected to give the rate equation 2EXP used in this work. The two lower levels, A_1 and E, can be regarded as a single level for the purposes of this work, as they are indistinguishable over the temperature range investigated, a result which also agrees well with that of Crosby *et al*,[53] who indicate the A_1 and E levels become well-resolved only at temperatures below 30 K. The obvious correlation to be made is that of the ΔE_2 term for the CA film studies of this work with the A_2-E splittings given by Crosby *et al*.[53,147] for

these complexes in polymethylmethacrylate film. From this work, $[Ru(phen)_3]^{2+}$ gives a splitting of (33±3) cm^{-1}, while $[Ru(bipy)_3]^{2+}$ gives (54±6) cm^{-1} for ΔE_2. These can be compared with the A_2-E splittings quoted by Crosby et al.[147] of 44 and 50.1 cm^{-1} respectively in PMM film. It is, therefore, apparent that the two sets of results given reasonable agreement with the phen complex having closer-spaced levels than the bipy analogue. A further point which can be made is that while the results in polymer film give good agreement, these are atypical, particularly in terms of ΔE_1, of results obtained in fluid media and, therefore, the correlation between photophysical results obtained in polymer matrices with photochemical results obtained in fluid media must be made with caution.

5-5 Detailed discussion of the proposed general model in terms of the individual complexes and the observed solvent effects

While a procedure involving the fitting of four variables makes accurate determination of these parameters difficult, particularly in the case of ΔE_2 and A_2, and over a restricted temperature range, a number of points about the values of these parameters can be made. In the case of $[Ru(bipy)_3]^{2+}$ in an aqueous environment ΔE_1 is in the range (47.85 ± 1.13) kJ mol^{-1} ((4,000 ± 95) cm^{-1}) while for organic solvents the term is not significantly different, as mentioned earlier, the values being within the range (49.9 ± 2.2) kJ mol^{-1} ((4,170 ± 984) cm^{-1}). Similarly, for $[Ru(phen)_3]^{2+}$, ΔE_1 spans a relatively narrow range of (45.82 ± 2.3) kJ mol^{-1} ((3,810 ± 192) cm^{-1}). As mentioned earlier, the luminescence spectra are not perturbed for any of the media used, and this

indicates that the changes in ΔE_1 reflect changes in the position of the high-energy triplet LF level. It is, however, significant that the frequency factors, A_1, for deactivation through this level are correspondingly high to allow efficient degradation, and it may be that these high values of A_1 reflect the effect of SOC in these complexes on the level, which may remove some of the 'forbiddenness' imparted by the triplet label to allow this process to be efficient. If this is the case, then the unusually low results for both A_1 and ΔE_1 obtained for the polymer film may be explained in terms of the non-radiative level becoming both lower in energy and more 'defined', resulting in a reduced SOC effect which would explain the 10^7-fold reduction in A_1.

The effect of solvent deuteration is most readily investigated in a 9 M LiCl aqueous medium which affords an extended temperature range to give a more precise determination of the contribution from ΔE_2. For $[Ru(phen)_3]^{2+}$ the higher-energy pathway gives an isotope effect of 1.06 at 298 K, whereas the lower-energy route shows an isotope effect of 1.8, the overall isotope effect being dependent upon the relative contribution of the two pathways to the observed rate constant at 298 K. Similarly for $[Ru(bipy)_3]^{2+}$, an isotope effect of 0.96 is apparent for the higher energy route at 298 K, while the lower energy route gives one of 1.74 at 298 K. It would appear, therefore, that the observed isotope effect is a result of the effect of deuteration on the lower energy pathway, and this result agrees with the report of van Houten and Watts[54] who consider the higher energy pathway to be a strongly coupled route, whereas the lower energy pathway is a weakly-coupled process, as indicated by the presence of a significant isotope effect.

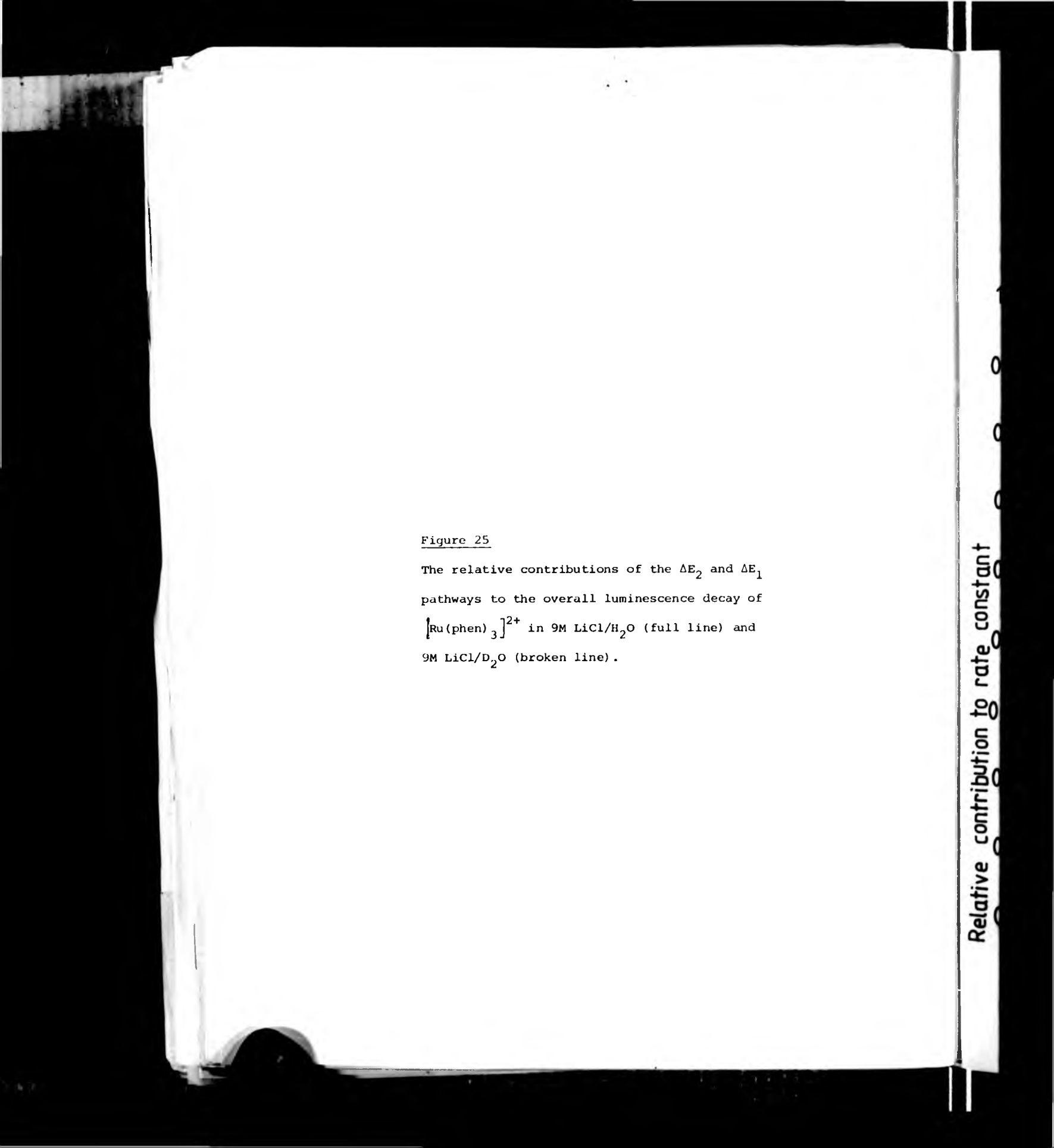

Figure 25

The relative contributions of the ΔE_2 and ΔE_1 pathways to the overall luminescence decay of $[Ru(phen)_3]^{2+}$ in 9M $LiCl/H_2O$ (full line) and 9M $LiCl/D_2O$ (broken line).

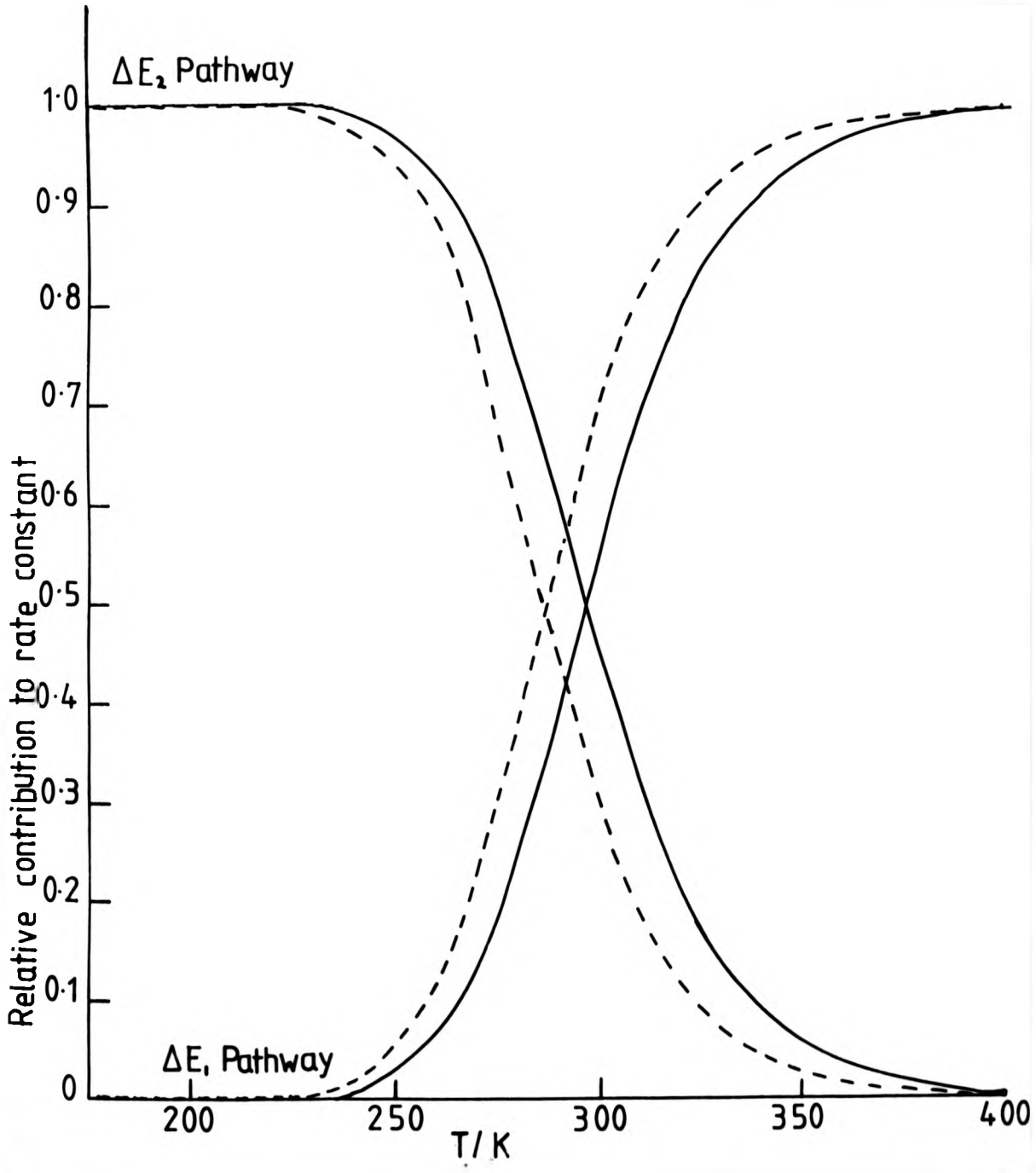
ΔE₂ Pathway
ΔE, Pathway
Relative contribution to rate constant
1·0
0·9
0·8
0·7
0·6
0·5
0·4
0·3
0·2
0·1
0
200
250
300
350
400
T/K

The effect on ΔE_2 of glassing of the 9 M LiCl medium is to lower the value to that comparable with the value of ΔE_2 obtained for CA film for both complexes, and this is coupled with a concomitant ∿ four-fold decrease in the frequency factor, a result which emphasises the environmental dependence of the ΔE_2 term which is typically higher in fluid solution than in a poorly solvating medium such as cellulose acetate film.

The contribution of the ΔE_2 pathway to the overall rate constant for the luminescence decay can be ascertained by reference to Figure 25 which shows the relative contribution of both pathways to the overall decay for $[Ru(phen)_3]^{2+}$ in 9 M $LiCl/H_2O$ and 9 M $LiCl/D_2O$ above 178 K. At temperatures below 220 K, the rate constant is essentially that described by the lower energy routes, while above this temperature there is a marked increase in the contribution of the higher energy pathway, the two contributions becoming equal at ∿287 K for 9 M $LiCl/D_2O$ and 297 K for 9 M $LiCl/H_2O$, the latter route becoming dominant at temperatures > 325 K. This figure illustrates the rapid changeover in the dominant term on raising the temperature, caused by the high frequency factors of the ΔE_1 term.

5-6 Summary

From this work, the overall equation required to explain the thermal activation of ruthenium(II) polypyridyl luminescence over the complete temperature range that has so far been investigated (0 to 400 K) is

Figure 26

Simplified Jablonski diagram for $[Ru(phen)_3]^{2+}$ in 9M $LiCl/H_2O$ at T > 178 K.

$_3]^{2+}$ in

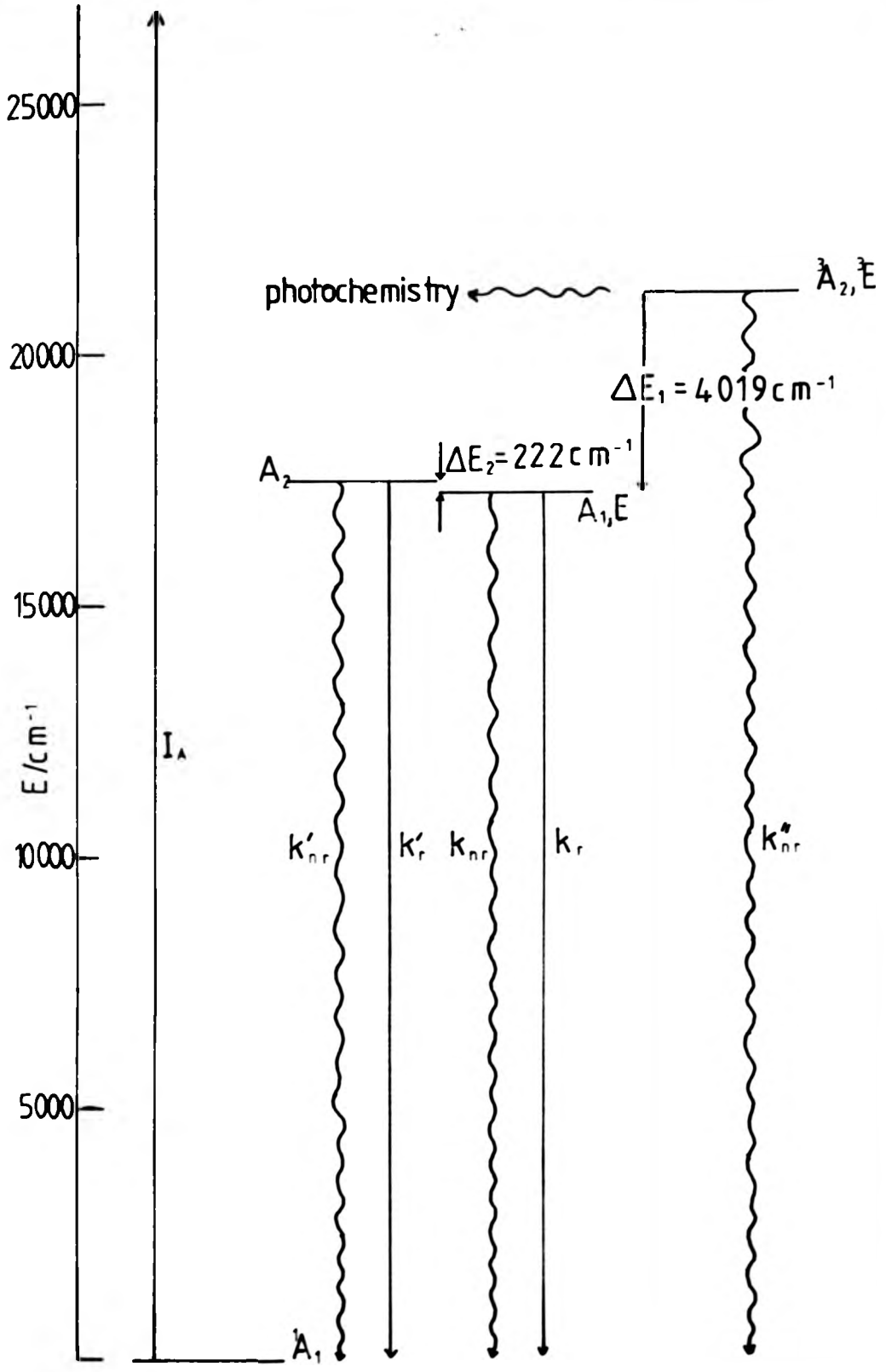
25000
20000
15000
10000
5000
E/cm⁻¹
I_A
photochemistry
³A₂, ³E
ΔE₁ = 4019 cm⁻¹
ΔE₂ = 222 cm⁻¹
A₂
A₁, E
k'nr
k'r
knr
kr
k"nr
¹A₁

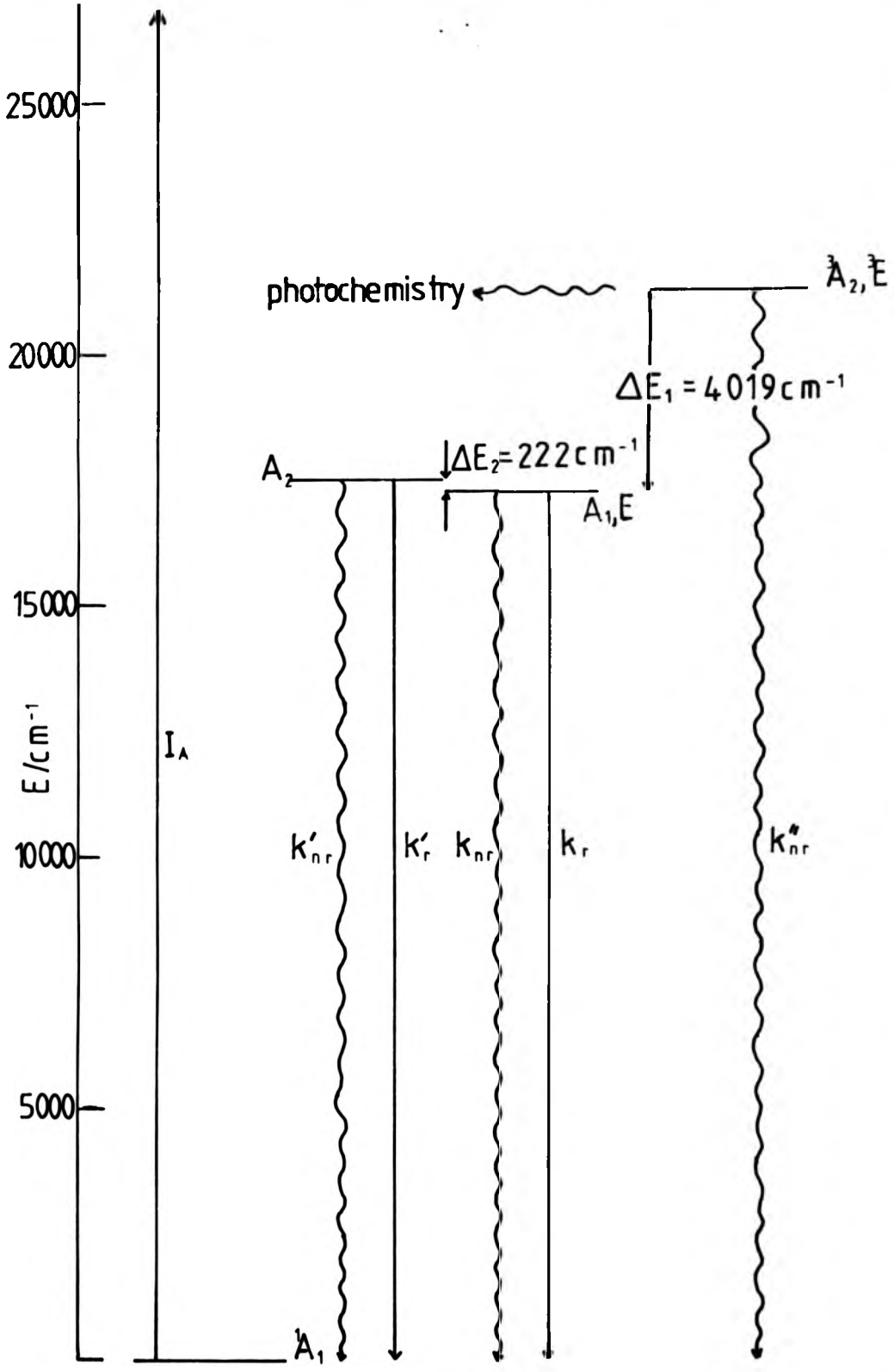
25000
20000
15000
10000
5000
E/cm⁻¹
I_A
photochemistry
$^3A_2, ^3E$
$\Delta E_1 = 4019\,cm^{-1}$
$\Delta E_2 = 222\,cm^{-1}$
A_2
A_1, E
k'_{nr}
k'_r
k_{nr}
k_r
k''_{nr}
$^1A_1$

$)_3]^{2+}$ in

$$k_{obs} = k_r + k_{nr} + A_3 \exp(-\Delta E_3/RT) + A_2 \exp(-\Delta E_2/RT) + A_1 \exp(-\Delta E_1/RT) \quad (5\text{-}3)$$

where k_r and k_{nr} refer to the radiative and non-radiative rate constants respectively for the lowest level of the low-lying triplet manifold, A_3 is the sum of the radiative and non-radiative rate constants for the second-lowest (E) level of the triplet with ΔE_3 representing the splitting (ca. 10 cm^{-1}) of this level from the lowest level. A_2, ΔE_2, A_1 and ΔE_1 have the same meanings as used in this work. However, at temperatures above 77 K, the first three terms of equation (5-3) can be neglected to give the expression (equation (5-1)) used in this work.

The temperature range for which these individual pathways becomesimportant can be found by using the appropriate data to produce plots such as Figure 25 over the entire temperature range. The results for $[Ru(phen)_3]^{2+}$ [147] show that the low-lying A_1 level is only dominant between 0 and 2 K, with the E level having a maximum contribution between ~ 8 and 15 K. The A_2 level is dominant from 30 to 220 K, with deactivation through the higher LF level becoming important at temperatures > 350 K. The precise changeover points will obviously change with environment and complex, although a similar pattern can be expected for all cases. The degradative routes for the excitation energy in the case of $[Ru(phen)_3]^{2+}$ in 9 M LiCl/H_2O for T > 178 K are represented in the Jablonski diagram of Figure 26 for the temperature range covered in this work. It has been assumed that ISC from the initially populated singlet state to the A_1 level occurs with unitary efficiency, and the levels have been given the labels adopted by Crosby *et al.*[53] for the low-lying level and that of van Houten and

Watts[54] to the higher level. This diagram, therefore, can be used to rationalise the luminescence behaviour of this complex at ambient temperatures, affording good comparison with the results of photochemical studies. Perhaps the most important points to be made are that (i) the value of ΔE_2 quoted by Crosby et al.[53,147] is only applicable to a polymer matrix environment, and use of this value for ambient temperature will give erroneous results due to the enhancement of ΔE_2 in a fluid solution, clearly indicating an environmental dependence, and (ii) the presence of an isotope effect on the low-energy pathway has been suggested to show the presence of some CTTS character in the low-lying triplet manifold. This may well be important when considering the electron transfer properties of this level.

In conclusion, this work has shown that the luminescence of polypyridyl complexes of ruthenium(II) occurs mainly through a thermally-activated pathway (ΔE_2) at temperatures > 77 K, representing the highest level of the Crosby[53] ^{3}CT model. A non-radiative thermally-activated route (ΔE_1) competes successfully with the pathway at temperatures > ∿ 320 K, and this has been labelled as a ^{3}LF photoreactive level by van Houten and Watts.[54] Solvent isotope studies indicate that the ^{3}CT level may have some CTTS character imparted to it. The results also indicate that $[Ru(phen)_3]^{2+}$ is less susceptible to thermal quenching than the bipyridyl analogue with an inherently longer lifetime for a given medium. This is in agreement with previous reports[147] and reflects the enhanced rigidity of the ligand framework.

CHAPTER 6

POLYPYRIDYL COMPLEXES OF OSMIUM(II)

RESULTS AND DISCUSSION

The effects of temperature and solvent on both the luminescence lifetime and spectrum of $[Os(bipy)_3]^{2+}$ and $[Os(phen)_3]^{2+}$ have been investigated with a view to establishing a model for the luminescence by comparison with the analagous ruthenium(II) complexes. The luminescence spectra of both complexes showed a negligible change with solvent in the position of the emission maximum for the systems investigated (± 2 nm). To afford investigation over a wide temperature range, the luminescence spectra were recorded in an aqueous LiCl medium. Lifetime measurements were taken over an extended temperature range in both aqueous and deuterated LiCl media as well as polymeric (cellulose acetate) film. Kinetic measurements were also made in other selected solvents at ∿ 295 and 77 K, which gave excellent agreement with literature values[136,154] where available, indicating both complexes to be pure.

6-1 Luminescence spectra

Both the changes in emission peak position and relative luminescence yield were recorded every few K over the temperature range 77 to 340 K for both complexes in an aqueous 9 M LiCl medium. An excitation wavelength of 466 nm was employed to avoid interference from the second-order scattering peak, with a band-pass of 20 nm for both excitation and emission monochromators being chosen to allow a reasonable spectral intensity at elevated temperatures. The results show that room-temperature spectra consist of a single peak centred at 725 and 728 nm (with a vestige of a shoulder at 700 nm) for the phen and bipy complexes respectively, which agrees well with previous reports.[136,154] When the temperature is lowered, however, there is a marked shift of intensity toward the blue edge of the spectrum with no change

Figure 27

Luminescence spectra of $\left[Os(phen)_3\right]^{2+}$ in 9M $LiCl/H_2O$; individual intensities are not related. (Spectra were recorded on different sensitivity settings and are uncorrected).

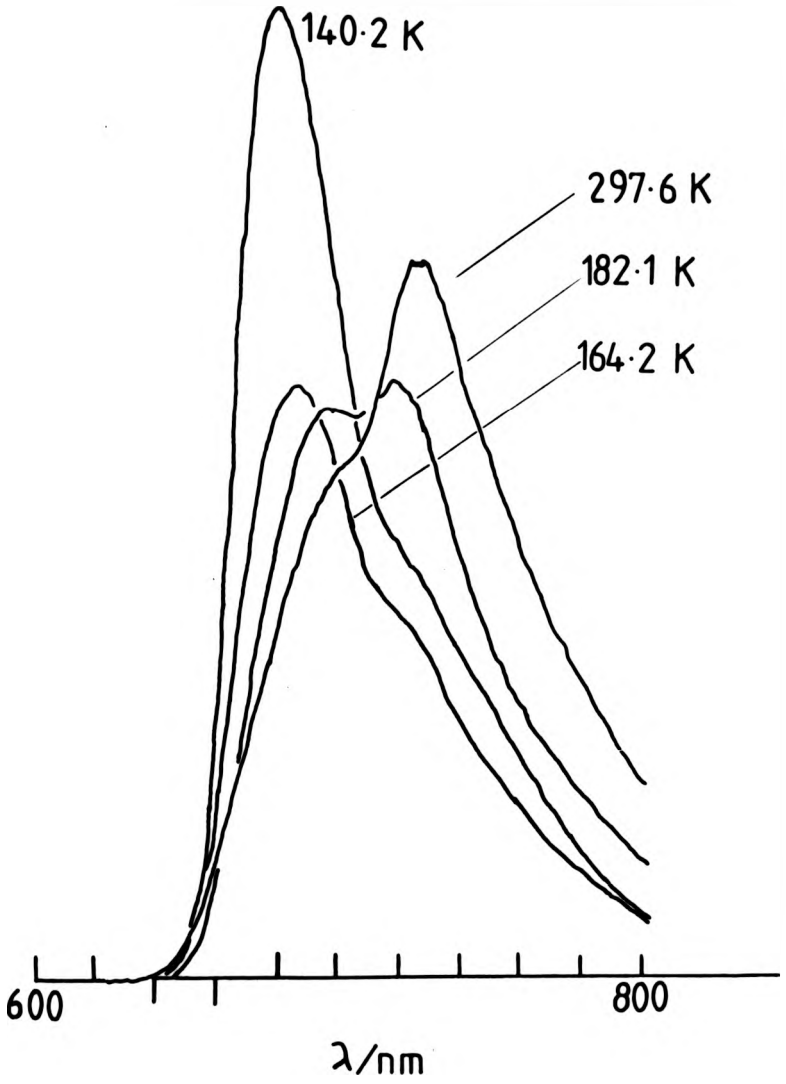
140·2 K
297·6 K
182·1 K
164·2 K
600
800
λ/nm

in the overall spectral region, which is depicted in Figure 27 for $[Os(phen)_3]^{2+}$. A similar situation was also found for $[Os(bipy)_3]^{2+}$ with a peak at 709 nm (cf. 695 nm with $[Os(phen)_3]^{2+}$) becoming apparent at 77 K, although resolution of structure was less apparent in this case. However, a constant separation for the two peaks of 530 ± 30 cm^{-1} was found for both complexes. This can be compared with a separation of ∿ 1300 cm^{-1} reported for the analogous ruthenium(II) systems, attributed to the vibronic progression caused by an M-L vibrational deactivation mode. The reduction of this frequency in the case of osmium(II) is reasonable in view of the increased mass of the central metal atom.

Further resolution of the osmium(II) spectra at 77 K was enabled by reducing the bandpass to 10 nm to give a shoulder at 790 nm. This can be compared with the spectra of Zuloaga and Kasha[138] who report emission maxima at 685, 721 and 790.5 nm for $[Os(phen)_3]^{2+}$, although Crosby et al[239] have reported an emission spectrum with peaks at ∿ 700, 790 and ∿ 900 nm for this complex, with no peak at 721 nm being apparent. Unfortunately, as in the case of ruthenium(II), it is not possible to resolve the positions of the individual radiative levels of the triplet manifold due to the small splitting (expected to be < 100 cm^{-1}) exhibited by these levels, although the observed shift of intensity would suggest that the upper level, at least, lies within the region of 14,400 cm^{-1} (695 nm) for $[Os(phen)_3]^{2+}$ and 14,100 cm^{-1} (709 nm) for $[Os(bipy)_3]^{2+}$. Perhaps studies of low temperature (4.2 K) solid state luminescence spectra may give the required resolution to allow evaluation of these parameters.

Figure 28

Temperature dependence of (relative) luminescence quantum yield for $[Os(phen)_3]^{2+}$ (upper curve, X) and $[Os(bipy)_3]^{2+}$ (lower curve, +).

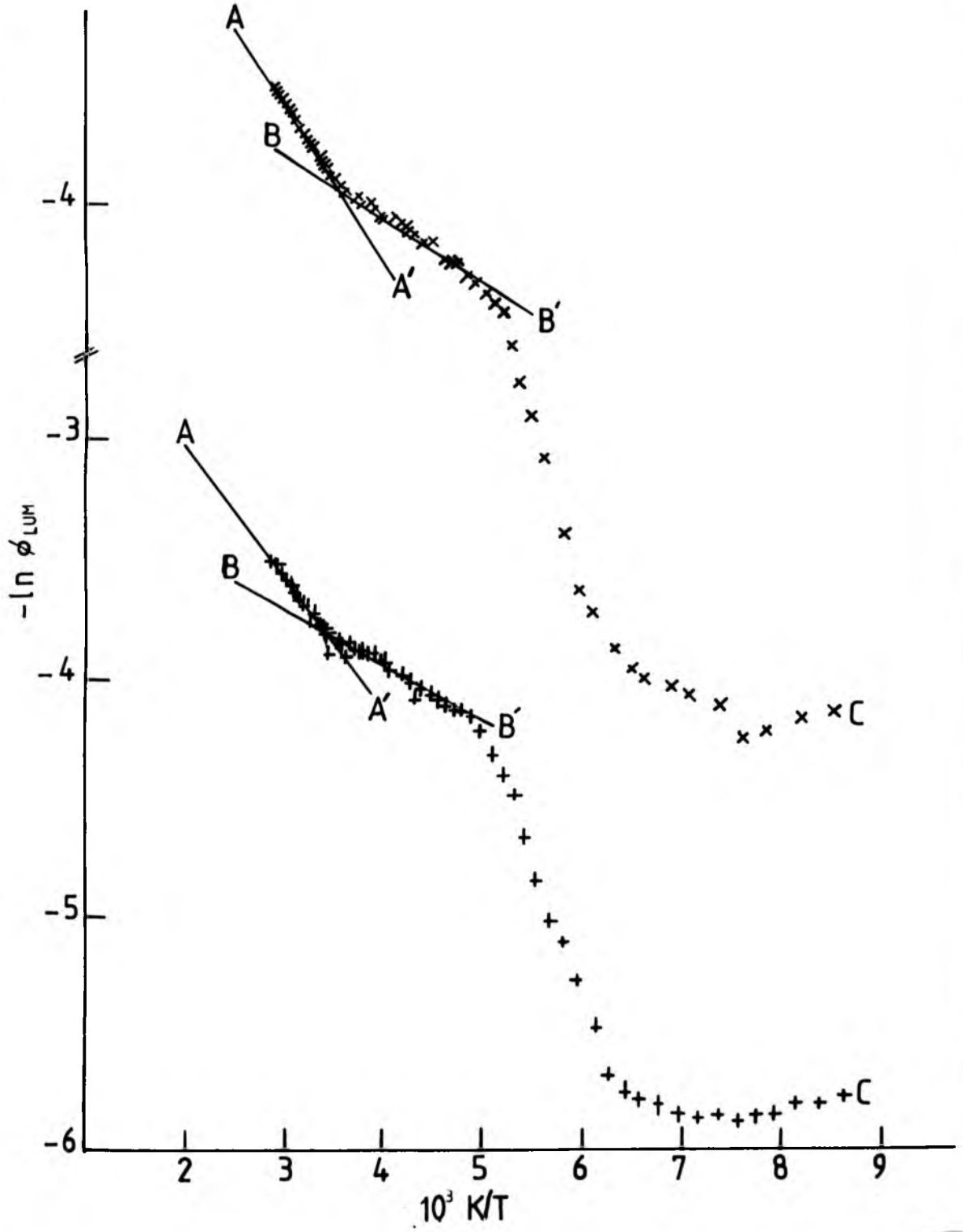
A
B
A'
B'
A
B
A'
B'
C
C
-4
-3
-4
-5
-6
2
3
4
5
6
7
8
9
$-\ln \phi_{LUM}$
10^3 K/T

The change in the relative luminescence yields, ϕ_{LUM}, with temperature is depicted in the form of $-\ln\phi_{LUM}$ vs. $1/T$ in Figure 28, for both complexes in an aqueous 9 M LiCl medium which affords good correlation with the kinetic obtained from flash photolysis (see later) since $\phi_{LUM} = k_r.\tau_{OBS}$ (see equation (1-36)), assuming $\phi_{ISC} = 1$. Figure 28 shows both complexes to give identical behaviour with the temperature profile of the luminescence yield falling into distinct regions, denoted by AA' and BB', which represent simple Arrhenius behaviour at > 286 K and 204 < T < 286 K respectively, with C denoting distinctly non-Arrhenius behaviour in the region 200 > T > 130 K. While a relative plot of this form does not yield absolute values for the frequency factors, the activation energies for AA' and BB' are 5.7 ± 0.2 kJ mol^{-1} and 2.28 ± 0.08 kJ mol^{-1} respectively for $[Os(phen)_3]^{2+}$ which can be compared with values of 4.3 ± 0.1 kJ mol^{-1} and 2.00 ± 0.08 kJ mol^{-1} respectively for $[Os(bipy)_3]^{2+}$. Region C is peculiar in that the luminescence yield increases rapidly with falling temperature to a position of maximum luminescence at T ∿ 132 K, from which a small decrease occurs on further lowering of the temperature. This would indicate that the luminescence observed where the point occurs through a thermally activated emitting state of higher luminescence quantum yield than the level responsible for luminescence below 132 K. The levels can be related to the upper A_2 state and the A_1,E manifold respectively of the low-temperature triplet model proposed[53] for this system and from which this result would be expected (see Introduction). Further discussion of these results will be continued later in relation to the results of direct kinetic studies given below.

6-2 Results of flash photolysis experiments

While the luminescence decay of both osmium(II) complexes followed strict first-order kinetics for all measurements, a small but distinct

Figure 29

Dependence of luminescence lifetime upon emission wavelength for $[Os(phen)_3]^{2+}$ in 9M $LiCl/H_2O$ at 77 K.

emission

$_2$O at

dependence of the luminescence lifetime on emission wavelength was found at 77 K as shown for $[Os(phen)_3]^{2+}$ in an aqueous 9 M LiCl glass in Figure 29. This showed an ∿ 35% decrease in lifetime between the extreme measurements at 660 and 850 nm (recorded with a 1 nm bandpass). This necessitated all other measurements to be made with a small bandpass, (2 nm) and these were recorded at 730 nm (unless otherwise stated).

Temperature dependence measurements (77 to 370 K) were made for both complexes under conditions which have been described in the preceding discussion and the results are shown in the Arrhenius plots of Figure 30 with the fitted activation parameters being given in Table 6-1. The best fit was obtained using the expression (for T < 170 K):-

$$k_{obs} = A_1 \exp(-\Delta E_1^{\dagger}/RT) + A_2 \exp(-\Delta E_2^{\dagger}/RT) \qquad (6\text{-}1)$$

which is identical to that used for the ruthenium(II) case (equation (5-1)) with the parameters having the same meaning (see Chapter 5). This implies a similar model in which $\Delta E_1^{\dagger}$ represents a temperature-activated radiative pathway through which the observed luminescence occurs predominantly throughout the temperature range investigated. $\Delta E_2^{\dagger}$ can be compared to the competitive non-radiative pathway cited in the ruthenium(II) case, although the exact nature of this state for the two systems may differ. The inappropriateness of a fit of the form of equation (5-2) is demonstrated by the dashed lines in these plots. Above 180 K the data could be fitted to a simple Arrhenius expression, the parameters being given in Table 6-1.

Lifetime measurements for both complexes in a number of solvents at ambient temperature (Table 6-2) indicated only slight dependences, with the luminescence decay being fastest in an aqueous medium and slowest in ethanol and acetonitrile. An isotope effect (k_{H_2O}/k_{D_2O}) of 1.4 and 1.9 was found for $[Os(bipy)_3]^{2+}$ and $[Os(phen)_3]^{2+}$ respectively and, although a slight decrease of lifetime is apparent in 9 M LiCl for both complexes, indicating a minimal quenching effect by chloride ions, this medium can be regarded simply as providing an extended temperature range to the aqueous environment.

Table 6-1 Rate and activation data for luminescence of Os(II) complexes

(a) 9 mol dm^{-3} aqueous LiCl solutions

Complex	Medium	T < 170 K				T > 180 K	
		$10^{-10}A_1/s^{-1}$	$\Delta E_1^{\dagger}$/kJ mol^{-1}	$10^{-6}A_2/s^{-1}$	$\Delta E_2^{\dagger}$/kJ mol^{-1}	$10^{-7}A/s^{-1}$	$\Delta E^{\dagger}$/kJ mol^{-1}
$[Os(bipy)_3]^{2+}$	H_2O-LiCl	5.17(± 1.98)[a]	13.50(± 0.64)	5.57(± 0.97)	0.712(± 0.150)	35.19(± 5.11)	5.13(± 0.32)
	D_2O-LiCl	1.03(± 0.62)	12.1(± 0.9)	3.96(± 0.34)	0.753(± 0.070)	22.99(± 2.47)	5.11(± 0.24)
$[Os(phen)_3]^{2+}$	H_2O-LiCl	1.37(± 0.67)	13.3(± 0.81)	2.71(± 0.37)	0.849(± 0.121)	14.07(± 1.43)	5.61(± 0.24)
	D_2O-LiCl	1.30(± 1.42)	14.3(± 1.65)	1.67(± 0.16)	0.779(± 0.081)	5.28(± 0.18)	4.80(± 0.08)

(b) Cellulose acetate (CA) film

		$10^{-7}A_1/s^{-1}$	$\Delta E_1^{\dagger}$/kJ mol^{-1}	$10^{-6}A_2/s^{-1}$	$\Delta E_2^{\dagger}$/kJ mol^{-1}
$[Os(bipy)_3]^{2+}$	CA	19.3(± 3.4)	7.26(± 0.52)	4.15(± 1.10)	0.751(± 0.229)
$[Os(phen)_3]^{2+}$	CA	3.08(± 0.60)	5.95(± 0.62)	1.62(± 0.39)	0.532(± 0.195)

[a] bracketed figures refer to one standard deviation

Figure 30

Temperature profiles of the luminescence lifetimes (730 nm) for $[Os(phen)_3]^{2+}$ and $[Os(bipy)_3]^{2+}$ in aqueous and polymeric media. Full curve-computer fit to equation 6-1; broken curve-computer fit to equation 5-2.

(a) $[Os(bipy)_3]^{2+}$ in 9M $LiCl/H_2O$ (top curve) and 9M $LiCl/D_2O$ (bottom curve).

(b) $[Os(phen)_3]^{2+}$ in 9M $LiCl/H_2O$ (top curve) and 9M $LiCl/D_2O$ (bottom curve).

(c) $[Os(phen)_3]^{2+}$ in CA film (bottom curve) and $[Os(bipy)_3]^{2+}$ in CA film (top curve).

Figure 30

Temperature profiles of the luminescence lifetimes (730 nm) for $[Os(phen)_3]^{2+}$ and $[Os(bipy)_3]^{2+}$ in aqueous and polymeric media. Full curve-computer fit to equation 6-1; broken curve-computer fit to equation 5-2.

(a) $[Os(bipy)_3]^{2+}$ in 9M $LiCl/H_2O$ (top curve) and 9M $LiCl/D_2O$ (bottom curve).

(b) $[Os(phen)_3]^{2+}$ in 9M $LiCl/H_2O$ (top curve) and 9M $LiCl/D_2O$ (bottom curve).

(c) $[Os(phen)_3]^{2+}$ in CA film (bottom curve) and $[Os(bipy)_3]^{2+}$ in CA film (top curve).

lifetimes
$]^{2+}$ in
-computer
er fit to

urve) and

urve) and

rve) and
).

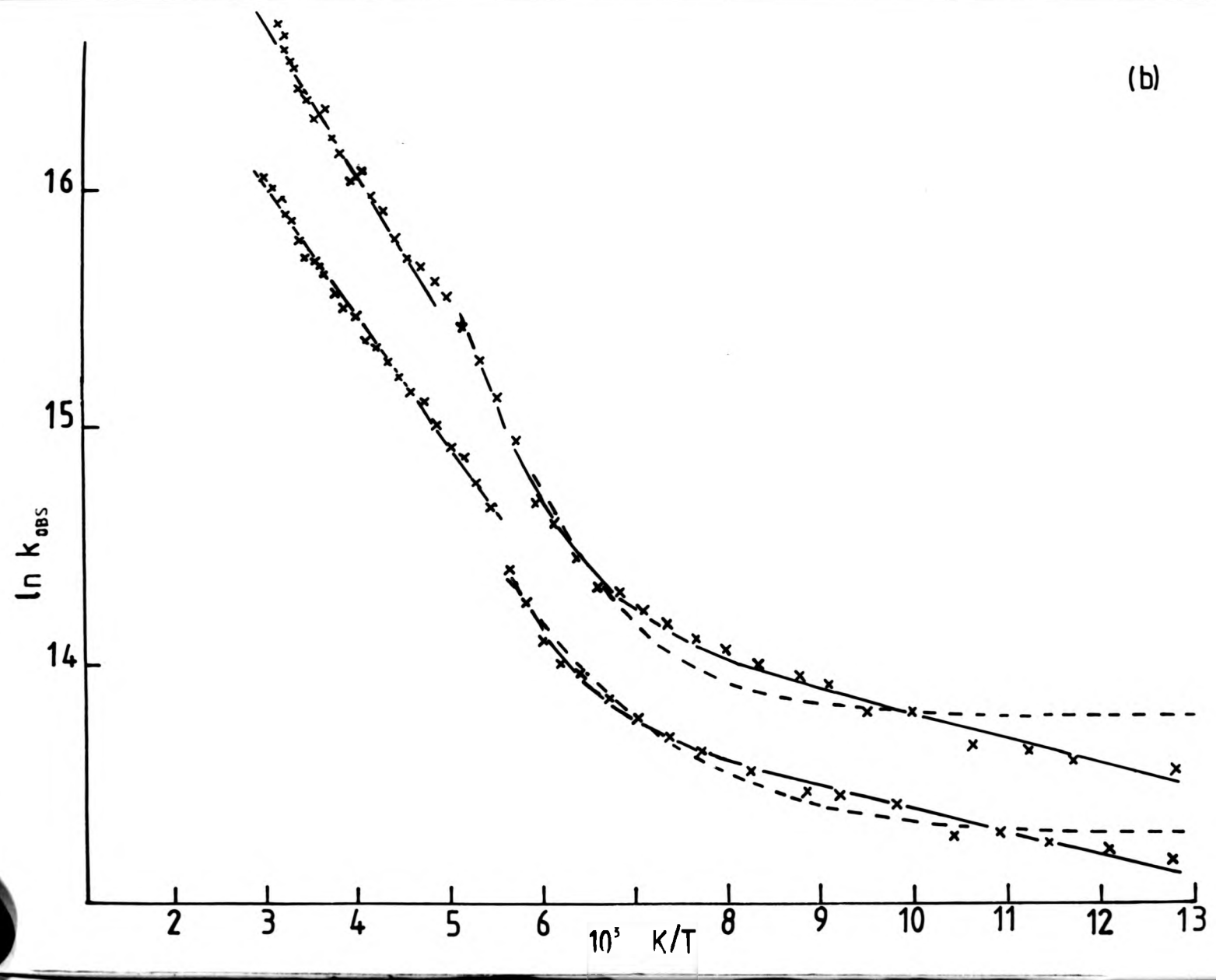
(b)
16
15
14
ln k_{OBS}
2
3
4
5
6
8
9
10
11
12
13
10^3 K/T

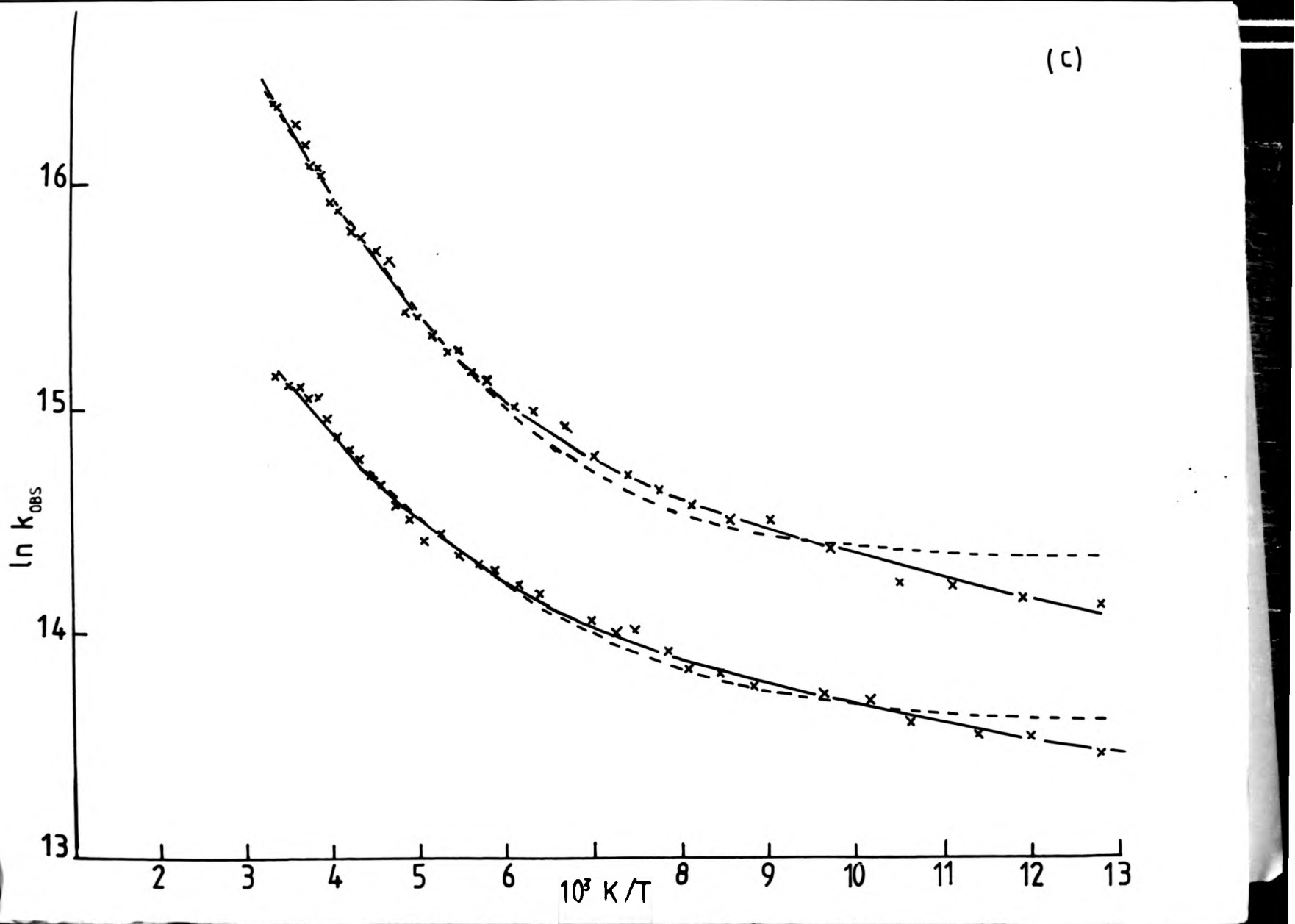
(c)
16
15
14
13
ln k_{OBS}
2
3
4
5
6
8
9
10
11
12
13
10^3 K/T

6-3 Discussion of results

The Arrhenius plots for 9 M LiCl solutions of both complexes differ from those of the analogous ruthenium(II) complexes in that the phase transition occurs at a point for which the high energy pathway is still important and results in a discontinuity (180 to 200 K) which highlights the different kinetic behaviour given in glassy and fluid media . The simple Arrhenius behaviour exhibited by both complexes in this medium above $\sim$ 200 K indicates the high-energy non-radiative pathway to be the dominant deactivation mode, although the position of this level changes dramatically from 1,128 cm^{-1} (13.5 kJ mol^{-1}) to 429 cm^{-1} (5.13 kJ mol^{-1}) for $[Os(bipy)_3]^{2+}$ in 9 M $LiCl/H_2O$ and from 1,111 cm^{-1} (13.3 kJ mol^{-1}) to 469 cm^{-1} (5.61 kJ mol^{-1}) for $[Os(phen)_3]^{2+}$ in 9 M $LiCl/H_2O$. This result suggests that while the environment produces large shifts in the levels, the nature of the ligand is more influential on the magnitude of the frequency factor, which would suggest that the ligand is implicated in the 'forbiddenness' of a transition, possibly through the ordering of the state which would explain the reduced frequency factors for the more rigid phenanthroline complex. $[Os(phen)_3]^{2+}$, in fact, exhibits a longer lifetime than $[Os(bipy)_3]^{2+}$ under all the conditions investigated (see Table 6-2). which seems to be a general trend for polypyridyl complexes (see Chapters 4 and 5). Both complexes, however, exhibit much shorter lifetimes than the equivalent ruthenium(II) complexes which may reflect both the lowering in position of the non-radiative level and the enhanced SOC effect. In particular, the short lifetime exhibited by $[Os(bipy)_3]^{2+}$ restricted measurements to T < 295 K at which a lifetime of $\sim$ 24 ns was recorded.

Table 6-2 Luminescence lifetimes for Os(II) complexes

(a) Ambient temperatures

Complex	Medium	Temperature/K	τ/ns	Reference
$[Os(bipy)_3]^{2+}$	H_2O	298	19.2	136
	H_2O	293.5	30 ± 2	This work
	D_2O	293.2	42 ± 1	This work
	9 M LiCl-H_2O	295.3	24.5 ± 1	This work
	9 M LiCl-D_2O	296.3	34.8 ± 2	This work
	MeOH	294	49	154
	MeOH	296.0	46.9 ± 1.2	This work
	CD_3OD	281.9	59 ± 1	This work
	EtOH	294.8	61.3 ± 1	This work
	i-PrOH	295.0	57.1 ± 1	This work
	CH_3CN	293.3	57.6 ± 1	This work
	DMF	295.3	46.1 ± 1	This work
	DMSO	295.8	43.7 ± 4	This work
$[Os(phen)_3]^{2+}$	H_2O	294.0	82 ± 1	This work
	D_2O	294.0	154 ± 6	This work
	9 M LiCl-H_2O	295.5	74.1 ± 2	This work
	9 M LiCl-D_2O	294.0	139 ± 2	This work
	MeOH	294	183	154
	MeOH	296.0	173 ± 2	This work
	CD_3OD	288.7	230 ± 10	This work
	EtOH	295.4	199 ± 5	This work
	i-PrOH	295.1	191 ± 11	This work
	CH_3CN	293.1	218 ± 8	This work
	DMF	294.8	160 ± 3	This work
	DMSO	296.0	142 ± 8	This work

(b) Cryogenic temperatures

Complex	Medium	Temperature/K	τ/ns	Reference
$[Os(bipy)_3]^{2+}$	CD_3OD	78.9	822 ± 1	This work
	EtOH-MeOH(4:1)	77	890	15
	9 M LiCl-H_2O	78	551	This work
	9 M LiCl-D_2O	78	765	This work
	Cellulose acetate	78	724	This work
$[Os(phen)_3]^{2+}$	CD_3OD	79.2	1790 ± 50	This work
	EtOH-MeOH(4:1)	77	2430	15
	9 M LiCl-H_2O	78	1275	This work
	9 M LiCl-D_2O	78	1877	This work
	Cellulose acetate	78	1427	This work

Comparison of these Arrhenius plots with the equivalent luminescence plots (Figure 28) mentioned earlier reveals that while both show a similar form below T_g the temperature profile above T_g differs. This suggests that while k_r can be regarded as temperature-insensitive, below T_g the expression $\phi_{LUM} = k_r.\tau_{OBS}$ does not hold above T_g and a temperature-dependence of k_r is implied. A full explanation for this behaviour is not immediately apparent, but the BB' region may be related to $\Delta E_2^{\dagger}$, whereas AA' may be representative of $\Delta E_1^{\dagger}$. That $\Delta E_1^{\dagger}$ is particularly sensitive to environment has been shown by the lifetime studies,and the activation energies quoted for AA' are of a similar magnitude to $\Delta E_1^{\dagger}$. The activation energy of BB' is $\sim$ 2 kJ mol^{-1} ($\sim$ 166 cm^{-1}) for both complexes, and it has been shown that $\Delta E_2^{\dagger}$ increases in fluid media to $\sim$ 160 cm^{-1} for $[Ru(bipy)_3]^{2+}$ in 9 M $LiCl/H_2O$. However, while this may give an indication as to the nature of AA' and BB', it does not explain why a similar situation is not found in lifetime studies, a result for which no explanation can be offered, although an experimental artefact seems unlikely as these experiments were repeated a number of times with the same result.

The temperature-dependence of the luminescence was also investigated in cellulose acetate film to eliminate the effect of the phase transition in 9 M LiCl glasses, and the results shown in Figure 30c and Table 6-1 show a distinct lowering of $\Delta E_1^{\dagger}$ for both complexes in this medium. A similar situation was found for ruthenium(II) (Chapter 5),and a similar explanation can be adduced. The value of 44 cm^{-1} (0.53 kJ mol^{-1}) for $\Delta E_2^{\dagger}$ for $[Os(phen)_3]^{2+}$ in CA film can be compared with the 40 cm^{-1} splitting of the A_2 and E levels in the low-temperature triplet manifold reported by Crosby[5] for $[Os(phen)_3]^{2+}$ in PMM film.

Figure 31

Temperature profiles of the luminescence lifetime of $[Os(phen)_3]^{2+}$ in 9M $LiCl/H_2O$ at emission wavelengths of 662 nm (bottom curve, X) and 830 nm (top curve, ·). Full curves are computer fits to equation 6-1.

lifetime of

wavelengths

op curve, ·).

6-1.

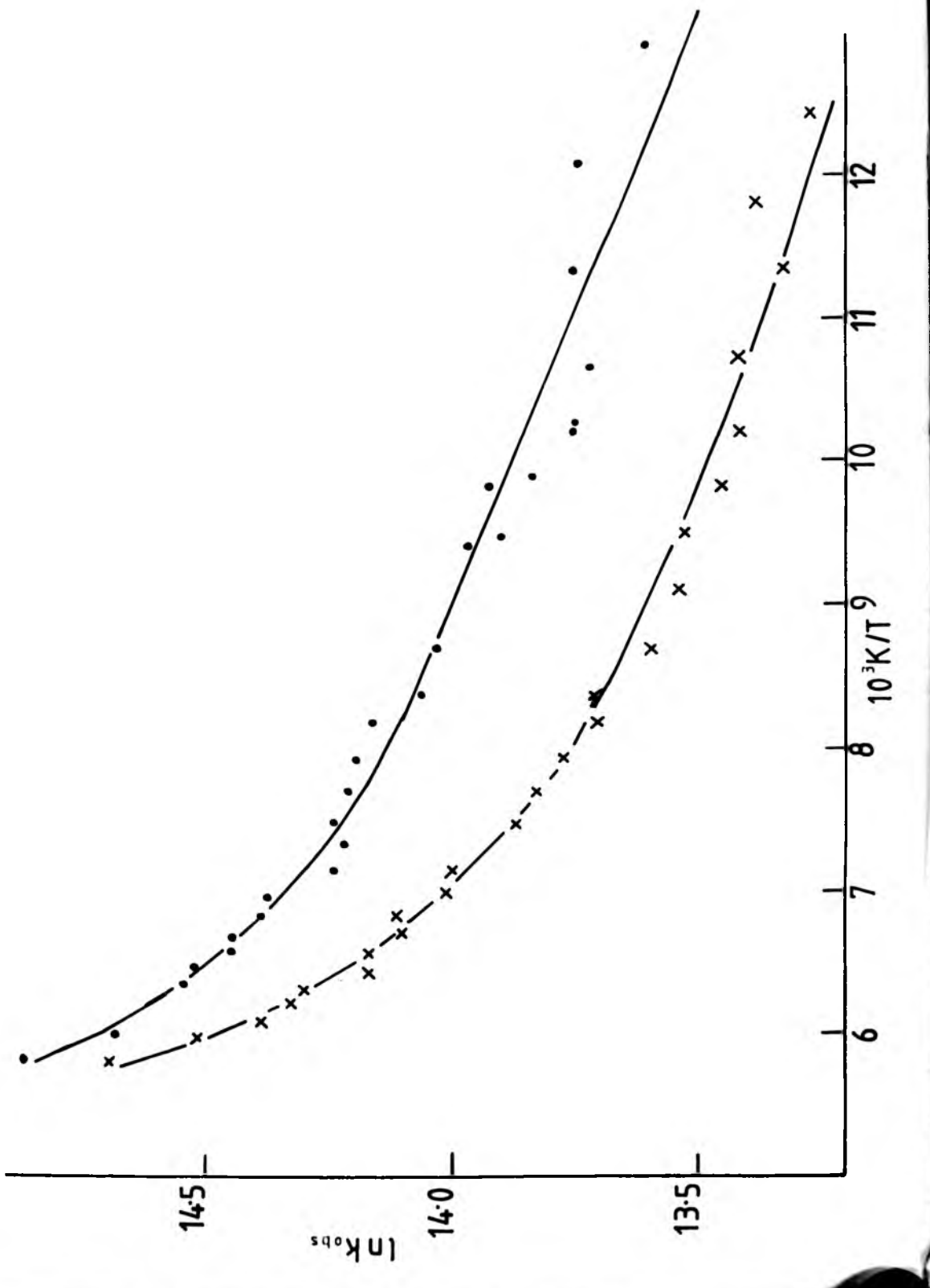

This gives weight to the assumption that $\Delta E_2^{\dagger}$ represents the upper level of the low-temperature triplet proposed by Crosby *et al.*[53]

The emission wavelength dependence of the luminescence lifetime suggests that emission occurs from two levels. A similar situation has been reported for iridium(III) complexes[51] although non-exponential kinetics are displayed by these systems, indicating the two emitting levels to be in good thermal communication, and it was possible to resolve the decay into two exponential components corresponding to the two levels. In this case, however, good first-order kinetics were given over the entire wavelength range, which suggests the presence of two near-lying levels which are not in thermal equilibrium but which decay quite independently, once populated. The temperature-dependences of the emission from $[Os(phen)_3]^{2+}$ in 9 M $LiCl/H_2O$ at the two extreme wavelengths (662 and 830 nm) were investigated (Figure 31), and the results of fitting the accumulated data to equation (6-1) are given in the table below, along with the activation parameters for the luminescence monitored at 730 nm for this system.

Activation parameters for the luminescence of $[Os(phen)_3]^{2+}$ in H_2O-LiCl at different emission wavelengths

λ/nm	$10^{-10}A_1/s^{-1}$	$\Delta E_1^{\dagger}$/kJ mol^{-1}	$10^{-6}A_2/s^{-1}$	$\Delta E_2^{\dagger}$/kJ mol^{-1}
662	1.68(± 1.69)[a]	13.7(± 1.5)	2.3(± 0.3)	0.97(± 0.12)
730	1.37(± 0.67)	13.3(± 0.81)	2.7(± 0.37)	0.84(± 0.121)
830	1.1(± 1.7)	13.2(± 0.2)	3.5(± 0.5)	0.99(± 0.11)

[a] bracketed figures refer to one standard deviation.

Unfortunately, the results are inconclusive as they do not reveal which of the four parameters is responsible for the observed wavelength dependence, probably due to the relatively small rate difference for the two extremes, although A_2 would seem to be of particular influence in view of the standard deviations quoted.

6-4 The proposed general model for luminescence from osmium(II) polypyridyl complexes

This work has shown that,while a basic model similar to that proposed for ruthenium(II) can be applied equally well to explain the luminescence from osmium(II) complexes, the latter differ in particular details. This has been shown by the complicating factors of (a) the slight but definite emission wavelength dependence of the luminescence lifetime and (b) the difference in the temperature profile of the relative luminescence yield from that of the luminescence lifetime, neither of which have been found for the ruthenium(II) case. The Arrhenius plots for the luminescence lifetime differ from those of the ruthenium(II) case in that the higher-energy pathway, $\Delta E_1^{\dagger}$, is still dominant at the phase transition rather than the low-energy $\Delta E_2^{\dagger}$ route, demonstrating a definite medium dependence of $\Delta E_1^{\dagger}$. It may well be the case, therefore, that both $\Delta E_1^{\dagger}$ and $\Delta E_2^{\dagger}$ are dependent upon environment for these systems. The observed solvent isotope effect indicates the low-lying triplet to have some CTTS character, also noted for ruthenium(II).

The Jablonski diagram in Figure 32 gives the basic scheme for deactivation of excited osmium(II) complex, the specific examples of $[Os(bipy)_3]^{2+}$ in 9 M $LiCl/H_2O$ and cellulose acetate film being shown. From previous discussion, it is almost certain that the

Figure 32

Summary of energy states important in the deactivation of $\left[Os(bipy)_3\right]^{2+}$ in 9M $LiCl/H_2O$ (left) and cellulose acetate film (right) in the temperature range 77 to 300 K.

e deactivation

nd cellulose

range 77 to

lower energy route corresponds to the upper level, A_2, of the low-lying Crosby triplet, whereas the lower level can be regarded as the A_1,E manifold of this triplet. In view of the noted wavelength dependence, however, it is uncertain that this low-energy pathway ($\Delta E_2^{\dagger}$) is responsible for the majority of the observed luminescence at all emission wavelengths or, indeed, for which region of the spectrum it is predominant.

The exact nature of the higher energy pathway is uncertain as this level is much lower than in the case of ruthenium(II), although it is unlikely that this level is of LF character as in the above case. The value of Δ for osmium(II) would be expected to be greater than that for the analogous ruthenium(II) case and, assuming a similar value of the Racah interelectronic repulsion parameter, C, then the observed splitting (Δ-3C) would be expected to be greater than in the latter case. $\Delta E_2^{\dagger}$ is, however, approximately one-third of the value of the equivalent activation energy in the ruthenium(II) case. A study of Figure 5 in ref. 148, however, indicates that $\Delta E_2^{\dagger}$ may correspond to an upper manifold of CT states of either $d\pi^*(a_2)$ or $d\pi^*(e)$ origin. If this is the case, then this higher manifold may contribute to the overall radiative decay of the excited complex, which would provide an alternative explanation for the observed behaviour of the luminescence intensity at elevated temperatures (Figure 28). Unfortunately, this argument is purely speculative,but a study of the photochemistry of osmium(II) complexes at elevated temperatures similar to that performed by van Houten and Watts for $\left[Ru(bipy)_3\right]^{2+}$ [157] may help in determining the nature of this upper level.

In conclusion, therefore, while the basic model developed for ruthenium can be applied to the equivalent osmium(II) systems, the nature of the luminescence, particularly at elevated temperatures, appears to be somewhat different.

CHAPTER 7

BIS(8-HYDROXYQUINOLINATO)PLATINUM(II) LUMINESCENCE

RESULTS AND DISCUSSION

Few studies have been reported for the luminescence of platinum(II) complexes in solution, and this work therefore has taken the form of a preliminary investigation into both the nature of the luminescence and the excited-state properties of bis(8-hydroxyquinolinato)platinum(II), denoted $[Pt(QO)_2]$, through the effect of changes in environment on the ground state absorption spectrum, and the emission spectrum and lifetime. The presence of an ESA spectrum has allowed the position of higher excited states to be determined.

7-1 Results and discussion of spectroscopic studies

The ground state absorption spectrum and luminescence spectrum of $[Pt(QO)_2]$ have been given in Chapter 2 (Figure 9). The luminescence spectrum resembles those of ruthenium(II) and osmium(II) in that it is highly structured with at least four peaks being apparent. Unfortunately, further resolution could not be obtained even at 77 K in cellulose acetate film, although the emission maximum (652 nm at 298 K) shifted to 620 nm at 77 K, which is in agreement with a previous report.[37] However, the structure has a spacing of $\sim$ 1,220 cm^{-1} (see Table 7-2), indicative of a vibrational progression due to an M-L type of deactivation mode,while the shift in the emission maximum is reminiscent of the situation found for ruthenium(II) and osmium(II).

Figure 9 would suggest that the luminescence occurs from an excited state with an apparent Stokes' shift of $\sim$ 5,700 cm^{-1} at ambient temperature, assuming the first observable absorption band to be responsible for the population of the emitting state. However, this would suggest that the emitting state is considerably distorted from the ground state geometry, and may therefore be expected to be quite reactive. However, no such photo-reaction

has been found even on prolonged exposure to high-intensity light. A more likely explanation may be that the absorption band related to the emitting state is extremely weak and, therefore, not well-resolved in the ground state absorption spectrum. The low energy absorption band may then represent an initially populated state from which ISC to the emitting state occurs with unitary efficiency (due to the large SOC effect). This argument gains validity from the overlapping of the luminescence spectrum at 77 K with the red tail of the low-energy absorption band (see Figure 1 of ref. 37). The luminescence excitation spectrum of $[Pt(QO)_2]$ in CA film shows peaks at 468 nm, 345 nm and 284 nm, with the intensity decreasing toward lower wavelength. These peaks, which correspond to the three lowest energy bands in the absorption spectrum, suggest that the low-energy absorption band at 468 nm is mainly responsible for the population of the emitting state, which accords with the above discussion.

The $[Pt(QO)_2]$ complex has been reported to have a redox potential of -0.89 V *vs.* SCE[240] and it would therefore be expected that the high intensity CT band will occur at reasonably low energies and may well envelope some of the weaker d-d bands. In particular, the first d-d spin-allowed transition is expected to occur above 303 nm[241] with an extinction coefficient (ε) of *ca.* 100 $dm^3\ mol^{-1}\ cm^{-1}$. The two low-energy bands which occur at 20,964 cm^{-1} (band A) and 28,985 cm^{-1} (band B) with $\varepsilon_{max} \sim$ 9,000 $dm^3\ mol^{-1}\ cm^{-1}$ and 10,000 $dm^3\ mol^{-1}\ cm^{-1}$ respectively in dimethyl-formamide at 298 K are therefore far too intense to be d-d transitions. The intensity of these bands suggest that they may be due to spin-allowed transitions, although the enhanced SOC effect for this system may well be instrumental in giving intensity to these transitions.

Figure 33

Correlation of ν_{MAX} with E_T values for bands A and B of the ground state absorption spectra of $\left[Pt(QO)_2\right]$ in various solvents. The designations of the points are given in Table 7-1.

ands A and

of

gnations

A solvatochromic shift of both bands A and B has been found, and the results are given below in Table 7-1.

Table 7-1 Bis(8-hydroxyquinolinato)platinum(II): absorption data (298 K) in various solvents

Solvent	ν_{max}/cm^{-1} (band A)	ν_{max}/cm^{-1} (band B)
1. MeOH	22 026	29 542
2. 2-Methoxyethanol	21 800	29 325
3. EtOH	21 750	29 112
4. n-PrOH	21 700	29 154
5. i-PrOH	21 500	28 940
6. t-BuOH	21 097	28 490
7. MeCN	21 367	29 369
8. DMSO	21 320	29 197
9. Me_2CO	21 160	29 028
10. CH_2Cl_2	21 140	29 028
11. C_5H_5N	20 986	28 900
12. $CHCl_3$	21 598	28 944
13. 1,4-Dioxan	20 812	28 735
14. DMF	20 964	28 985
15. cellulose acetate film	21 552	29 940

This shift has been correlated to the Dimroth parameter, E_T, for the solvent[242] as shown in Figure 33. This parameter, the origin of which has been given in Chapter 4, gives a relative indication of the solvent polarity through its solvating power. Figure 33 shows that band A appears at 22,026 cm^{-1} in methanol and red-shifts in solvents of lower polarity, appearing at 20,812 cm^{-1} in the least polar 1,4-dioxan. A similar situation is found for band B, although the effect is not so pronounced in case (29,542 cm^{-1} in methanol to 28,735 cm^{-1} in 1,4-dioxan). Both plots (Figure 33) show two distinct linear regions, one referring to hydroxylic solvents and the other to non-hydroxylic solvents, with the distinction being especially marked for band B.

This behaviour reflects the difference between this system and the organic systems which provide the E_T scale, and it illustrates the problem of providing a single solvent parameter applicable to all situations.[243] A similar dependence has been shown for the positions of the MLCT bands in a number of complexes of Mo, W and Fe[244,245] and, in particular, the observed shifts show both the same direction and magnitude as found for band A. This would suggest that band A is an MLCT band, probably d-π*, and such an assignment is certainly in line with the high extinction coefficient. Band B, however, is more likely to be a ligand centred π-π* transition as the free QO^- ligand has been reported to have a maximum at 28,653 cm^{-1} [37] in dimethylformamide solution saturated with KOH, which closely corresponds to the value of 28,985 cm^{-1} found for band B in this solvent. The relatively greater solvent-sensitivity found for band A, therefore, suggests that the solvent achieves intimate contact with the platinum metal core, probably *via* axial co-ordination.

In contrast, the emission maximum (*ca.* 15,200 cm^{-1}) shows a shift of only 230 cm^{-1} over the solvent range ethanol to dimethyl sulphoxide (see Table 7-2) when excited at 468 nm, which implies that the luminescent state is different to that populated directly by excitation into band A. although the origin may be the same (*i.e.* they may differ only in multiplicity). The discussion in Chapter 2.2-6 gives a similar description of the luminescence from other platinum(II) complexes in solvent glasses at 77 K, and suggests the emitting state for these complexes to be CT in origin. This would, therefore, imply that the emitting state for $[Pt(QO)_2]$ is a ^{3}CT(d-π*) state, assuming that band A refers to a spin-allowed singlet-singlet absorption of d-π* character. This inference is substantiated by (i) the reported excited state redox

potential of -0.89 V[240] which is similar to that reported for ruthenium(II) and (ii) the reported dynamic electron-transfer quenching processes from this state. In particular, the observation of the transient absorption of the reduced species for quenching by $[Cr(bipy)_3]^{3+}$ confirms this mechanism which was proposed after the quenching rate constant, k_q, for a series of quinones and nitroaromatics was found to be dependent on the reduction potential of the quencher.[240] However, it has been shown that ^{3}(d-d) states can also undergo electron-transfer processes, e.g. for chromium(III)[246], while a metal-centred transition could also explain the insensitivity of the luminescence spectrum to solvent, and a LF luminescent state has been described for some platinum(II) systems (see Chapter 2.2-6). However, the readiness with which the complex undergoes electron-transfer reactions, as illustrated by a moderately efficient photooxidation reaction which occurs in an aerated solution of acetonitrile at 293 K, and the high values of k_q (> 10^{10} for a number of aromatic quenchers)[240] suggests a ^{3}CT state to be the more likely explanation, although the spin-labelling of this state may not be particularly meaningful in view of the expected large contribution of SOC to this system.

7-2 Luminescence kinetics

The luminescence lifetime of $[Pt(QO)_2]$ has been recorded in a number of solvents, both at ambient temperatures and 77 K, the results being given in Table 7-2. A definite oxygen quenching effect was apparent for these systems on both the lifetime and emission spectrum (see Table 7-2) and all measurements were made in deaerated solutions. No dependence of the lifetime on emission wavelength was found with 90% of the points giving a lifetime of

Table 7-2 Bis(8-hydroxyquinolinato)platinum(II): luminescence characteristics

Solvent	Emission maxima (nm)	τ(μs)* (air-equilibrated solutions) 296 K	τ(μs)* (argon-flushed solutions)	τ(μs)* (77 K)
DMF	659,717	0.15**	3.1 ± 0.1 (296.0 K)	12.0 ± 0.8
DMSO	663,721	0.371	2.9 ± 0.3 (296.0 K)	13.7 ± 0.2
CH_3CN	659,716	0.16	3.5 ± 0.2 (296.0 K)	11.8 ± 0.1
MeOH	658,715	0.086	3.72† (296.0 K)	13.0 ± 0.1†
EtOH	653,717	0.11 ± 0.02	5.0 ± 0.1 (296.1 K)	13.5 ± 0.3
$CHCl_3$	654,714	0.17 ± 0.03	4.15 ± 0.09 (296.4 K)	17.7 ± 0.5
C_5H_5N	658,719	0.150 ± 0.004	4.30 ± 0.03 (296.6 K)	11.9 ± 0.8
$(CH_3)_2CO$	656,714	0.084 ± 0.004	2.21 ± 0.05 (295.6 K)	12.9 ± 0.1
C.A. film	632,657,716	-	8.05 (296.0 K)	18.0
CD_3OD	-	-	4.3 ± 0.1 (296.1 K)	17.4 ± 0.8

* Lifetimes recorded at λ(emission) with greatest intensity

** A similar quenching effect was observed in the intensity of the emission spectrum, e.g. $\frac{\phi \text{ argon}}{\phi \text{ air}} = 13.0$, cf. $\frac{\tau \text{ argon}}{\tau \text{ air}} = 17.3$

† Isotope effect At 296 K, $\frac{\tau CD_3OD}{\tau CH_3OH} = \frac{4.3}{3.7} = 1.16$; at 77 K $\frac{\tau CD_3OD}{\tau CH_3OH} = \frac{17.4}{13.0} = 1.34$

(3.1 ± 0.1) μs for a dimethylformamide solution of the complex at 296.7 K. Table 7-2 shows that the emission lifetime of $Pt(QO)_2$ is not particularly sensitive to solvent with the exception of cellulose acetate film, which would be expected from the enhanced rigidity of this medium. An isotope effect of 1.16 at 296 K and 1.34 at 77 K for $\tau_{CD_3OD}/\tau_{CH_3OH}$ has been noted in Table 7-2, which is similar to that found for both ruthenium(II) (see Chapters 5 and 6), and implies a small component of CTTS character in the luminescence transition. The persistence of this effect at 77 K implies that the solvent participation is not diffusional,but intimate contact of the solvent with the complex is suggested.

The lifetime of the complex also appears to be relatively insensitive to temperature with only a two-to-four-fold increase in τ being shown for a reduction of the temperature by over 200 K from ∿ 296 K to 77 K (see Table 7-2). This can be compared with a ten-to-twenty-fold increase for the ruthenium(II) and osmium(II) systems investigated.

7-3 Temperature dependence studies of the luminescence

The temperature dependence of the luminescence has only been investigated for three contrasting media in view of the behaviour described in the preceding section. The temperature profile of the relative luminescence yield has been determined in deaerated dimethylformamide over the range 273 to 333 K, while cellulose acetate film and methanol afforded lifetime studies over the range of 295 to 77 K.

The temperature profile of the relative luminescence yield, shown in Figure 34, indicates a simple Arrhenius behaviour with an activation energy of (7.5 ± 0.2) kJ mol^{-1}. The temperature

Figure 34

Temperature dependence of (relative) luminescence quantum yield of $[Pt(QO)_2]$ in DMF solution.

2·1
2·0
1·9
$\log_{10}\phi_{lum(rel)}$
3·0
3·2
3·4
3·6
$10^3 K/T$

Figure 35

Temperature profile of the luminescence of $\left[Pt(QO)_2\right]$ in (a) methanol and (b) CA film.

Full line-computer fit to equation 7-1.

of

film.

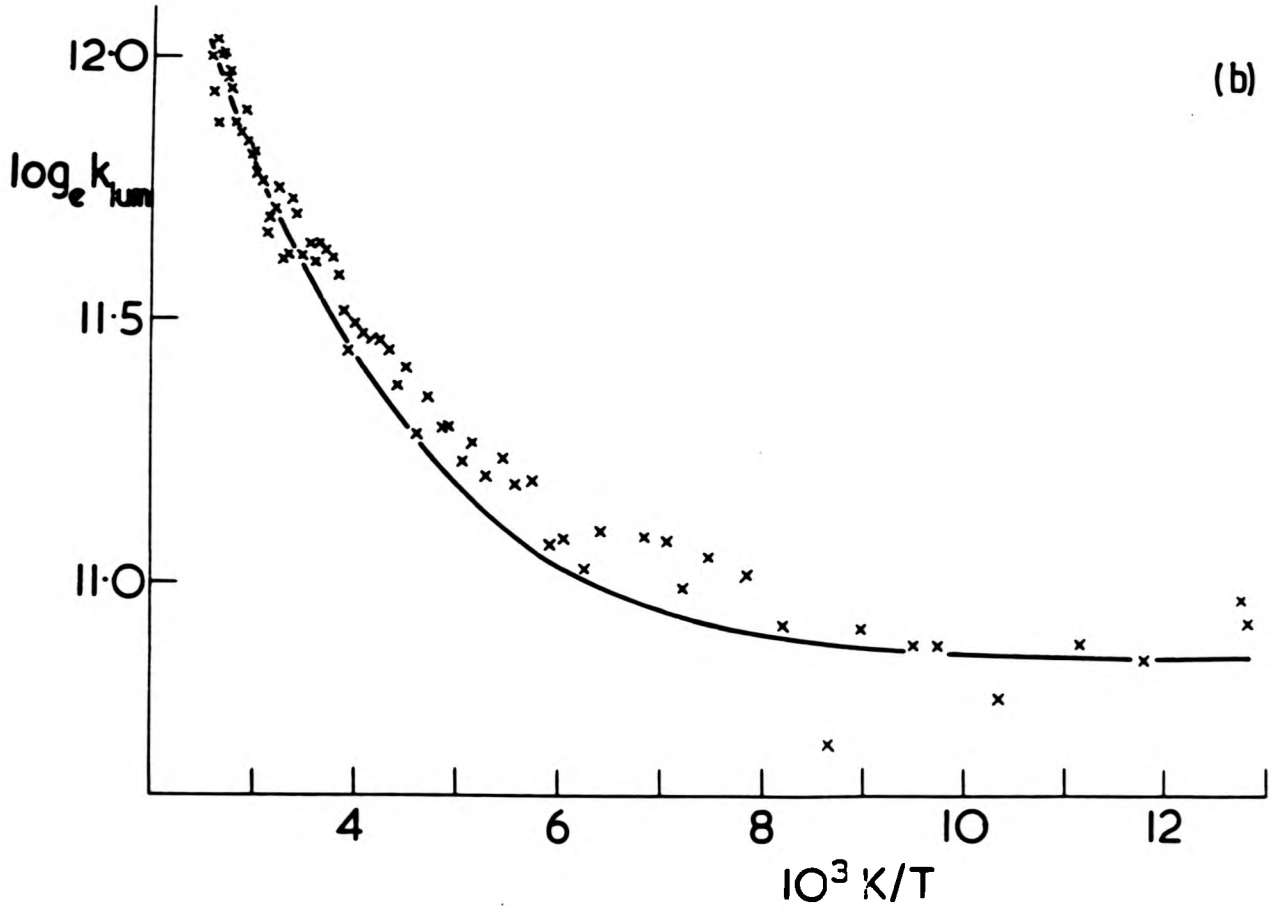
12·0
11·5
11·0
log$_e$ k$_{un}$
(b)
4
6
8
10
12
10^3 K/T

dependence of the luminescence lifetime over a wider temperature range showed a more complicated behaviour, as depicted in Figure 35, with the data being fitted to the expression:-

$$k_{lum} = A \exp(-E_A/RT) + B \qquad (7\text{-}1)$$

which is identical to that used in the study of chromium(III) luminescence (Chapter 4), with B representing the sum of the temperature-independent radiative and non-radiative rate constants, while A is the limiting rate of the temperature-dependent pathway. E_A is the activation energy of this route, and R is the gas constant. The fitted values of A, E_A and B are given below in Table 7-3 along with the fluorimetry result for comparison.

Table 7-3 Bis(8-hydroxyquinolinato)platinum(II): activation parameters for luminescence deactivation based on equation: $k_{lum} = B + A(\exp(-E_A/RT)$

Solvent	$A(s^{-1})$	E_A(kJ mol^{-1})	$B(s^{-1})$
DMF*	-	(7.5 ± 0.2)	-
C.A. film	(6.9 ± 1.4) x 10^5	(5.9 ± 0.6)	(5.21 ± 0.6) x 10^4
MeOH†	(4.2 ± 3.9) x 10^7	(14.2 ± 2.1)	(1.53 ± 0.03) x 10^5

* Fluorimetry data between 273 and 333 K

† Temperature run showed a phase transition at $\frac{1000}{T} = 5.5$. Computer fit is to data at T > 182 K

Attempts to fit the lifetime data to a two-exponential expression such as that used for both ruthenium(II) and osmium(II) (equation (5-1)) resulted merely in the second exponential being regressed to zero, indicating equation (7-1) to provide the better description of the temperature profile. The plot for $[Pt(QO)_2]$ in methanol shows a discontinuity at 182 K which is attributed to a phase transition caused by the glassing of the solvent medium, and a value of B of (7.3 ± 0.8) x 10^4 s^{-1} is apparent for T < 140 K

which is in reasonable agreement with that obtained in cellulose acetate film. The presence of this phase transition illustrates the sensitivity of the temperature-independent non-radiative pathway to environment.

The temperature profile of the relative luminescence yield of $[Pt(QO)_2]$ in DMF (Figure 34) is similar to that given by the lifetime studies in the relevant temperature region (273 to 333 K) and suggests a direct relationship between the luminescence yield and lifetime can safely be assumed with no unusual behaviour such as that given by osmium(II) complexes being apparent (Chapter 6).

The fitted values of E_A (Table 7-3) show that, as in the case of osmium(II) and ruthenium(II), the value for cellulose acetate film is unexpectedly low and can be compared with the chromium(III) systems (Chapter 4), for which an unusually high value of E_A was given by the polymeric medium. This implies that the thermally-activated route corresponds to deactivation through a higher level whose position is solvent sensitive, rather than a thermally activated non-radiative process of the emitting state involving an M-L vibrational deactivation mode as suggested for chromium(III). However, this pathway accounts for only 47% of the dissipated energy in methanol solution, and 55% in cellulose acetate film at 298 K, which suggests that the temperature-independent non-radiative pathway is equally as important at ambient temperatures.

7-4 Excited state absorption spectrum of $[Pt(QO)_2]$

Flash photolysis of deaerated solutions of $[Pt(QO)_2]$ in DMSO at 298 K in the absorption mode revealed an intense transient absorption with a lifetime identical to that of the emission for all wavelengths in this solvent, as indicated by

Figure 36

ESA spectrum of $\left[Pt(QO)_2\right]$ in deaerated DMSO solution at 296 K following 20 ns laser pulse excitation (2 cm cell):

(inset) oscillogram featuring matching of decay rates of luminescence (ascending curve) and ESA (descending curve).

) solution

ation

decay rates

descending

the inset of Figure 36. This shows that the same excited state is responsible for both the emission and absorption. The ESA spectrum was determined between 400 and 950 nm, and is given in Figure 36; the apparently zero extinctions in the 450 to 500 nm region and 640 to 680 nm are due to the influence of the ground-state absorption and emission spectrum respectively in these regions. There is a clear peak at 560 nm (17,857 cm^{-1}) and a possibly structured band at 830 to 930 nm (12,048 to 10,572 cm^{-1}), although the absorptions in the latter region could not be determined very precisely as the signal-to-noise ratio was low as a result of fall-off in both photomultiplier response and the output of the analysing lamp. The intensity of these peaks indicates that they represent allowed transitions from the emitting level. Unlike the cases of the polypyridyl complexes of ruthenium(II) and osmium(II),[126] there is no obvious correlation of the ligand anion absorption spectrum with the ESA spectrum which would give conclusive evidence of an essentially ligand-centred or CTTL luminescence. The absorption spectrum of QO^- has been reported to have maxima at 349 and 403 nm [240] which, unfortunately, are not within the range over which the ESA spectrum could be studied, although there is a suggestion of a peak ca. 400 nm.

7-5 A basic model for $[Pt(QO)_2]$ luminescence in solution

The results of this work are summarised by Figure 37 which shows the specific case of $[Pt(QO)_2]$ in methanol. The ground state absorption spectrum shows two low-energy bands at 22,026 and 29,542 cm^{-1} which have been labelled as CTTL and π-π^* transitions respectively. Absorption of 347 nm light into the π-π^* band produces both an ESA and emission transient which decay with identical lifetimes, indicating a common excited state to be

Figure 37

State diagram for lower electronic levels of $[Pt(QO)_2]$ deduced from absorption, ESA and luminescence spectra and kinetic data.

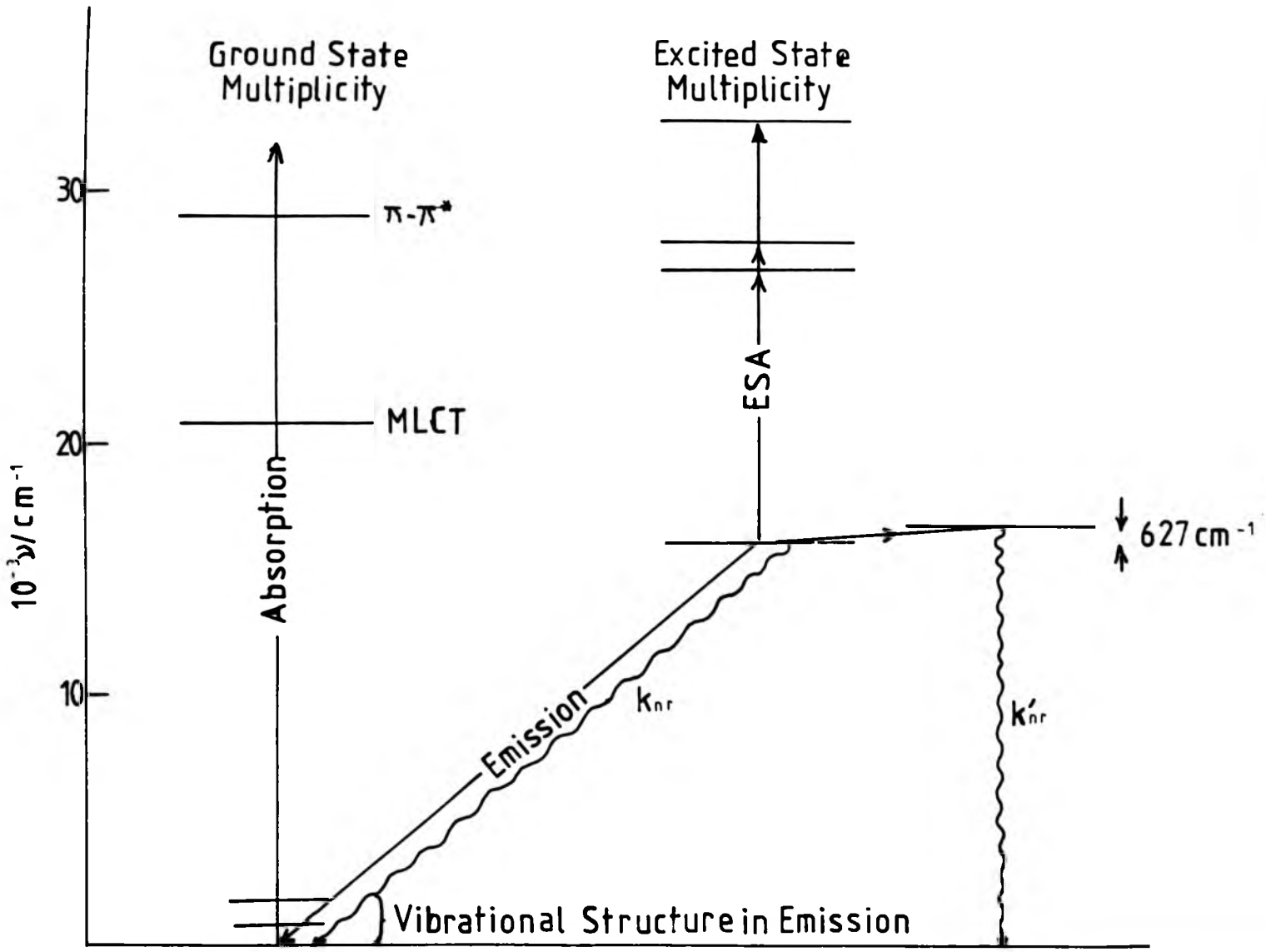
Ground State
Multiplicity
Excited State
Multiplicity
30
20
10
$10^{-3}\tilde{\nu}/cm^{-1}$
π-π*
MLCT
ESA
Absorption
627 cm⁻¹
Emission
k_{nr}
k'_{nr}
Vibrational Structure in Emission

responsible for both the luminescence and the ESA. The ESA spectrum shows two definite peaks at 17,857 and between 10,752 and 12,048 cm^{-1}, which are considered to be due to allowed transitions from the emitting state because of their high extinctions. The luminescence spectrum shows a vibronic progression of $\sim$ 1,220 cm^{-1}, suggesting the radiative route to involve an M-L vibration as a deactivation mode, while the lifetime of 3.72 μs at 296 K suggests the luminescence to involve a partially forbidden transition.

Temperature dependence studies indicate a thermally-activated non-radiative process to be operative which involves deactivation through a close-lying level. This pathway, however, only accounts for $\sim$ 50% of the dissipated energy at ambient temperature and would suggest that the low frequency factor for this route indicates that this level differs in character from the emitting state.

The emitting level has been assigned as a ^{3}CT state mainly because of the observed electron-transfer processes[240] which are concurrent with the quenching of the luminescence at ambient temperatures. Although this may be purely speculative, the results suggest that a spin-forbidden state is responsible for the luminescence, and previous reports (see Chapter 2-2) suggest that either an LF or CT state is the most likely nature of this state. In particular, it has been suggested that the ordering of these states can change with environment, and it may be that emission occurs from the CT level with non-radiative deactivation occurring through the close-lying LF state or <u>vice versa</u>.

CHAPTER 8

The Luminescence of the Uranyl Ion $[UO_2]^{2+}$, in Solution

The luminescence kinetics of the uranyl ion have been investigated in a wide variety of solvents including non-aqueous inorganic media, water-based solutions, and both photoinert and photoreactive organic media. Through studying these systems over as wide a temperature range as was allowed either by the solvent or the instrumentation, it was possible to rationalise the luminescence decay in terms of two distinct pathways which provided a basis for discussion of the observed lifetime dependences upon environment.

8-1 Results of Luminescence Studies

As mentioned in Chapter 2.3, $[UO_2]^{2+}$ displays an ESA spectrum as well as intense luminescence, and hence lifetime measurements were made either at the emission maximum (510 nm) or by monitoring the ESA transient at its peak position of 585 nm, with both transients showing identical kinetics, as expected (Chapter 2.3). All measurements were made using a 0.2 mol dm^{-3} $[UO_2]^{2+}$ concentration which afforded good absorption of the 347 nm laser pulse, and although no detectable oxygen effect on the luminescence lifetime has been found, all solutions were deoxygenated as a precautionary measure. The emission lifetime was found to be almost invariant, with emission wavelength at 77 K in conc.H_2SO_4 allowing a wide bandpass to be used when necessary.

The Arrhenius plots in those cases where only a restricted temperature range ($T > 285$ K) could be covered, showed normal Arrhenius behaviour, whereas over an extended temperature range definite curvature was apparent which resulted in a horizontal plateau region at temperatures typically below 150 K. For curvature given over a restricted temperature range, the behaviour could be equally well explained by either a single-

Figure 38

Temperature profiles of the luminescence lifetime of $[UO_2]^{2+}$ in water-based solutions. Straight line - linear least squares analysis; full curve - computer fit to equation 8-1 (individual parameters are given in Table 8-1).

(a) H_2O (X) and D_2O (·)

(b) 0.2 mol dm^{-3} $HClO_4/H_2O$ (X) and 0.2 mol dm^{-3} $HClO_4/D_2O$ (·)

(c) 35% $HClO_4$

(d) 70% $HClO_4$

(e) 0.22 mol dm^{-3} $HClO_4$

(a) + 2.0 mol dm^{-3} $NaClO_4$ (top curve, X)

(b) + 2.0 mol dm^{-3} NaF (bottom curve, +)

(f) 6 mol dm^{-3} $LiCl/H_2O$ (X); 9 mol dm^{-3} $LiCl/H_2O$ (O) and 9 mol dm^{-3} $LiCl/D_2O$ (·)

2·0 4·0 6·0 8·0 $10^3 K/T$ 10·0 12·0

lifetime

aight line -

ve - computer

rs are given

mol dm^{-3}

ve, X)

ve, +)

^{3} $LiCl/H_2O$ (O)

(a)

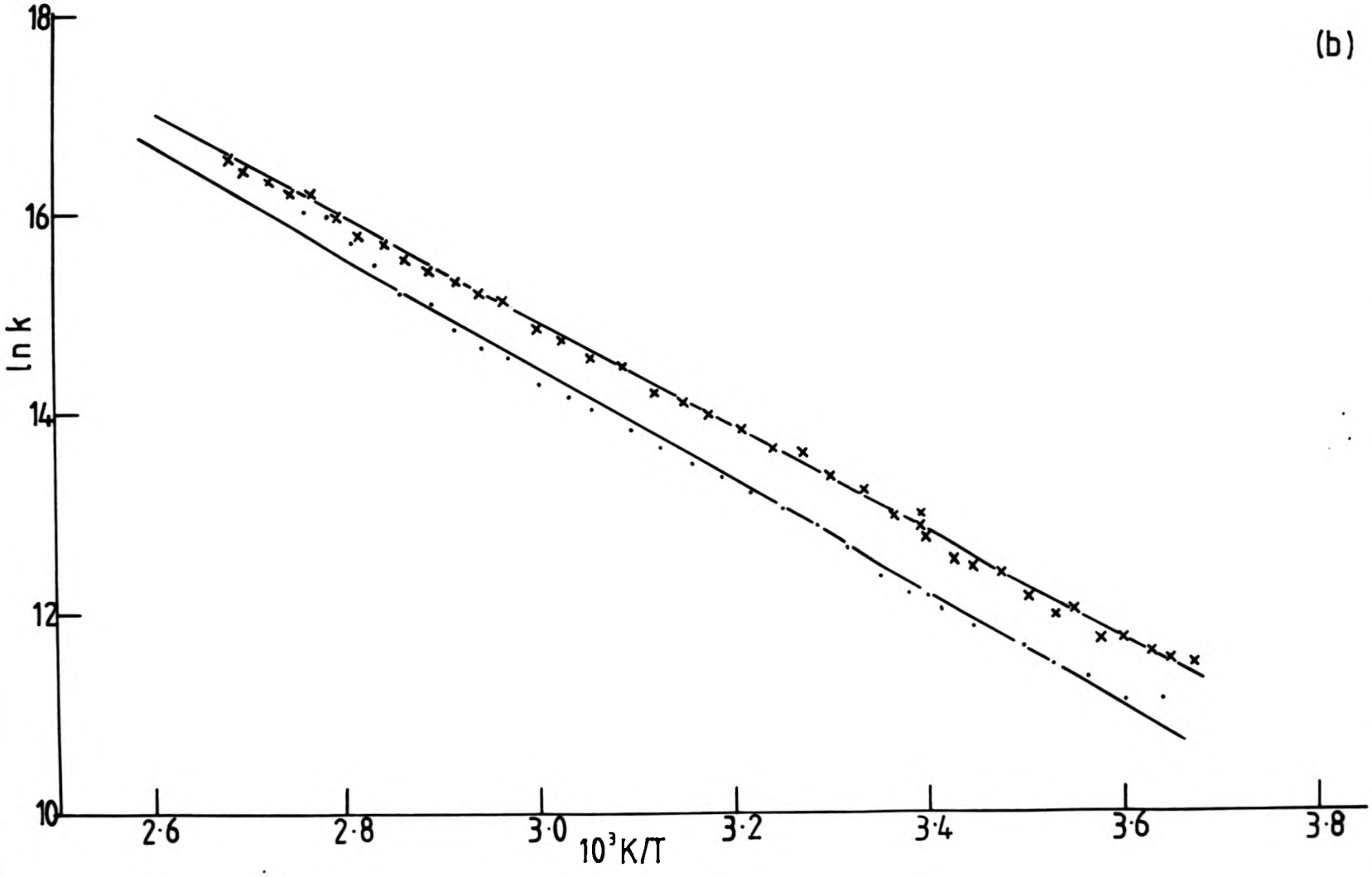
(b)
18
16
14
12
10
ln k
2·6
2·8
3·0
3·2
3·4
3·6
3·8
10³K/T

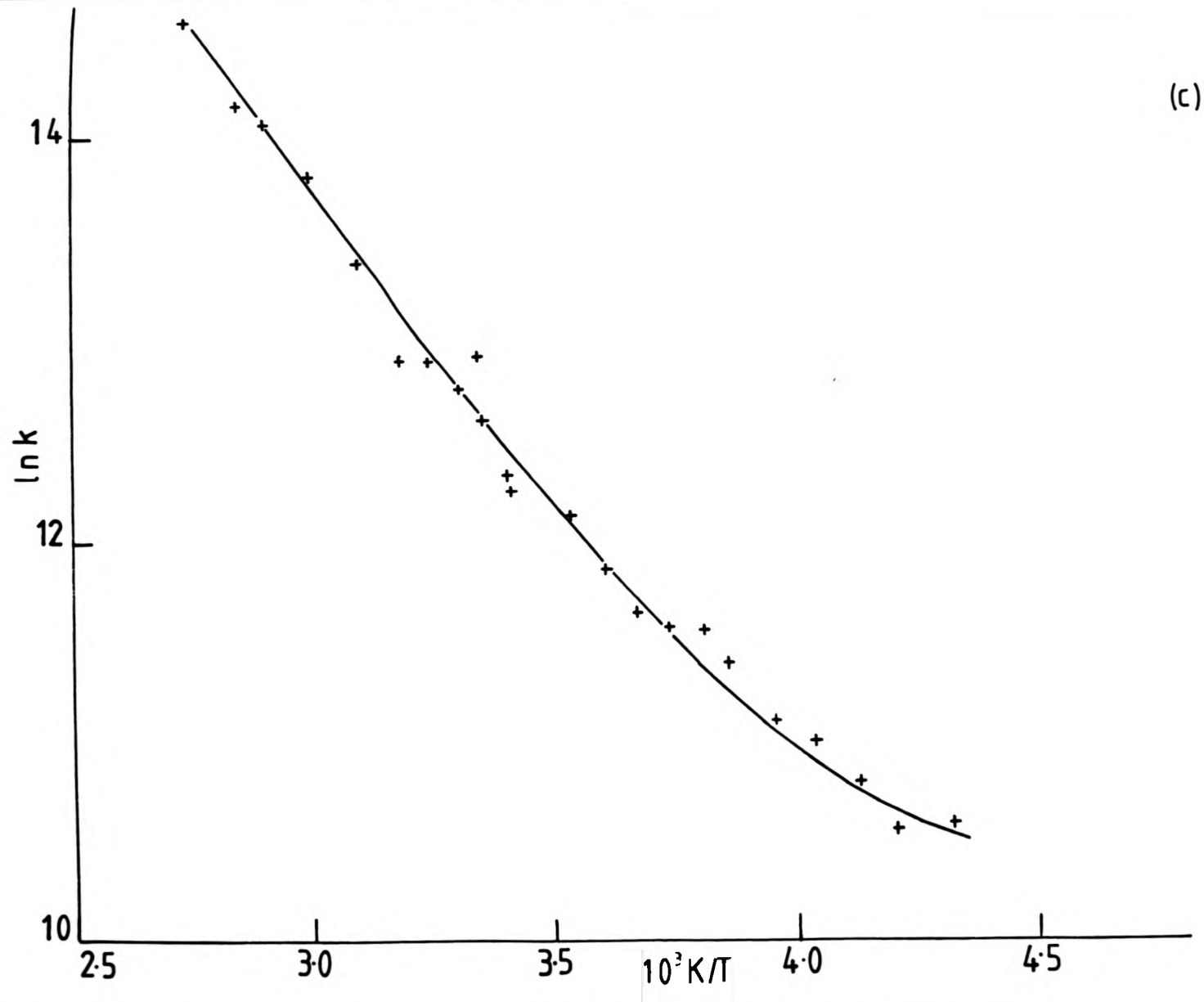
(c)
14
12
10
ln k
2·5
3·0
3·5
4·0
4·5
10³ K/T

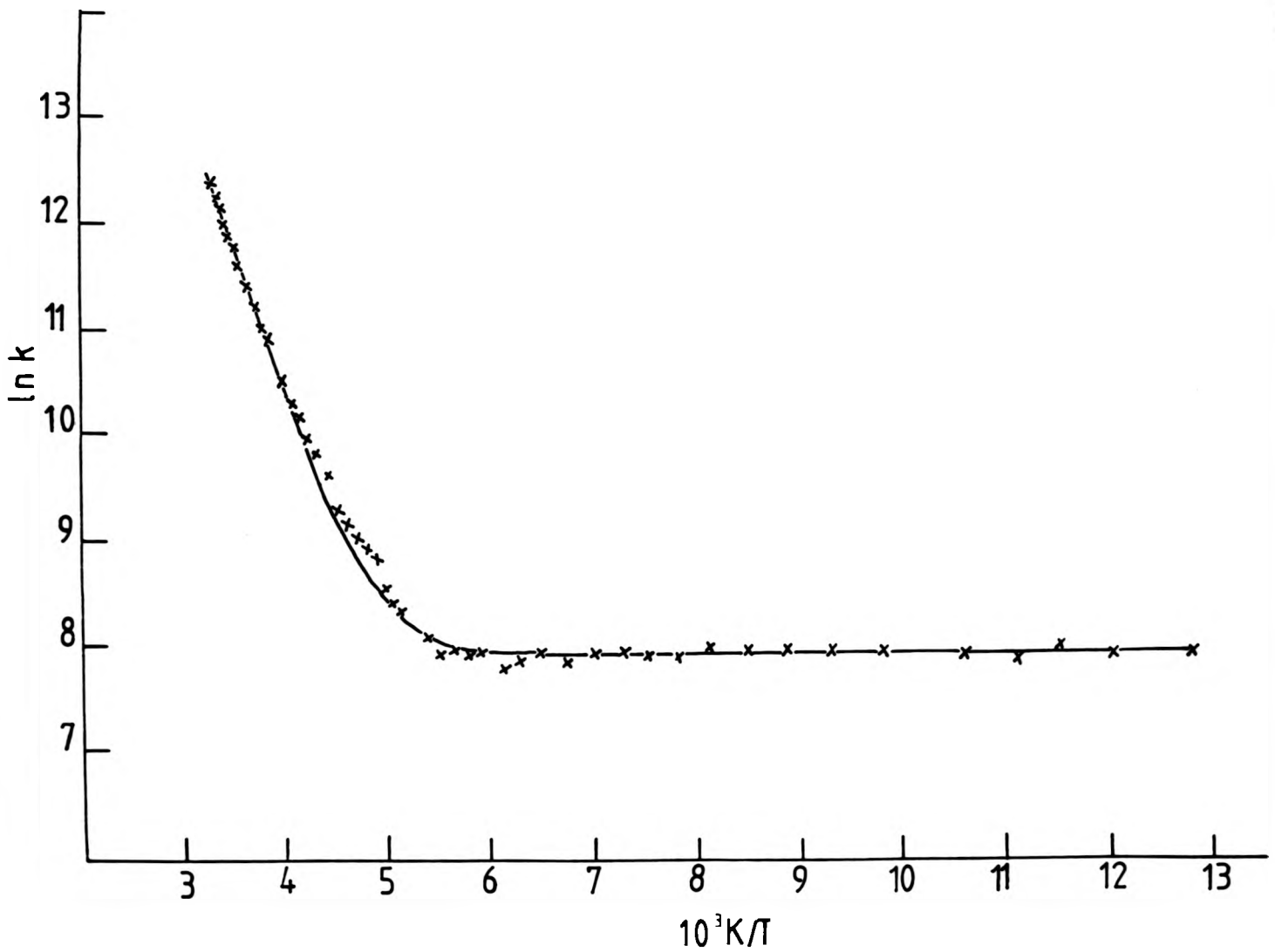
(d)
13
12
11
10
9
8
7
ln k
3
4
5
6
7
8
9
10
11
12
13
10³K/T

(e)

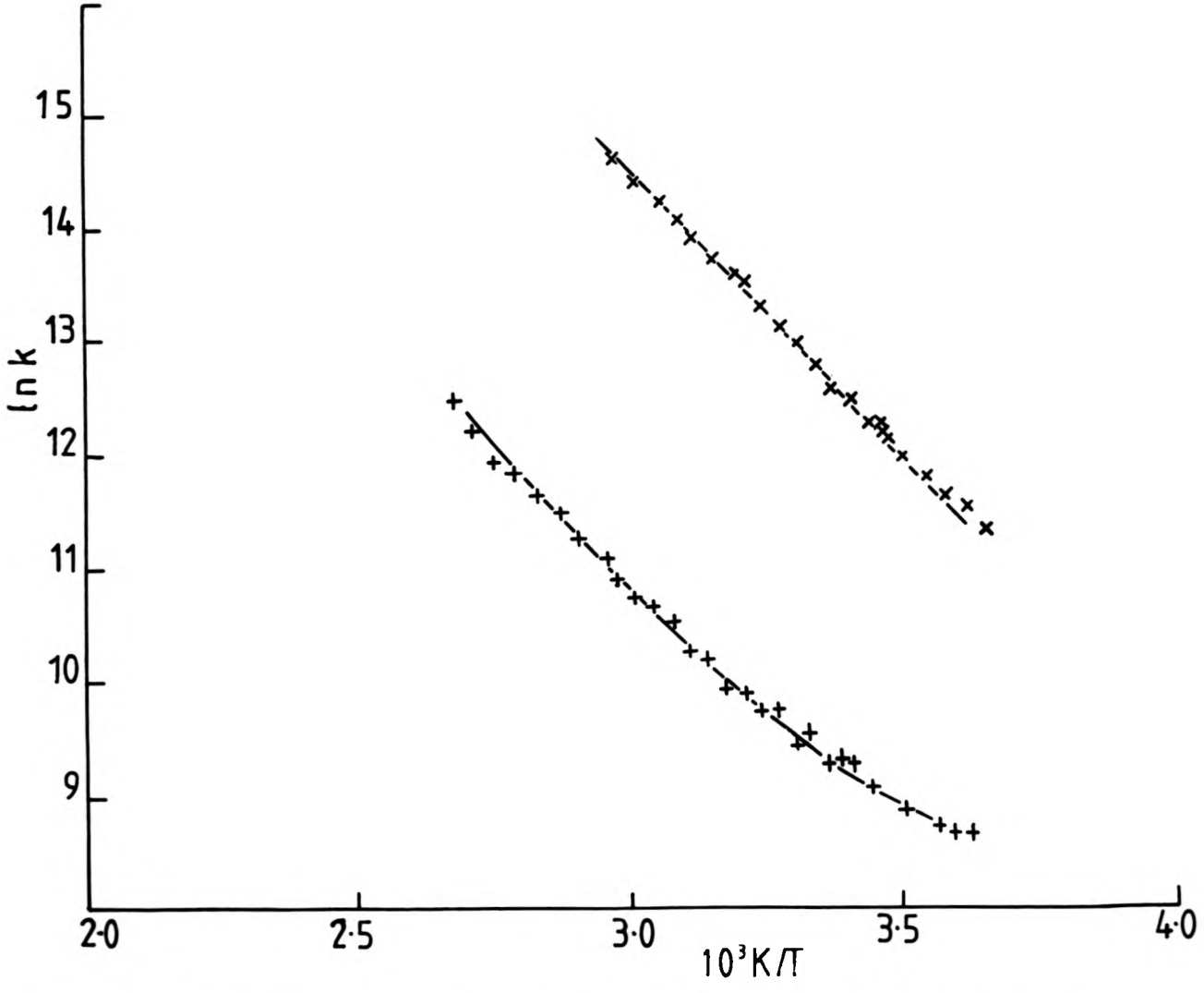

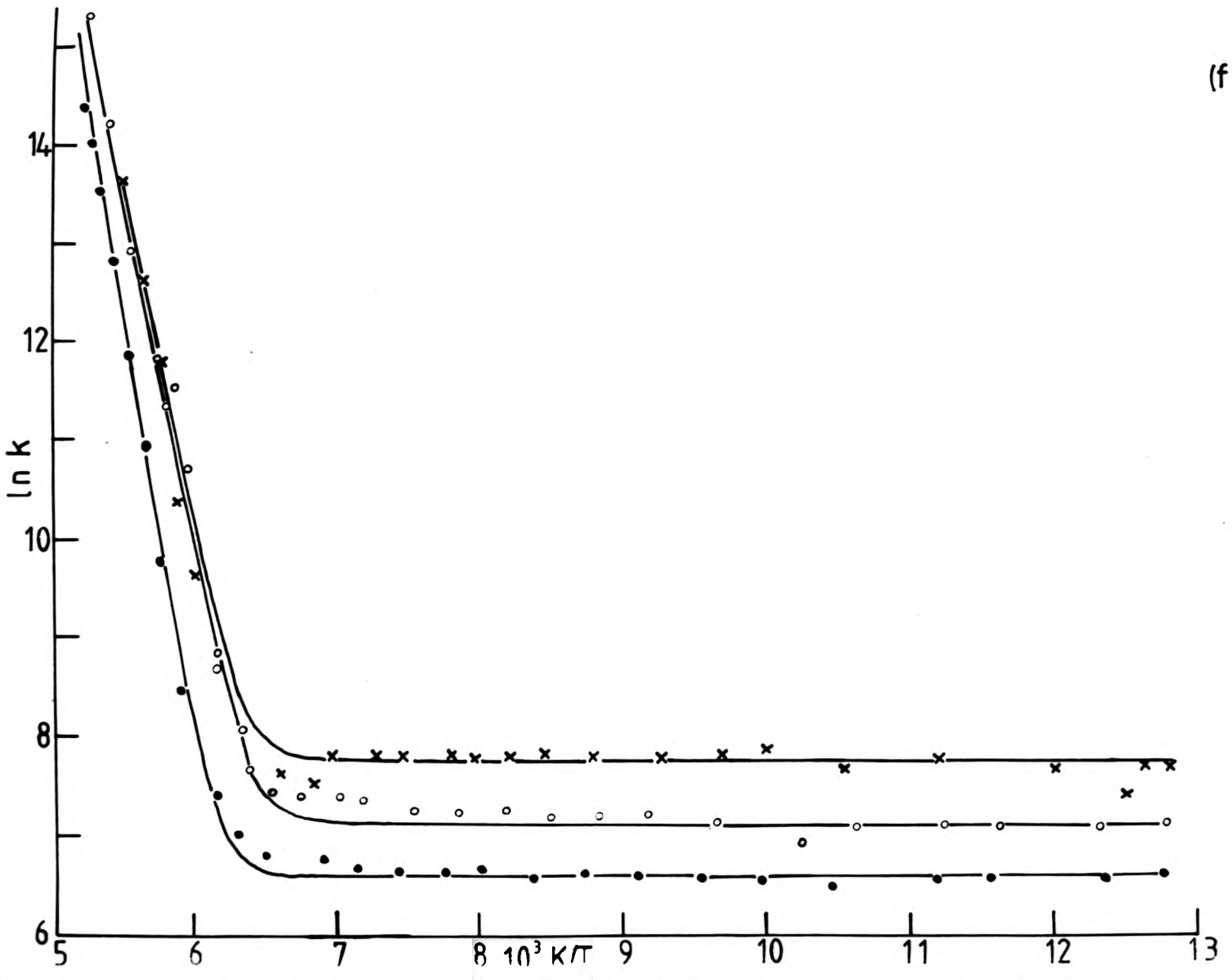
(f)
14
12
10
8
6
ln k
5
6
7
8
9
10
11
12
13
10^3 K/T

exponential expression such as equation (7-1) or a double-exponential form such as equation (5-1). However, over a complete temperature range (77 to 370 K), the plots could be fitted unambiguously to an expression identical to that given by equation (7-1), i.e.

$$k = A \exp(-E_A/RT) + B \qquad (8\text{-}1)$$

with the parameters having the same general meaning, indicating this expression to give the correct interpretation of the observed behaviour. The simple Arrhenius behaviour given by those systems which allowed investigation over only an elevated temperature range (T > 273 K) can, therefore, be assumed to represent the high temperature limit of this expression for which the contribution from the B term is negligible.

The Arrhenius plots and the fitted parameters will be discussed in terms of the general types of systems studied since, as indicated in Chapter 2.3, the uranyl ion can assume a number of different roles, depending upon the nature of the environment.

8-2 Results and Discussion for Water-based Solutions

The fitted activation parameters for these systems are summarised in Table 8-1 with the Arrhenius plots being given in Figure 38 , and the Arrhenius data shown more accurately in tabulated form in Appendix II. From Table 8-1, it is apparent that the energetics of the uranyl ion are susceptible to both added acid and anions. In particular, the presence of a high concentration of lithium chloride imparts a marked reduction in the lifetime at 298 K. In the case of added acid, only the systems involving 35% $HClO_4$ and 70% $HClO_4$ showed definite curvature, with the latter system being the only one to enable a complete temperature study,which may explain the

Table 8-1 Rate and activation parameters* for the excited uranyl ion (0.2 mol dm^{-3}) in water-based solutions

Medium	$10^{-4}\ k_{298}{}^{\dagger}/s^{-1}$	A/s^{-1}	E_A/kJ mol^{-1}	B/s^{-1}	Data source
H_2O (>273K)	52.6	$(7.2 \pm 3.6) \times 10^{9}$	23.6 ± 0.8		This work
D_2O (>273K)	29.7	$(3.6 \pm 1.8) \times 10^{9}$	23.3 ± 0.8		This work
0.01 mol dm^{-3} $HClO_4$			40.2		ref. 191[e]
0.1 mol dm^{-3} $HClO_4$			44.4		ref. 191[e]
0.2 mol dm^{-3} $HClO_4$	45.2	$(2.17 \pm 0.37) \times 10^{13}$	43.8 ± 0.5		This work
0.2 mol dm^{-3} $HClO_4/D_2O$	24.6	$(5.0 \pm 1.3) \times 10^{13}$	47.4 ± 0.8		This work
0.23 mol dm^{-3} $HClO_4$	53.8	9.0×10^{12}	41.2 ± 0.7		ref. 183[d]
1.0 mol dm^{-3} $HClO_4$			51.9		ref. 191[e]
5.85 mol dm^{-3} (35%) $HClO_4$	30.0	$(2.29 \pm 0.07) \times 10^{10}$	28.1 ± 0.09	$(2.74 \pm 0.14) \times 10^{4}$	This work[a]
11.7 mol dm^{-3} (70%) $HClO_4$	20.7	$(2.99 \pm 0.59) \times 10^{9}$	23.9 ± 0.5	$(2.80 \pm 0.03) \times 10^{3}$	This work
0.22 mol dm^{-3} $HClO_4$ + 2.0 mol dm^{-3} $NaClO_4$	55.0	$(9.4 \pm 2.9) \times 10^{12}$	42.5 ± 0.8		This work[b]
0.22 mol dm^{-3} $HClO_4$ + 1.9 mol dm^{-3} NaF	1.15	$(7.4 \pm 2.4) \times 10^{11}$	46.2 ± 1.0	[c]	This work[b]
6 mol dm^{-3} LiCl	9.24×10^{8}	$(9.8 \pm 20.0) \times 10^{23}$	62.9 ± 3.1	$(2.37 \pm 0.52) \times 10^{3}$	This work
9 mol dm^{-3} LiCl	4.35×10^{8}	$(1.99 \pm 0.49) \times 10^{23}$	60.82 ± 0.39	$(1.23 \pm 0.04) \times 10^{3}$	This work
9 mol dm^{-3} $LiCl/D_2O$	4.53×10^{9}	$(4.6 \pm 10) \times 10^{26}$	74.2 ± 3.6	$(7.3 \pm 8.7) \times 10^{2}$	This work

† values calculated from fitted parameters

* errors refer to one standard deviation

[a] these data also fitted equally well to a double-exponential expression $k = (2.36 \pm 0.16) \times 10^{10} \exp(-28200 \pm 220)/RT + (4.50 \pm 4.56) \times 10^{4} \exp(-1000 \pm 2030)/RT$

[b] $[UO_2]^{2+}$ concentration of 10^{-2} mol dm^{-3}

[c] B temperature-dependent, viz. $(4 \pm 10) \times 10^{4} \exp(-5000 \pm 5000)/RT$

[d] $[UO_2]^{2+}$ concentration of 0.04 mol dm^{-3}

[e] $[UO_2]^{2+}$ concentration of 0.01 mol dm^{-3}

difference in the B terms as due to the unavoidably incomplete analysis in the case of 35% $HClO_4$.

The activation energy of 43.8 kJ mol^{-1} obtained for a 0.2 mol dm^{-3} $HClO_4$ solution of 0.2 mol dm^{-3} $[UO_2]^{2+}$ from this work compares quite well with those reported by other workers for similar systems (see Table 8-1). Similarly the lifetime at 298 K for this system of 2.21 μs can be compared with reported values of 1.86 μs[183] and 1.6 μs[191] for solutions of 0.04 mol dm^{-3} $[UO_2]^{2+}$ in 0.23 mol dm^{-3} $HClO_4$ and 0.01 mol dm^{-3} $[UO_2]^{2+}$ in 0.1 mol dm^{-3} $HClO_4$ respectively at 298 K, although direct comparison is hindered by the reported lifetime dependence on the uranyl concentration.[183] However, the good agreement of the reported and observed activation energies indicates this parameter to be almost insensitive to uranyl ion concentration.

The activation energy for the pure aqueous medium is considerably lower than that found even in mildly acidic media. k_{298}, however, is not significantly different for all but the strongly acidic media, indicating A and E_A to be affected in a parallel manner in all but the above mentioned cases. It should be noted that the transient decay in both H_2O and D_2O showed slight deviation from good first-order kinetics at T > 258 K through the presence of an initially fast component in the overall decay. This was assumed to be due to the presence of more than one complexed form of $[UO_2]^{2+}$, and was ignored in favour of the predominant slower decay, to which the activation data given in this work refers.

The unusually low values of E_A for 35% and 70% $HClO_4$ would suggest that these systems should be considered as fundamentally different from the aqueous system, whereas the case of dilute acidic media can be considered as slightly modified aqueous media.

This view is supported by considering the complete temperature profiles of the 70% $HClO_4$ and H_2O systems (Figures 38d and 38a). The former shows a continuous curve which can be fitted to equation (8-1) with no apparent effect at the glassing point of the solution. In contrast, pure water shows more complicated behaviour with several regions being defined. While the expected behaviour above the freezing point is apparent, there is a marked increase in lifetime at the freezing point of the solution (4.6 μs to ∿ 550 μs) which then remains unchanged on lowering the temperature until ca. 220 K, when τ shortens as the temperature is lowered further until ∿ 200 K when τ goes through a slight maximum before levelling out at ∿ 170 K to give a lifetime of ∿ 220 μs below this temperature. A similar profile is also given for D_2O which indicates the behaviour to be genuine, although the exact positions of these regions were found to be dependent upon whether the glassing point was approached from above or below this temperature. This profile probably reflects the changes in the internal structuring of the water molecules on going through the phase transition rather than any inherent deactivation pathway of the uranyl ion, as no such behaviour has been found in any other medium studied, although this behaviour is reminiscent of the report concerning a series of H_2SO_4 solutions of differing concentrations in which the uranyl thermoluminescence was considered to follow the structural changes in the medium on increasing the temperature from 77 K[201] (see Chapter 2.3). While no detailed explanation of this behaviour can be offered it would seem that environmental changes influence both the thermally-activated and temperature-independent deactivation modes. The initial act of freezing, which induces the longest lifetime, suggests

that there is a certain amount of disorder in the system in this region which hinders efficient participation of the solvent in the deactivation modes. As the temperature is lowered further, the system becomes more ordered until at ∿ 200 K, the profile returns to the expected form which is represented by the slight maximum, indicating the thermally activated route to continue to make a slight contribution at this temperature. Further lowering of the temperature results in the expected plateau region by the complete 'freezing-out' of the thermally-activated route.

That the lengthening of the lifetime at 298 K is due to the presence of H^+ rather than the counter-ion is illustrated by the addition of 2.0 mol dm^{-3} $NaClO_4$ to a solution of $[UO_2]^{2+}$ in 0.22 mol dm^{-3} $HClO_4$ which shows only marginal changes in both lifetime and activation parameters from the salt-free solution (see Table 8-1). However, anions such as Cl^- and F^- have a pronounced effect on the lifetime of the uranyl ion. The presence of F^- results in a large reduction of the pre-exponential factor for this system,coupled with distinct curvature in the Arrhenius plot (Figure 38e),and the transient decays were found to be composed of a minor, fast initial component, followed by a major slower decay which was exponential over several half-lives and which was used to obtain the activation parameters given in this work. At the concentration of F^- used, the uranyl ion is present as $[UO_2F_3]^-$ and $[UO_2F_4]^{2-}$ which have similar lifetimes of ∿ 150 μs at 298 K:[246] this can be compared with our value of 87 μs at 298 K obtained in the presence of 0.22 mol dm^{-3} $HClO_4$ which presumably deactivates the excited complexes.

The choride ion is known to be an efficient quencher of the uranyl luminescence with a quenching constant of 1.7 x 10^9

$dm^3\ mol^{-1}\ s^{-1}$ at 298 K[211] and the exceedingly short lifetime extrapolated from Figure 38f at this temperature of 0.23 ps for a 9 mol dm^{-3} LiCl medium is therefore not surprising. The absence of a phase effect for this medium, however, allowed further insight into the effect of temperature on the kinetic isotope effect which will be discussed later. The unusually high activation energies of > 60 kJ mol^{-1} probably reflect the combined temperature activation of the electron transfer from Cl^- to $[UO_2]^{2+*}$ and the diffusion coefficients of the reactants in the viscous medium. A curious result, however, is that the lifetime in 6 mol dm^{-3} LiCl is shorter than in a 9 mol dm^{-3} solution of the salt, which may reflect the more vitreous character of the stronger solution. The convergence of all three Arrhenius plots for this medium (Figure 38f) also indicates a common mechanism of quenching of $[UO_2]^{2+*}$ by Cl^- to be operative at ambient temperatures for all three solutions.

8-3 Mechanistic Aspects of the Deactivation of $[UO_2]^{2+*}$ in an Aqueous Medium

$[UO_2]^{2+}$ is photochemically inert as regards its own photodestruction in an aqueous medium, and therefore three possible mechanisms have been proposed for its deactivation (see Chapter 2.3).

(i) Fast, reversible hydrogen abstraction[170]

$$[UO_2]^{2+*} + H_2O \rightleftharpoons [UO_2H]^{2+} + \dot{O}H$$

(ii) Fast, reversible electron-transfer[191]

$$[UO_2]^{2+*} + H_2O \rightleftharpoons [UO_2]^{+} + H_2O^{\cdot}$$

(iii) For low temperatures (77 K), a physical quenching mechanism[170,190]

$$[UO_2]^{2+*} + H_2O \longrightarrow [UO_2]^{2+} + H_2O^{*}$$

The elaborate scheme involving exciplex formation devised by Marcantonatos,[198] as discussed in Chapter 2.3, seems improbable

in the light of no direct evidence for an emitting exciplex. Further, the key step in this scheme is:-

$$[UO_2]^{2+*} + H_2O \rightleftharpoons [UO_2H]^{2+*} + OH\cdot$$

While this involves a hydrogen atom abstraction mechanism cf. (i) above, it considers the process to leave the U(V) species in an electronically excited state. The redox potential of the excited state of $[UO_2]^{2+}$ is, however, $\sim$ 2.7 eV[191] and the energy required for hydrogen abstraction is expected to be ca. 2.82 - 0.059 pH (the redox potential for the reaction $\cdot OH + H^+ + e \longrightarrow H_2O$ at 298 K[191]), which, although showing the overall process to be energetically feasible, would indicate that the excited uranyl ion is deactivated by this process.

The presence of a small, but real, kinetic isotope effect for the aqueous medium (Figure 38a) detracts from the possibility of a fast, reversible electron-transfer mechanism for which the presence of an isotope effect is not readily explicable. This mechanism, proposed by Moriyasu et al.,[191] who ruled out hydrogen abstraction on the grounds of the known photostability of the solution, also requires a fast back-reaction to explain the absence of any detectable or scavengeable intermediates ($H_2O^{+\cdot}$ or $\cdot OH$) which is also a necessary requirement of the hydrogen-abstraction mechanism.

The temperature profiles for the uranyl ion in H_2O and D_2O suggest that,while a temperature-independent non-radiative pathway is dominant at temperatures below 170 K, the behaviour of the excited uranyl ion at ambient temperatures is dominated by a thermally-activated non-radiative pathway. The rate constant at 77 K for H_2O (k_{H_2O}) and D_2O (k_{D_2O}) of 4.5 x 10^3 s^{-1} and 1.28 x 10^3 s^{-1} respectively yield an isotope effect of 3.5 which agrees only moderately well with that of Joshi et al[190], who find k_{H_2O} = 4.0

x 10^3 s^{-1} and k_{D_2O} = 6.67 x 10^2 s^{-1} yielding an isotope effect of 6.0. However, a sample of D_2O from a different source gave k_{D_2O} = 6.32 x 10^2 s^{-1} at 77 K, but revealed a shorter lifetime at 298 K than the sample of D_2O actually employed and was therefore rejected. The explanation of this isotope effect as due to a physical quenching mechanism involving deactivation through the vibrational modes of the co-ordinated solvent molecules proposed by Joshi *et al*[190] seems reasonable, although the extension of this explanation to ambient temperatures seems less likely. The reduced isotope effect of 1.6 at 77 K for 9 mol dm^{-3} LiCl may well be indicative of the more vitreous nature of this medium with the lifetime at 77 K for the protonated medium being longer (813 μs) than that for H_2O (222μs), suggesting restriction of the deactivation mode. This approach would also explain the intermediate lifetime of 422 μs obtained for 6 mol dm^{-3} LiCl at 77 K.

The kinetics of the excited uranyl ion at ambient temperatures is dominated by the thermally activated non-radiative pathway, E_A. The isotope effect on this pathway is 1.77 at 298 K for H_2O and D_2O, which reflects the reduced frequency factor for D_2O (see Table 8-1) with the activation energies being approximately equal. In contrast, while the isotope effect for the uranyl ion in 0.2 mol dm^{-3} $HClO_4$ gives a similar value of 1.84, both A and E_A are affected by deuteration in this case (see Table 8-1). This result, therefore, is somewhat ambiguous since the former result would suggest a physical quenching mechanism, in which the O-H bond is not chemically involved in the initial deactivation step, whereas the latter case gives the expected behaviour for a chemical mechanism involving hydrogen abstraction. However, where such small

Figure 39

Barclay-Butler plot for the activation parameters of the uranyl ion in aqueous media. (Data taken from Table 8-1).

Slope = (0.42 ± 0.01) kJ mol^{-1}

ı parameters

(Data taken

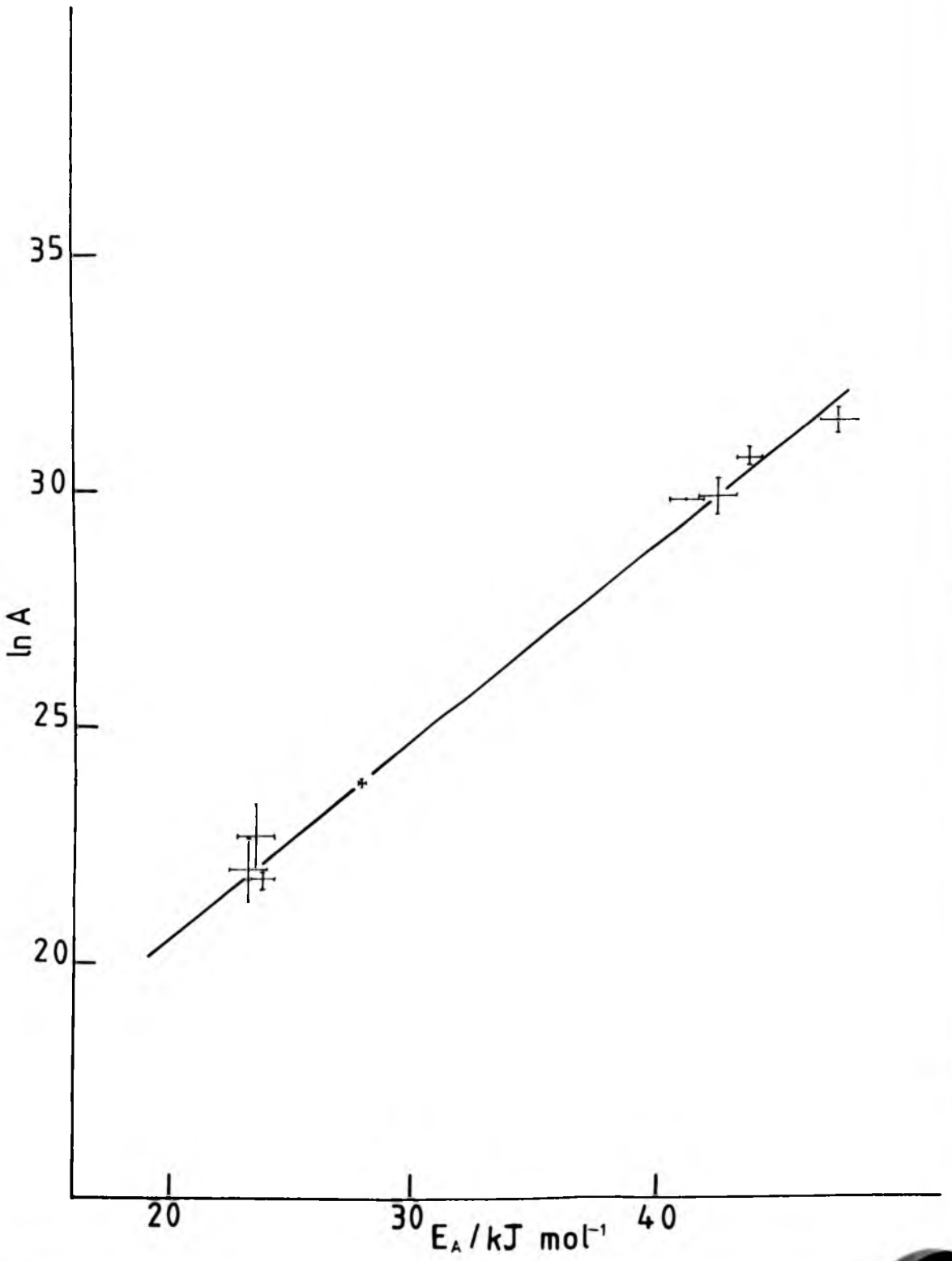

isotope effects are involved, it is difficult to apportion contribution from the A and E_A terms at all accurately.

As mentioned earlier, the presence of even a small amount of acid has a considerable effect on both A and E_A, and it may be that the deactivation mode,even in a mildly acidic medium, differs from that operating in water. This explanation, however, is unlikely as indicated by the adherence to a Barclay-Butler plot (Figure 39) for all acidic media, using the activation data given in Table 8-1 (the correlation coefficient is 0.996). Perhaps what is more significant is that the activation data for both the lithium chloride and methanol systems (see later) do not conform to this plot. While the lithium chloride result may not be surprising,in view of the expected contribution to the activation energy of the electron-transfer quenching process, that with methanol suggests a unique pathway for photoreactive organic media. This conclusion would suggest that a physical quenching mechanism is active in the aqueous case, since there is strong evidence for a hydrogen-abstraction mechanism in the alcohol case from the spin-trapping of either an alkyl radical[247] or a hydroxyalkyl radical.[193] The effect of deuteration on the activation energy for 0.2 mol dm^{-3} $HClO_4$ must, therefore, be caused by some form of complicated behaviour in the acidic medium which is not readily explained.

In order to investigate further the effect of acid, the acidity dependence of the lifetime of the uranyl ion at 295 K in both H_2O and D_2O was studied, and the results are given in Figure 40 . While the results show considerable scatter, the isotope effect at 0.2 mol dm^{-3} acid ($\sim$ 2.33) compares closely with the results at 0.1 mol dm^{-3} acid (2.29) and zero acidity (2.19) which further indicates that the water molecule plays a

Figure 40

Acidity dependence of luminescence lifetime of $[UO_2]^{2+}$ in H_2O (lower line) and D_2O (upper line). Straight lines refer to least squares analysis of data.

:ime of

)er line).

ıalysis

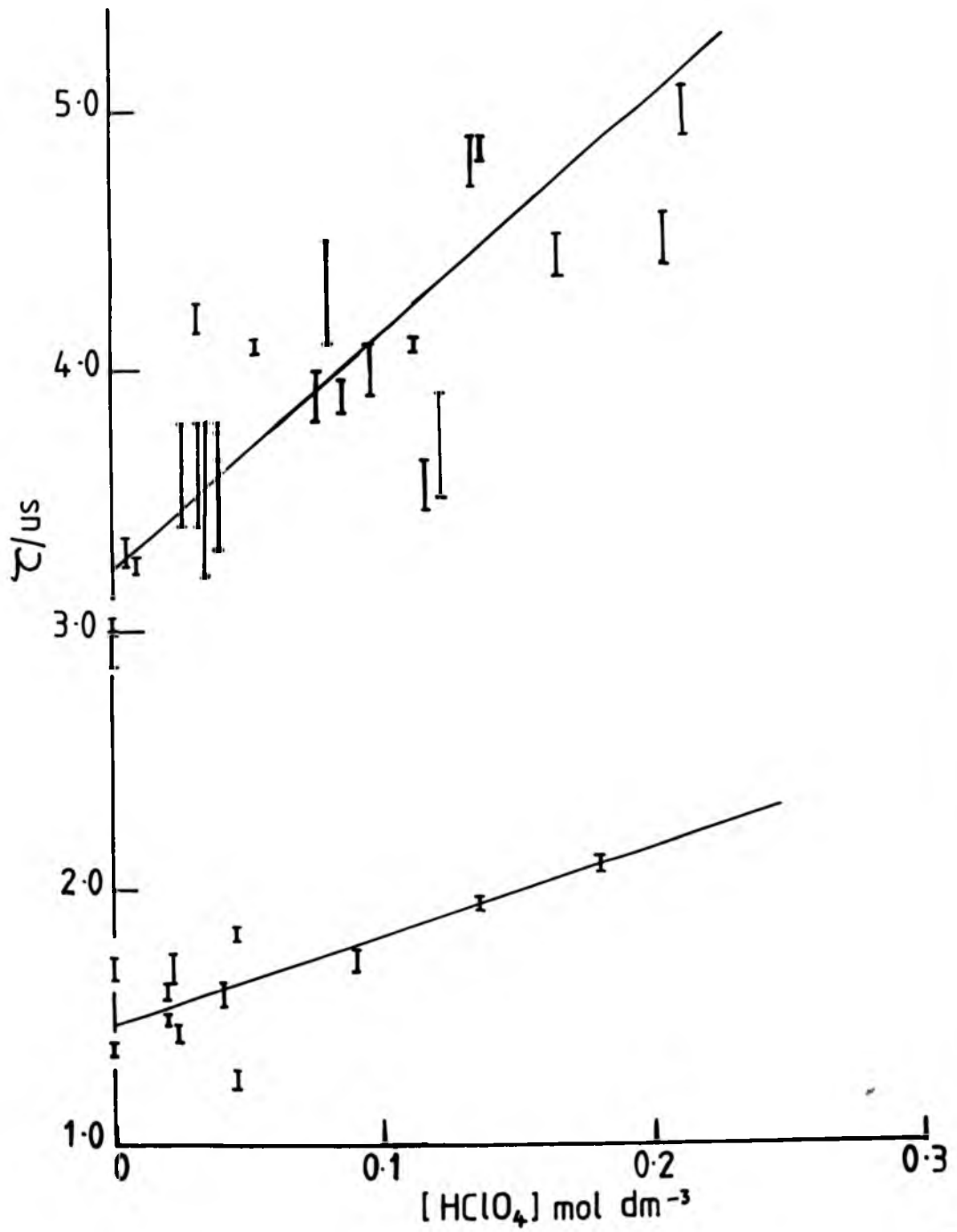

Figure 41

Acidity dependence (added $HClO_4$) of luminescence lifetime of $[UO_2]^{2+}$ in CH_3CN (with least squares analysis).

minescence

ast squares

single role in these acidic media. A further study of the acidity dependence of the lifetime in acetonitrile (Figure 41) at 295K revealed that the addition of acid shortens the lifetime in this solvent,which suggests that the 'stabilising' effect of added acid is peculiar to water.

In conclusion, therefore, it would appear that while deactivation of $[UO_2]^{2+*}$ in low-temperature glasses occurs through a physical quenching mechanism involving the vibrational modes of the co-ordinated solvent, the onset of diffusional modes in fluid solution at ambient temperature enables a dominant thermally-activated non-radiative process which is affected by both added acid and isotopic substitution of the solvent. The presence of an isotope effect suggests that the process refers either to a physical quenching or a hydrogen-abstraction mechanism, with the adherence of the activation data to a Barclay-Butler plot, suggesting a common mechanism to operate for all acidic media. Although there is no direct evidence for either mechanism, the poor fitting of the activation parameters in both LiCl and alcoholic media to Barclay-Butler plot suggest a physical mechanism to be more likely for water. However, too much importance cannot be attached to this plot since it refers to the joining of two sets of clustered points. The solvent exchange rate of co-ordinated with bulk solvent in $[UO_2]^{2+}$ solutions has been estimated as $> 1.25 \times 10^4\ s^{-1}$ [191] which would indicate a dynamic process to be more likely than the static process involved in the physical quenching mechanism at low temperatures.

The exact nature of the effect of acid on the aqueous environment of the uranyl ion is uncertain, but the results of this work indicate it to be both peculiar to water and to

Figure 42

Temperature activation plots for luminescent decay of uranyl nitrate in (a) H_2SO_4 (bottom line, X) and (b) H_3PO_4 (top curve, ·). Full curves are computer fits to equation 8-1; (individual parameters given in Table 8-2).

iescent

(bottom

. Full

3-1;

8-2).

involve H^+ rather than the counter-ion. The explanation[191] that the 'stabilising effect' of the acid is due to appreciable formation of H_3O^+ is unacceptable at such low acid concentration while the proposal involving acid-accentuated formation of an emitting exciplex[198] still requires more convincing evidence for this emitting species. However, the increase in the activation energy by added acid would suggest that the acid must depress the deactivation mode, possibly by disordering the structured aqueous environment. The lowering of the activation energy in more concentrated acidic media might, therefore, reflect a new structuring of the aqueous environment which results in less efficient deactivation of the excited uranyl ion.

8-4 Results and Discussion for Non-aqueous Inorganic Media

Unlike water, both examples of this type of system (H_2SO_4 and H_3PO_4) enabled work to be performed over a wide temperature range to give a clear indication of the complete temperature profile with no phase effects being apparent. The Arrhenius plots for these systems are given in Figure 42 and the fitted parameters in Table 8-2.

Table 8-2 Rate and fitted* activation parameters for the excited uranyl ion in a non-aqueous inorganic media

Medium	$10^{-4} k_{298}$ /s^{-1}	B/s^{-1}	A/s^{-1}	E_A/kJ mol^{-1}
H_2SO_4	7.09	$(1.10\pm0.11)\times10^3$	$(3.42\pm0.52)\times10^9$	31.3 ± 0.5
H_3PO_4	1.23	$(1.21\pm0.48)\times10^3$	$(4.97\pm1.46)\times10^{10}$	33.4 ± 0.8
		$(9.22\pm6.23)\times10^3$	$(2.04\pm2.68)\times10^{19}$	127.3 ± 5.7
Silicate glass		$(1.41\pm0.12)\times10^3$	$(6.06\pm2.80)\times10^{15}$	100.6 ± 2.0

* errors refer to one standard deviation

Figure 43

Temperature activation plots for the two components of the luminescent decay of uranyl sulphate in silicate glass. Full curves represent computer fits to equation 8-1; (individual parameters are given in Table 8-2).

wo components

phate in

t computer

meters are

Both media show rather similar behaviour with E_A lying between 31 and 33 kJ mol^{-1} and almost identical B terms, although the values of A differ by an order of magnitude. These results can be compared with 70% $HClO_4$ (Table 8-1) which gives generally similar behaviour although the reduced values of E_A and the lifetime at 77 K may reflect the aqueous content of the medium. The results for H_2SO_4 are in good agreement with those of Galanin[248] who reports a lifetime of 850 μs at 77 K (cf. 910 μs obtained from this work), but conflict with those of Kazakov et al.[201] who report neither the lifetime nor the luminescence yield to vary smoothly with temperature over the range 80 to 320 K, but to give a series of discontinuities reflecting the structural changes of the environment. However, there is a general agreement with the reported lifetime of 850 μs at 80 K and a 'break' in the temperature profile at ∿ 200 K, the glassing point of the solvent. The discrepancies in the low-temperature lifetimes probably lie in the thermal history of the sample during the experiment, which could well influence the position of the phase transitions.

The similarity of the activation parameters for H_2SO_4 and H_3PO_4 may be explained simply in terms of a temperature-independent radiative pathway $k_R \sim 1.1 \times 10^3\ s^{-1}$ and a temperature-activated non-radiative pathway for these two cases.

A further example of this type of medium is that of a silicate block doped with $[UO_2]^{2+}$. However, this system displays unusual kinetics and is considered to be a special case: the transient decays for $[UO_2]^{2+}$ were decidedly non-exponential and could be fitted to a two-term expression:-

$$-d[UO_2]^{2+*}/dt = k_1[UO_2]^{2+*} + k_2[UO_2]^{2+*}$$

where k_1 and k_2 represent the two individual rate constants making up the overall decay. The two resultant Arrhenius plots and sets of fitted activation parameters are given in Figure 43 and Table 8-2 respectively. The plots, which show considerable scatter, reflect the inherent inaccuracy in decomposing the multi-exponential decays, feature an extremely sharp rise in both k_1 and k_2 above 370 K, giving a value of $E_A > 100$ kJ mol^{-1} which may well reflect the endothermicity of the deactivation process in this rigid medium.

A similar two-exponential decay has been reported for other uranyl-doped glasses,[185] although this is not a general trend for these systems as a number of glasses have been reported to give good first-order kinetics. For a phosphate glass containing 1% by weight of $[UO_2]^{2+}$, two first-order decays were resolved with lifetimes of 115 and 367 μs at 300 K, although lower concentrations gave a single decay of ∿ 400 μs.[185,249] The dual nature of the luminescence is explained in terms of multiple site emission with the shorter-lived component possibly resulting from a small concentration of uranyl pairs, with a short U-U distance, formed during the cooling of the molten glass, and may result in a self-quenching effect giving the shorter lifetime.[185] In the case of the silicate block, the two exponential components may result from borate and silicate centres. The Arrhenius plots show the two components to differ mainly in the magnitude of the temperature-independent B term which is larger by a factor of 6.5 for the shorter lived component.

8.5 Results and Discussion for Organic Media

The temperature activation of the uranyl luminescence has been investigated in both photoinert and photoreactive organic media, and the fitted parameters are given in Table 8-3 with the

Table 8-3 Rate and fitted* activation parameters for the excited uranyl ion in organic media

Medium	$10^{-4}\ k_{298}/s^{-1}$	A/s^{-1}	E_A/kJ mol^{-1}	B/s^{-1}
	(a) Photoinert organic media			
$(CH_3)_2CO$	73	$(3.12 \pm 0.55) \times 10^8$	15.0 ± 0.3	-
$(CD_3)_2CO$	31.7	$(1.06 \pm 0.13) \times 10^7$	8.70 ± 0.3	-
CH_3CN	26	$(5.91 \pm 1.08) \times 10^7$	13.4 ± 0.4	-
CF_3CO_2H	129	$(7.60 \pm 1.5) \times 10^9$	21.5 ± 0.5	-
	(b) Photoreactive organic media			
CH_3OH	2.78×10^3	$(1.2 \pm 0.2) \times 10^{11}$	20.8 ± 0.3	$(5.7 \pm 1.1) \times 10^3$
CH_3OD	3.33×10^3	$(3.3 \pm 0.7) \times 10^{11}$	22.8 ± 0.5	$(2.9 \pm 0.6) \times 10^3$
CD_3OH	1.21×10^3	$(4.2 \pm 1.1) \times 10^{11}$	25.9 ± 0.6	$(4.4 \pm 0.2) \times 10^3$
CD_3OD	1.23×10^3	$(1.2 \pm 0.4) \times 10^{11}$	22.8 ± 0.5	$(2.2 \pm 1.6) \times 10^3$
cellulose acetate	4.22×10^4	$(1.9 \pm 2.4) \times 10^{14}$	55 ± 2	2.6×10^3 a

* errors refer to one standard deviation

a estimated value

Figure 44

Temperature activation plots for the luminescent decay of uranyl nitrate in photoinert organic media. Full lines refer to least squares analysis of data;(individual parameters are given in Table 8-3).

(a) acetone (X) and acetone-d^6 (O)

(b) trifluoracetic acid (X) and acetonitrile (O)

uminescent

organic

ares analysis

en in Table

onitrile (O)

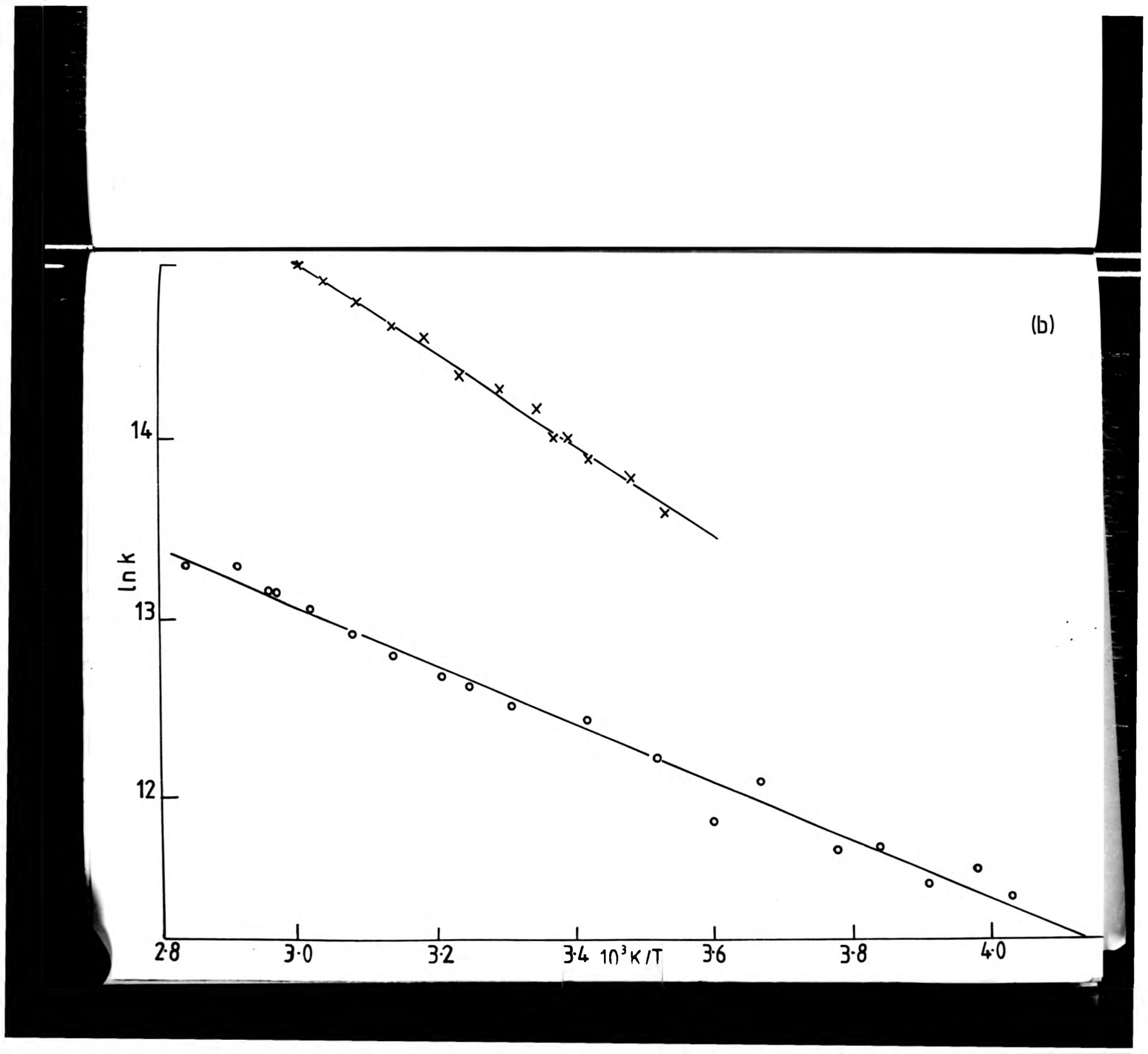
(b)
14
13
12
ln k
2·8
3·0
3·2
3·4
10³ K/T
3·6
3·8
4·0

Arrhenius plots being given in Figures 44 and 45.

As noted in Chapter 2.3, the excited uranyl ion interacts with a wide variety of organic functional groups and it is therefore not surprising that only a few organic media can be found which fail to quench strongly its luminescence at ambient temperature. In this work, acetone (and deuterated acetone), acetonitrile and trifluoroacetic acid have been used, which are normally fairly inert to one-electron oxidative attack and therefore allowed a detectable luminescence over their fluid range. These systems gave lifetimes at 298 K which were similar to those of water (cf. Tables 8-3 and 8-1) and displayed simple Arrhenius behaviour, although this is probably due to their restricted temperature range. The fitted activation parameters (Table 8-3) show both the frequency factors (A) and the activation energies (E_A) are much lower than in water, with the exception of trifluoroacetic acid, which gave a value of E_A only slightly lower than that of water. It would seem, therefore, that the main reason for the observed luminescence from these systems is reflected in the low values of A, which suggests the thermally-activated deactivation route to be somewhat inefficient.

E.s.r. data[192] have shown that hydrogen-atom abstration is the predominant photochemical redox process for solutions of $[UO_2]^{2+}$ in acetonitrile at 77 K, whereas the presence of $\cdot CF_3$ radical on photolysis of the uranyl-trifluoroacetic acid system suggests that oxidative decarboxylation operates in this case. Photolysis of the uranyl-acetone system[192] produced a mixture of $\cdot CH_3$ and $\cdot CH_2COCH_3$ at 77 K, with the latter becoming predominant at 125 K, indicating a hydrogen-atom abstraction mechanism to be dominant at higher temperatures. These results suggest that the thermally-activated non-radiative pathway refers

Figure 45

Temperature activation plots for the luminescent decay of uranyl nitrate in photoreactive organic media. Full curves refer to computer fit to equation 8-1; (individual parameters are given in Table 8-3).

(a) CH_3OH (X); CH_3OD (·); CD_3OH (+); CD_3OD (O)

(b) CA film

inescent

organic

t to

given in

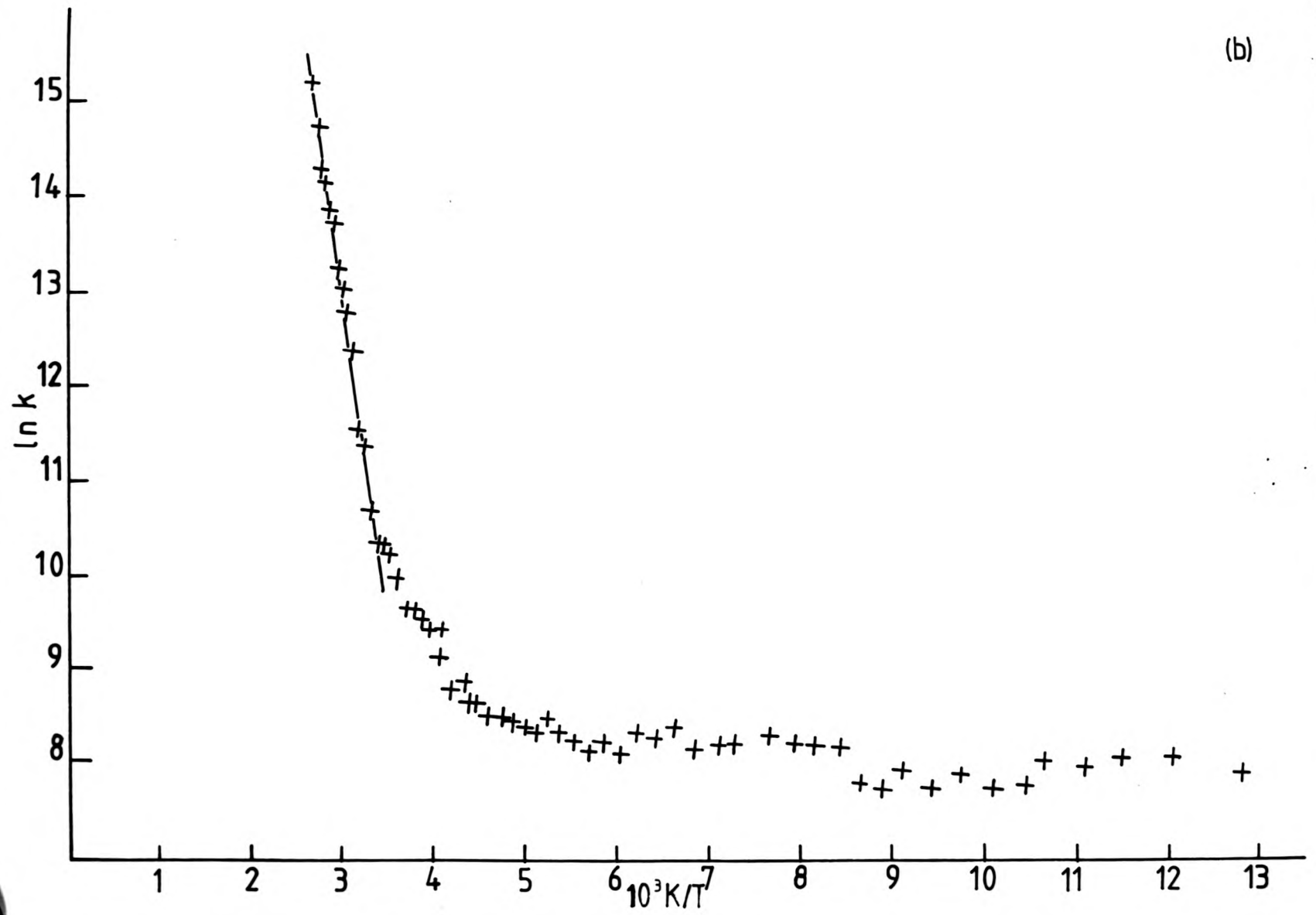
(b)
15
14
13
12
11
10
9
8
ln k
1
2
3
4
5
6
7
8
9
10
11
12
13
10³K/T

to the appropriate chemical mechanism with the relatively low frequency factors indicating an intrinsic barrier to this mechanism. In particular, the isotope effect for acetone confirms a hydrogen-abstraction mechanism in this instance, although the scatter in the experimental points (Figure 44a) makes any quantitative analysis inappropriate.

The weak luminescence at 298 K of $[UO_2]^{2+}$ found in the methanol systems was not surprising, as an efficient chemical quenching of $[UO_2]^{2+}$ by methanol with $k_q = 6.4 \times 10^6$ dm^3 mol^{-1} s^{-1} at 298 K has been reported, although the strong luminescence obtained for this system at 77 K implies restriction of this mechanism at low temperatures. This medium allowed study of the luminescence lifetime over the complete temperature range of 77 to 300 K and the fitted Arrhenius parameters for both methanol and its deuterated forms are given in Table 8-3 with the Arrhenius plots being depicted in Figure 45a . The plots show two main trends, namely (i) at high temperatures (T > 250 K), the rates for CH_3OH and CH_3OD are identical, but are considerably higher (by a factor of $\sim$ 2.5) than those for CD_3OH and CD_3OD, which also exhibit identical behaviour in this temperature region, and (ii) as the temperature is lowered, the rates within each pair begin to diverge until,when what appears to be one mechanism is frozen out (near 145 K), two new 'pairs', each with similar temperature-independent rates emerge, i.e. CH_3OH and CD_3OH (in which decay is faster) and CH_3OD and CD_3OD. A further point which can be made about these plots is that the fitted curve gives consistently poor agreement with the observed data at the freezing point of the solution, which suggests the presence of a slight phase effect.

The fitted parameters for all four cases give remarkably similar values of E_A to that found for water, although the A term

is higher by two orders of magnitude, which is indicative of the efficient chemical quenching process mentioned previously. Further evidence that E_A refers to a chemical process comes from the production of U(IV) for this system on photolysis at 298 K. The B term for the O-H systems is similar to the decay rate of $[UO_2]^{2+*}$ in H_2O at 77 K (4.5×10^3 s^{-1}), although the O-D systems give a somewhat higher value than D_2O which gives 1.28×10^3 s^{-1} at this temperature.

The solvent isotope effects for this system are given below:-

Isotope effect	System	298 K	77 K
k(CH/CD)	$\frac{CH_3OH}{CD_3OH}$	2.3	1.3
k(CH/CD)	$\frac{CH_3OD}{CD_3OD}$	2.7	1.3
k(OH/OD)	$\frac{CH_3OH}{CH_3OD}$	0.83	2.0
k(OH/OD)	$\frac{CD_3OH}{CD_3OD}$	0.98	2.0

These results can be compared with those of Joshi *et al.*[190] who find for k(OH/OD) for CH_3OH/CH_3OD a value of $4.0 \times 10^3/2.22 \times 10^3$ = 1.80 at 77 K, and with those of Kemp *et al*[188] for aqueous solutions of CH_3OH and CD_3OH in H_2O (for which k(CH/CD) = 2.76 ± 0.08) and in D_2O (for which k(CH/CD) = 2.39 ± 0.11). Experiments on CH_3OH (in H_2O) and CH_3OD (in D_2O) yielded k(OH/OD) = 0.98 ± 0.03, whilst those on CD_3OH (in H_2O) and CD_3OD (in D_2O) yielded k(OH/OD) = 0.85 ± 0.03.[188] These values accord with those found in this work and, in particular, the close agreement with the isotope effect found for the quenching of the aqueous $[UO_2]^{2+}$ luminescence by methanol indicates the thermally-activated route to be chemical.

The solvent isotope effects give a clear indication that attack of $[UO_2]^{2+*}$ on the C-H bonds of methanol is a dominant mode at 298 K, while deactivation through the O-H bonds of the solvent is predominant at 77 K. E.s.r. studies have demonstrated the presence of MeO· during the photo-oxidation of neat methanol by $[UO_2]^{2+}$ at room temperature,[247] although in studies at 215 K only $\cdot CH_2OH$ radicals were spin-trapped,[193] which the authors suggest may relate to a secondary radical formed by the fast attack of MeO· upon MeOH. However, our results suggest that either the primary route involving MeO· formation must have a very low isotope effect or $\cdot CH_2OH$ formation is the dominant route at room temperature. The latter conclusion is substantiated by studies of aqueous methanolic $[UO_2]^{2+}$ at room temperature for which both the spin-trapping of $\cdot CH_2OH$ only on photolysis[247] and the similar isotope effects,[188] as outlined above, have been reported. It is also unlikely that hydrogen-abstraction[192] is responsible for the low-temperature isotope effects since this process would then appear to involve no activation energy and the seemingly negligible activation energy would suggest a purely physical mode involving direct energy transfer to the O-H bonds of the neighbouring solvent molecules to be more appropriate, as proposed by Joshi *et al.*[190]

A brief study of $[UO_2]^{2+}$ in cellulose acetate film was also undertaken, and the results are shown in Figure 45b . These results could not be fitted to equation (8-1), but the plot is in general agreement with the other uranyl systems studied, and two clearly defined regions are apparent, with a strongly temperature-activated region with E_A = (55 ± 2) kJ mol^{-1} dominant at high temperatures (T > 300 K) while a temperature-independent region with k = 2.56 x 10^3 s^{-1} is manifest at low temperature.

E_A for this system is expected to refer to the attack on the polymer by $[UO_2]^{2+*}$, with the high value reflecting the restricted mobility of the reactants. The report of radical formation on uranyl-sensitised photolysis of cellulose at 77 K supports this assignment.[192]

8.6 General Summary

The photophysics of the uranyl ion can be resolved into two processes over the temperature range 77 to 300 K. At low temperatures (T < 270 K), deactivation of the excited uranyl ion occurs mainly through a temperature-independent non-radiative pathway which is thought to be a physical quenching mechanism involving the neighbouring solvent molecules. At ambient temperatures, the deactivation of the excited state is dominated by a strongly thermally activated process, the nature of which is dependent upon the solvent medium. For organic media, this pathway is expected to represent a chemical process, the exact mechanism of which depends upon the solvent medium. For methanol, hydrogen atom abstraction involving a C-H bond seems most likely from the isotope effects at the ambient temperature reported, although e.s.r. studies indicate hydrogen abstraction from the O-H bond to be preferred on photolysis at 298 K.[247] For the other organic media studied, a chemical process has been proposed on the basis of low-temperature e.s.r. results, although the above discussion would indicate that direct comparison with spin-trapping results may well be inappropriate.

The photophysics of the aqueous uranyl ion gives a more confused picture, with the absence of any detectable radical intermediates requiring a fast, reversible chemical process in order for such a mechanism to describe the observed behaviour. However, the results of this work suggest a physical quenching

mechanism to be more appropriate, although this conclusion is based on a Barclay-Butler plot which involves the joining of two clustered sets of points. An interesting comparison can be drawn between the activation parameters obtained for methanolic solutions (Table 8-3), and those of the pure water (Table 8-1). These parameters indicate the essential difference between the two systems lies in the A term which reflects the efficiency of the activation process. This would suggest that the differing mechanisms proposed for these two systems may well reflect steric restrictions on the O-H bond of the water molecule compared with the C-H bond in the alcohol. The 'stabilising' effect of added acid seems to be peculiar to the aqueous environment, and reflects an increase in E_A rather than a reduction in the frequency factor. While no detailed explanation for this effect can be offered, the cause must lie in the structuring of the solvent medium rather than in an important deactivating role for H_3O^+.[191]

CHAPTER 9

An initial investigation of an unusual luminescence from a series of Pt(O) complexes

9-1 The case for genuine luminescence

A series of Pt(0) complexes with the general formula of $[(PPh_3)_2Pt(L)]$ where L = tetracyanoethylene (tcne), fumaronitrile (fmn), O_2 or C_2H_4 plus $[(AsPh_3)_2Pt(fmn)]$ have been reported to give what appears to be a highly structured luminescence,[250] which occurs between 310 and 366 nm in a cellulose acetate film medium. A typical luminescence spectrum is given for $[(PPh_3)_2Pt(tcne)]$ in Figure 46 for which the observed structure was analysed in terms of a vibronic progression of (420 ± 30) cm^{-1}, with similar results being given by the other complexes as shown below.

Table 9-1

Spectroscopic and kinetic characteristics† of selected $(MPh_3)_2Pt(L)$ complexes

M	L	medium	λ^{EM}_{max} /nm	λ^{ABS}_{max} /nm	vibronic structure/cm^{-1}	lifetime* /ns
P	tcne	C A film	366	258	423	200 ± 2
		EtOH,CH_2Cl_2	365			
		C_6H_6	362			
P	C_2H_4	C A film	322	268	405	42 ± 4
		MeOH	356			238 ± 10
P	fmn	C A film	336	260	403	47.8 ± 0.4
		MeOH	350			45 ± 3
P	O_2	C A film	310	267	410	420 ± 30
		MeOH	313			2020 ± 80
As	fmn	C A film	316	268	405	41 ± 6
		MeOH	355			231 ± 12

*measured at 298 K in C A film

†recorded in aerated solutions as no O_2 quenching effect was detected

That this luminescence is genuine is suggested by both the invariance in the position of the emission spectrum with changes in excitation wavelength and the spectral 'blank' of the C A film, which was preferred to solvents with C-H or O-H bonds which gave

Figure 46

Emission spectrum of $\left[(PPh_3)_2Pt(tcne)\right]$ in CA film at 298 K (λ_{ex} = 260 nm). Base line - pure CA film; vibrational progression = (420 ± 30) cm^{-1}.

CA film

re CA film;

.

interfering Raman bands as well as almost unresolved structure. The obvious similarity between the emission of all the complexes investigated would suggest that it is the $-Pt(PPh_3)_2$ part of the molecule which is responsible for the luminescence with the third ligand acting merely as a perturbing influence. Further, the emission spectrum of the free ligand, PPh_3, at 298 K closely resembles that of of $[(PPh_3)_2Pt(tcne)]$ (Figure 46) with an emission maximum of 360 nm, similar bandwidth and structure. This would suggest that the observed emission is a π-π^* luminescence although the possibilities of either free ligand impurity or chemiluminescence from the photodissociated complex have to be considered. However, the slight but definite changes in emission maxima for different complexes suggests an impurity to be unlikely. This assignment differs from that suggested for the parent complex, $[Pt(PPh_3)_3]$, which has been reported to give a bright red luminescence under u.v. excitation with an emission spectrum similar (in shape) to that of the free ligand.[38] The absence of an absorption band at the luminescence excitation maximum (ca. 360 nm) in the absorption spectrum of the free ligand led to the assignment of the luminescence as CTTL(d-π^*).

A number of peaks were found in the i.r. spectra of these complexes in the region of the calculated vibronic progression so that assignment to a precise peak was impossible. However, the presence of this structure in the PPh_3 luminescence spectrum implies a P-Ph vibration to be involved as a deactivation mode. The lifetimes of the luminescence were measured at the emission maxima in C A film at 298 K, using a frequency quadrupled (264.8 nm) neodymium laser with the transient decays showing complicated behaviour through the presence of two well-resolved decays in all but the case of $[(PPh_3)_2Pt(tcne)]$. The lifetime of

the latter in liquid methanol was immeasurably fast (<50 ns), and poor transmission at 77 K made lifetime measurements at this temperature impossible. However, the lifetime for all the complexes is considerably shorter than that of the phosphorescence from the free ligand (14.5 ms at 77 K)[251] which would be expected from the increased influence of SOC caused by the heavy-metal centre, with negligible effect of temperature (298 to 77 K) on both the position and the yield of the luminescence being apparent.

9-2 Factors making the assignment of a genuine luminescence questionable

While the observed luminescence is almost certainly due to the presence of complex, as no such emission is apparent in an identical system with no complex present, the complicated behaviour of the luminescence lifetime is puzzling. A more disturbing fact is the inability to obtain realistic excitation spectra for either the complexes or the free PPh_3 ligand with attempts resulting merely in a very intense, sharp peak at the selected emission wavelength. This would suggest that the observed luminescence may be an artefact, possibly due to a form of excitation light-scattering effect, and further definite evidence is required before a genuine luminescence can be unquestionably assumed for either complex or ligand, although the ligand has been reported to luminesce at 77 K.[251]

In order to examine the validity of this luminescence it was decided to use pulse radiolysis which does not involve any form of light excitation and thereby removes any possibility of light artefacts. Unfortunately, deaerated solutions of both $[(PPh_3)_2Pt(tcne)]$ and PPh_3 in benzene produced no detectable luminescence over the entire region of 200 to 500 nm on irradiation

with a 5 ns pulse of 3 MeV electrons. However, it was possible to detect the benzene fluorescence decay in the pure solvent at 275 nm which indicates that efficient energy transfer occurs between solvent and the added solute, but either this does not result in luminescence of the latter or the luminescence yield is extremely small, with an efficient radiationless process certainly operating.

From this work, it appears that while the reported luminescence for $[(PPh_3)_2Pt(L)]$ complexes is due to the presence of the PPh_3 ligand, the exact cause of this emission is uncertain, and further work is required before a complete explanation can be given. However, the possibility of a series of high-energy sensitisers makes this work of special interest.

I wish to thank Dr. A. Salmon of the Cookridge High Energy Radiation Centre (University of Leeds) for both instruction and help with the techniques of pulse radiolysis. I am also grateful to Dr. F. Wilkinson of the University of East Anglia for access to the neodymium laser equipment used in lifetime measurements.

CHAPTER 10

Concluding Remarks and Suggestions for Further Work

10.1 Concluding Remarks

One of the recurring themes throughout inorganic photochemistry has been the lack of photophysical data for inorganic compounds under photochemical conditions, making comparison between the two difficult. This work was undertaken to try and remedy this situation for luminescent complexes by using a fast relaxation technique (laser flash photolysis) which affords measurement of luminescence lifetime down to $\tau \sim 50$ ns, so that it was possible to study the excited state kinetics of a number of luminescent compounds at ambient temperatures. Through studying the lifetimes over a complete temperature range (77 to 300 K) , it was possible to evaluate both low- and high-temperature results in terms of one general model for each system.

While the basic models need more refinement in order to give a complete description for the individual systems, they do, however, fall into two categories, namely (i) those which contain both a thermally-activated radiative and non-radiative route (ruthenium(II) and osmium(II)) and (ii) those which only have a single,thermally-activated non-radiative route (chromium(III), $[UO_2]^{2+}$ and platinum(II)). However, both types of model predict the thermally-activated non-radiative process to dominate at ambient temperature, while either the temperature-independent or smaller thermally-activated route becomes important at low temperatures. This illustrates the basis of the previously expressed difficulties of comparison between photochemical results determined at ambient temperatures and low-temperature photophysical data.

A comparison between the trends of the activation energies with environment for these two types of model reveals a method

by which the nature of the thermally-activated process may be distinguished. In the case of deactivation through a higher electronic level, the increased viscosity of a cellulose acetate film is associated with a reduction of E_A, while an increase in E_A is given for the cases where deactivation occurs through a thermally-activated route involving an M-L vibration.

These two general models can be applied to the various types of systems we have studied. The 'heavy-metal' luminescence for ruthenium(II), osmium(II) and platinum(II) all adhere to a general scheme involving deactivation through a higher electronic level at ambient temperatures, while solvent isotope effects suggest partial CTTS character to be imparted to the emitting state which is considered to be CTTL in origin for all three cases. The absence of a thermally-activated emitting level for $[Pt(QO)_2]$ is probably due to both the differing geometry and enhanced SOC effect fot this complex, while the exact nature of the higher level may well differ for individual complexes, although this level is considered to be a ^{3}LF state for ruthenium(II). There is also a close resemblance in the shape of the luminescence spectra for these systems, with structure becoming more well-resolved as the contribution for SOC increases. This structure is considered to represent the radiative deactivation mode through the M-L vibrations of the complex. The luminescence has been explained in the case of ruthenium(II) and osmium(II) in terms of a manifold of close-lying spin-orbit states of CTTL origin, to which the platinum(II) case also appears to adhere,although the exact splitting of the state for this system will obviously differ.

In contrast, the 'light-metal' luminescence of chromium(III) complexes has been considered in terms of well-defined levels

with the reduced effect of SOC in these systems resulting in absence of close-lying levels which could effect efficient deactivation either radiatively or non-radiatively. Similarly, the greater reluctance for chromium(III) to undergo CT transitions results in a good separation of the LF and CT levels for these complexes, so that only the low-lying LF levels need be considered. In this case, therefore, the description of the thermally-activated pathway as due to a non-radiative M-L vibrational or photochemical deactivation of the emitting ^2E metal-centred state is consistent with the proposed model for which no close-lying levels are available. $[UO_2]^{2+}$ also adheres to the same general model as chromium(III), but the nature of the thermally-activated process in this case is less certain and is dependent upon the solvent environment. A chemical process is suggested for organic media, but the nature of this pathway for the important case of water is uncertain.

10.2 Suggestions for Further Work

While the general model for the luminescence of all the complexes studied has been evaluated, the exact nature of some of the processes and states involved remains unclear. The lack of a more exact description of the photophysics for chromium(III) complexes is mainly due to the customary absence of fluorescence. This means no direct observation of the first excited quartet state is possible for many chromium complexes with the consequence that both the position and lifetime of the fluorescent state are uncertain, so that distinction between a photochemical reaction directly from the phosphorescent doublet state or back-ISC to the 'thexi' quartet state as the thermally-activated non-radiative process, is not easily made. The resolution of this problem

requires further work to be directed towards the fluorescence rather than phosphorescence of chromium(III) complexes in order to determine the excited-state parameters for the 'thexi' quartet state.

The description of the luminescence from the polypyridyl complexes of ruthenium(II) is quite complete,and perhaps further work should be focussed on other luminescent complexes of ruthenium(II). However, the osmium(II) case shows considerably more complicated behaviour, while adhering to the same general model. In particular, the nature of the higher level is uncertain and a photochemical investigation at elevated temperatures such as that described by Van Houten and Watts[157] for $[Ru(bipy)_3]^{2+}$ may well give a further indication of the nature of this level. Moreover, both the discrepancy between the temperature profile of the luminescence yield and the lifetime, and the emission-wavelength dependence of the lifetime require further investigation before a complete description of the luminescence from these osmium(II) systems can be attempted.

Our study of the luminescence from $[Pt(QO)_2]$ has only taken the form of a preliminary investigation, and there is an obvious need for further work on most aspects of this system. In particular, the nature of both the emitting and higher non-radiative levels need to be fully defined. While the nature of the latter level may become clearer through photochemical experiments at elevated temperatures, as outlined for osmium(II), the precise nature of the emitting state may well be evaluated by further quenching studies at ambient temperature, with preliminary results showing a dynamic electron - transfer mechanism, indicative of a CT state, to be operative.[240] In

particular, the detection of intermediates such as $[Pt(QO)_2]^+$ or quencher radicals should help in the defining of the exact nature of this CT mode.

The nature of the thermally-activated deactivation for $[UO_2]^{2+}$ in water is still uncertain; although a Barclay-Butler plot (Figure 39) has been used to suggest it, it is decidedly different from the (C-H) hydrogen-abstraction mechanism given in organic media. However, further work is required to provide more points for this plot before a definite conclusion can be drawn.

Preliminary results have also been obtained for a number of luminescent Pt(O) complexes, and these could well form the basis of a more complete study of these novel systems.

REFERENCES

1. S.C. Pyke and M.W. Windsor, J. Amer. Chem. Soc., 1978, 100. 6518.
2. E. Rabinowitch and R.L. Belford, Spectroscopy and Photochemistry of Uranyl Compounds (Pergamon, London, 1964).
3. J.B. Birks, Photophysics of Aromatic Molecules (Wiley-Interscience, London, 1970).
4. C.A. Parker, Photoluminescence of Solutions (Elsevier, Amsterdam, 1968).
5. G.A. Crosby in Inorganic Compounds with Unusual Properties, Adv. Chem. Series, 1976, 150, 149.
6. H.L. Schläfer and G. Gliemann, Basic Principles of Ligand Field Theory (Wiley, London, 1969).
7. H.E. White, Introduction to Atomic Spectra (McGraw-Hill, Tokyo, 1934).
8. Y. Tanabe and S. Sugano, J. Phys. Soc. Japan, 1954, 9, 753.
9. C.K. Jorgensen, Progress in Inorg. Chem., 1962, 4, 73.
10. R.A. Palmer and T.S. Piper, Inorg. Chem., 1966, 5, 864.
11. A.W. Adamson, W.L. Waltz, E. Zinato, D.W. Watts, P.D. Fleischauer and R.D. Lindholm, Chemical Reviews, 1968, 68, 541.
12. S.J. Strickler and R.A. Berg, J. Chem. Phys., 1962, 37, 814.
13. G.B. Porter and H.L. Schläfer, Z. Phys. Chem. (Frankfurt), 1963, 37, 109.
14. T.R. Thomas and G.A. Crosby, J. Mol. Spectroscopy, 1971, 38, 118.
15. J.N. Demas and G.A. Crosby, J. Amer. Chem. Soc., 1971, 93, 2841.
16. M.K. de Armond, Acc. Chem. Res., 1974, 7, 309.
17. G.A. Crosby, K.W. Hipps. W.H. Elfring, Jr., J. Amer. Chem. Soc., 1974, 96, 629.
18. T.L. Kelly and J.F. Endicott, J. Phys. Chem., 1972, 76, 1937.
19. A.D. Kirk, Mol. Photochem., 1973, 5, 127.
20. P.D. Fleischauer, A.W. Adamson and G. Sartori, Progress in Inorg. Chem., 1972, 17, 1.
21. J.I. Zink, Mol. Photochem., 1973, 5, 151.
22. M. Wrighton, H.B. Gray and G.S. Hammond, Mol. Photochem., 1973, 5, 165.

23. L.G. Vanquickenbourne and A. Ceulemans, J. Amer. Chem. Soc., 1977, 99, 2208.

24. J.F. Endicott in Concepts of Inorganic Photochemistry, edited by A.W. Adamson and P.D. Fleischauer (Wiley, New York, 1975).

25. J.F. Endicott and M.Z. Hoffman, J. Amer. Chem. Soc., 1965, 87, 3348.

26. P.P. Zarnegar and D.G. Whitten, J. Amer. Chem. Soc., 1971, 93, 3776.

27. P.C. Ford, G. Malouf, J.D. Petersen and V.A. Durante in Inorganic Compounds with Unusual Properties, Adv. Chem. Series, 1976, 150, 187.

28. R.J. Watts, G.A. Crosby and J.L.Sansegret, Inorg. Chem., 1972, 11, 1474.

29. V. Balzani, L. Moggi, M.F. Manfrin and F. Bolletta, Coord. Chem. Reviews, 1975, 15, 321.

30. H.D. Gafney and A.W. Adamson, J. Amer. Chem. Soc., 1972, 94, 8238.

31. N. Sabbatini and V. Balzani, J. Amer. Chem. Soc., 1972, 94, 7587.

32. V. Balzani, L. Moggi, F. Bolletta and M.F. Manfrin in Inorganic Compounds with Unusual Properties, Adv. Chem. Series, 1976, 150, 160.

33. C. Creutz and N. Sutin, Inorg. Chem., 1976, 15, 496.

34. R. Matsushima, J. Amer. Chem. Soc., 1972, 94, 6010.

35. J.N. Demas and G.A. Crosby, J. Amer. Chem. Soc., 1970, 92, 7262.

36. P.D. Fleischauer and P. Fleischauer, Chemical Reviews, 1970, 70, 199.

37. R. Ballardini, M.T. Indelli, G. Varani, C.A. Bignozzi and F. Scandola, Inorg. Chim. Acta, 1978, 31, L423.

38. R.F. Ziolo, S. Lipton and Z. Dori, J.C.S. Chem. Comm., 1970, 1124.

39. J.P. Paris and W.W. Brandt, J. Amer. Chem. Soc., 1959, 81,5001.

40. G.B. Porter and H.L. Schläfer, Ber. Bunsenges. phys. Chem., 1964, 68, 316.

41. G.A. Crosby, W.G. Perkins and D.M. Klassen, J. Chem. Phys., 1965, 43, 1498.

42. J.N. Demas and G.A. Crosby, J. Mol. Spectr., 1968, 26, 72.

43. F.E. Lytle and D.M. Hercules, J. Amer. Chem. Soc., 1969, 91, 253.
44. A.W. Adamson in Inorganic Compounds with Unusual Properties, Adv. Chem. Series, 1976, 150, 128.
45. G.B. Porter and H.L. Schläfer, Z. Phys. Chem. (Frankfurt), 1963, 38, 227.
46. N.A.P. Kane-Maguire and C.H. Langford, J.C.S. Chem. Comm., 1971, 895.
47. R.J. Watts and G.A. Crosby, J. Amer. Chem. Soc., 1971, 93, 3184.
48. D.H.W.Carstens and G.A. Crosby, J. Mol. Spectr., 1970, 34, 113.
49. J. Hillis and M.K. de Armond, J. Luminescence, 1971, 4, 273.
50. R. Englman and J. Jortner, Mol. Phys., 1970, 18, 145.
51. R.J. Watts, M.J. Brown, B.G. Griffith and J.S. Harrington, J. Amer. Chem. Soc., 1975, 97, 6029.
52. L.S. Forster in Inorganic Compounds with Unusual Properties, Adv. Chem. Series, 1976, 150, 172.
53. G.D. Hager and G.A. Crosby, J. Amer. Chem. Soc., 1975, 97, 7031.
54. J. van Houten and R.J. Watts, J. Amer. Chem. Soc., 1976, 98, 4853.
55. L.S. Forster and K. de Armond, J. Chem. Phys., 1961, 34,2193.
56. H.L. Schläfer, J. Phys. Chem., 1965, 69, 2201.
57. R.A. Plane and J.P. Hunt, J. Amer. Chem. Soc., 1957, 79, 3343.
58. M.R. Edelson and R.A. Plane, J. Phys. Chem., 1959, 63, 327.
59. A.W. Adamson and A.H. Sporer, J. Amer. Chem. Soc., 1958, 80, 3865.
60. A.W. Adamson, J. Inorg. Nuclear Chem., 1960, 13, 275.
61. S.T. Spees and A.W. Adamson, Inorg. Chem., 1962, 1, 531.
62. E.E. Wegner and A.W. Adamson, J. Amer. Chem. Soc., 1966, 88, 394.
63. R.D. Lindholm, E. Zinato and A.W. Adamson, J. Phys. Chem., 1967, 71, 3713.
64. A.W. Adamson, J. Phys. Chem., 1967, 71, 798.
65. A.W. Adamson, Coord. Chem. Reviews, 1968, 3, 169.
66. A.W. Adamson, Pure Appl. Chem., 1970, 24, 451.

67. E. Zinato in Concepts of Inorganic Photochemistry edited by A.W. Adamson and P.D. Fleischauer (Wiley, New York, 1975).
68. S-N. Chen and G.B. Porter, Chem. Phys. Letters, 1970, 6, 41.
69. S.-N. Chen and G.B. Porter, J. Amer. Chem. Soc., 1970, 92, 3196.
70. C.H. Langford and L. Tipping, Can. J. Chem., 1972, 50, 887.
71. N.A.P. Kane-Maguire and C.H. Langford, J. Amer. Chem. Soc., 1972, 94, 2125.
72. R. Ballardini, G. Varani, F. Wasgestian, L. Moggi and V. Balzani, J. Phys. Chem., 1973, 77, 2947.
73. H.F. Wasgestian, J. Phys. Chem., 1972, 76, 1947.
74. J.L. Laver and P.W. Smith, J.C.S. Chem. Comm., 1970, 1497.
75. H.L. Schläfer, H. Gausmann and H. Witzke, Z. Phys. Chem. (Frankfurt), 1967, 56, 55.
76. F.D. Camassei and L.S. Forster, J. Chem. Phys., 1969, 50, 2603.
77. W. Targos and L.S. Forster, J. Chem. Phys., 1966, 44, 4342.
78. J.L. Laver and P.W. Smith, Aust. J. Chem., 1971, 24, 1807.
79. W. Coleman and W. Schaap, J.C.S. Chem. Comm., 1975, 226.
80. C.F.C. Wong and A.D. Kirk, Inorg. Chem., 1976, 15, 1519.
81. D.B. Yang and C. Kutal, J.C.S. Chem. Comm., 1978, 363.
82. M. Maestri, F. Bolletta, L. Moggi, V. Balzani, M.S. Henry and M.Z. Hoffman, J. Amer. Chem. Soc., 1978, 100, 2694.
83. A.W. Adamson, Pure Appl. Chem., 1979, 51, 313.
84. R.T. Walters and A.W. Adamson, Acta Chem. Scand. A., 1979, 33, 53.
85. F. Castelli and L.S. Forster, J. Phys. Chem., 1977, 81, 403.
86. N.A.P. Kane-Maguire, J.E. Phifer and C.G. Toney, Inorg. Chem., 1976, 15, 593.
87. N.A.P. Kane-Maguire, D.E. Richardson and C.G. Toney, J. Amer. Chem. Soc., 1976, 98, 3996.
88. A.R. Guttierrez and A.W. Adamson, J. Phys. Chem., 1978, 82, 902.
89. C. Conti, F. Castelli and L.S. Forster, Inorg. Chim. Acta, 1979, 33, L171.
90. A.D. Kirk, P.E. Hoggard, G.B. Porter, M.G. Rockley and M.W. Windsor, Chem. Phys. Letters, 1976, 37, 199.

91. J.T. Yardley and J.K. Beattie, J. Amer. Chem. Soc., 1972, 94, 8925.

92. S.-N. Chen and G.B. Porter, J. Amer. Chem. Soc., 1970, 92, 2189.

93. N.A.P. Kane-Maguire, J. Conway and C.H. Langford, J.C.S. Chem. Comm., 1974, 801.

94. G.B. Porter and A.D. Kirk, Poster on 'Room Temperature Phosphorescence of Chromium(III) Complexes', 3rd Microsymp. on Photochem. and Photophysics of Coordination Compounds, 31st July to 1st August, 1978, Köln, Germany.

95. M. Maestri, F. Bolletta, L. Moggi, V. Balzani, M.S. Henry and M.Z. Hoffman, J.C.S. Chem. Comm., 1977, 491.

96. R. Dingle, J. Chem. Phys., 1969, 50, 1952.

97. F. Castelli and L.S. Forster, J. Amer. Chem. Soc., 1975, 97, 6306.

98. F. Bolletta, M. Maestri and V. Balzani, J. Phys. Chem., 1976, 80, 2499.

99. V. Balzani and V. Carassiti, Photochemistry of Coordination Compounds (Academic Press, New York, 1970).

100. M.F. Manfrin, L. Moggi and V. Balzani, Inorg. Chem., 1971, 10, 207.

101. A.D. Kirk, J. Amer. Chem. Soc., 1971, 93, 283.

102. S.C. Pyke and R.G. Linck, J. Amer. Chem. Soc., 1971, 93, 5281.

103. C. Bifano and R.G. Linck, Inorg. Chem., 1974, 13, 609.

104. M.F. Manfrin, D. Sandrini, A. Juris and M.T. Gandolfi, Inorg. Chem., 1978, 17, 90.

105. C. Kutal and A.W. Adamson, J. Amer. Chem. Soc., 1971, 93, 5581.

106. C. Kutal and A.W. Adamson, Inorg. Chem., 1973, 12, 1990.

107. L.G. Vanquickbourne and A. Ceulemans, Inorg. Chem., 1979, 18, 897.

108. C. Furlani, Theoret. Chim. Acta, 1974, 34, 233.

109. C.F.C. Wong and A.D. Kirk, Inorg. Chem., 1977, 16, 3148.

110. R.E. Wright and A.W. Adamson, Inorg. Chem., 1977, 16, 3360.

111. C.D. Flint in Advances in Infrared and Raman Spectroscopy, vol. 2 (Heyden, London, 1976).

112. W.J. Michell and M.K. de Armond, J. Luminescence, 1971, 4, 137.

113. C.D. Flint and A.P. Matthews, J.C.S. Chem. Comm., 1971, 954.
114. K.K. Chatterjee and L.S. Forster, Spectrochimica Acta, 1964, 20, 1603.
115. N.A.P. Kane-Maguire, R.C. Kerr and J.R. Walters, Inorg. Chim. Acta, 1979, 33, L163.
116. K. de Armond and L.S. Forster, Spectrochimica Acta, 1963, 19, 1687.
117. K. de Armond and L.S. Forster, Spectrochimica Acta, 1963, 19, 1393.
118. K. de Armond and L.S. Forster, Spectrochimica Acta, 1963, 19, 1403.
119. R. Dannöhl-Fickler, H. Kelm and F. Wasgestian, J. Luminescence, 1975, 10, 103.
120. A. Pfeil, J. Amer. Chem. Soc., 1971, 93, 5395.
121. M.S. Henry, J. Amer. Chem. Soc., 1977, 99, 6138.
122. M.S. Henry and M.Z. Hoffman in Inorganic and Organometallic Photochemistry, Adv. Chem. Series, 1978, 168, 91.
123. J.N. Demas and A.W. Adamson, J. Amer. Chem. Soc., 1973, 95, 5159.
124. C.-T. Lin, W. Böttcher, M. Chou, C. Creutz and N. Sutin, J. Amer. Chem. Soc., 1976, 98, 6536.
125. C. Creutz and N. Sutin, Proc. Natl. Acad. Sci. (USA), 1975, 72, 2858.
126. N. Sutin and C. Creutz in Inorganic and Organometallic Photochemistry, Adv. Chem. Series, 1978, 168, 1.
127. G. Sprintschnik, H.W. Sprintschnik, P.P. Kirsch and D.G. Whitten, J. Amer. Chem. Soc., 1976, 98, 2337.
128. G. Sprintschnik, J.W. Sprintschnik, P.P. Kirsch and D.G. Whitten, J. Amer. Chem. Soc., 1977, 99, 4947.
129. B. Durham, W.J. Dressick and T.J. Meyer, J.C.S. Chem. Comm., 1979, 381.
130. G. Navon and N. Sutin, Inorg. Chem., 1974, 13, 2159.
131. P.J. de Laive, J.T. Lee, H.W. Sprintschnik, H. Abruna, T.J Meyer and D.G. Whitten, J. Amer. Chem. Soc., 1977, 99, 7094.
132. W.D.K. Clark and N. Sutin, J. Amer. Chem. Soc., 1977, 99, 4676.
133. W.J. Albery and A.W. Foulds, J. Photochem., 1979, 10, 41.
134. C. Kutal in Inorganic and Organometallic Photochemistry, Adv. Chem. Series, 1978, 168, 158.

135. E. Finkenberg, P. Fisher, S.Y. Huang and H.D. Gafney, J. Phys. Chem., 1978, 82, 526.

136. C.-T. Lin and N. Sutin, J. Phys. Chem., 1976, 80, 97.

137. F. Diomedi Camassei, L. Ancarani-Rossiello and F. Castelli, J. Luminescence, 1973, 8, 71.

138. F. Zuloaga and M. Kasha, Photochem. Photobiol., 1968, 7, 549.

139. E.E. Mercer and R.R. Buckley, Inorg. Chem., 1965, 4, 1692.

140. D.M. Klassen and G.A. Crosby, Chem. Phys. Letters, 1967, 1, 127.

141. D.M. Klassen and G.A. Crosby, J. Chem. Phys., 1968, 48, 1853.

142. I. Fujita and H. Kobayashi, Inorg. Chem., 1973, 12, 2758.

143. R.W. Harrigan and G.A. Crosby, J. Chem. Phys., 1973, 59, 3468.

144. R.J. Watts and G.A. Crosby, J. Amer. Chem. Soc., 1972, 94, 2606.

145. R.J. Watts, R.W. Harrigan and G.A. Crosby, Chem. Phys. Letters, 1971, 8, 49.

146. G.A. Crosby, D.E. Lacky and B.J. Pankuch, Abstracts of 169th A.C.S. Meeting (Philadelphia, 1975), no. INOR 69.

147. G.D. Hager, R.J. Watts and G.A. Crosby, J. Amer. Chem. Soc., 1975, 97, 7037.

148. K.W. Hipps and G.A. Crosby, J. Amer. Chem. Soc., 1975, 97, 7042.

149. I. Hanazaki and S. Nagakura, Inorg. Chem., 1969, 8, 648.

150. H.C. Stynes and J.A. Ibers, Inorg. Chem., 1971, 10, 2304.

151. D.C. Baker and G.A. Crosby, Chemical Physics, 1974, 4, 428.

152. C. Creutz and N. Sutin, J. Amer. Chem. Soc., 1976, 98, 6384.

153. R.C. Young, F.R. Keene and T.J. Meyer, J. Amer. Chem. Soc., 1977, 99, 2468.

154. J.N. Demas, E.W. Harris, C.M. Flynn, Jr. and D. Diemente, J. Amer. Chem. Soc., 1975, 97, 3838.

155. J. van Houten and R.J. Watts, J. Amer. Chem. Soc., 1975, 97, 3843.

156. J.S. Winterle, D.S. Kliger and G.S. Hammond, J. Amer. Chem. Soc., 1976, 98, 3719.

157. J. van Houten and R.J. Watts, Inorg. Chem., 1978, 17, 3381.

158. R. Bensasson, C. Salet and V. Balzani, J. Amer. Chem. Soc., 1976, 98, 3722.

159. M. Wrighton and J. Markham, J. Phys. Chem., 1973, 77, 3042.

160. I.A. Khirstikov, Tr. Gos. Optich. Inst. Leningrad, 1937, 12, 3; Chem. Abs., 32, 2432.

161. D.L. Webb and L. Ancarani- Rossiello, Inorg. Chem., 1971, 10, 2213.

162. D.L. Webb and L. Ancarani-Rossiello, Inorg. Chem., 1970, 9, 2622.

163. T. Kobayashi, K.D. Straub and P.M. Rentzepis, Photochem. Photobiol., 1979, 29, 925.

164. R. Ballardini, G. Varani, M.T. Indelli and F. Scandola, Poster on 'Luminescent Properties and Electron-transfer Quenching of $Pt(QO)_2$ ', 3rd Microsymp. on Photochem. and Photophysics of Coordination Compounds, 31st July to 1st August, 1978, Köln. Germany.

165. P.C. Ford, R.E. Hintze and J.D. Petersen in Concepts of Inorganic Photochemistry edited by A.W. Adamson and P.D. Fleischauer (Wiley, New York, 1975).

166. F. Scandola, O. Traverso and V. Carassiti, Mol. Photochem., 1969, 1, 11.

167. J.N. Demas and A.W. Adamson, J. Amer. Chem. Soc., 1971, 93, 1800.

168. V.S. Sastri and C.H. Langford, J. Amer. Chem. Soc., 1969, 91, 7533.

169. F. Bolletta, M. Gleria and V. Balzani, J. Phys. Chem., 1972, 76, 3934.

170. H.D. Burrows and T.J. Kemp, Chem. Soc. Rev., 1974, 3, 139.

171. e.g. W.G. Leighton and G.S. Forbes, J. Amer. Chem. Soc., 1930, 52, 3139.

172. (noted by) J.T. Bell and R.E. Biggers, J. Mol. Spectr., 1965, 18, 247.

173. S.P. McGlynn and J.K. Smith, J. Mol. Spectr., 1961, 6, 164.

174. J.B. Newman, J. Chem. Phys., 1965, 43, 1691.

175. R.L. Belford and G. Belford, J. Chem. Phys., 1961, 34, 1330.

176. C.A. Coulson and G.R. Lester, J. Chem. Soc., 1956, 3650.

177. C. Görller-Walrand and S. de Jaegere, Spectrochimica Acta, 1972, 28A, 257.

178. J.T. Bell and R.E. Biggers, J. Mol. Spectroscopy, 1968, 25, 312.

179. M. Moriyasu, Y. Yokoyama and S. Ikeda, J. Inorg. Nuclear Chem., 1977, 39, 2205.

180. C.K. Jorgensen and R. Reisfeld, Chem. Phys. Letters, 1975, 35, 441.

181. P. Brint and A.J. McCafferty, Mol. Phys., 1973, 2, 311.

182. C. Görller-Walrand and L.G. Vanquickenbourne, J. Chem. Phys., 1972, 57, 1436.

183. P. Benson, A. Cox, T.J. Kemp and Q. Sultana, Chem. Phys. Letters, 1975, 35, 195.

184. D.D. Pant and H.B. Tripathi, J. Luminescence, 1974, 8, 492.

185. N. Lieblich-Sofer, R. Reisfeld and C.K. Jorgensen, Inorg. Chim. Acta, 1978, 30, 259.

186. L.V. Volod'ko and E.A. Turetskaya, Zh. Prikl. Spektroskopii Akad. Nauk Belorussk. SSR, 1965, 3, 248 (Russ.); Chem. Abs., 64, 7548c.

187. G.I. Sergeeva, A.K. Chibisov, A.V. Karyakin, L.V. Levshin, A.A. Nemodruk and B.F. Myasvedov, J. Applied Spectrosc., 1975, 19, 1132 (English Trans.).

188. R.J. Hill, T.J. Kemp, D.M. Alberi and A. Cox, J.C.S. Faraday I, 1974, 70 847.

189. H.B. Tripathi, G.C. Joshi and D.D. Pant, Indian J. Pure Appl. Phys., 1973, 11, 377.

190. G.C. Joshi, H.P. Tripathi and D.D. Pant, Current Sci. (India), 1975, 44, 185.

191. M. Moryasu, Y. Yokoyama and S. Ikeda, J. Inorg. Nuclear Chem., 1977, 39, 2211.

192. D. Greatorex, R.J. Hill, T.J.Kemp and T.J. Stone, J.C.S. Faraday I, 1972, 68, 2059.

193. D. Greatorex, R.J. Hill, T.J. Kemp and T.J. Stone, J.C.S. Faraday I, 1974, 70, 216.

194. J.L. Kropp and M.W. Windsor, J. Chem. Phys., 1965, 42, 1599.

195. R.A. Marcus, J. Phys. Chem., 1963, 67, 853.

196. V.P. Kazakov, R.G. Bulgakov, Yu. E. Nikitin and G.L. Sharunov, Opt. Spektrosk., 1976, 41, 1091 (Russ): Chem. Abs., 86, 8113q.

197. H.D.Burrows and S.J. Formosinho, J.C.S. Faraday II, 1977, 73, 201.

198. M.D. Marcantonatos, Inorg. Chim. Acta, 1978, 26, 41.

199. M.D. Marcantonatos, Inorg. Chim. Acta, 1977, 25, L101.

200. R.N. Sylva and M.R. Davidson, J.C.S. Dalton, 1979, 465.

201. V.P. Kazakov, V.N. Korbeinikov, Yu. N. Chuvelin, V.V. Rykova and I.G. Kovelgon, Opt. Spectrosc. (English edition), 1973, 35, 576.

202. H.D. Bist, Proc. Chem. Symp. 1st, 1969 (pub. 1970), 2, 276 (Chemistry and Metallurgy Comm. of Dept. of Atomic Energy, Bombay, India).

203. G. Sergeeva, A. Chibisov, L. Levshin and A. Karyakin, J.C.S. Chem. Comm., 1974, 159.

204. M.D. Marcantonatos, Inorg. Chim. Acta, 1977, 24, L37.

205. S. Sakuraba, S. Mimura and R. Matsushima, Bull. Chem. Soc. Japan, 1973, 46, 2784.

206. R. Matsushima, J. Amer. Chem. Soc., 1972, 94, 6010.

207. R. Matsushima and S. Sakuraba, J. Amer. Chem. Soc., 1971, 93, 7143.

208. H.D. Burrows, S.J. Formosinho, M. da Graca Miguel and F. Pinto Coelho, J.C.S. Faraday I, 1976, 72, 163.

209. R. Matsushima, H. Fujimori and S. Sakuraba, J.C.S. Faraday I, 1974, 70, 1702.

210. Y. Yokoyama, M.Moriyasu and S. Ikeda, J. Inorg. Nuclear Chem., 1974, 36, 385.

211. Y. Yokoyama, M.Moriyasu and S. Ikeda, J. Inorg. Nuclear Chem., 1976, 38, 1329.

212. A.G. Brits, R. van Eldik and J.A. van den Berg, J. Inorg. Nuclear Chem., 1977, 39, 1195.

213. A. Okyashi and K. Ueno, J. Inorg. Nuclear Chem., 1974, 36, 379.

214. A.G. Brits, R. van Eldik and J.A. van den Berg, Inorg. Chim. Acta, 1978, 30, 17.

215. S.R. Allsopp, A. Cox, S.H. Jenkins, T.J. Kemp and S.M. Tunstall, Chem. Phys. Letters, 1976, 43, 135.

216. R.W. Harrigan and G.A. Crosby, Spectrochimica Acta, 1970, 26A, 2225.

217. R.G.W. Norrish and G. Porter, Nature, 1949, 164, 658.

218. G. Porter and M.R. Topp, Nature, 1968, 220, 1228.

219. P.R. Hammond, J. Chem. Phys., 1979, 70, 3884.

220. A. Yariv, Introduction to Optical Electronics, end Edn. (Holt, Reinehart and Winston, U.S.A., 1976).

221. S.L. Murov, Handbook of Photochemistry, (Marcel Dekker, 1973).

222. W.H. Melhuish and R. Hardwick, Trans. Faraday Soc., 1962, 58, 1908.

223. F.C. Unterleitner and E.I. Hormats, J. Phys. Chem., 1965, 69, 2516.

224. W. Windhager, S. Schneider and F. Dörr, J. Photochem., 1976, 6, 69.

225. T. Ohno and S. Kato, Bull. Chem. Soc. Japan, 1970, 43, 8.

226. G. Brauer, Handbook of Preparative Inorganic Chemistry, 2nd Edn., vol. II (Academic Press, London, 1965).

227. N. Serpone and F. Bolletta quoted by V. Balzani, F. Bolletta, M.T. Gandolfi and M Maestri, Top. Curr. Chem., 1979, 75, 1.

228. B. Brunschwig and N. Sutin, J. Amer. Chem. Soc., 1978, 100, 7658.

229. A.L. Phipps and R.A. Plane, J. Amer. Chem. Soc., 1957, 79, 2458.

230. F.H. Burstall, J. Chem. Soc., 1936, 173.

231. F.H. Burstall, F.P. Dwyer and E.C. Gyarfas, J. Chem. Soc., 1950, 953.

232. U. Belluco, Organometallic and Coordination Chemistry of Platinum, ch. 6, (Academic Press, London, 1973).

233. R.A. Krause, I. Trabjerg and C.J. Ballhausen, Chem. Phys. Letters, 1969, 3, 297.

234. F. Castelli and L.S. Forster, Chem. Phys. Letters, 1975, 30, 465.

235. C.H. Langford, Lecture on "Solvation and Photonucleophilicity", 3rd Microsymp. on Photochem. and Photophysics of Coordination Compounds, 31st July to 1st August, 1978, Köln, Germany.

236. R.C. Young, J.K.Nagle, T.J. Meyer and D.G. Whitten, J. Amer. Chem. Soc., 1978, 100, 4773.

237. C.H. Langford, private communication.

238. R.G. Bennett and P.J. McCartin, J. Chem. Phys., 1966, 44, 1969.

239. G.A. Crosby, D.M. Klassen and S.L. Sabath, Mol. Cryst., 1966, 1, 453.

240. M.T. Indelli, F. Scandola, M.A. Scandola-Rampi, C.A. Bignozzi and V. Carassiti, paper submitted for A.I.C.I. Conference, Trieste, Italy, 1979.

241. W.R. Mason, III and H.B. Gray, J. Amer. Chem. Soc., 1968, 70, 5721.

242. C. Reichardt, Angew. Chemie (Int. Edn.), 1965, 4, 29.

243. W. Liptay, Angew. Chemie (Int. Edn.), 1969, 8, 177.

244. J. Burgess, Spectrochimica Acta, 1970, 26A, 1369.

245. J.N. Demas, T.F. Turner and G.A. Crosby, Inorg. Chem., 1969, 8, 674.

246. R. Matsushima and S. Sakuraba, J. Amer. Chem. Soc., 1971, 93, 5421.

247. A. Ledwith, P.J. Russell and L.H. Sutcliffe, Proc. Roy. Soc. A, 1973, 332, 151.

248. M.D. Galanin, Zhur. ekop. teor. Khim., 1951, 21, 126.

249. G. Blasse and J.P.M. van den Dungen, J. Inorg. Nuclear Chem., 1978, 40, 2037.

250. O. Traverso, private communication.

251. D. McClure, J. Chem. Phys., 1949, 17, 905.

APPENDIX I

COMPUTER PROGRAMS

(a) Programs used in analysis of ESA and emission transients

The inputted form of the data for each individual trace is given below:-

Form	Comments
TRACE REFERENCE NUMBER	
NUMBER OF DATA POINTS	preferably between 12 and 15
TIMEBASE ON WHICH TRACE WAS RECORDED (IN ns)	halved to compensate for 2 x enlargement
I_o	put equal to 1.0 for emission measurement
ESTIMATE OF RATE CONSTANT V(1)	a rough guide to the reciprocal of the timebase (in seconds^{-1})
TEMPERATURE (^{o} C)	
OFFSET VALUE	only used when I_o > 16.1
DATA	digitised points fed in as sets of I_t and t values

The information in this form is stored on a data file (...../DATA) for further inspection by the program V1EOX which converts that data, either ESA or emission, into an appropriate form ready for first-order analysis by the subroutine VB01A which is called by this program. VB01A is a modified version of an ICL 1900 library copy from the University of East Anglia and is the key program in this work as it provides for both analysis of the Arrhenius-type data as well as the first-order decays. The program is essentially a least squares approximation program in which the pertinent equation and the partial derivatives of this equation with respect to the unknown variables are fed in through the subroutine DERIV. The program, which minimises the sum of the squares of the difference between the observed and calculated points for the function, S, utilises the basic criterion that the partial

derivative of S with respect to each of the unknown variables, dS(I), must be equal to 0 for S to be a minimum. The subroutine MA04A, called by VB01A, estimates the change needed in V(I), the set of unknown variables, to produce this condition for each partial derivative. The changed values of V(I) are then used in reiteration of the procedure until the square of the change required in V(I) is less than the standard deviation of V(I), or to ten iterations, whichever happens first. In the latter case, a satisfactory fit has not been found, due to either bad initial estimates or use of the wrong theoretical equation. The subroutine then gives an output consisting of the values of V(I), their standard deviations, and the observed and calculated data points. The subroutine then returns the values of V(I) to V1EOX which then proceeds to write the first-order rate constant, its natural logarithm and the lifetime (in μs) of the transient. The temperature and trace reference number are also given. The programme V1EOX and the subroutines VB01A, MA04A and DERIV, along with samples of the input and output format, are given (in Fortran IV) at the back of this appendix.

For analysis of a two-exponential transient decay, V12EX is used instead of V1EOX. This program calls VB01A to fit the data to the appropriate equations given in the subroutine DERIV4. This program is also tabulated at the back of the appendix.

(b) Programs used in analysis of Arrhenius type data

V1EOX (and V12EX) produce an output file (...../ARRHENIUS) which contains the rate constants and equivalent temperatures for a given experiment. The estimates for the Arrhenius

parameters are added to the end of this file, and the curve-fitting procedure of VBOlA then utilised through the calling of a relevant subroutine (DBEXP, VHEXP or SEXP) which ensures the correct subroutine (DERIV4, DERIV3 or DERIV2) is used to give the required 'theoretical' equation together with the presentation of the parameters in the appropriate form (activation energies in kJ mol^{-1} and pre-exponential factors in s^{-1}). The Arrhenius data are fed to the subroutine VBOlA by means of a program (...../FIT) which allows variation in the weighting of the points and reiteration of the procedure with the fitted Arrhenius parameters to ensure a 'best-fit' has been obtained and the results do not reflect a false minimum. In order to obtain a fit for many of the curves, it was necessary to restrict the action of the subroutine VBOlA in changing the estimates of the Arrhenius parameters as it was found that the subroutine often over-compensated for 'large' estimates by putting the estimates negative which caused the program to 'blow up'. The restriction imposed was that the Arrhenius estimates could only be changed by, at the most, half of their value for each iteration. Once a good fit had been found, these restrictions were lifted to allow any free change by the subroutine which might occur in the case of false minima. These programmes are listed at the back of this appendix, and the output is in the same form as that given for VlEOX, with the first-order parameters replaced by the relevant Arrhenius parameters.

For linear Arrhenius plots, a simple linear least squares subroutine was used (WLSSRA) which was called from the programme LINE, and allowed alteration of the weighting of the

data points. This program, also listed at the back of this appendix, was used for analysis of linear plots in general.

```
@FILE (UWMSRAS)VIEWX ON USERPK
$RESET LINEINFO
$SET AUTOBIND
$BIND=FROM (UWMSRAS)OBJECT/SRALIB
$RESET FREE
FILE   51(KIND=DISK,TITLE="OBS/DATA")
FILE   60(KIND=DISK,TITLE="ARRHENIUS",MAXRECSIZE=14,AREASIZE=60,
       1BLOCKSIZE=420,PROTECTION=SAVE)
       REAL TEMP, DD(40), T(40), W(40), Z(40), V(2), E(2), B(3,21), OFFSET
    1  OFFSET=0
       READ(51,/)MM
       WRITE(6,2)MM
       IF(MM.LE.0)STOP
       READ(51,/)N,S,AI,V(1),TEMP
       IF(AI.LT.1.1)  GO TO 3
       IF(AI.GE.16.1)READ(51,/)OFFSET
       READ(51,/) (DD(J), T(J), J =1,N)
    4  DO 5 JJ =1,N
       W(JJ) = 1.0
       DD(JJ) = ALOG10(AI/(DD(JJ)+OFFSET))
    5  T(JJ) = T(JJ)*S/1.0E+09
       GO TO 6
    3  READ(51,/) (DD(J), T(J), J=1,N)
       DO 7 JJ =1,N
       W(JJ) = 1.0
    7  T(JJ) = T(JJ)*S/1.0E+09
    6  V(2) = DD(1)
       CALL VBILA(T,DD,W,Z,N,V,E,2,6,3,IT)
       WRITE(6,8)V(1)
       DEC = 1/(V(1)*1.0E-36)
       WRITE(6,9)DEC
       DEC = ALOG(V(1))
       WRITE(6,10)DEC
       TEMP=273.16+TEMP
       WRITE(60,11)TEMP,V(1)
       TEMP=10000/TEMP
       WRITE(6,12)TEMP
       GO TO 1
    2  FORMAT(1H1,33X,22HTRACE REFERENCE NUMBER,3X,I3,/)
    8  FORMAT(1X,//,13X,23HDECAY CONSTANT      =,E16.8,/)
    9  FORMAT(1X,//,13X,23HLIFETIME (IN USEC) =,1PE16.8,/)
   10  FORMAT(1X,//,13X,23HLN(DECAY CONSTANT) =,2PE16.8,/)
   11  FORMAT(1X,E16.8,1H,,E16.8,1H,)
   12  FORMAT(1X,//,13X,23H10000/T(DEG.K)      =,1PE16.8,//)
       END
$RESET LIST
$
```

A TYPICAL OUTPUT FROM VIEW IS GIVEN BELOW:

I	V(I)	S.D. OF V(I)
1	.49433338E+17	.48135766E+15
2	.22851183E+01	.13211399E-01

NUMBER OF DATA POINTS = 11

RESIDUAL SUM OF SQUARES= .24153412E-02

X	OBS Y	FITTED Y	OBS.Y - FITTED Y
1.	.22711111E+01	.22851183E+01	-.15119263E-01
.51111111E-17	.18111111E+01	.17847281E+01	.15271881E-01
.13111111E-16	.14111111E+01	.13939123E+01	.63876946E-02
.15111111E-16	.13811111E+01	.13886765E+01	-.86764711E-02
.23111111E-16	.87111111E+00	.85328351E+00	.19719494E-01
.25111111E-16	.68111111E+00	.66438796E+00	.15212338E-01
.31111111E-16	.51111111E+00	.51896743E+00	-.18667449E-01
.35111111E-16	.41111111E+00	.41511081E+00	-.53979786E-02
.41111111E-16	.31111111E+00	.31638491E+00	-.63849117E-02
.45111111E-16	.22111111E+00	.24711364E+00	-.27113644E-01
.51111111E-16	.21111111E+00	.19299343E+00	.71163333E-02

DECAY CONSTANT = .49433333E+17

LIFETIME (IN USEC) = 2.02314979E-11

LN(DECAY CONSTANT) = 15.41343982E+00

INTERCEPT = 3.35391394E+00

```
FILE (UMSRAS)SRALIB.UN USERPK
4733        SUBROUTINE VARIA(X,Y,N,Z,N,V,E,M,A,IA,MAXIT)
4833        DIMENSION X(N),Y(N),W(N),Z(N),V(M),E(M),A(IA,21)
4933        DIMENSION VV(20),F(20)
5033        IF(MAXIT.LE.10)GO TO 51
5133        WRITE(6,775)
5233        WRITE(6,776)
5333        GO TO 99999
5433   51   WRITE(6,777)
5533        WRITE(6,778)
5633    775 FORMAT(23X,21HITERATIONS RESTRICTED,)
5733    776 FORMAT(23X,21H**********,//)
5833    777 FORMAT(23X,25HNON-RESTRICTED ITERATIONS,)
5933    778 FORMAT(23X,25H**********,//)
6033  99999 CONTINUE
6133        MP1=M+1
6233        M1=M-1
6333        II=0
6433        NDF=N-M
6533    776 DO 433 I=1,M
6633        VV(I)=V(I)
6733    433 CONTINUE
6833     11 S=0.0
6933        DO 1 I=1,M
7033        A(I,MP1)=0.0
7133        DO 2 J=1,I
7233        A(I,J)=0.0
7333      2 CONTINUE
7433      1 CONTINUE
7533        DO 3 K=1,N
7633        IF(M.EQ.2.AND.MAXIT.LE.10)CALL DERIV(X(K),V,F,Z(K))
7733        IF(M.EQ.2.AND.MAXIT.GT.10)CALL DERIV2(X(K),V,F,Z(K))
7833        IF(M.EQ.3)CALL DERIV3(X(K),V,F,Z(K))
7933        IF(M.EQ.4)CALL DERIV4(X(K),V,F,Z(K))
8033    433 WS=Y(K)-Z(K)
8133        S=S+WS**2*W(K)
8233        WS=WS*W(K)
8333        DO 4 I=1,M
8433        A(I,MP1)=A(I,MP1)+F(I)*WS
8533        DO 5 J=1,I
8633        A(I,J)=A(I,J)+F(I)*F(J)*W(K)
8733      5 CONTINUE
8833      4 CONTINUE
8933      3 CONTINUE
9033        DO 12 I=1,M1
9133        JJ=I+1
9233        DO 13 J=JJ,M
9333        A(I,J)=A(J,I)
9433     13 CONTINUE
9533     12 CONTINUE
9633        CALL MATAA(A,M,IA)
9733    333 ZZZZZZ=NDF
9833        WSI=S/(100.0*ZZZZZZ)
9933        DO 16 I=1,M
10033        E(I)=WSI*A(I,I)
10133     16 CONTINUE
```

```
V3M1A CONTINUED.......


#FILE (JWMSRAS)SRALIB ON USERPK
13233         IF (IT) 131,17,131
13333   131   DO 116 I=1,M
13433         IF(MAXIT.GT.10.AND.(A(I,MP1)**2-3.1*E(I)).GT.0.0)GO TO 17
13533         IF(A(I,MP1)**2-E(I))116,116,17
13633    116  CONTINUE
13733     35  XXXXXX=NOF
13833         VAR=S/XXXXXX
13933         DO 21 I=1,M
14033         DO 21 J=1,M
14133         A(I,J)=A(I,J)*VAR
14233     21  CONTINUE
14333         E(I)=SQRT(A(I,I))
14433     27  CONTINUE
14533         WRITE(6,122)
14633    122  FORMAT(1X,/,6X,1HI,13X,4HV(I),16X,12HS.D. OF V(I), ///)
14733         DO 23 I=1,M
14833         WRITE(6,24) I, V(I),E(I)
14933     23  CONTINUE
15033     24  FORMAT(I5,2E27.8)
15133         WRITE(6,26)N
15233     26  FORMAT(///,1X,24HNUMBER OF DATA POINTS = ,I3,/)
15333         WRITE(6,25)S
15433     25  FORMAT(/,1X,24HRESIDUAL SUM OF SQUARES=,E16.8,///)
15533         WRITE(6,28)
15633     28  FORMAT(1H1,9X,1HX,12X,5HOBS Y,12X,8HFITTED Y,6X,
15733        116HOBS.Y - FITTED Y,////)
15833         DO 29 K=1,N
15933         YZ = Y(K) - Z(K)
16033         WRITE(6,33) X(K),Y(K),Z(K),YZ
16133     29  CONTINUE
16233     33  FORMAT(4E17.8,/)
16333    534  RETURN
16433     22  WRITE(6    ,34)IT
16533     34  FORMAT(22H TERMINATED, MORE THAN   I3,11H ITERATIONS  ///)
16633         GO TO 35
16733     17  IT = IT + 1
16833         IF(IT.GE.MAXIT)GO TO 22
16933         DO 31 I=1,M
17033         VV(I)=V(I)
17133         IF(MAXIT.LE.10)GO TO 53
17233         IF(A(I,MP1).LT.0.0)IAA=-1
17333         IF(A(I,MP1).GT.0.0)IAA=+1
17433         IF(ABS(A(I,MP1)).GT.0.5*V(I))A(I,MP1)=0.5*V(I)*IAA
17533    53   V(I)=VV(I)+A(I,MP1)
17633     31  CONTINUE
17733         WRITE(6,43) IT,S,(VV(I),V(I),I=1,M)
17833     43  FORMAT(13H1ITERATION,I3,2X,2HS=,E16.8,//(2E27.8))
17933         SI=S
18033         GO TO 11
18133         END
18233
18333
*
```

```
#FILE (UMSRAS)SRALIB ON USERPK
15733          SUBROUTINE MATINV(A,M,IA)
15833          DIMENSION A(IA,21),C(133),IND(133)
15933          MP1=M+1
16033      133 AMAX=0.0
16133          DO 2 I=1,M
16233          IND(I)=I
16333          IF(ABS(A(I,1))-AMAX)2,2,3
16433        3 AMAX = ABS(A(I,1))
16533          I4=I
16633        2 CONTINUE
16733          MM=M-1
16833          DO 111 J=1,MM
16933          IF(I4-J)6,6,4
17033        4 ISTO=IND(J)
17133          IND(J)=IND(I4)
17233          IND(I4)=ISTO
17333          DO 5 K=1,MP1
17433          STO = A(I4,K)
17533          A(I4,K)=A(J,K)
17633          A(J,K)=STO
17733        5 CONTINUE
17833        6 AMAX=0.0
17933          JJ=J+1
18033          DO 11 I=JJ,M
18133          A(I,J)=A(I,J)/A(J,J)
18233          DO 13 K=JJ,MP1
18333          A(I,K)=A(I,K)-A(I,J)*A(J,K)
18433          IF (K-JJ)14,14,13
18533       14 IF(ABS(A(I,K))-AMAX)13,13,17
18633       17 AMAX=ABS(A(I,K))
18733          I4=I
18833       13 CONTINUE
18933       11 CONTINUE
19033      111 CONTINUE
19133       19 DO 127 II=1,M
19233          I=M+1-II
19333          IF(M-I)327,327,28
19433       28 I2=I+1
19533          DO 32 K=I2,M
19633          A(I,MP1)=A(I,MP1)-A(I,K)*A(K,MP1)
19733       32 CONTINUE
19833      327 A(I,MP1)=A(I,MP1)/A(I,I)
19933      127 CONTINUE
```

```
SUBROUTINE MATAA CONTINUED.....

FILE (ON4SRAS)SRALIB ON JSERPK
      65 DO 149 II=1,MM
         I=M+1-II
         I2=I-1
         DO 41 JJ=1,I2
         J=I2+1-JJ
         J2=J+1
         AI=-A(I,J)
         IF(I2-J2)141,43,43
      43 DO 42 K=J2,I2
         AI=AI-A(K,J)*C(K)
      42 CONTINUE
     141 C(J)=AI
      41 CONTINUE
         DO 47 K=1,I2
         A(I,K)=C(K)
      47 CONTINUE
     149 CONTINUE
         DO 159 II=1,M
         I=M+1-II
         I2=I+1
         N=A(I,I)
         DO 56 J=1,M
         IF (I-J)52,53,54
      52 AI=1.0
         GO TO 55
      53 AI=1.0
         GO TO 55
      54 AI=A(I,J)
      55 IF(II-1)156,156,57
      57 DO 58 K=I2,M
         AI=AI-A(I,K)*A(K,J)
      58 CONTINUE
     156 C(J)=AI
      56 CONTINUE
         DO 59 J=1,M
         A(I,J)=C(J)/N
      59 CONTINUE
     159 CONTINUE
         DO 61 I=1,M
      63 IF(IND(I)-I)71,63,61
      61 J=IND(I)
         DO 62 K=1,M
         STO=A(K,I)
         A(K,I)=A(K,J)
         A(K,J)=STO
      62 CONTINUE
         ISTO=IND(J)
         IND(J)=I
         IND(I)=ISTO
         GO TO 63
      69 CONTINUE
      64 RETURN
         END
```

```
$
$FILE (JNMSRAS)SRALIB ON JSERPK
      SUBROUTINE DERIV(T,V,F,FUNC)
      DIMENSION F(2),V(2)
      FUNC=V(2)*EXP(-V(1)*T)
      F(1)=-FUNC*T
      F(2)=FUNC/V(2)
      RETURN
      END



      SUBROUTINE DERIV4(T,V,F,FUNC)
      DIMENSION F(4),V(4)
      FUNC=V(1)*EXP(-V(2)/(8.3142*T))+V(3)*EXP(-V(4)/(8.3142*T))
      F(1)=EXP(-V(2)/(8.3142*T))
      F(2)=(-V(1)/(8.3142*T))*EXP(-V(2)/(8.3142*T))
      F(3)=EXP(-V(4)/(8.3142*T))
      F(4)=(-V(3)/(8.3142*T))*EXP(-V(4)/(8.3142*T))
      RETURN
      END



      SUBROUTINE DERIV3(T,V,F,FUNC)
      DIMENSION F(3),V(3)
      FUNC=V(1)*EXP(-V(2)/(8.3142*T))+V(3)
      F(1)=EXP(-V(2)/(8.3142*T))
      F(2)=(-V(1)/(8.3142*T))*EXP(-V(2)/(8.3142*T))
      F(3)=1.0
      RETURN
      END



      SUBROUTINE DERIV2(T,V,F,FUNC)
      DIMENSION F(2),V(2)
      FUNC = V(1)*1.0*EXP(-V(2)/(8.3142*T))
      F(2) = -FUNC /(8.3142*T)
      F(1) = FUNC/V(1)
      RETURN
      END
$RESET LIST
$
```

```
@FILE (JW/SRAS)V12EX ON USERPK
100 $RESET LINEINFO
200 $SET AUTOBIND
300 $BIND=FROM (JW/SRAS)OBJECT/SRALIB
400 $RESET FREE
500 FILE  50(KIND=DISK,TITLE="OBS/DATA")
600 FILE  60(KIND=DISK,TITLE="ARRHENIUS",MAXRECSIZE=14,AREASIZE=60,
700       1BLOCKSIZE=420,PROTECTION=SAVE)
800       REAL TEMP, OD(40),T(40),N(40),Z(40),V(4),E(4),B(5,21),OFFSET
900     1 OFFSET=0
1000       READ(50,/)MM
1100       WRITE(6,2)MM
1200       IF(MM.LE.0)STOP
1300       READ(50,/)N,S,AI,V(1),TEMP
1400       IF(AI.LT.1.1) GO TO 3
1500       IF(AI.GE.16.1)READ(50,/)OFFSET
1600       READ(50,/) (OD(J), T(J), J =1,N)
1700     4 DO 5 JJ =1,N
1800       N(JJ) = 1.0
1900       OD(JJ) = ALOG10(AI/(OD(JJ)+OFFSET))
2000     5 T(JJ) = T(JJ)*S/1.0E+09
2100       GO TO 6
2200     3 READ(50,/) (OD(J), T(J), J=1,N)
2300       DO 7 JJ =1,N
2400       N(JJ) = 1.0
2500     7 T(JJ) = T(JJ)*S/1.0E+09
2600     6 CONTINUE
2700       V(3)=V(1)/13.3
2800       V(2)=OD(1)/2.0
2900       V(4)=V(2)
3000 C*    READ(50,/)(V(J),J=1,4)
3100       CALL V831A(T,OD,N,Z,N,V,E,4,6,5,33)
3200       WRITE(6,8)V(1)
3300       WRITE(6,23)V(3)
3400       DEC = 1/(V(1)*1.0E-36)
3500       WRITE(6,9)DEC
3600       DEC=1/(V(3)*1.0E-36)
3700       WRITE(6,21)DEC
3800       DEC = ALOG(V(1))
3900       WRITE(6,10)DEC
4000       DEC=ALOG(V(3))
4100       WRITE(6,22)DEC
4200       TEMP=273.16+TEMP
4300       WRITE(60,11)TEMP,V(1),V(3)
4400       TEMP=1000/TEMP
4500       WRITE(6,12)TEMP
4600       GO TO 1
4700     2 FORMAT(1H1,33X,23HTRACE REFERENCE NUMBER,3X,I3,/)
4800     8 FORMAT(11X,23HIST DECAY CONSTANT =,E16.8,)
4900    23 FORMAT(11X,23H2ND DECAY CONSTANT =,E16.8,)
5000     9 FORMAT(11X,23HIST LIFETIME (USEC)=,1PE16.8,)
5100    21 FORMAT(11X,23H2ND LIFETIME (USEC)=,1PE16.8,)
5200    10 FORMAT(11X,23HLN(1ST DECAY CONST)=,2PE16.8,)
5300    22 FORMAT(11X,23HLN(2ND DECAY CONST)=,2PE16.8,)
5400    11 FORMAT(1X,E16.8,1H,,E16.8,1H,,E16.8,1H,,)
5500    12 FORMAT(11X,23H1000/T(DEG.K)       =,1PE16.8,/)
5600       END
5700
$
```

VI2EX CONTINUED.....

```
#FILE (UWMSRAS)VI2EX ON USERPK
5800
5900
6000          SUBROUTINE DERIV4(T,V,F,FUNC)
6100          DIMENSION F(4),V(4)
6200          FUNC=V(2)*EXP(-V(1)*T) + V(4)*EXP(-V(3)*T)
6300          F(1)=-T*V(2)*EXP(-V(1)*T)
6400          F(2)=EXP(-V(1)*T)
6500          F(3)=-T*V(4)*EXP(-V(3)*T)
6600          F(4)=EXP(-V(3)*T)
6700          RETURN
6800          END
6900 $RESET LIST
&
```

```
#FILE (UMMSRAS)SRALIB ON  JSERPX
25833         SUBROUTINE  DBEXP(T,K,N,Z,N,V,IMAX)
25933         REAL  T(N),K(N),N(N),Z(N),V(4),E(4),G(5,21),DIF
26033         CALL  V33IA(T,K,N,Z,N,V,E,4,G,5,IMAX)
26133         WRITE(6,1)
26233     1   FORMAT(1H1,/,4X,12H1/T  OBS K,5X,7HOBS LNK,13X,13HFITTED
        $ LNK,
26333        17X,15H(OBS-FITTED)LNK,//)
26433         DO  2  I = 1,N
26533         T(I)=1000/T(I)
26633         K(I)=ALOG(K(I))
26733         Z(I)=ALOG(Z(I))
26833         DIF=K(I)-Z(I)
26933         WRITE(6,3) T(I),K(I),Z(I),DIF
27033     3   FORMAT(1X,2E15.5,6X,2E15.5,/)
27133         K(I)=EXP(K(I))
27233         T(I)=1000.0/T(I)
27333     2   CONTINUE
27433         V(2)=V(2)/1000.0
27533         WRITE(6,4)V(1)
27633         WRITE(6,5)V(2)
27733         V(2)=V(2)*1000.0
27833         V(4)=V(4)/1000.0
27933         WRITE(6,6)V(3)
28033         WRITE(6,7)V(4)
28133         V(4)=V(4)*1000.0
28233     4   FORMAT(1X,//,13X,26HFIRST PRE-EXPONENTIAL TERM =,E20.8,2X
        $,5HSEC-1)
28333     5   FORMAT(1X,//,13X,26HFIRST ACTIVATION ENERGY     =,E20.8,2X
        $,7HKJ/MOLE)
28433     6   FORMAT(1X,//,13X,26HSND PRE-EXPONENTIAL TERM =,E20.8,2X
        $,5HSEC-1)
28533     7   FORMAT(1X,//,13X,26HSND ACTIVATION ENERGY     =,E20.8,2X
        $,7HKJ/MOLE)
28633         RETURN
28733         END
28833
28933
$
```

```
#FILE (UWMSRAS)SRALIB ON USERPK
29333       SUBROUTINE VMEXP(T,K,N,Z,N,V,IMAX)
29433       REAL T(N),K(N),N(N),Z(N),V(3),E(3),G(4,21),DIF
29533       CALL V811A(T,K,N,Z,N,V,E,3,G,4,IMAX)
29633       WRITE(6,1)
29733     1 FORMAT(1H1,/,4X,12H1/T DEG K,5X,7HOBS LNK,10X,10HFITTED LNK,
         $ /,
29833        17X,10H(OBS-FITTED)LNK,//)
29933       DO 2 J = 1,N
30033       T(J)=1000/T(J)
30133       K(J)=ALOG(K(J))
30233       Z(J)=ALOG(Z(J))
30333       DIF=K(J)-Z(J)
30433       WRITE(6,3)T(J),K(J),Z(J),DIF
30533     3 FORMAT(1X,2E15.5,6X,2E15.5,/)
30633       K(J)=EXP(K(J))
30733       T(J)=1000./T(J)
30833     2 CONTINUE
30933       V(2)=V(2)/1000.
31033       WRITE(6,4)V(1)
31133       WRITE(6,5)V(2)
31233       V(2)=V(2)*1000.
31333       WRITE(6,6)V(3)
31433     4 FORMAT(//,19X,33HINST PRE-EXPONENTIAL TERM      =,E23.8,2X,
         $ 5HSEC-1)
31533     5 FORMAT(//,19X,21HINST ACTIVATION ENERGY,8X,1H=,E23.8,2X,7HKJOU
         $ /MOLE)
31633     6 FORMAT(//,19X,33HTEMPERATURE INDEPENDENT TERM =,E23.8,2X,
         $ 5HSEC-1)
31733       RETURN
31833       END
31933
32033
$
```

```
FILE (UWMSRAS)SRALIB ON USERPK
      SUBROUTINE SEXP(T,X,W,Z,N,V,IMAX)
      REAL T(N),X(N),W(N),Z(N),V(2),E(2),G(3,21),DIF
      CALL V3PIA(T,X,W,Z,N,V,E,2,G,3,IMAX)
      WRITE(6,1)
    1 FORMAT(1H1,/,4X,12H1 T/T DEG K,5X,7H OBS LNK,13X,13HFITTED LNK,
     1 /,
     2 17X,15H(OBS-FITTED)LNK,//)
      DO 2 I = 1,N
      T(I)=1000/T(I)
      X(I)=ALOG(X(I))
      Z(I)=ALOG(Z(I))
      DIF=X(I)-Z(I)
      WRITE(6,3)T(I),X(I),Z(I),DIF
    3 FORMAT(1X,2E15.5,6X,2E15.5,/)
      X(I)=EXP(X(I))
      T(I)=1000./T(I)
    2 CONTINUE
      V(2)=V(2)/1000.0
      WRITE(6,4)V(1)
      WRITE(6,5)V(2)
      V(2)=V(2)*1000.0
    4 FORMAT(1X,//,13X,26HFIRST PRE-EXPONENTIAL TERM =,E21.8,2X,
     1 5HSEC-1)
    5 FORMAT(1X,//,13X,25HFIRST ACTIVATION ENERGY    =,E21.8,2X,
     1 7HCAL/MOLE)
      RETURN
      END
```

```
$FILE (JAMSRAS)LINE ON USERPK
$RESET LINEINFO
$SET AUTOBIND
$BIND =FROM(JAMSRAS)OBJECT/SRALIB
$RESET FREE
      FILE   S3(KIND=DISK,TITLE="LINE/DATA")
      REAL X(43),Y(43),W(43),M,SM,C,SC
    3 READ(S3,/) N
      WRITE(6,2) N
    2 FORMAT(1X,24HNUMBER OF POINTS =      ,I3,//)
      IF(N.LE.3)STOP
      READ(S3,/) (X(J),Y(J),J=1,N)
      DO 1 J=1,N
    1 W(J)=1.0
      CALL WLSSRA(X,Y,W,N,M,SM,C,SC)
      GOTO 3
      END
$RESET LIST
$
```

```
#FILE (UW#SRAS)SRALIB ON USERPK
C
      SUBROUTINE WLSSRA(X,Y,W,N,M,SM,C,SC)
      REAL X(100),Y(100),W(100),SW,SWXY,SWX
      REAL SWY,SWXX,SWYY,DEL,M,C,SM,SC,Z,SY
      INTEGER N,I
      SW = 0.0
      SWXY = 0.0
      SWX = 0.0
      SWY = 0.0
      SWXX = 0.0
      SWYY = 0.0
      DO 1 I = 1,N
      SW = SW + W(I)
      SWXY = SWXY + (W(I)*X(I)*Y(I))
      SWX = SWX + (W(I)*X(I))
      SWY = SWY + (W(I)*Y(I))
      SWXX = SWXX + (W(I)*X(I)*X(I))
    1 CONTINUE
      DEL = (SW*SWXX) - (SWX*SWX)
      M = ((SW*SWXY) - (SWX*SWY))/DEL
      C = ((SWY*SWXX) - (SWX*SWXY))/DEL
      DO 6 I=1,N
      Y(I) = (M*X(I) + C - Y(I))
      SWYY = SWYY + (Y(I)*Y(I)*W(I))
    6 CONTINUE
      SY = SQRT((SWYY)/(N - 2))
      SM = SY*SQRT(SW/DEL)
      SC = SY * SQRT(SWXX/DEL)
      WRITE(6,2)M
    2 FORMAT(/,10X,25HSLOPE                          =,  E23.8)
      WRITE(6,4)SM
    4 FORMAT(/,10X,25HSTD. DEV. OF SLOPE             =,  E23.8)
      WRITE(6,3)C
    3 FORMAT(/,10X,25HINTERCEPT                      =,E23.8)
      WRITE(6,5)SC
    5 FORMAT(/,10X,25HSTD. DEV. OF INTERCEPT         =,  E23.8,/)
      RETURN
      END
```